Report Prepared by:
Alberto A. Sagüés
Eric I. Moreno*
Walter Morris
Carmen Andrade† (Section 2)
*Permanent Affiliation: CINVESTAV-Mérida, México
†Instituto Eduardo Torroja, Madrid, Spain

CARBONATION IN CONCRETE AND EFFECT ON STEEL CORROSION

Final Report, State Job No. 99700-3530-119
WPI 0510685
Prof. Alberto A. Sagüés, Ph.D., P.E.
Principal Investigator
June, 1997
Department of Civil and Environmental Engineering

College of Engineering
University of South Florida
Tampa Florida 33620

1. Report No.	2. Government Accession No.	3. Recipient's Catalog No.
WPI 0510685		

4. Title and Subtitle

CARBONATION IN CONCRETE AND EFFECT ON STEEL CORROSION

5. Report Date: June, 1997

6. Performing Organization Code

8. Performing Organization Report No

7. Author's

Alberto A. Sagüés, Eric. I. Moreno, Walter Morris and Carmen Andrade

9. Performing Organization Name and Address

Department of Civil and Environmental Engineering
University of South Florida
Tampa, FL 33620

10. Work Unit No. (TRAIS)

11. Contract or Grant No: B-8383

13. Type of Report and Period Covered

Final Report
August 1993 - February 1997

12. Sponsoring Agency Name and Address

Florida Department of Transportation
605 Suwannee Street
Tallahassee, FL 32399-0450

14. Sponsoring Agency Code

15. Supplementary Notes

Prepared in cooperation with the U.S. Department of Transportation and the Federal Highway Administration

16. Abstract

An investigation was conducted to establish a prognosis for carbonation-induced corrosion of steel in concrete in present and future Florida highway structures. A survey of 18 existing bridges built between 1939 and 1981 (ages 14 years < t < 56 years) revealed carbonation depths $x_c \leq 50$ mm with a median of ≈ 10 mm. Carbonation coefficients $K_c = x_c\, t^{-1/2}$ ranged from 0 to 14 mm/y$^{1/2}$, with a median value of 1.4 mm/y$^{1/2}$. The highest values of K_c were observed on the decks of inland bridges. The projected time to corrosion initiation for the combination worst 10-percentile K_c values and lowest 10-percentile reinforcement cover was ≥66 years. Only a very small fraction of the present inventory of Florida D.O.T. bridges is expected to exhibit carbonation-induced corrosion over a 75-year service life. Laboratory tests were conducted to determine the influence of mix design on the carbonation resistance of concretes to be used in new Florida D.O.T. construction. The results indicate that the time for initiation of carbonation-induced corrosion may be shortened by ≈60% when the fly ash cement replacement is increased from 20% to 50%. The initiation time may be shortened by ≈35 when cement replacement is increased from 20% fly ash to 20% fly ash plus 8% silica fume.

17. Key Words	18. Distribution Statement
Reinforcing Steel, Corrosion, Carbonation, Concrete, Fly Ash, Silica Fume, Bridges	No restrictions. This document is available to the public through the National Technical Information Service, Springfield, VA 22161

19. Security Classif.(of this report)	20. Security Classif. (of this page)	21. No. of Pages	22. Price
Unclassified	Unclassified	251	

Form DOT F 1700.7 (8-72)

CONVERSION FACTORS, US CUSTOMARY TO METRIC UNITS

Multiply	*by*	*to obtain*
inch	25.4	mm
foot	0.3048	meter
square inches	645	square mm
cubic yard	0.765	cubic meter
pound/cubic yard	0.593	kg/cubic meter
gallon/cubic yard	4.95	liter/cubic meter
standard cubic feet/hour	466.67	ml/minute
ounces	28.35	gram
pound	0.454	kilogram
pound (lb)	4.448	newtons
kip (1000 lb)	4.448	kilo newton (kN)
pound/in^2	0.0069	MPa
kip/in^2	6.895	MPa
ft-kip	1.356	kN-m
in-kip	0.113	kN-m

ACKNOWLEDGMENT

This investigation was supported by the State of Florida Department of Transportation, and this report is prepared in cooperation with the State of Florida Department of Transportation and the U.S. Department of Transportation. The opinions, findings, and conclusions expressed here are those of the authors and not necessarily those of the Florida Department of Transportation or the U.S. Department of Transportation.

The authors are indebted to Dr. S. Kranc for valuable discussions. The extensive technical support and many helpful discussions provided by Rodney G. Powers, and the assistance of the Corrosion Section of the FDOT Materials Office are gratefully acknowledged. One of the authors (E.Moreno) acknowledges the scholarship provided by the National Council for Science and Technology (CONACYT-México).

TABLE OF CONTENTS

EXECUTIVE SUMMARY

Corrosion of reinforcing steel in concrete often occurs in the substructure of Florida marine bridges as a result of chloride ions from seawater. The chloride ions penetrate through the concrete cover and cause breakdown of the otherwise protective passive layer on the steel surface. A slower process that also causes steel passivity breakdown is carbonation of the concrete due to chemical reaction with atmospheric carbon dioxide. A low pH, reacted layer of concrete forms at the surface and penetrates inward to a depth x proportional to the square root of the exposure time t ($x = K_c t^{1/2}$, where K_c is called the carbonation coefficient). When x is equal to the rebar cover depth, steel depassivation takes place and corrosion begins. This process does not require chloride ions and may eventually affect the entire FDOT bridge inventory. Progress in preventing chloride-induced corrosion has now significantly extended the design service life of new structures, and slower forms of deterioration such as carbonation-induced corrosion merit serious consideration when attempting to achieve a 75-year service life goal. Moreover, thousands of existing FDOT bridges both over seawater and inland are reaching service lives at which carbonation-induced corrosion can be of concern.

The present investigation was conducted to establish a prognosis for carbonation-induced corrosion in present and future FDOT structures. Specific objectives included

(a) determining the state of the art knowledge of the carbonation-corrosion process;
(b) conduct a survey of bridges in the FDOT inventory to determine the extent of concrete carbonation, establishing quantitative service life predictions and compare with the effects of chloride-induced corrosion;
(c) conduct a laboratory investigation to determine the influence of mix design parameters on the carbonation resistance of concretes to be used in new construction.

The results from the knowledge base developed under objective (a) were used to select structures in the State with the most propitious conditions for carbonation. To address objective (b) a total of 18 structures was identified for examination, incorporating bridges built between 1939 and 1981 in Dade, Duval, Hillsborough and Monroe Counties. Sixteen of the bridges showed evidence of significant concrete carbonation, but only one (built in 1962) showed corrosion damage attributable to carbonation.

Concrete carbonation depths observed in the bridges were as high as 50 mm, with an average value of ≈10 mm. The carbonation coefficients measured from bridge-extracted cores ranged from 0 to 14 mm/y$^{1/2}$, with a median value of 1.4 mm/y$^{1/2}$. Cores extracted from bridge decks presented higher values of x_c and K_c compared with the substructure. This difference was most pronounced on bridges built over water, where the average values of x_c were 12.3 and 2.1 mm for the deck and the

substructure respectively. The most severe conditions for carbonation-induced corrosion were obtained on the decks of bridges built overland (highest 10 percentile $K_c > 4.35$ mm/y$^{1/2}$).

Measurements of concrete covers in the bridges examined showed that in 10% of the cases the cover was < 3.8 cm. The estimated time for corrosion initiation assuming the combination of worst 10-percentiles for carbonation coefficient and cover indicated above (4.35 mm/y$^{1/2}$ and 3.8 cm) was ≈ 70 years. Time to carbonation-induced corrosion projections for the median conditions were much in excess of 100 years. As expected, evaluation of the propensity for chloride-induced corrosion in substructure of the marine bridges included in the survey resulted in much lower projections of time to corrosion. The results of the field survey suggest that only a small fraction (on the order of 1%) of the present FDOT bridge inventory is expected to show significant carbonation-induced corrosion during a 75-year service life.

Objective (c) stemmed from FDOT concrete formulations for new construction that are relying increasingly on pozzolanic additions (primarily class F fly ash) for increased performance. Because the pozzolanic reaction consumes part of the calcium hydroxide reserve of concrete, its resistance to carbonation may be compromised. Laboratory experiments were designed to determine the carbonation resistance of concretes with 20% fly ash cement replacement (typical of high

performance Section 346 concretes) and an extreme case of 50% replacement. Variations with additional pozzolan (8% silica fume), and chloride contamination were also examined. Test specimens were exposed to accelerated carbonation test atmospheres containing 0.5% CO_2 (16 times more than normal atmospheric content) and the carbonation coefficients were determined after 100 days of exposure. Comparison between carbonation coefficients obtained in the the accelerated test exposure and initial atmospheric conditions confirmed the theoretical expectations that $K_c \propto \%CO_2^{½}$. The results from the accelerated tests could then be reasonably correlated with predicted behavior under atmospheric conditions.

The tests revealed that for concretes with the same amount and type of cementitious material the carbonation depth increased directly proportional to the water-to-cementitious (w/ct) ratio, and decreased when the compressive strength increased. When w/ct was kept constant, the carbonation depth increased as the cement content decreased, and also increased as the water-to-cement ratio (w/c) increased. The estimated carbonation-induced corrosion initiation period can be shortened by about 60% if the amount of fly ash cement replacement is increased from 20% to 50%. The initiation time can be shortened by about 35% when cement replacement is increased from 20% fly ash to 20% fly ash plus 8% silica fume. In general, the results indicate that excessive cement replacement by pozzolanic additions may significantly impair carbonation resistance.

The overall results from this investigation indicate that past FDOT construction practices have provided reasonable protection against high incidence of carbonation-induced corrosion. Only a very small fraction of the FDOT bridge inventory is likely to exhibit this form of corrosion over a service span of 75 years. New concrete formulations using moderate fly ash replacement of concrete offer similarly good performance, but caution should be exercised to avoid excessive pozzolanic cement replacement.

Section 1. INTRODUCTION

Corrosion of reinforcing steel in concrete begins when the initially passive condition of the steel surface is disrupted. Subsequent accumulation of corrosion products causes concrete cover spalls and other structural deterioration. The most common cause for steel passivity disruption in Florida highway structures is the presence of chloride ions in the concrete next to the reinforcing steel; the chloride ions penetrate from the external concrete surface in contact with seawater. Corrosion induced by chloride ions has been frequently observed in marine substructure after service times on the order of only a few years. Improvements in design and concrete quality over the last decades have considerably extended the expected time for the onset of steel depassivation (known as the length of the corrosion *initiation period*) in the case of chloride-induced corrosion. Consequently, design service lives approaching a 75-year design goal appear to be within reach.

However, the improved resistance to chloride-induced deterioration has led to concern about a normally slower form of steel depassivation that results from *concrete carbonation*. Concrete carbonation results from the chemical reaction between the hydrated cement components (notably the calcium hydroxide but also the calcium-silicate-hydrate and other compounds) and atmospheric carbon dioxide. This reaction lowers the pH of the concrete pore solution to a level where passivity of the steel surface is no longer supported, causing the initiation of corrosion and

consequent damage. Concrete carbonation begins at the external surface and progresses inward at a rate that decreases with time, but that is expected to remain finite so that the reinforcing steel depth is eventually reached.

Recent observations of significant concrete carbonation depths in some FDOT bridges, combined with the aforementioned progress in mitigating chloride induced corrosion, led to the formulation of the present investigation, aimed at establishing the prognosis for carbonation-induced corrosion in present and future FDOT structures. The objectives of this investigation were as follows:

Objective (a): Determine the state-of-the-art knowledge of the processes responsible for carbonation-induced corrosion of carbonation steel; including a bibliographic search and compilation of methods used to predict rate of concrete carbonation. The findings pertaining to this objective are introduced in **Section 2** of this report.

Objective (b): Conduct a field survey of bridges in the FDOT inventory to determine the extent of concrete carbonation, and establish a prognosis for corrosion-limited service life. Whenever appropriate, compare with concurrent chloride-induced corrosion processes. The findings are presented in **Section 3** of this report.

Objective (c): Conduct a laboratory investigation to determine the influence of mix design parameters on the carbonation rate of concrete to be used for future long term durability FDOT applications. The findings are presented in **Section 4** of this report.

Section 2. Objective (a): STATE OF THE ART KNOWLEDGE

Objective (a) is to determine the state-of-the-art knowledge of the processes responsible for carbonation-induced corrosion of carbonation steel; including a bibliographic search and compilation of methods used to predict rate of concrete carbonation.

This portion of the investigation was conducted as part of a subcontract to the E. Torroja Institute of Construction Sciences, Superior Council of Scientific Research, Madrid, Spain. The findings are presented in the appendix for Section 2 (pp. 161-213).

Section 3. Objective (b): FIELD INVESTIGATION

Objective (b) is to conduct a field survey of bridges in the FDOT inventory to determine the extent of concrete carbonation, and establish a prognosis for corrosion-limited service life. Whenever appropriate, compare with concurrent chloride-induced corrosion processes.

The approach to attain this objective was to select a number of suitable FDOT bridges built one or more decades ago, and measure the extent of concrete carbonation and any related corrosion. Concrete cores were extracted from those structures. The results were used to determine carbonation coefficients and obtain a picture of the distribution of carbonation severity as a function of structure location, age, and type of structural member. The distribution of concrete rebar cover depths was also obtained. The results were then used to obtain projections of the length of service time before carbonation-induced corrosion would be observed in typical and severe exposure conditions. Additional determinations were made of the extent of chloride ion contamination and the projected times for development of chloride-induced corrosion.

The test plan was developed by first examining the environmental conditions present in the State to determine geographic regions with the highest potential for development of concrete carbonation. The bridge inventory in those regions was examined to select bridges within the appropriate age range. Eighteen bridges were selected for detailed examination; these structures are

listed in Table I.1 and indicated in the map in Figure I.13. Experimental activities were conducted both in the field and in the laboratory.

During field visits of each structure determinations were made of the visual appearance, approximate carbonation depth, concrete electrical resistivity, half cell potentials, and internal concrete relative humidity (selected structures). Concrete cores were then extracted from the substructure and the deck, and initial determinations of concrete cover thickness were made.

Laboratory examination of field-extracted samples included detailed measurement of carbonation depth, measurement of chloride concentration profiles whenever applicable, measurement of concrete resistivity in the wet condition, characterization of the coarse aggregate, determination of concrete porosity, and measurement of corrosion rate of embedded rebar segments in selected cases.

A detailed indication of the test techniques and the findings is given in the following subsections.

3.1 PROCEDURE

3.1.1 Field Investigation

A group of possible locations within the State were initially proposed for field inspections, taking into account existing records of structures that had

shown signs of deterioration presumably due to concrete carbonation. The climatic conditions that influence carbonation were also considered for the selection of the structures. The bridge selection criterion was adjusted during the project, based on the ongoing findings and the experience gathered after each inspection. The main aspects considered for the selection are indicated below:

3.1.1.1 Environmental Conditions

The environmental conditions at which a structure has been exposed during its service life influence the carbonation process. The conditions under which carbonation will more likely take place are described below:

3.1.1.1.1 Relative Humidity in the range of 50 to 70%. The air relative humidity (***RH***) experiences considerably diurnal and yearly variation. Nevertheless, the carbonation process will be more severe on those structures that are exposed to an environment where the ***RH*** is in the range of 50 to 70% [I.1, I.2, I.3]. When the ***RH*** is higher than 70%, the concrete pores tend to saturate with water making the diffusion of CO_2 through the concrete very slow. On the other hand, when the relative humidity is lower than 50%, the pores tend to become dry and the dissolution of $Ca(OH)_2$ and CO_2 necessary for the carbonation reaction does not takes place.

The annual maximum and minimum average values of ***RH*** in the state of Florida are illustrated in the maps shown in Figure I.1-A and I.1-B. The information was provided by the Southeast Region Climate Center and reflects the data obtained between 1931 and 1990.

3.1.1.1.2 High Temperatures. The carbonation reaction rate increases with temperature. It is then expected to find higher carbonation depths on those regions with higher nominal temperatures. Figure I.2 shows a map with the nominal values of temperatures in the state of Florida.

3.1.1.1.3 Low Rain Precipitation. When the concrete surface is wetted by rain, the diffusion of CO_2 is momentarily blocked as the pores get filled with water. The diffusion of CO_2 will continue once the concrete starts drying. Carbonation is then expected to be more severe in those regions with low precipitation and particularly on those parts of the structures that remain sheltered from the rain. A map illustrating the nominal values of annual precipitation's in the state of Florida is presented in Figure I.3.

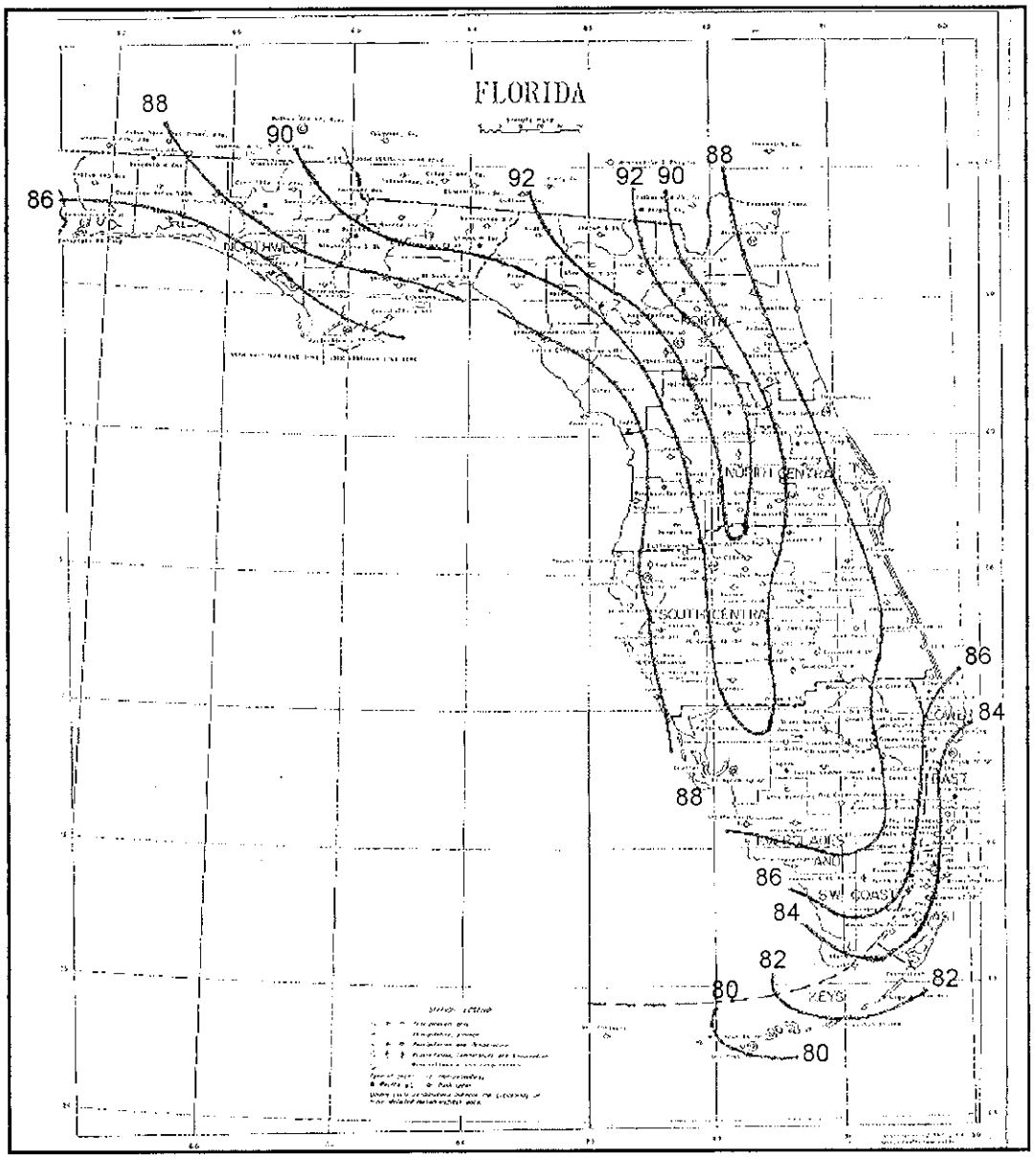

Figure I.1-A. Annual maximum average values of air relative humidity %(*RH*) in the state of Florida. The information was provided by the Southeast Region Climate Center and reflect the average values corresponding to the period 1931 - 1990.

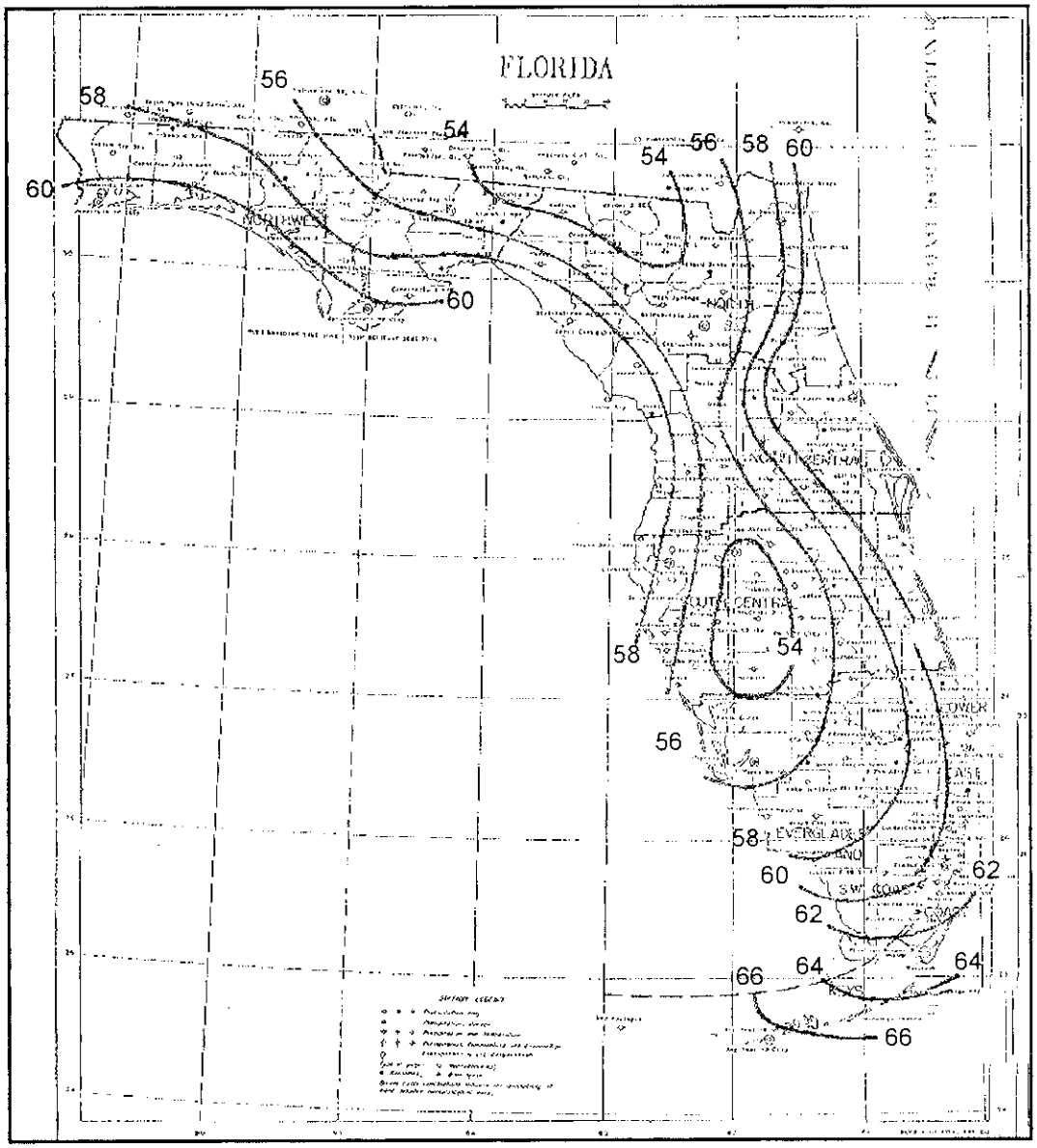

Figure I.1-B. Annual minimum average values of air relative humidity %(*RH*) in the state of Florida. The information was provided by the Southeast Region Climate Center and reflect the average values corresponding to the period 1931 - 1990.

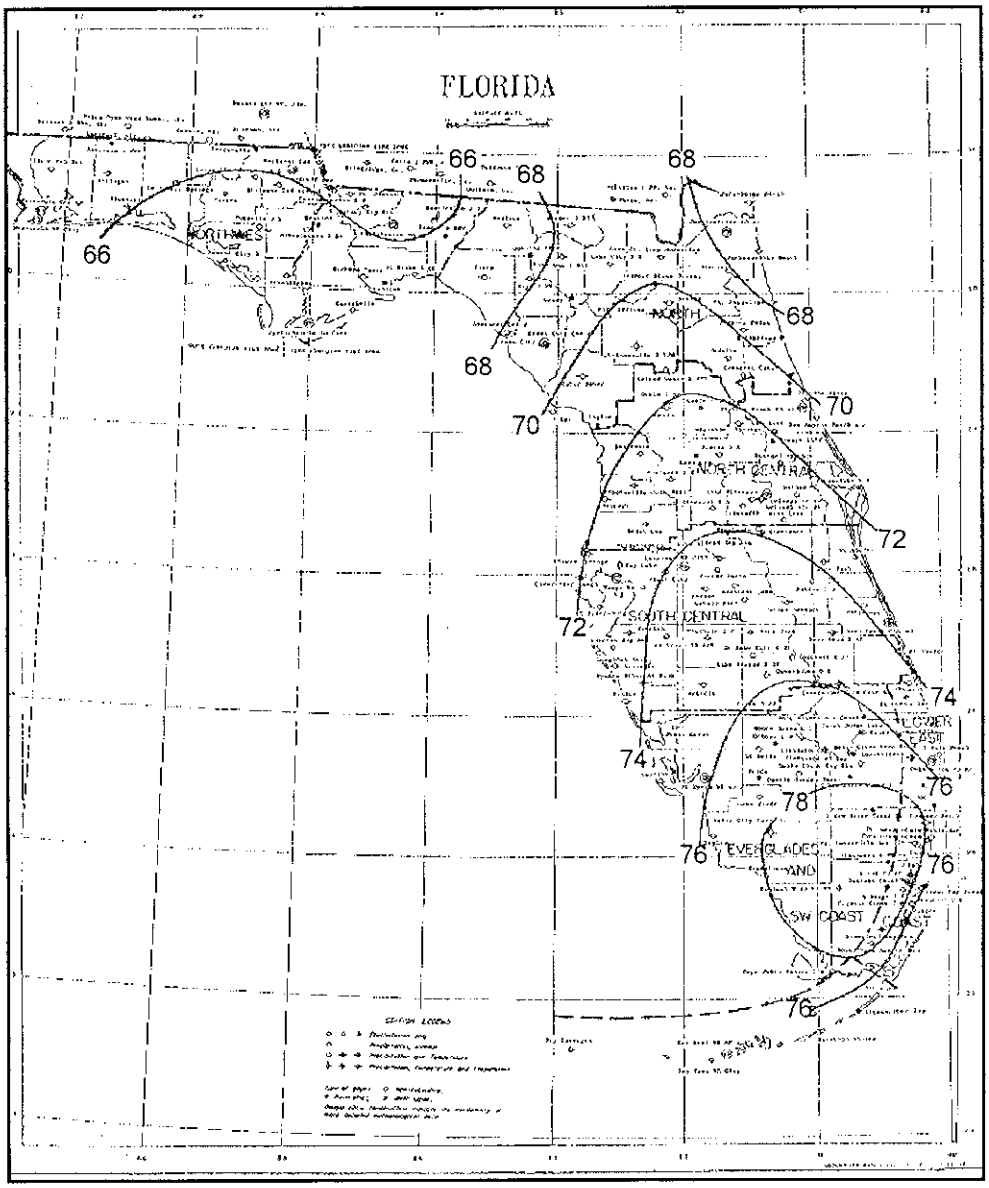

Figure I.2. Annual average values of temperature (°F) in the state of Florida. The information was provided by the Southeast Region Climate Center and reflect the average values corresponding to the period 1931 - 1990.

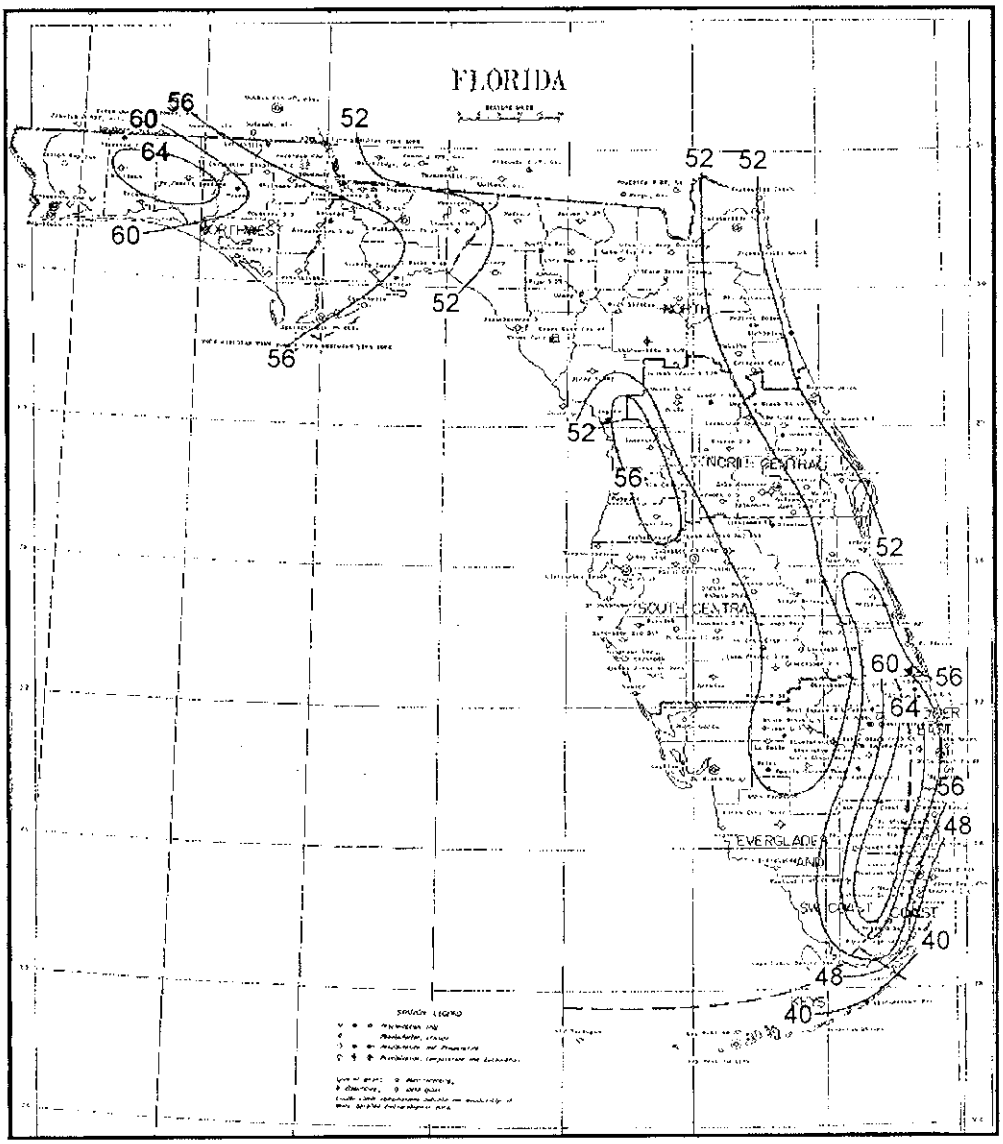

Figure I.3. Nominal values of annual rain precipitation (in *inches*) in the state of Florida. The information was provided by the Southeast Region Climate Center and reflect the average values corresponding to the period 1931 - 1990.

3.1.1.1.4 High Concentration of CO_2. The normal concentration of CO_2 in the atmosphere is approximately 0.03%. However, in certain areas as in bridges with heavy traffic, or close to industrial areas the level of CO_2 contamination may

reach and even exceed 0.1 % concentration [I.4]. Under these circumstances the carbonation penetration increases proportional to the square root of the external CO_2 concentration [I.3].

3.1.1.2 Age of the Structure

The carbonation depth also increases with the square root of time [I.4, I.5, I.6]. Accordingly, older bridges were chosen wherever possible for the field inspection. The information regarding the year of construction and structure characteristics was obtained from the National Bridge Inventory (*NBI*), and provided by the Florida Department of Transportation (FDOT).

3.1.1.3 Structure Type of Exposure Conditions (Over land & over water)

In addition to the climatic conditions that characterize a particular region, the type of exposure conditions, meaning whether the bridge is located over water or over land were considered when selecting the structures. In the following, the inspected structures will be referred as "over water" or "over land" depending on whether it is an over water or a highway overpass bridge. Figure I.4 and I.5 shows an over water and an over land bridge respectively, inspected during the project.

Figure I.4. Over water structure located on the Florida keys (South (right) and North (left) bound Bahia Honda Bridge built in 1969 and 1972 respectively).

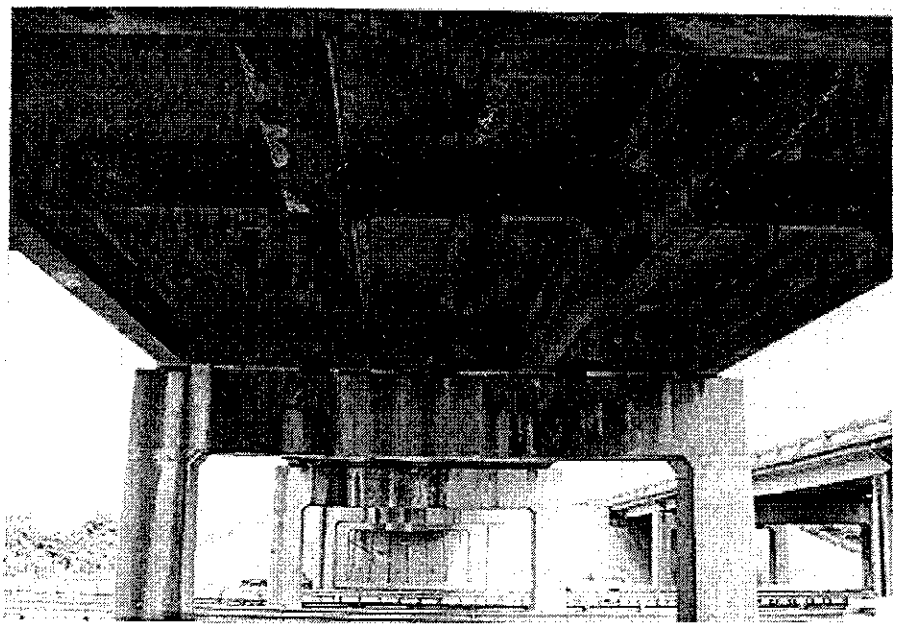

Figure I.5. Over land bridge located on the city of Tampa (West bound I-4 over Orient road, built in 1961).

3.1.2 Site Activities

3.1.2.1 Visual Examination and Soundings

Each structure was first visually examined for evidence of concrete spalls, cracks, and rust marks. Once the visual inspection was completed, two to three bents were selected for further detailed examination. Hammer sounding tests were performed on the selected locations of the structure in order to detect delaminated concrete.

3.1.2.2 Carbonation Depth

The concrete carbonation depth (x_c) was determined by spraying a pH indicator on freshly exposed concrete surfaces [I.7]. The pH indicator changes in color depending on the pH of the tested solution. Two types of pH indicators were initially tested in the field, a 1% solution of phenolphthalein in ethyl alcohol and a solution of 0.05% thymolphthalein. The phenolphthalein turns from colorless to red when the pH increases through the range 8.2 to 10. Likewise, the thymolphthalein turns from colorless to blue when the pH increases through the range 9.4 to 10.6. The phenolphthalein gave better contrast when it was sprayed over the concrete surface and it was used in most of the applications. Preliminary measurements of x_c were performed in the field by chipping off

pieces of concrete at different parts of the structure and spraying the pH indicator over these spots. Figure I.6 shows a column where the external concrete surface was chipped off at the edge, and sprayed with the phenolphthalein solution. The carbonation depth is determined by the uncolored region, measured perpendicular to the external surface.

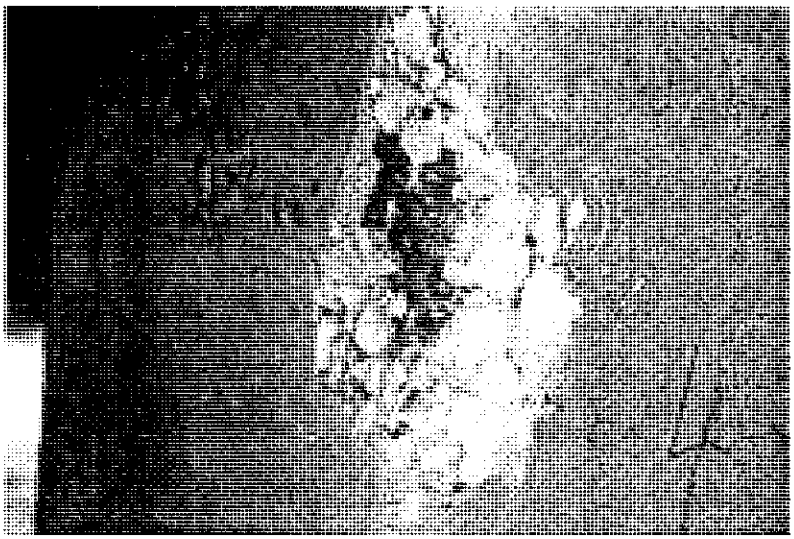

Figure I.6. Field determination of concrete carbonation depth on a column of a highway bridge (I 95 over Trout river near Jacksonville). The measurement is taken after chipping the concrete and spraying a pH indicator (1% solution of phenolphthalein in ethyl alcohol) over the freshly exposed concrete.

When the carbonation depth was measured at the edge (corner) of a structural component, as in the case shown in the Figure I.6, the measurement was taken with respect to one of the flat surfaces of the column, to minimize the corner effect.

3.1.2.3 Electrical Resistivity Measurements

The electrical resistivity of concrete in service can be an important aid to assess the corrosion durability of reinforced concrete structures [I.8]. The measurement of the concrete resistivity in conjunction with half-cell potential mapping provides a quick and inexpensive way of assessing the risk of rebar corrosion.

Concrete resistivity measurements were performed using a C.N.S. RM MKII four point Wenner array probe with electronic driver/analyzer set for a 1.5 *inch* (3.81 *cm*) inter-point spacing. The probe operated at a controlled current and frequency of about 20μA and 13 *Hz* respectively. The contact probes were 3 mm diameter wooden tips. The readings were taken by triplicate at different elevations above high tide (***EAHT***) and above floor level (***EAFL***) on over water and on over land structures respectively. The measurements were performed placing the probe far from the edges of the tested component to avoid errors due to uneven current distributions. As the readings can be affected by the presence of reinforcing steel underneath the concrete cover where the probe is positioned, measurements were taken placing the probe array in a vertical and horizontal position. The average value of all readings at a given elevation was considered as the representative value of the concrete resistivity.

3.1.2.4 Concrete Cores

Concrete cores with a diameter of 1.75" (4.44 *cm*) were drilled using a hollow bit cooled with fresh water. Usually 2 or more cores were extracted from each inspected site of the bridge. In the bridge substructure, the cores were extracted at different elevations above high tide (***EAHT***) or above the floor level (***EAFL***) depending if the bridge was located over water or over land. Figure I.7 shows the coring equipment set up at 10 *ft.* ***EAHT*** on a prestressed pile of an over water bridge.

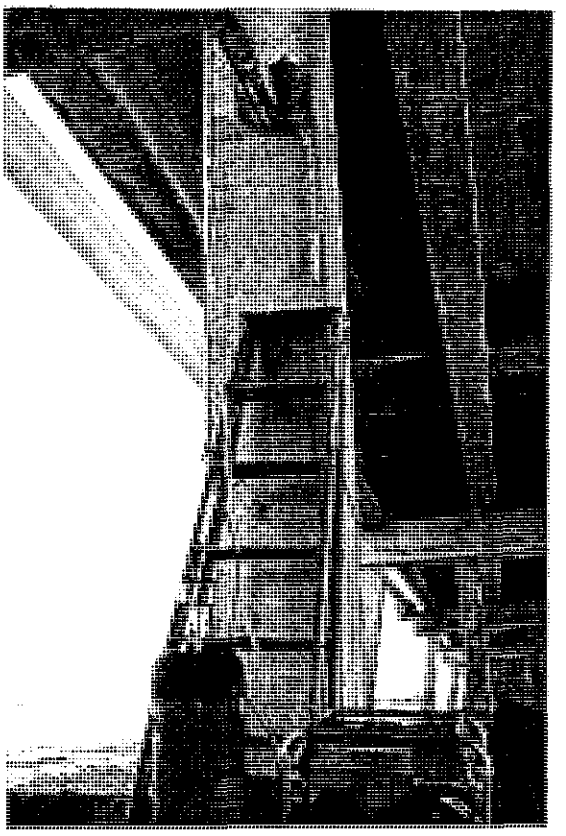

Figure I.7. Coring equipment set up at 10 *ft.* above high tide on a prestressed pile of the south bound Boca Chica Bridge located at the Florida Keys.

The cores from the bridge deck were drilled through the slab from the top of the deck. This procedure usually required drilling two or more holes to obtain a complete core. Appendix 3.2 shows a list of all the cores extracted, indicating the original bridge from where they were drilled and other characteristics. The cores were labeled, indicating the date, bent and pile number, and bridge number and placed in plastic bags for further laboratory evaluations.

3.1.2.5 Half-Cell Potentials

The half cell potential can give an indication of the rebar corrosion state. Half-cell potentials measurements were obtained from those locations where the coring bit intersected rebars or prestressed tendons, leaving bare steel exposed. The measurements were performed generally following the ASTM C- 876 standard test procedure. An electrical contact was established between the steel and a voltmeter with high internal resistance, and the corrosion potential (E_{corr}) was measured using a copper-copper sulfate reference electrode (***CSE***). Potential readings were taken by placing the reference electrode tip in contact with the concrete surface around the core hole and at different elevations (***EAHT/EAFL***). In the over water structures, an additional measurement was performed immersing the reference electrode tip in the water next to the pile or column tested. This reading was labeled as the potential of the steel corresponding to the high tide level (***EAHT*** = 0).

3.1.2.6 Internal Concrete Relative Humidity

There is a general agreement that the internal concrete relative humidity (***IRH***) affects the penetration rate of aggressive species like CO_2 and Cl^- into concrete, as well as the rebar corrosion rate once it is initiated [I.2, I.9]. The ***IRH*** gives an indication of the moisture content and indirectly the degree of pore saturation in the concrete [I.10-I.12]. Although, no clear quantitative relationship between these parameters has still been presented in the literature, the ***IRH*** nevertheless was measured for an effective depth of 1.5 in. (3.81 *cm*) on different parts of the structure. A 7/8" (2.22 *cm*) diameter hole was drilled into the concrete with a dry masonry bit, and a plastic fitting with a removable cap was attached in the hole, as shown in Figure I.8.

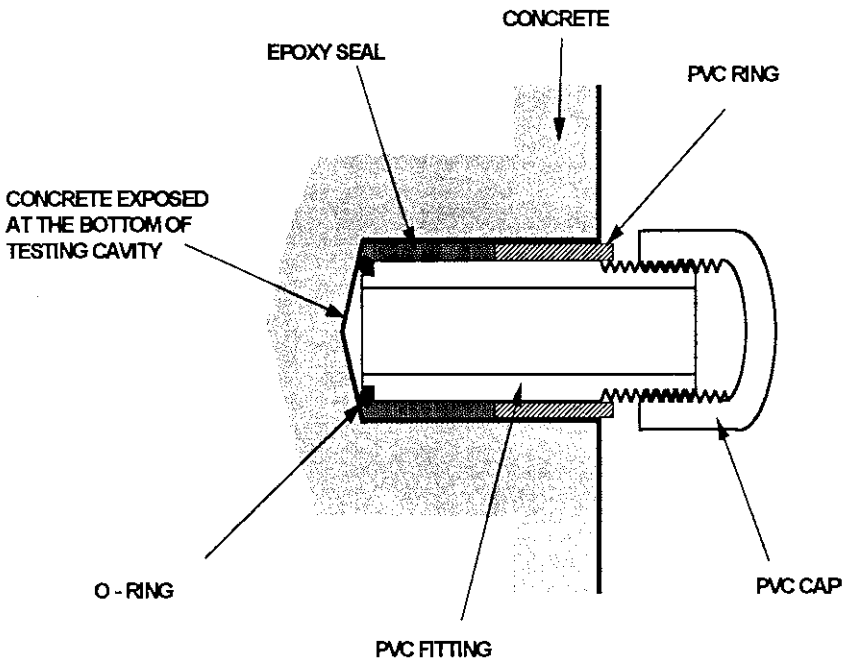

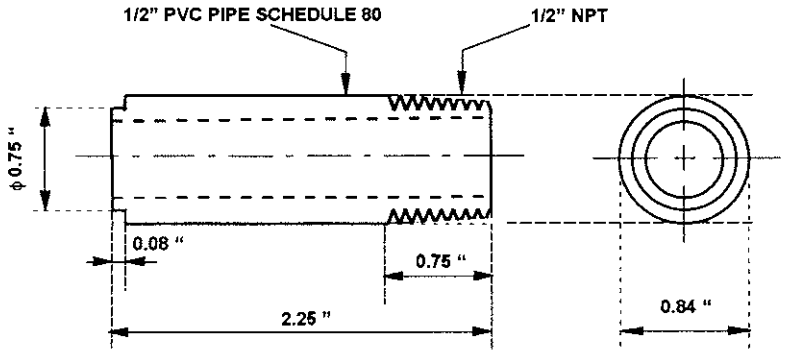

Figure I.8. Characteristics and dimensions of relative humidity probe for the measurement of the internal relative humidity (***IRH***) of concrete.

A first set of ***IRH*** readings were taken 48 *hr.* after the fitting was placed, to allow the inside relative humidity to stabilize and approach a representative value. ***IRH*** measurements were repeated at later visits during the year to observe possible seasonal effects. Following the procedure of Andrade et al [I.2], the measurements were performed after removing the cap and introducing the sensing end of a relative humidity probe inside the cavity. The probe dimensions were such that a tight fit with the plastic fitting was achieved during the measurement. As the opening operation slightly modified the internal cavity conditions and that the probe itself did not stabilize immediately, several readings were taken at different time steps. The value of ***IRH*** was determined extrapolating the experimental data recorded by means of a mathematical curve fit, assuming a power law dependence of the ***IRH*** readings with time (see Appendix 3.3). Figure I.9 shows the relative humidity testing device during the measurement of ***IRH*** in a concrete column of an over land bridge.

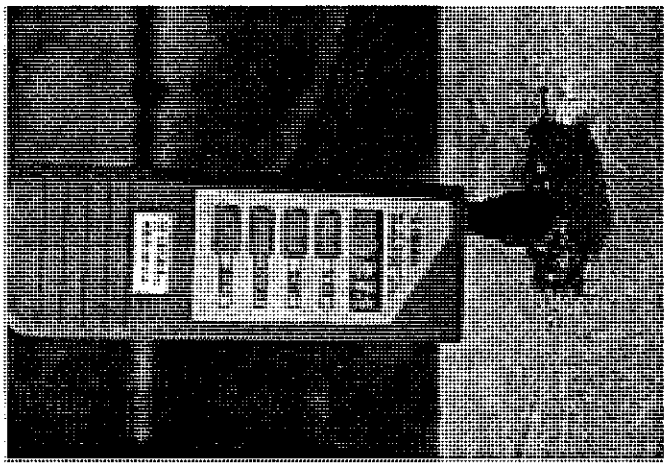

Figure I.9. Internal relative humidity (***IRH***) measurement on a column of an over land bridge.

3.1.2.7 Concrete Cover Thickness

The concrete cover thickness (***cc***) was measured directly on those cores that exposed rebars or prestressed tendons. The ***cc*** was measured as the perpendicular distance from the core surface originally exposed to the external environment, up to the rebar surface (if remains attached to the core), or eventually to the rebar mark at the cracked end of the core. As the field inspection was not focused on the extraction of steel samples, only one third of the total number of cores extracted (116) reached the reinforcement.

3.1.3 Laboratory Evaluation of Field Samples

The laboratory tests were performed on the cores extracted from the field. The cores were first classified and logged according to the type of structure from where they were extracted (reinforced - prestressed), the location (over water - over land), and the part of the structure (deck - substructure).

3.1.3.1 Carbonation Depth

The carbonation depth (x_c) was measured with more accuracy in the laboratory repeating the pH indicator procedure utilized in the preliminary measurements performed in the field. The core end originally exposed to the

external environment was cracked longitudinally and the pH indicator (1% phenolphthalein in ethyl alcohol) was sprayed on both cracked surfaces. The values of x_c were recorded in *mm* measuring the distance between the core end and the carbonation front (color boundary defined by the pH indicator), as indicated in Figure I.10. The maximum and minimum values of carbonation depth (x_{max} and x_{min}) [I.7] were also recorded on those cores that presented irregular carbonation fronts. Figure I.10 shows a schematic representation of the carbonation depth measured on a concrete core. The influence of the coarse aggregate on the carbonation front was examined, determining its influence in x_c.

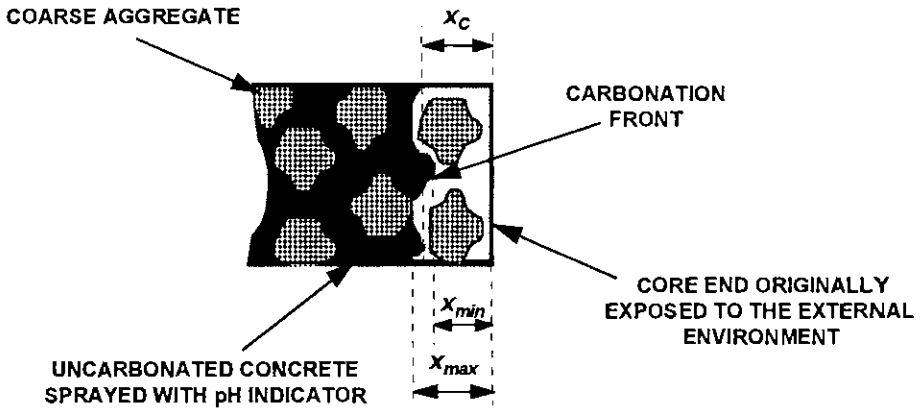

Figure I.10. Schematic representation of the carbonation depth (x_c) measurement on a concrete core.

The values of carbonation coefficient **Kc** ($mm/y^{1/2}$) were calculated using equation **(1)**, based on the measurements of x_c and the age of the inspected structures.

$$x_c = Kc\sqrt{t} \qquad \textbf{(1)}$$

3.1.3.2 Chloride Concentration Profile

Chloride concentration profiles were determined by cutting the core in slices 0.5 *mm* thick the first two and 1 *mm* thick the remainding 4. Each slice was pulverized and the powders were analyzed for chloride content following the acid soluble procedure detailed in FDOT Research Report 203 [I.13]. The chloride concentration profiles were mathematically processed for the determination of the apparent effective chloride diffusion coefficient (D_{eff}). A curve fitting program based on the solution of Fick's second law for a certain value of bulk concentration (C_o) and an estimated value of superficial chloride concentration (C_s) was used for these calculations.

An approximate estimation of the time for corrosion initiation due to chloride induced corrosion was determined assuming a typical concrete cover thickness and a chloride threshold value for corrosion initiation of 1.2 *pcy* of concrete (0.71 kg/m^3).

3.1.3.3 Wet Resistivity

The electric resistivity of concrete is a function of the concrete pore structure and the amount and type of solution present in the pores. This parameter, conveniently calibrated or standardized to reference values, could give information about the proportion of saturated concrete pores, which at the

same time may give an indication of the rate of CO_2 and Cl^- penetration [I.14, I.15].

A group of cores were selected for the determination of the wet resistivity (ρ_w). The cores were placed in a 100% relative humidity chamber and periodically monitored taking weight and electrical resistivity measurements. The value of ρ_w was measured after the cores achieved constant weight. The resistivity measurements were taken using a C.N.S. RM MKII meter with a 4-point Wenner array using 1 inch (2.54 *cm*) or larger inter-point spacing. The 4 point probe array was placed longitudinally centered on the core side as shown in Figure I.11.

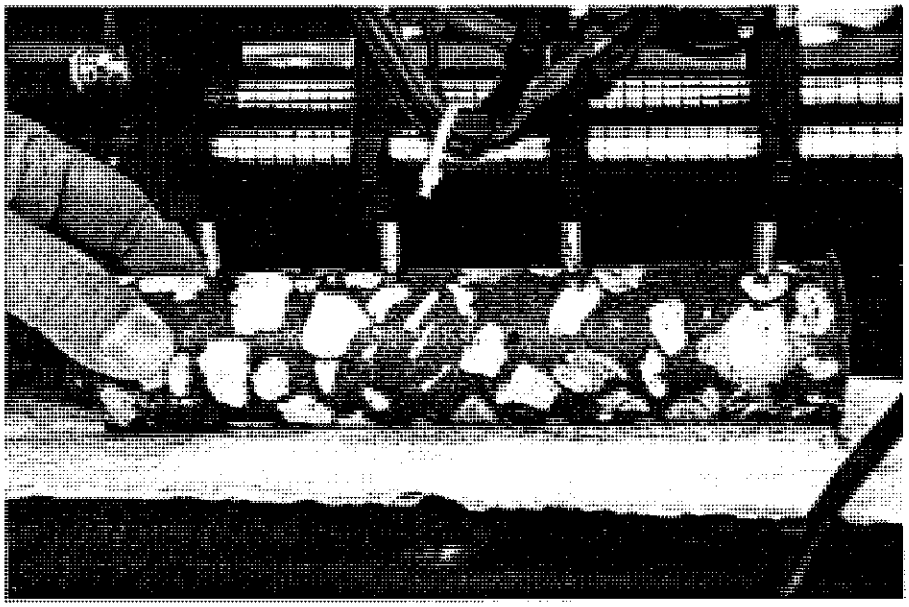

Figure I.11. Measurement of apparent concrete resistivity (ρ_{app}) on a concrete core using the 4 point probe Wenner array device with a 2 *inch* (5.08 *cm*) inter-point distance.

Three different tangential positions around the core (120° one from the other) were tested, to overcome the variability effect introduced by the coarse aggregate [I.16]. The measuring device is calibrated for taking measurements on surfaces of structures that can be considered as semi-infinite. When the measurement is performed on a finite body as a concrete core, the device measures an apparent value of resistivity (ρ_{app}) that is higher than the real value of resistivity (ρ). The value of ρ_w should be then calculated as

$$\rho_w = \frac{\rho_{app}}{K} \quad (2)$$

where K is defined as the geometrical cell constant and depends on the dimensions of the core and the inter-probe spacing. For a core diameter of 1.75" (4.45 *cm*) and an inter-point spacing of 1" (2.54 *cm*) the value of K varies from 3.15 to 2.9 for a core length of 3" (7.62 *cm*) and 5" (12.5 *cm*) or larger respectively [I.16].

3.1.3.4 Aggregate Characterization

The coarse aggregate in the cores was visually examined for size distribution and type (limestone or river rock). The porosity of a typical limestone coarse aggregate was independently determined, running the ASTM C 642-90 standard test on three samples randomly picked from a FDOT stock pile. The

maximum aggregate size was 3/4" (1.9 *cm*). The average of the three values was considered as a representative value of the limestone coarse aggregate porosity, and used in further calculations.

3.1.3.5 Concrete Porosity

The percentage of voids or concrete porosity, was determined on a group of cores according to the ASTM C 642-90 standard test. The procedure consists in weighing the concrete samples in three different conditions; after oven drying at 105 $^{\circ}C$ (**A**); after immersion in water for 24 *hr.* and boiling for 6 *hr.*(**B**); and weighing the sample immersed in cold water (**C**) after having implemented conditions **A** and **B**. Calling $\mathbf{W_A}$, $\mathbf{W_B}$ and $\mathbf{W_C}$ the weights obtained in each of the three conditions, the percentage of voids or porosity was thus calculated as:

$$\%\text{voids} = \frac{W_B - W_A}{W_B - W_C} \times 100 \qquad (3)$$

3.1.3.6 Corrosion Rate of Rebars

Electrochemical tests were performed with selected cores that had segments of rebars that were cut during the coring procedure and remained attached to the concrete. The good determination of the exposed metallic area

being tested and the ease of the experiment set up made the test attractive to estimate the rebar corrosion rate (***CR***). The selected cores were kept in sealed plastic bags until the moment of running the test to preserve the original conditions of the concrete, preventing it from drying and from further carbonation. A small threaded hole was made in the rebar end and a screw was placed to allow a good electrical contact. As shown on Figure I.12, the working electrode of the potentiostat was connected to the rebar. A titanium mesh was placed at one of the ends of the core and used as a counter electrode. A wet paper towel was placed between the titanium mesh and the core end to improve the electrical contact. A ***CSE*** reference electrode was placed with its tip in contact to the concrete at the same level of the rebar.

Polarization resistance (Rp) tests were performed with each specimen using a CMS100 Corrosion Measurement System manufactured by Gamry, Inc. using a scan rate of 0.1 *mV/s*. Electrochemical impedance spectroscopy (EIS) tests were performed sweeping the frequency range 100 *kHz* to 1 *mHz*. A lock in amplifier Model 5210 and a potentiostat Model 273 manufactured by EG&G (Princeton Applied Research) controlled by the Model 398 EIS software were used for these tests.

The tests were run at open circuit potential. The corrosion potential (E_{corr}) and the resistance (***R***) between the working (rebar) and reference electrode were recorded before starting the experiment. The corrosion current density

(i_{corr}) values obtained by means of both electrochemical techniques (Rp and EIS) were compared.

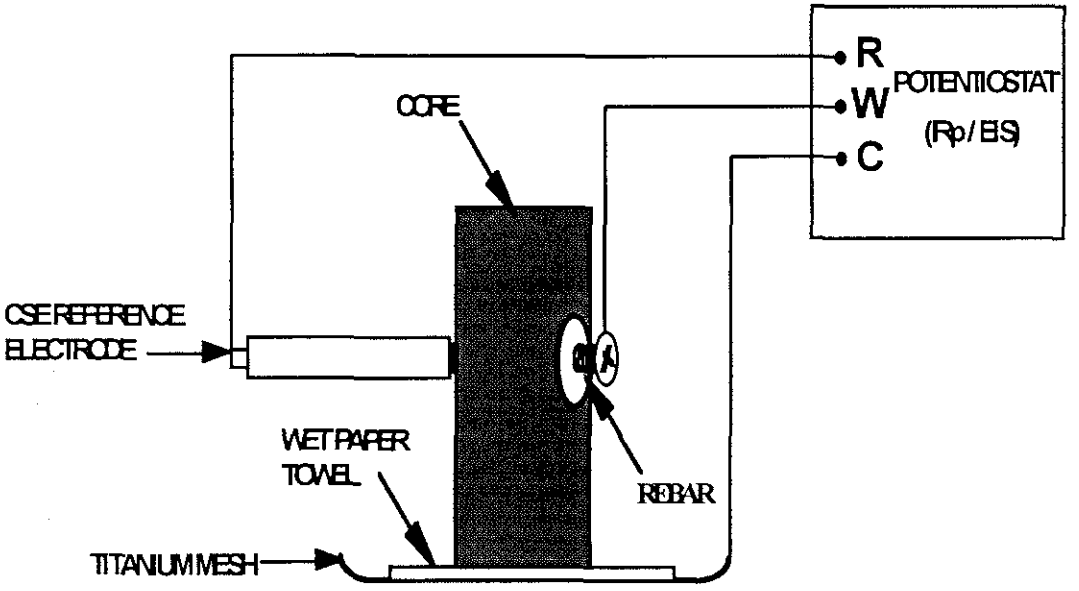

Figure I.12. Test setup for electrochemical test performed on concrete cores that had segments of rebar that were cut during the coring procedure and remained attached to the concrete.

3.2 RESULTS

A total of 18 highway bridges were selected to perform the field activities. The locations of the inspected structures are shown on Figure I.13. The first part of the field survey was carried out on a group of nine over water bridges, while the second part was performed on a group of nine over land highway overpasses. Table I.1 indicates the bridges inspected during the project, specifying the bridge number, date of inspection, year of construction, location and type of exposure condition. The structures are listed in the order in which they were inspected.

A total of 144 concrete cores were extracted from different locations of the 18 structures inspected for further analysis in the laboratory.

3.2.1 Results from Field Inspection

Appendix 3.1 presents a summary of the results obtained from the tests performed during the field inspections. Evidence of concrete carbonation in progress was found in 16 out of 18 of the bridges examined. Concrete spalls and rebar corrosion damage originated by concrete carbonation was found in one highway overpass bridge located in Tampa, (bridge no. 100172; see Table I.1). Severe rebar corrosion damage due to chloride induced corrosion was observed on five bridges (4 to 8 in Figure I.13) located in the Florida Keys.

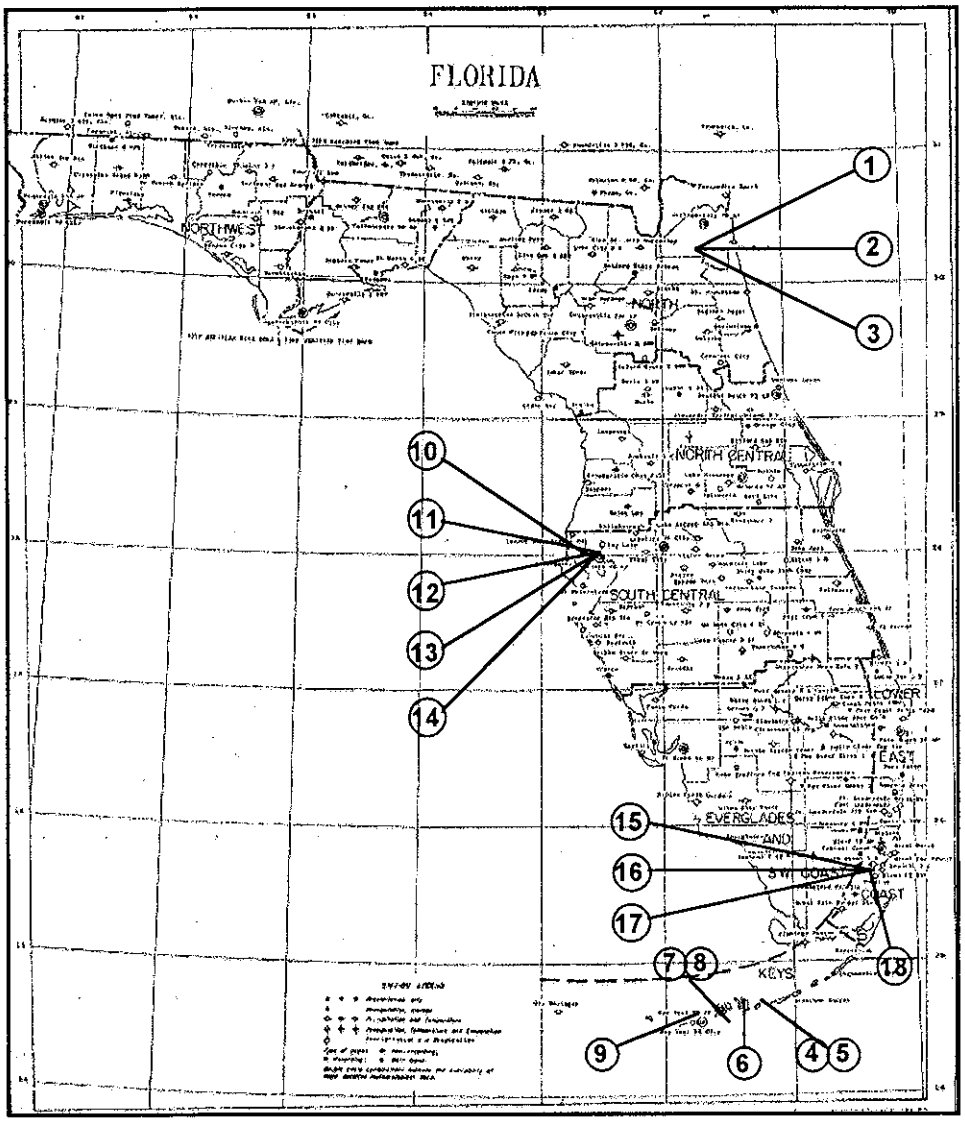

Figure I.13. Location of inspected bridges (see Table I.1 for bridge information).

Table I.1. List and specifications of bridges inspected.

Ident. # on map	Bridge Name	Bridge Abbr.	Bridge Number	Inspection Date	Const. Year.	County	Exposure condition
1	I 95, Eastbound over Trout river	I95	720011	05/05/94	1981	Duval	Over water (river)
2	Moncrief Creek over St. Johns river	MC	700352	05/05/94	1965	Duval	Over water (river)
3	Dunn Creek over St. Johns river	DC	720057	05/05/94	1973	Duval	Over water (river)
4	US 1, Boca Chica Southbound	BCS	900003	10/18/94	1981	Monroe	Over water (sea)
5	US 1, Boca Chica northbound	BCN	900037	10/18/94	1973	Monroe	Over water (sea)
6	US 1, Niles Channel	NC	900011	10/19/94	1981	Monroe	Over water (sea)
7	US 1, Bahía Honda Southbound	BHS	900016	10/20/94	1969	Monroe	Over water (sea)
8	US 1, Bahía Honda Northbound	BHN	900045	10/20/94	1972	Monroe	Over water (sea)
9	A 1 A at Key West	KW	900035	10/20/94	1960	Monroe	Over water (sea)
10	I 275 Westbound Howard Frankland	HF	150107	05/31/95	1959	Hills-borough	Over water (sea)
11	Orient road & I 4 Westbound	O&4	100172	08/03/95	1961	Hills-borough	Over land
12	22nd ST. & I 4 Westbound	22&4	100153	08/03/95	1962	Hills-borough	Over land
13	Palm Av. & I 275 Southbound	P&275	100198	08/03/95	1964	Hills-borough	Over land
14	Hillsborough over Hillsborough river	HILL	100920	08/03/95	1939	Hills-borough	Over water (river)
15	SR 826 & 37 ST. Westbound	826&37	870034	03/19/96	1964	Dade	Over land
16	SR 826 & 42 ST. Westbound	826&42	870049	03/19/96	1965	Dade	Over land
17	SR 826 & 47 ST. Westbound	825&47	870081	03/19/96	1965	Dade	Over land
18	SR 826 & 57 ST. Westbound	826&57	870053	03/20/96	1963	Dade	Over land

3.2.1.1 Carbonation Depth

The preliminary measurements of carbonation depth (x_c) obtained in the field by spraying a pH indicator over chipped concrete showed that most of the over water bridges presented values of x_c that were lower than 1/4" (6.3 *mm*). However, in the Florida Keys bridges values of x_c as high as 1/2" (12.7 *mm*) were observed on the higher areas of the substructure and in the deck. Higher values of carbonation depth were typically observed on over land structures, finding up to 1.5" (38.1 *mm*) on bridge no. 100172 (item 11 in Table I.1) which presented concrete spalls and rebar corrosion damage on caps and columns.

3.2.1.2 Concrete Resistivity

The concrete resistivity (***r***) measurements performed on the field (see Appendix 3.1) showed a strong dependence on the elevation above high tide or above floor level (***EAHT*** or ***EAFL***) at which the readings were taken. The values were consistent on piles and columns of the same structure, but varied considerably from bridge to bridge. Figure I.14 shows the average resistivity values as a function of ***EAHT - EAFL*** measured on piles and columns of the same bridge. A difference of more than one order of magnitude is observed between the values of ***r*** measured on over water and over land structures, which are indicated with empty and full symbols in the figure respectively.

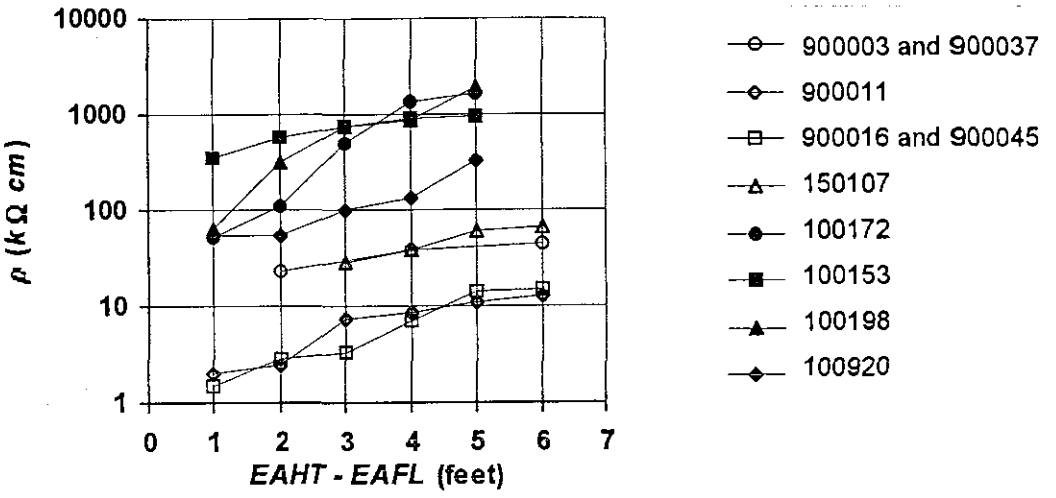

Figure I.14. Average values of field measurements of concrete resistivity (ρ) as a function of the elevation above high tide (***EAHT***) or *elevation above floor level* (***EAFL***). Empty and filled symbols correspond to over water and over land bridges respectively (see Table I.1 for bridge identification).

3.2.1.3 Half-Cell Potentials

Figure I.15 shows the variation of the average half-cell potential values, or corrosion potential values (E_{corr}), measured on piles and columns of over water bridges exposed to marine environment, as a function of ***EAHT.*** The values of E_{corr} in these bridges presented a common pattern, varying from typical active values for steel in concrete (-550 *mV* vs. ***CSE***) at the water level, to passive values at higher elevation (-50 *mV* vs. ***CSE***). The dependence of the E_{corr} values with the elevation above high tide can be approximated with the linear relationship $E_{corr}(mV)$ = 58 ***EAHT*** - 560 *mV*. Cracks, spalls, and rust marks

were observed in several piles and columns where active potentials were measured. With the exemption of bridge no. 100172 (see Table I.1) where active potentials were found next to spalled areas, in the rest of the over land bridges typical passive potentials values, varying between -50 and 100 *mV* vs. ***CSE*** were observed.

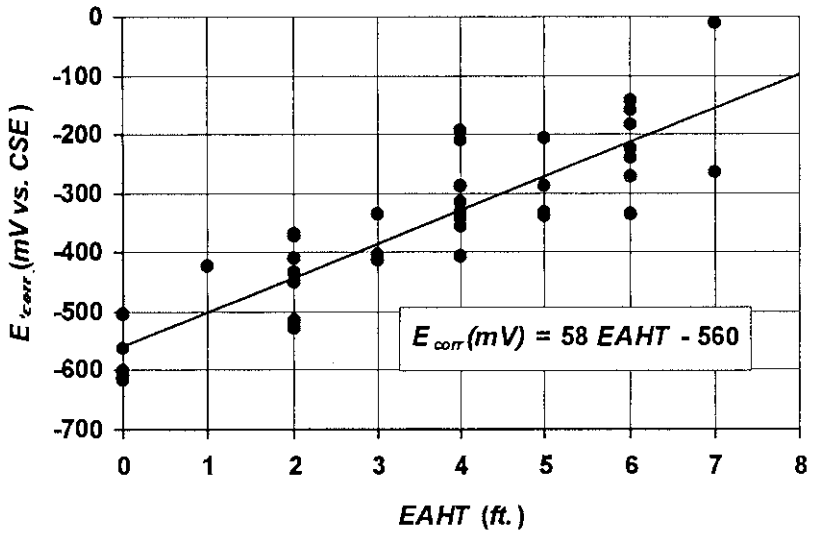

Figure I.15. Average values of corrosion potentials (E_{corr}) measured in over water bridges exposed to marine environment vs. the elevation above high tide (***EAHT***).

3.2.1.4 Internal Concrete Relative Humidity

Appendix 3.1 presents the measured and calculated values of internal relative humidity (***IRH***) of concrete obtained from different sites on over land and over water structures. In the case of over land bridges, two sets of readings were

taken, one during the summer and the other during the winter, in order to reveal the possible existence of a seasonal effect. Figure I.16 shows a bar diagram indicating the internal relative humidity values measured in each site during both seasons. The average ***IRH*** value for the winter is approximately 8 points higher than the average of readings obtained during the summer. Only one set of readings were taken on over water bridges because of the difficulty to access to the testing locations.

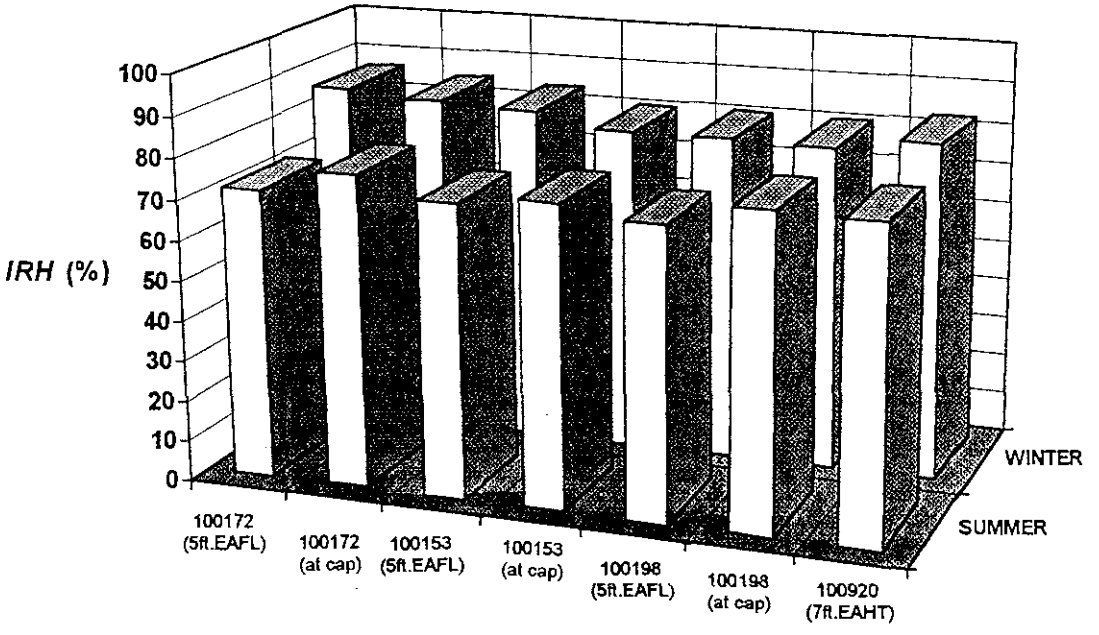

Figure I.16. Seasonal effect over internal relative humidity (***IRH***) measurements taken at different sites of over land bridges (see Table I.1 for bridge designation).

3.2.1.5 Concrete Cover

Figure I.17 shows a plot representing the cumulative % of cores that intersected rebar during the coring procedure versus the concrete cover thickness (***cc***). The data correspond to about one third of the total number of cores examined (144). The values of ***cc*** varied between approximately 1" and 4.5" (25.4 *mm* and 114.3 *mm*). The lower values were usually found on the bottom cover of cores extracted from the deck of over land bridge, while the higher values were found on prestressed piles of over water structures. As it can be observed in the figure, approximately 50% of the cores examined presented values of ***cc*** higher than 2.5" (63.5 *mm*) and about 10 % of the cores presented concrete cover values that were 1.5" (38.1 *mm*) or less.

The current FDOT design concrete cover thickness guidelines [I.17] specify values of ***cc*** varying from 1.75" to 2.5" (44.4 *mm* to 63.5 *mm*) for the superstructure, depending on the type of structural component and the exposure conditions. Likewise, the values of ***cc*** specified for the substructure vary from 3" to 4" (76.2 *mm* to 101.6 *mm*).

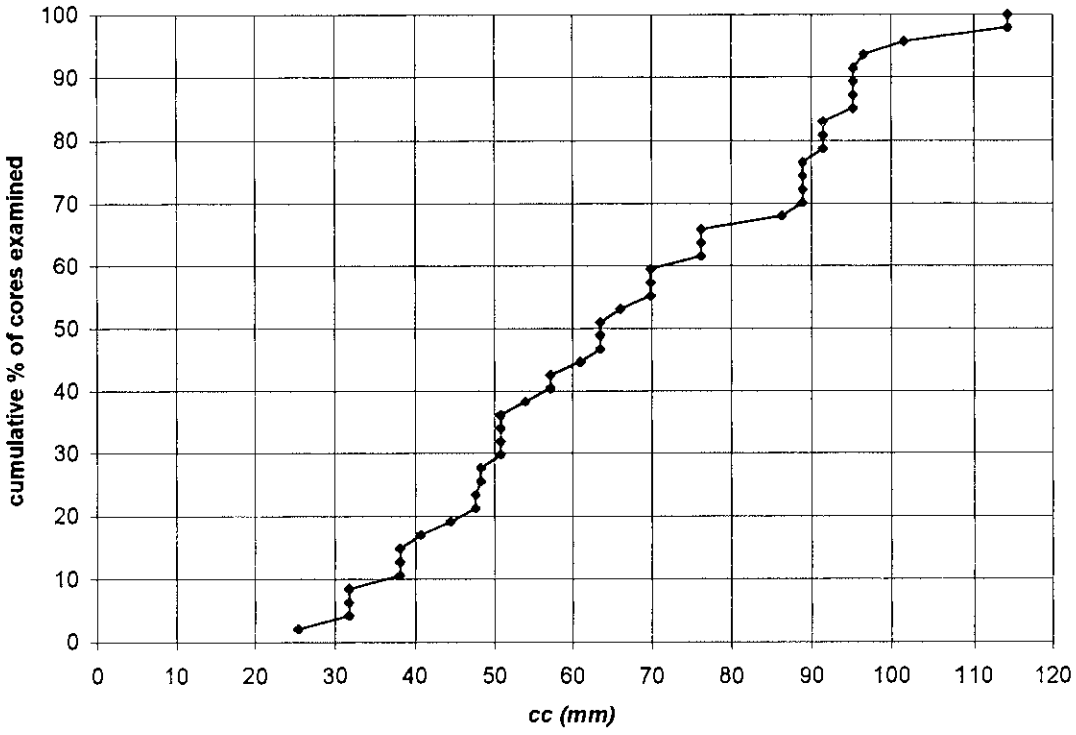

Figure I.17. Cumulative percentage of cores examined vs. the concrete cover thickness (***cc***).

3.2.2 Results from Laboratory Evaluation of Field Samples

Appendix 3.2 provides the summary of results obtained from different tests performed on cores extracted from bridges 1 to 14 (see Figure I.13).

3.2.2.1 Carbonation Depth

The carbonation depth measurements performed on field extracted cores in the laboratory showed great variability from core to core, but still confirmed

the preliminary field findings. Figure I.18 shows the cumulative % distribution of the carbonation depth measurements represented in a semi-log scale.

The lowest finite value of x_c recorded was 1 *mm*, which was adopted as the detection limit. Carbonation depths distinctly lower than 1 *mm* were recorded as zero. Values higher than 1 *mm* were recorded with a numeric precision of 0.5 *mm* or coarser. Since the data do not follow a simple normal distribution, the average value x_c = 9.8 *mm* did not match the median value $x_{c(50\%)}$ = 7.5 *mm* evident in Figure I.18.

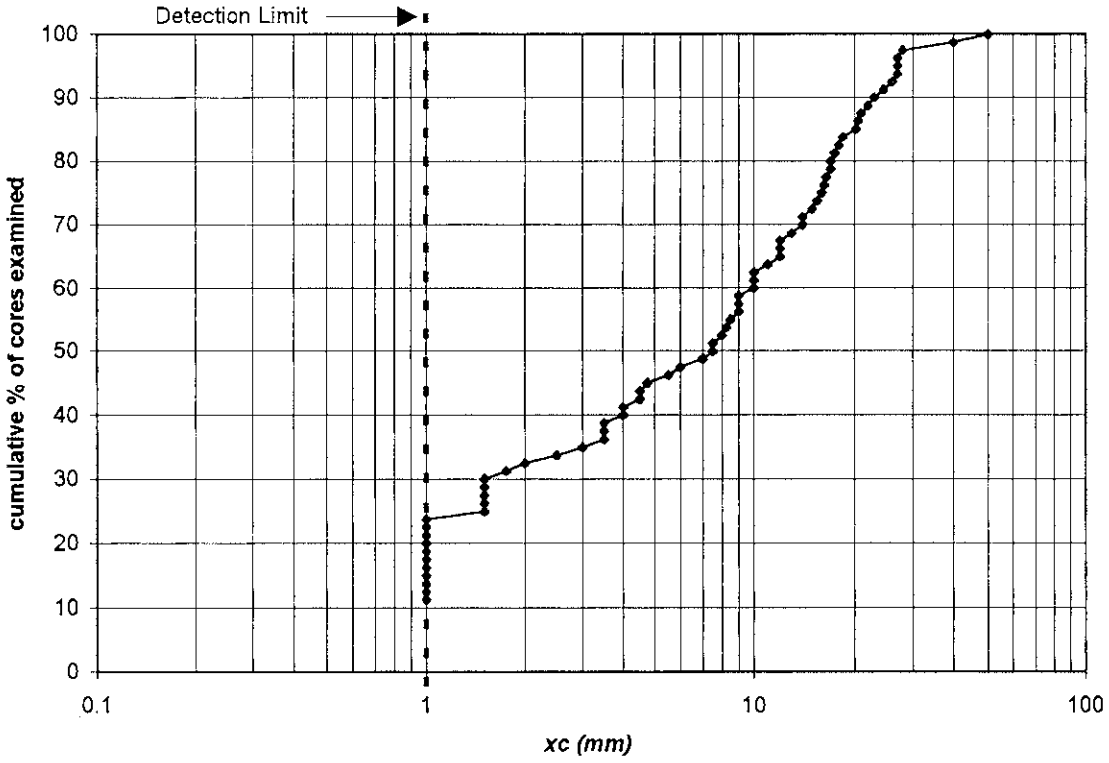

Figure I.18. Cumulative % distribution of the carbonation depth (x_c) data represented in a semi-log plot. The dashed line indicates the detection limit below which carbonation depth is recorded as zero.

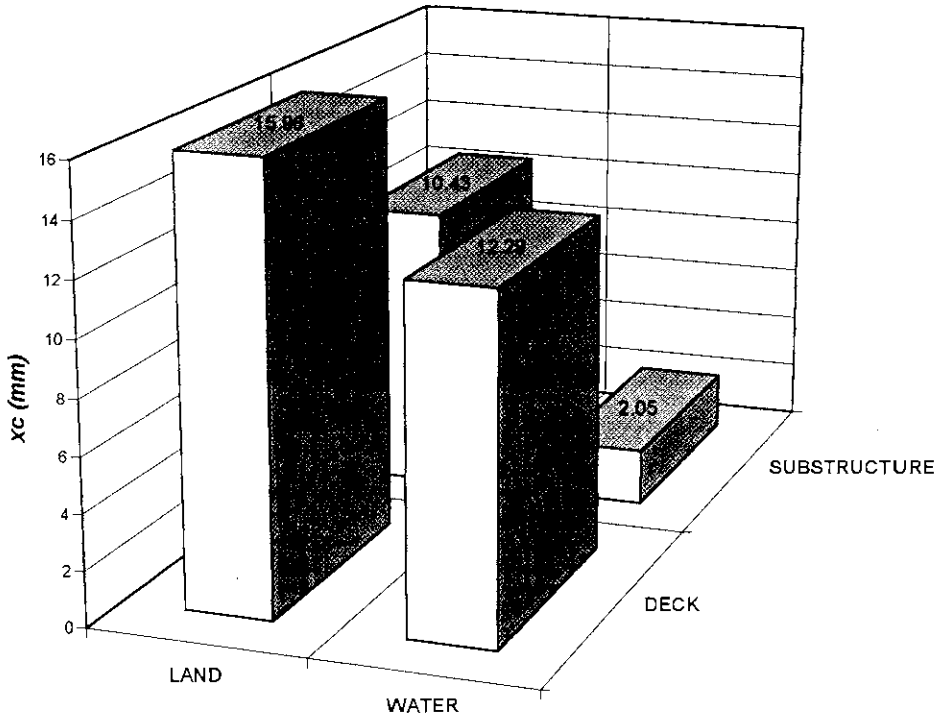

Figure I.19. Average values of concrete carbonation depth (x_c) measured on concrete cores extracted from the field.

Table I.2. Average values and range of variation of the carbonation depth measurements for different exposure conditions.

		Carbonation depth (x_c)			
Exposure Condition	Part of Substructure	Number of specimens	Average (mm)	Range (mm) Max.	Min.
Over Water	Deck	14	12.3	50	1
	Substructure	20	2.1	9	<1
Over Land	Deck	29	16	28	<1
	Substructure	17	10.4	27	<1

Only one over water bridge (bridge no. 900037 in Table I.1) presented carbonation depth values as high as 40 and 50 *mm* on the upper side of two cores extracted from the deck (see Figure I.20 (*right*)). However, these readings were not representative of most specimens from this group, as both cores had clear signs of bad concrete consolidation. Values between 20 and 25 *mm* were not uncommon in cores extracted from over land bridges. Figure I.20 (*left*) shows the carbonation front on a core extracted from the substructure of an over land bridge after spraying with the phenolphthalein indicator.

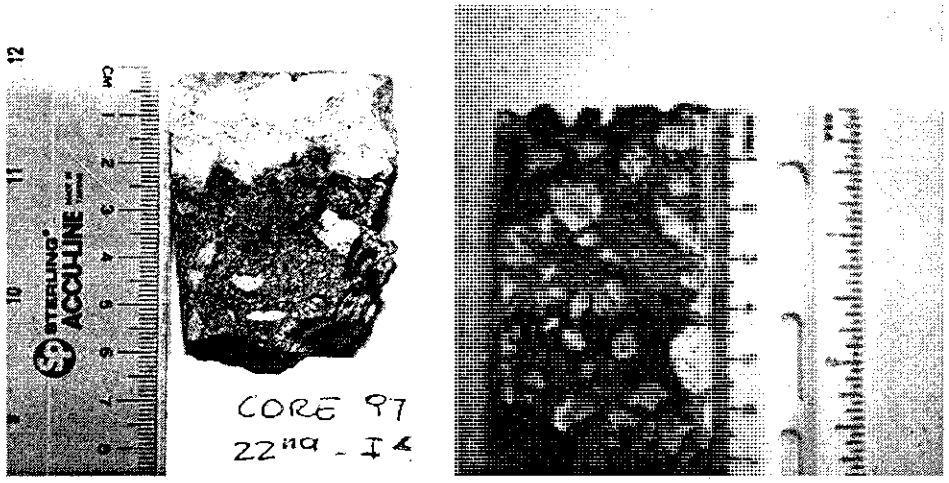

Figure I.20. Carbonation depth measurement on concrete cores. Right, core 27 corresponding to the upper side of the deck of bridge no. 900037. Left, core 97, extracted from the substructure of bridge no. 100153.

3.2.2.2 Carbonation Coefficients

The calculated values of carbonation coefficients (***Kc***) varied over a wide range depending on the carbonation depth (x_c) and the age of the inspected

structure. Figure I.21 shows a semi-logarithmic plot representing the cumulative percentage of cores examined versus the values of ***Kc*** ($mm/y^{1/2}$). The carbonation coefficients that result from the nominal values of x_c = 1 *mm* are indicated with empty symbols.

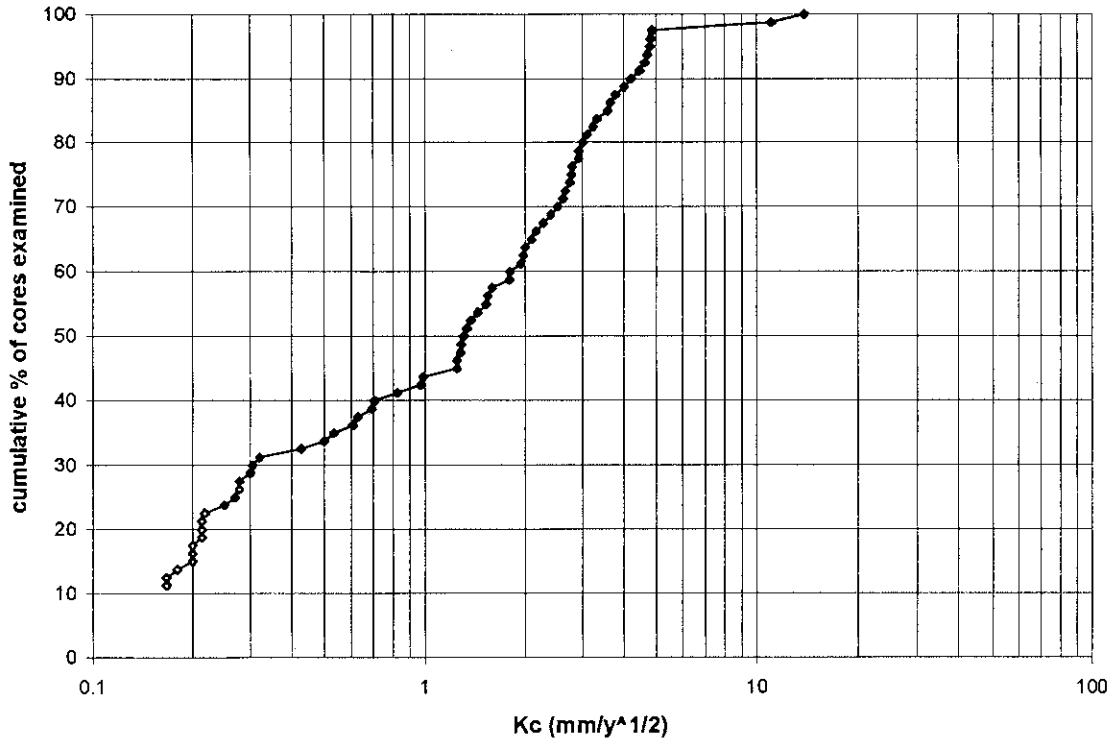

Figure I.21. Cumulative % of cores examined versus the overall calculated values of carbonation coefficients (***Kc***). Empty symbols indicate the values of ***Kc*** determined when for x_c = 1 *mm* (carbonation depth detection limit).

The distribution of the ***Kc*** values varied depending on the part of the structure from where the cores were extracted (deck or substructure). Figure I.22 shows the ***Kc*** data grouped as cores extracted from the deck and cores extracted from the substructure. As it can be observed, the results from the deck corresponds typically to higher ***Kc*** values than those from the substructure. The

same data, but now grouped according to the type of exposure condition (over water and over land) is shown in Figure I.23. In this case, the cores extracted from over land bridges presented the higher values of carbonation coefficients.

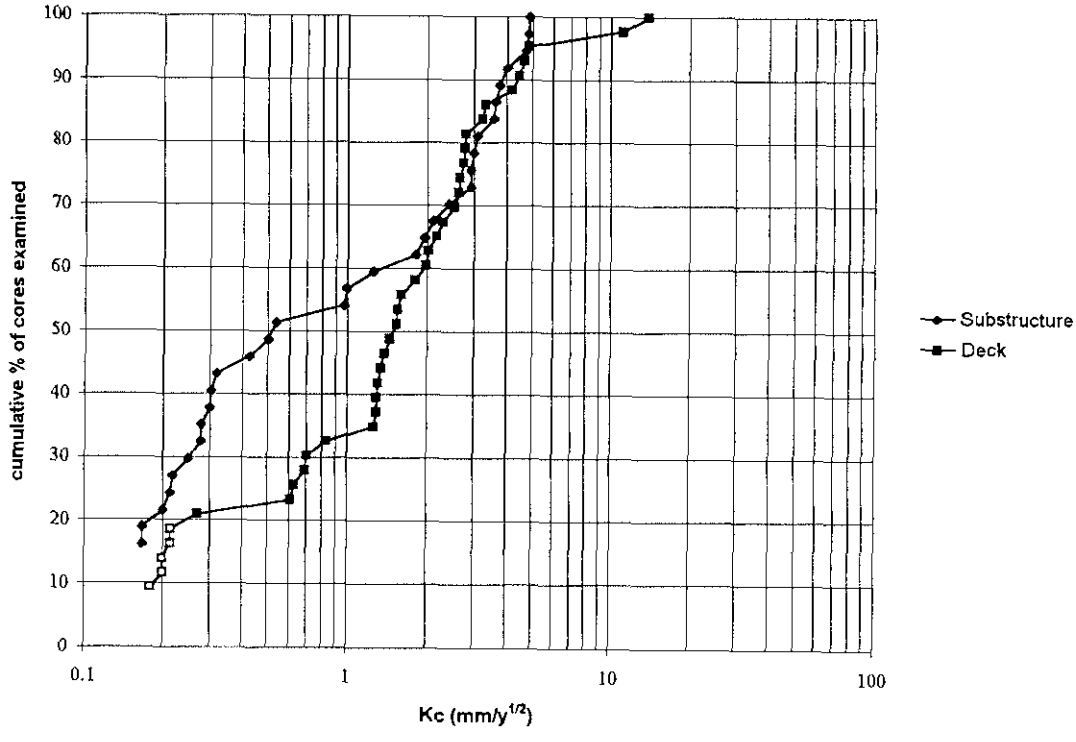

Figure I.22. Cumulative % plots of cores examined versus the carbonation coefficients data (***Kc***) grouped according to the part of the structure Inspected (deck - substructure). Empty symbols indicate the value of ***Kc*** determined when x_c = 1 *mm* (Carbonation depth detection limit).

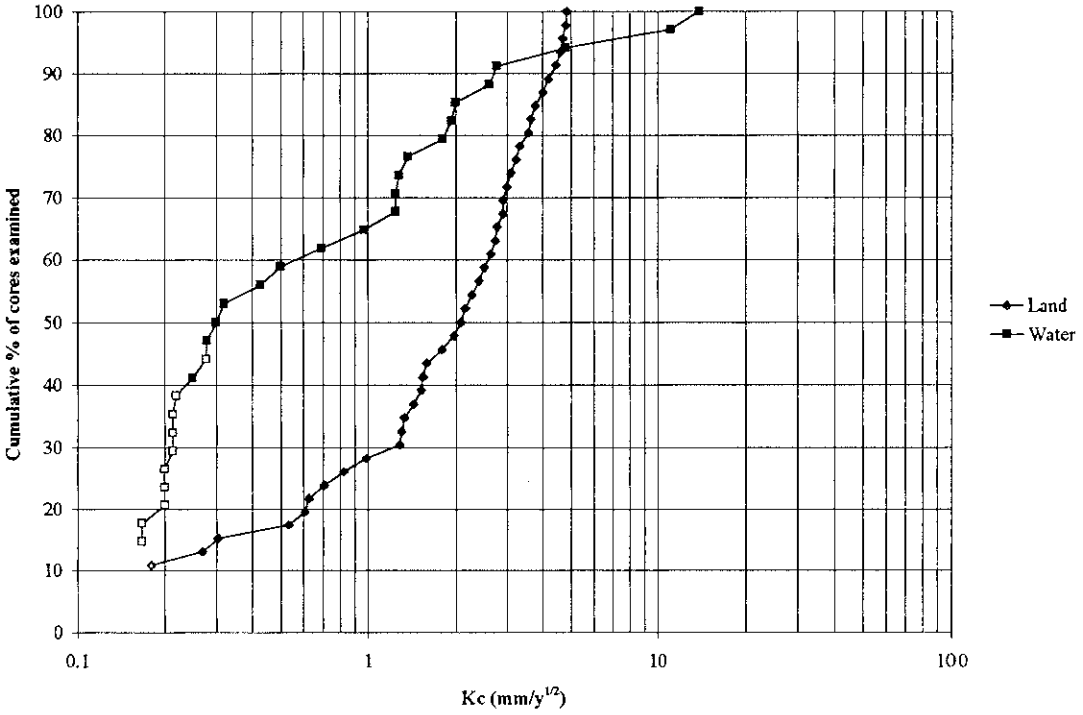

Figure I.23. Cumulative % plots of cores examined versus the carbonation coefficients data (***Kc***) grouped according to the type of exposure condition (over water over land). Empty symbols indicate the value of ***Kc*** determined when x_c = 1 *mm* (Carbonation depth detection limit).

3.2.2.3 Chloride Profiles

Figures I.24 and I.25 show the chloride concentration profiles obtained from cores extracted from the substructure and the deck of over water structures, exposed to marine environment. These structures are indicated in Table I.1 as over water (marine). Each profile is identified in the figure by core number as " C - #" (see Appendix 3.2). As the cores from the deck had both ends exposed to

the external environment (the upper and under side of the deck), an increase in the chlorides concentration in each end is observed in some samples. Figure I.26 shows the chlorides profiles obtained from cores extracted from over land bridges (represented by filled symbols) together with the profiles obtained from cores extracted from over water (river) bridges (represented by empty symbols). The over water (river) bridges (see Table I.1) were not exposed to severe salt contamination. The cores extracted from these structures presented chloride concentration levels in the same range as for cores extracted from over land structures. Much smaller levels of chloride concentrations were observed in this group compared with the over water (marine) group. The 1.2 *pcy* (0.71 kg/m^3) nominal chloride threshold value for corrosion initiation is indicated in each plot with a dashed line. As it can be observed in Figure I.24, the cores from the substructure of over water (marine) bridges presented at typical rebar depths chloride concentrations values that are much higher than the threshold value.

A computational fitting procedure was used to evaluate the apparent effective chloride diffusion coefficient (D_{eff}) as well as the calculated chloride surface concentration (***Cs***). This analysis was not performed on cores # 46 and # 51 as their chloride concentration profile deviated markedly from the Fick type of profile. The calculated values of ***Cs*** and D_{eff} for each of the cores analyzed is presented on the master table shown in Appendix 3.2.

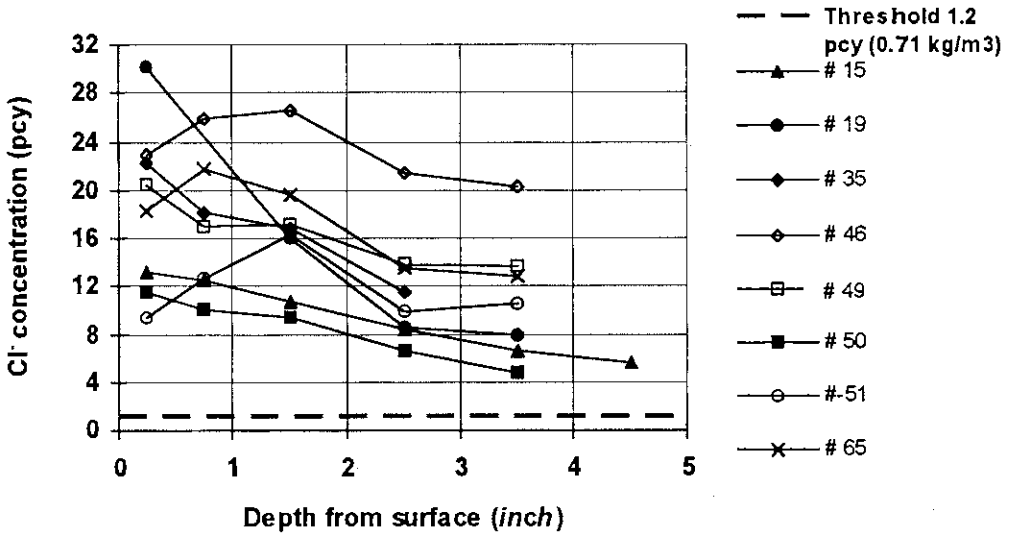

Figure I.24. Chloride concentration profiles obtained from cores extracted from the substructure of over water (marine) structures. The labels in the figure indicate the core number in Appendix 3.2.

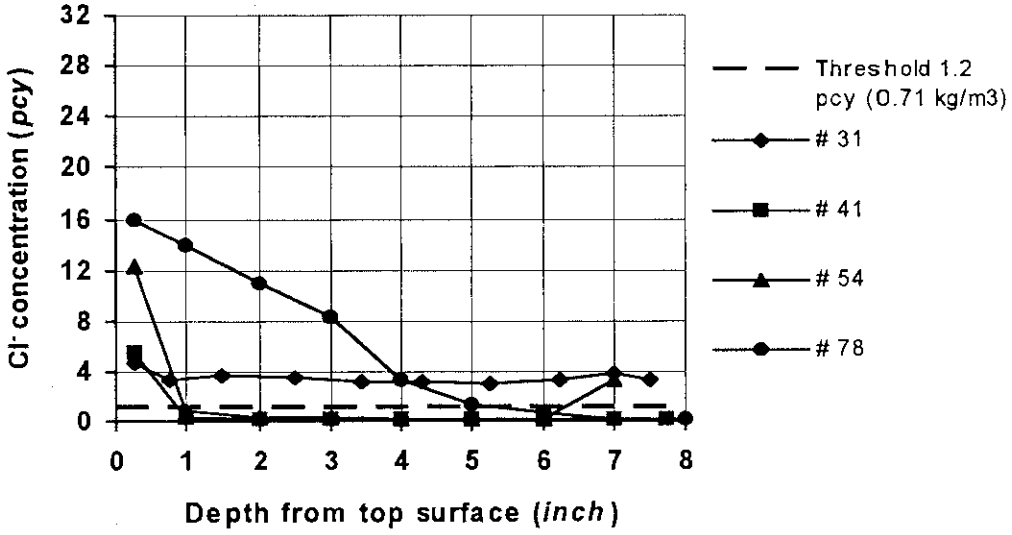

Figure I.25. Chloride concentration profiles obtained from cores extracted from the deck of over water (marine) structures. See Appendix 3.2 for identification by core number.

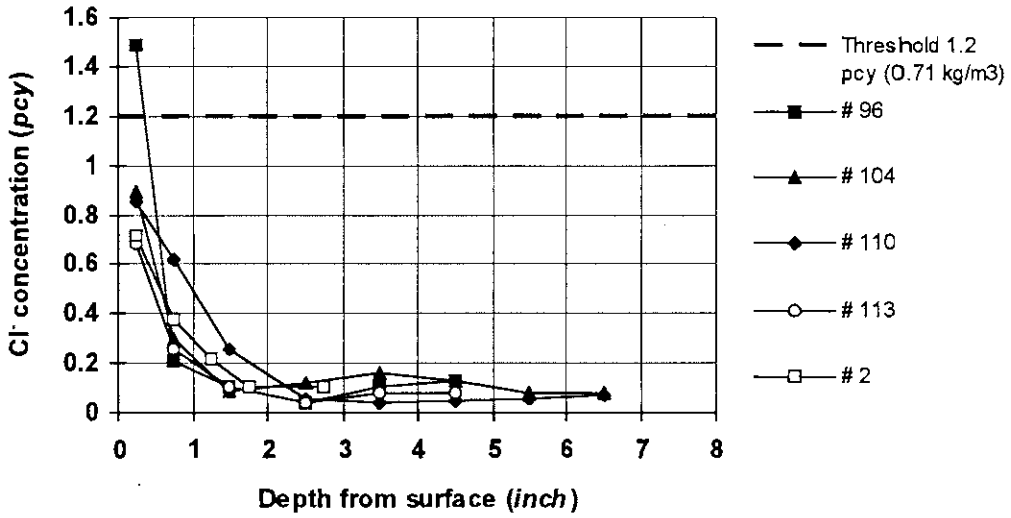

Figure I.26. Chloride concentration profiles obtained from cores extracted from the substructure and the deck of over land and over water (river) structures. See Appendix 3.2 for identification by core number.

Table I.3 shows the average values and the range of variation for the calculated values of ***Cs*** and D_{eff}, obtained from the analysis of cores extracted from over water (marine) substructures, upper and underside of over water (marine) decks, and over land and over water (river) bridges together. Most cores from over land and over water (river) bridges presented values of ***Cs*** that were lower than the threshold value for corrosion initiation, reflecting mild environment aggressiveness.

The highest values of ***Cs*** and D_{eff} were found in the substructure of over water bridges exposed to marine environment. The average values of D_{eff} observed in the bridge decks were approximately one order of magnitude smaller than those observed in the bridge substructures. Figure I.27 shows the

average values of D_{eff} grouped according to the bridge inspected. The calculation of D_{eff} based on the assumption of constant **Cs** values may give misleading results on cores extracted from over land bridges where the actual value of **Cs** may be instead slowly increasing with time due to chloride precipitation from spray from seashores miles away [I.18]. This results in very low calculated values of D_{eff} that do not reflect the actual chloride penetration process taking place.

Table I.3. Average values and range of variation of calculated **Cs** and D_{eff} values for the different exposure conditions analyzed.

Group	# of specimens tested	**Cs** (*pcy*)		D_{eff} (in^2/y)	
		Avrg.	Range Max./Min.	Avrg.	Range Max./Min.
Over water (marine) Substructure	6	20.9	32.0 / 12.0	$6.9\ 10^{-1}$	1.10 / 0.22
Over water (marine) Deck	4	12.0	20.4 / 4.2	$8.6\ 10^{-2}$	0.18 / 0.01
Over land & Over water (river)	5	1.4	2.7 / 0.9	$9.4\ 10^{-3}$	0.03 / 0.003

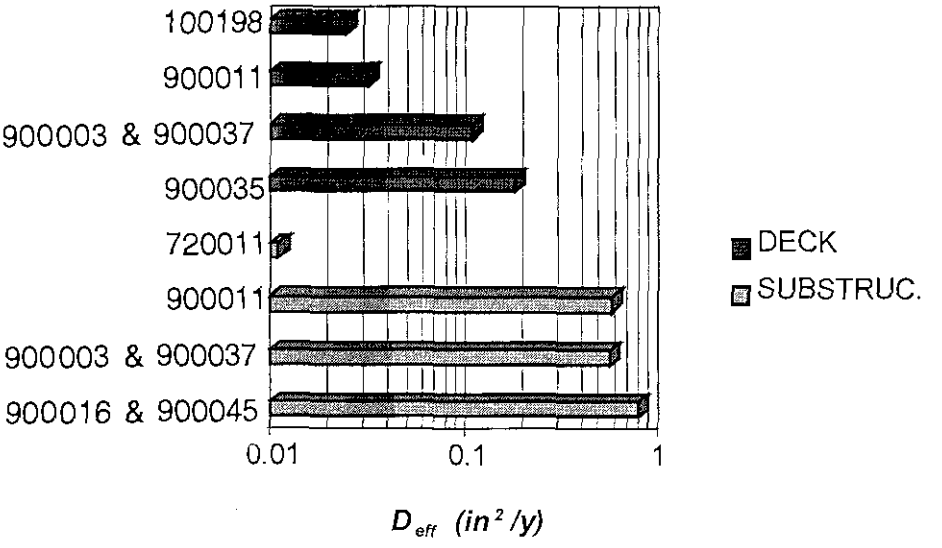

Figure I.27. Average effective chloride diffusion coefficients (D_{eff}) grouped according to bridge and bridge part (deck and substructure).

3.2.2.4 Wet Resistivity

Figure I.28 shows the average values of wet resistivity (r_W) measured on cores extracted from the substructure and the deck of over water and over land structures respectively. Table I.4 indicates the average values and the range of variation of the r_W values obtained in each group. Great variability was observed on the r_W values corresponding to over water bridges. Nevertheless, the cores extracted from the decks of over water bridges presented the highest average values of r_W.

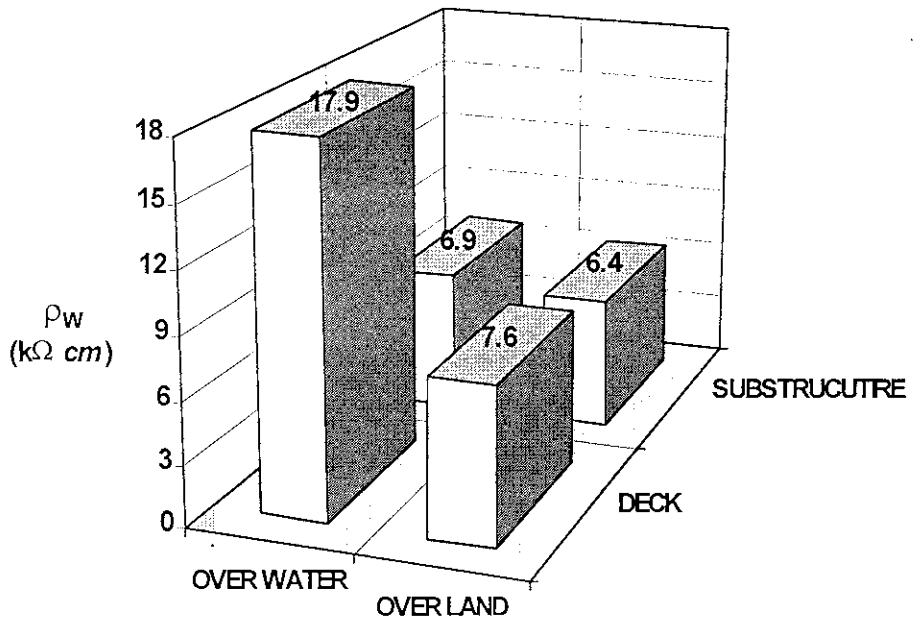

Figure I.28. Wet resistivity (ρ_w) measured on cores extracted from the substructure and the deck of over water and over land bridges.

Table I.4. Average and range of variation of r_w grouped according to the part of the structure and the type of exposure conditions.

	ρ_w (kW cm)			
	Over water bridges		Over land bridges	
	Substructure	Deck	Substructure	Deck
Average	6.9	17.9	6.4	7.6
Maximum	21.2	31.6	9.2	10.9
Minimum	1.5	3.5	4.6	6.3

3.2.2.5 Aggregate Characterization

With the exception of the bridge no. 100920 in Table I.1 (located on Hillsborough Av. over the Hillsborough river), built in 1939, which had river rock aggregate, the remaining structures used limestone as coarse aggregate. Almost all the cores examined had a maximum aggregate size (***MAS***) of 3/4" (1.90 *cm*). Aggregates of 1" (2.54 *cm*) ***MAS*** were found on cores from bridge no. 150107 (located on I 275 over the Tampa bay). A nominal porosity value for limestone coarse aggregate of 14.2 % was assumed based on the results of the ASTM C 642-90 standard test performed on three samples randomly picked from a stock pile.

3.2.2.6 Concrete Porosity

The ASTM porosity results for concrete were consistently differentiated when the values were grouped according to the type and part of the structure of origin. Figure I.29 shows the porosity average values obtained from cores that presented the same type of aggregate originated from prestressed piles, columns, decks, and footers.

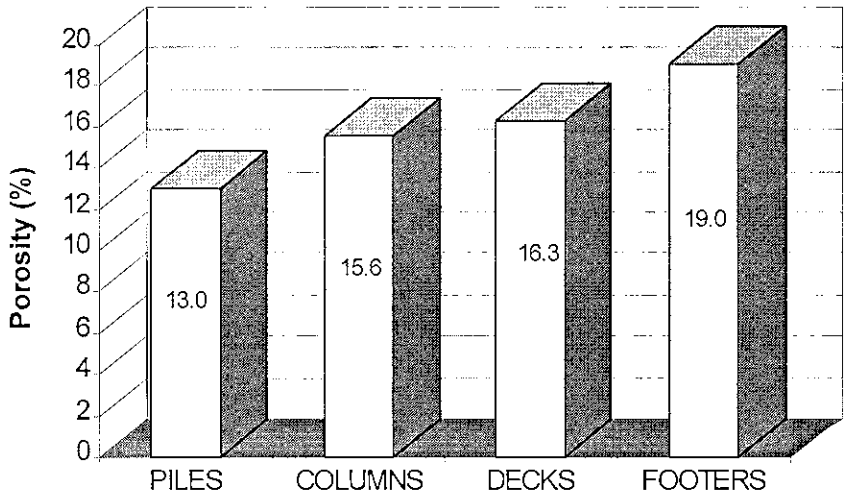

Figure I.29. Average concrete porosity measured in cores with limestone coarse aggregate as a function of structural origin.

3.2.2.7 Corrosion Rate Measurements

Table I.5 shows the values of corrosion current density and corrosion potentials measured on rebar segments embedded in the concrete cores. The values were obtained conducting polarization resistance (Rp) and electrochemical impedance spectroscopy (EIS) tests. The corrosion current densities were calculated by means of the Stern Geary equation assuming activation polarization conditions where $\beta_a = \beta_c = 120\ mV$.

The cores tested (# 109 and # 115) were extracted from the deck of bridge nos. 100198 and 100920 (see Table I.1) respectively. The concrete cover thickness (***cc***) and the carbonation depth (x_c) measured were ***cc*** = 1" (25.4 *mm*)

and x_c = 18.5 *mm* for core # 109 and ***cc*** = 1.5" (38.1 *mm*) and x_c = 10 *mm* for core 115. As in both cases the values of x_c are smaller than the corresponding values of ***cc,*** this would indicate that the rebar should be in the passive state and no active corrosion is taking place. However, as the rebar may become active at a pH higher than the one detected by the pH indicator, indications of active corrosion may be observed even when the carbonation front has not yet reached the rebar.

Table I.5. Corrosion parameters from electrochemical tests.

		Rp	EIS
Core # 109	i_{corr} ($\mu A/cm^2$)	0.43	0.39
	E_{corr} (mV vs. CSE)	-419	-420
Core # 115	i_{corr} ($\mu A/cm^2$)	0.83	0.61
	E_{corr} (mV vs. CSE)	-272	-270

The values of corrosion current density obtained fall in the low to moderate range (see Table I.9 on section **3.3.4.3.2**). However these measurements might be affected by localized active areas at the rebar edges were bare steel is exposed from the coring procedure. In such case the corrosion rate may have been overestimated.

3.3 DISCUSSION

3.3.1 Discussion of the Carbonation Depth Results

The results from the field survey of 18 bridges showed carbonation in progress in 16 out of 18 bridges inspected. Severe concrete spalling and rebar corrosion damage induced by concrete carbonation was observed on caps and columns of bridge no. 100172 located on I4 over Orient road in Tampa.

The results presented in section **3.2.2.1** showed that the over land structures presented typically higher values of carbonation depth (x_c) than the over water bridges. This was also reflected on the values of carbonation coefficients (***Kc***), where the higher values corresponded typically to the over land bridges (see Figure I.22). The reason for this may be higher levels of CO_2 concentration existing in the urban areas where the over land bridges examined are located. Papadakis et al [I.3], indicated that the carbonation depth is proportional to the square root of the CO_2 concentration. On the other hand, the over water bridges may be affected by presence of mist or fog during part of the day that maintains the concrete saturated and consequently reduce the rate of CO_2 penetration into the concrete.

The values of x_c and ***Kc*** obtained on cores extracted from the deck of both over water and over land bridges, were consistently higher than those observed in the substructure. The cores extracted from the substructure of over

water bridges presented as a group the lowest values of x_c and ***Kc.*** A previous carbonation field study [I.15], performed on structures exposed to marine environment reported similar results, attributing the low carbonation depths to the high moisture conditions present in over water bridges.

Appendix 3.4 presents a statistical approach to determine the probability of finding structures presenting rebar corrosion initiated by concrete carbonation. The study was based on the data distribution plots presented in section **3.2.1.5** and **3.2.2.1** for concrete cover thickness (***cc***) and carbonation depth (x_c). The x_c measurements were performed on 54 cores extracted from 14 highway bridges were at least one core from each bridge was tested. According to this analysis, there is approximately a 1% chance of finding cores having $x_c >$ ***cc***, which means that at the most one core out of 54 could meet this condition. Therefore, considering that approximately 3 cores were tested per bridge, only one bridge out of 14 may have been expected to show rebar corrosion initiated by concrete carbonation. This expectation agrees with the observation in the field.

The internal concrete relative humidity (***IRH***) values measured at a depth of 1.5" (3.8 *cm*) in the concrete cover, did not evidence any significant difference between the over land and over water structures inspected. As indicated in section **3.2.1.4**, the average of the ***IRH*** readings taken during the winter season was nearly 83% for both over land and over water bridges. The ***IRH*** data do not provide then any information to help explain the differences observed in the

values of x_c obtained in over land and over water bridges. As indicated by Andrade et al [I.19], persistent influence of the external environmental conditions on the ***IRH*** may be limited to the first 1 or 2 *cm* of the concrete cover depending on the quality of the concrete. Thus, ***IRH*** measurements at shallow depth may be best to provide information about the influence of the type of exposure conditions on the carbonation rate taking place in a concrete structure. As shown in Figure I.16, a seasonal effect was observed on the ***IRH*** measurements. The average of the internal relative humidity readings taken on over land structures during the winter was approximately 8 relative humidity units higher than the average ***IRH*** value measured during the summer.

3.3.2 Discussion of Chlorides Concentration Results

The chloride concentration profiles corresponding to the cores extracted from the substructure of over water marine bridges presented very high concentrations all through the core length, significantly exceeding the assumed chloride concentration threshold for corrosion initiation (1.2 *pcy* (0.71 kg/m^3)). As expected, evidence of corrosion damage was observed on several piles of these structures.

As shown in Figure I.24, several cores presented chloride concentration profiles that deviated markedly from the ideal Fick type of distribution. These cores were extracted from low elevations above high tide (***EAHT***), where the

external concrete surface was alternately wetted with sea water. Under these circumstances the mechanism of chlorides transport into the concrete is not only diffusion and may be dominated by absorption or capillary suction [I.20]. In these cores, the higher chloride concentrations were not observed at the concrete surface but instead between 1 to 2" (2.54 to 5.08 *cm*) from the external surface. This portion of the core may represent the part of the concrete cover that is affected by the external wetting. Beyond this depth, a monotonic decreasing trend with distance in the chloride concentrations is observed.

The chloride concentration profiles obtained from cores extracted from the decks of over water marine structures are shown in Figure I.25. As both ends of the cores were exposed to the external environment an increase in the chloride concentration was observed on each end (upper and under side of the deck), showing the higher values on the upper side of the deck. The over land and over water (river) bridges presented very low chloride concentrations as a result of the milder exposure conditions.

The calculated values of chloride superficial concentration (***Cs***) confirmed the relative severity of each exposure condition. The higher values of ***Cs*** were obtained on the cores extracted from the substructure of over water (marine) bridges. The cores extracted from the deck of over water bridges exposed to marine environments presented comparatively milder but still high values of ***Cs***. Finally, the cores extracted from over land and over water (river) structures presented the lower values of ***Cs***. Coincidentally, higher values of ***Cs*** were

typically associated with high values of chloride effective diffusion coefficients (D_{eff}). The calculation of D_{eff} based on the assumption of constant ***Cs*** values with time may conduct to misleading results particularly on cores extracted from over land bridges where the actual value of ***Cs*** may be increasing slowly with time (typical chloride deposition may proceed at an approximate rate of 10 to 23 g/m^2y [I.18]).

3.3.3 Service Life Prediction

An assessment of the initiation period or time for corrosion initiation (t_o), for the case of concrete carbonation (indicated as t_{Ca}) and chlorides induced corrosion (indicated as t_{Cl}) is presented below based on the results presented in section **3.2.2.2** and **3.2.2.3**. An estimation of the propagation period or time of corrosion propagation (t_p) is determined based on assumed values of corrosion rate (***CR***) obtained from the literature. Special emphasis is given to those cases where the estimation of ***SL*** is lower than a structure nominal service life (***NSL***) target of 75 years.

3.3.3.1 Estimation of t_{Ca} for Concrete Carbonation

As it was indicated before, the duration of the initiation period in the case of concrete carbonation (t_{Ca}) is idealized as a function of the carbonation coefficient (***Kc***) and the concrete cover thickness (***cc***). However, in reality these

parameters may vary over a wide range, and the consideration of simple average value in each individual case may be misleading. As shown in section **3.2.2.2** the calculated values of ***Kc*** vary between 0 and 14 ($mm/y^{1/2}$), and depend on the type of exposure condition (over water or over land) as well as the part of the structure inspected (deck or substructure). In addition, the ***cc*** may also vary significantly from part to part of a structure, and as shown in Figure I.17, values from approximately 1" (25.4 *mm*) to 4.5" (114.3 *mm*) or higher were recorded.

In order to obtain a representative estimation of t_{Ca}, a statistical type of analysis was carried out where two different cases were considered based on the data distribution plots for ***cc*** and ***Kc*** presented in section **3.2.1.5** and **3.2.2.2** respectively. These were a *median* case, represented by the values of ***Kc*** and ***cc*** that exceed 50% of the measurements reported, and a *severe* case represented by a high value of carbonation coefficient (***Kc*** exceeding 90% of the measurements reported) and a small value of concrete cover thickness (***cc*** exceeding 10% of the measurements reported). In the following analysis these conditions are referred as $Kc_{(50\%)}$, and $cc_{(50\%)}$ for the *median* case, and $Kc_{(90\%)}$ and $cc_{(10\%)}$ for the *severe* case.

Values of t_{Ca} were calculated for several exposure situations defined by how the carbonation coefficients were grouped. An overall estimation of t_{Ca} was obtained by considering values of $Kc_{(50\%)}$ and $Kc_{(90\%)}$ from the carbonation coefficient distribution plot for the entire data set presented in Figure I.21. The

influence of the different parts of the structure inspected (deck - substructure) and the influence of the exposure conditions (over water - over land) were evaluated by considering the values of $Kc_{(50\%)}$ and $Kc_{(90\%)}$ for each of the subsets, which were represented in Figures I.22 and I.23. The results are labeled by Kc_T for the entire set of carbonation coefficients, and by Kc_D, Kc_S, Kc_{OW}, and Kc_{OL} for each of the four selected subsets indicated above. Table I.6 shows the calculated carbonation coefficients values that correspond to the *median* and *severe* cases for each exposure situation.

Table I.6. Carbonation coefficients considered for the estimation of t_{Ca}.

Case	Carbonation Coefficients ($mm/y^{1/2}$)				
	Entire Data set	Grouped by part of the structure		Grouped by exposure condition	
	Kc_T	Kc_D	Kc_S	Kc_{OW}	Kc_{OL}
severe	4.20	4.35	3.90	2.67	4.32
median	1.31	1.48	0.52	0.30	2.09

The concrete cover thickness (**cc**) values were statistically classified in the same manner as the carbonation coefficients. Thus, the cumulative percentage plot presented in Figure I.17 yielded **cc** $\approx$ 64 *mm* for the *median* case and **cc** $\approx$ 37 *mm* for the *severe* case. The distribution of **cc** was assumed to be the same for all exposure conditions, although a more refined analysis would need to take into consideration that the concrete cover is usually thinner in the bridge superstructure. In the following calculations the values of concrete cover

thickness corresponding to each case are approximated to the closest half inch distance. Thus, values of $cc_{(50\%)}$ = 2.5" (63.5 *mm*) and $cc_{(10\%)}$ = 1.5" (38.1 *mm*) are considered for the *median* and *severe* case respectively.

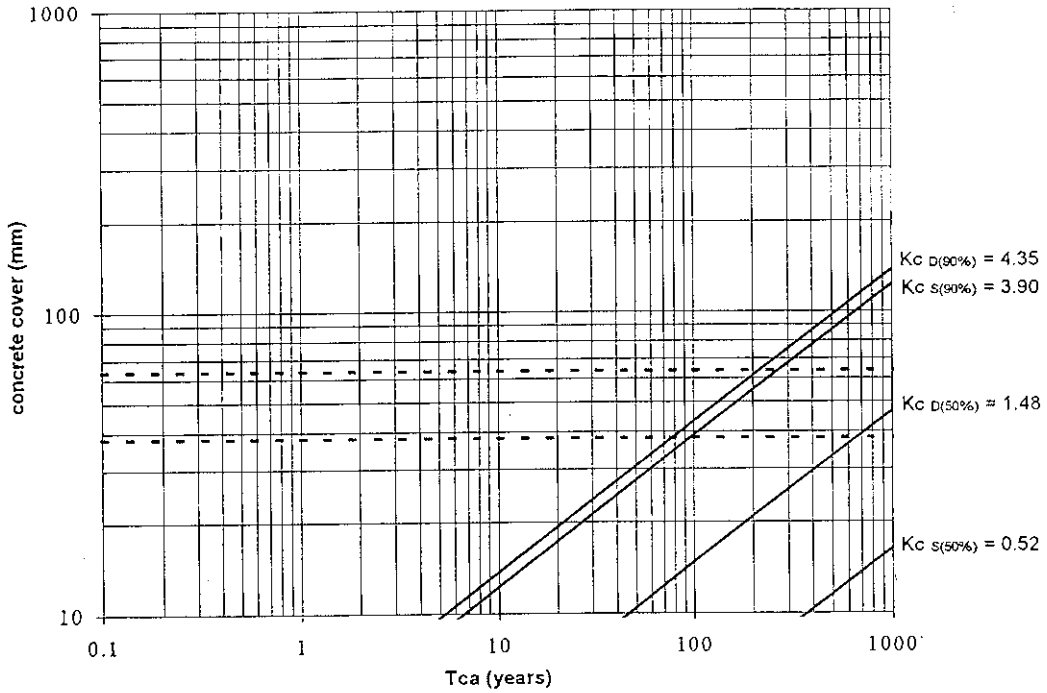

Figure I.30. Time for corrosion initiation by concrete carbonation (t_{Ca}) indicating the values of ***Kc*** ($mm/y^{1/2}$) corresponding to the *median* and *severe* cases, grouped according to the part of the structure examined (deck and substructure).

The values of t_{Ca} that resulted from analyzing each of the conditions presented in Table I.6 are represented in a log-log diagram. Figure I.30 presents the estimations of t_{Ca} for the values of ***Kc*** grouped according to the part of the structure (deck or substructure) that correspond to the *median* and *severe*

cases. Analogously, Figure I.31 show the estimations of t_{Ca} for the values of ***Kc*** grouped according to the type of exposure condition (over water and over land).

The values of t_{Ca} that result from considering the carbonation coefficients and concrete cover thickness corresponding to the *median* case may not represent a significant problem from the structure durability point of view as they already exceed the nominal service life target of 75 years. It is of more interest to consider the estimated values of t_{Ca} that result from the *severe* case given by $Kc_{(90\%)}$ and $cc_{(10\%)}$, which are presented in Table I.7.

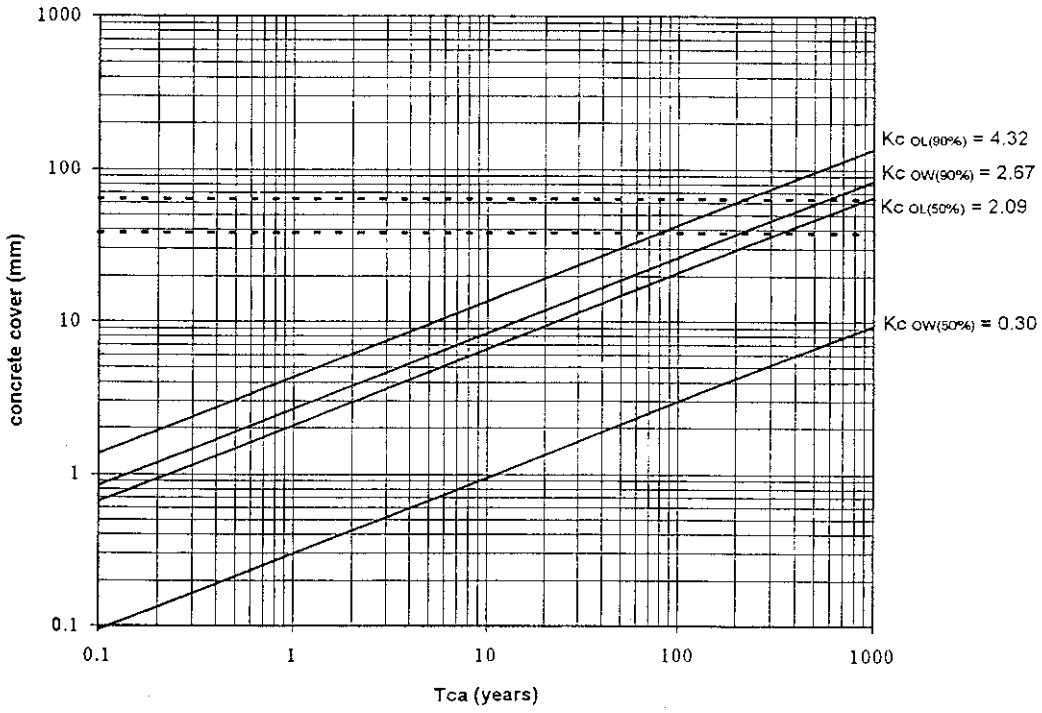

Figure I.31. Time for corrosion initiation by concrete carbonation (t_{Ca}) indicating the values of ***Kc*** ($mm/y^{1/2}$) corresponding to the *median* and *severe* cases , grouped according to the type of exposure condition (over water and over land).

Table I.7. Estimated values of time for corrosion initiation due to concrete carbonation (t_{Ca}) for the *severe* condition.

Concrete Cover	t_{Ca} (years)				
	$Kc_{T(90\%)}$	$Kc_{D(90\%)}$	$Kc_{S(90\%)}$	$Kc_{OW(90\%)}$	$Kc_{OL(90\%)}$
(10%)	75	70	90	190	72

The worst conditions from the point of view of concrete carbonation are projected for the bridge decks where the combination of $Kc_{D(90\%)}$ and $cc_{(10\%)}$ results in an estimated time for corrosion initiation of 70 years. On the other hand, carbonation induced corrosion is likely to be less of a problem in the bridge substructures where larger estimated values for t_{Ca} were obtained.

An overall value of t_{Ca} is obtained for the *severe* case when considering the value of $Kc_{T(90\%)}$ obtained from the entire carbonation coefficients data set and assuming $cc_{(10\%)}$. For this case t_{Ca} = 75 years.

3.3.3.2 Estimation of t_{Cl} for Chlorides Induced Corrosion

Nominal times for chloride induced corrosion initiation (t_{Cl}) were calculated based on the average values of chloride surface concentration (**Cs**) and chloride effective diffusion coefficients (D_{eff}) presented in Table I.3 of section **3.2.2.3**. A chloride concentration threshold for corrosion initiation at the rebar surface of 1.2 *pcy* (0.71 kg/m^3) was assumed in all instances. As in the

previous section, two values of concrete cover thickness ($cc_{(10\%)}$ = 38.1 *mm* and $cc_{(50\%)}$ = 63.5 *mm*) were selected for the calculations.

The initiation time was estimated using [1.21]:

$$t_{Cl} = \frac{cc^2}{4\,D_{eff}\left[erf^{-1}\left(1 - \frac{C_{threshold}}{Cs}\right)\right]^2} \qquad (4)$$

Figure I.32 represents in a manner similar to Figure I.30 and I.31 the estimated values of t_{Cl} for the three conditions considered in section **3.2.2.3.** These conditions are, the substructure of over water (marine) bridges, the deck of over water (marine) bridges and the over land together with over water (river) bridges. As t_{Cl} is inversely proportional to cc^2 , each condition is represented by straight lines in the log-log plot.

Table I.8 summarizes the results for the *median* and *severe* cases. The worst results corresponded to the substructure of over water (marine) bridges where t_{Cl} was a fraction of one year, when a concrete cover thickness of 1.5" (38.1 *mm*) was considered. This condition reflects the information obtained from cores extracted from a group of five bridges (map identification nos. 4 to 8 in Table I.1) located in the Florida Keys. This region of the state presents a tropical marine type of environment which is one of the most aggressive exposure conditions from the point of view of reinforced concrete durability. Under these circumstances, chloride induced corrosion is the major factor limiting the service life of structures. These results agree with a previous investigation for the assessment of corrosion of epoxy coated rebars that included several bridges of

comparable concrete type and construction located in this part of the State [I.21, I.22]. The calculations for the marine bridge are presented as an illustration only, since the data set is small and the actual concrete cover distribution is not well established. Reference [1.21] should be consulted for a representative sampling of substructure chloride-induced corrosion in Florida.

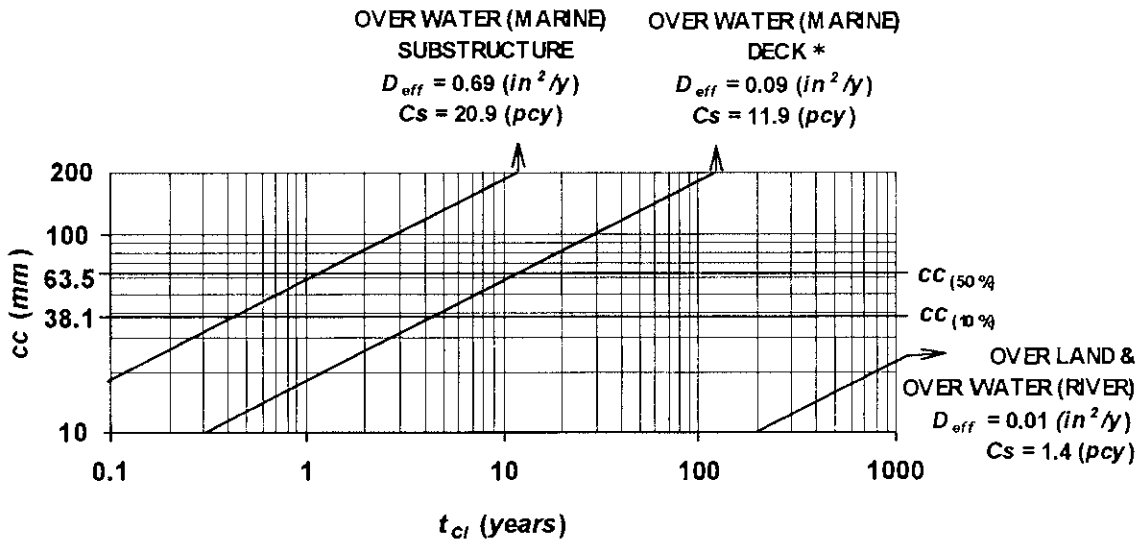

Figure I.32. Nominal time for chlorides induced corrosion initiation (t_{Cl}) assuming a chlorides threshold value of 1.2 *pcy* (0.71 *kg/m*^{3}). * For illustration only.

In the case of the over land and over water (river) bridges, the combination of ***Cs*** values comparable to the threshold value (1.2 *pcy* (0.71 *kg/m*^{3})) and low calculated D_{eff}, gave rise to essentially unlimited values of t_{Cl}.

Table I.8. Nominal time for chloride induced corrosion initiation (t_{Cl}) for different exposure conditions and concrete cover thickness (cc). * For Illustration only

	t_{Cl} (*years*)		
Concrete cover	Over water (marine)		Over land & Over water (river)
	Substructure	Deck *	
$cc_{(10\%)}$	0.4	4.4	$> 10^3$
$cc_{(50\%)}$	1.2	12.2	$> 10^3$

3.3.3.3 Estimation of the Propagation Period (t_p)

3.3.3.3.1 Service Life Criteria. The duration of the propagation period (t_p) is governed by the rebar corrosion rate (***CR***) and limited by a service life criterion that establishes the unacceptable degree of damage, before the structure must be either repaired or replaced. The unacceptable degree of damage of a structure due to rebar corrosion can be defined by alternative performance criteria, depending on the user's requirement.

A ***structural strength*** criterion assumes that t_p has been reached when the lead-bearing capability of the structure has been seriously degraded by loss of rebar cross-section. For the purposes of this work, a 10 % reduction of the rebar cross section (about 5 % reduction of the rebar diameter) is considered as a limit for the structure service life.

A ***corrosion repair need*** criterion assumes that t_p has been reached when a certain fraction of the structure surface shows cracks or concrete cover

spalls due to corrosion. This condition may not affect by itself the overall structural integrity very much, but expensive repair may be required because of aesthetic reasons, to avoid the onset of rapid subsequent corrosion to prevent dangerous debris falls, or to restore traffic surfaces on a bridge deck. The condition for this criterion is reached much sooner than for the structural integrity case. Concrete spalls typically appear after a reduction of about 1 % or less in the rebar diameter (approximately 2 % reduction or less in rebar cross section) is reached.

3.3.3.3.2 Estimation of t_p Based on the Structural Strength Criterion. The internal relative humidity (***IRH***) of concrete and the environmental exposure conditions of the structure exhibit considerable variation under daily and annual basis. These variations may also affect the ***CR*** which may show significant variations during the structure service life [I.2, I.4, I.23].

Section **3.1.3.6** presented a method for measuring the ***CR*** in concrete cores that had segments of rebar that were cut during the coring procedure and remained attached to the concrete. Although these measurements may be affected by changes in the original conditions of the concrete during the coring procedure and while the specimens are stored until the test is performed, the results provide nevertheless an estimation of the severity of the attack and of the rebar corrosion rate itself. The values of i_{corr} obtained represent the particular case of two specimens which were undergoing moderate corrosion. In order to

present a representative scenario of the different corrosion conditions observed in reinforced concrete, the estimations of t_p were done assuming typical values of ***CR*** obtained from the literature [I.4]. Andrade et al [I.19, I.24, I.25] has presented a classification for different levels of corrosion damage risk, as a function of ***CR***, based on the type of aggressive agent initiating corrosion (CO_2 or Cl^-) and the moisture condition of the concrete. These values are shown in Table I.9.

The estimation of t_p is a function of the original rebar diameter $\varnothing_o$. If a rebar type No. 4 with a diameter of 1/2". (1.27 *cm*) is considered, the 10% reduction of cross-section is given by a final diameter $\varnothing_c$ = 0.47" (1.20 *cm*). Figures I.33 shows the estimations of t_p that result from replacing the values of ***CR*** listed above on equation **(19)** for $\varnothing_o$ = 1/2" (1.27 *cm*) and assuming a *structural strength* criterion outlined by a 10 % rebar cross section reduction.

Table I.9. Typical values of corrosion rate for reinforcing steel in concrete.

Risk of Damage	Range of ***CR*** $\mu A/cm^2$ (*mpy*)	Condition
Very Low	< 0.1 (< 0.05)	very dry and carbonated concrete with no chloride contamination
Low	0.1 - 0.5 (0.05 - 0.23)	dry concrete, carbonated or with mild chloride contamination
Moderate	0.5 - 1 (0.23 - 0.46)	humid concrete, carbonated or with mild chloride contamination
High	1 - 10 (0.46 - 4.60)	high humidity concrete, carbonation or affected by chlorides attack
Very High	> 10 (> 4.60)	high humidity and highly contaminated with chlorides

Therefore, the estimated propagation period (*structural strength criterion*) of a reinforced concrete structure that is exposed to very high chloride concentrations and undergoes a ***CR*** = 10 $\mu A/cm^2$ is approximately 2.8 years. If the ***CR*** = 1 $\mu A/cm^2$, the estimated value of t_p is approximately 28 years and if ***CR*** = 0.5 $\mu A/cm^2$ the estimated t_p is approximately 57 years.

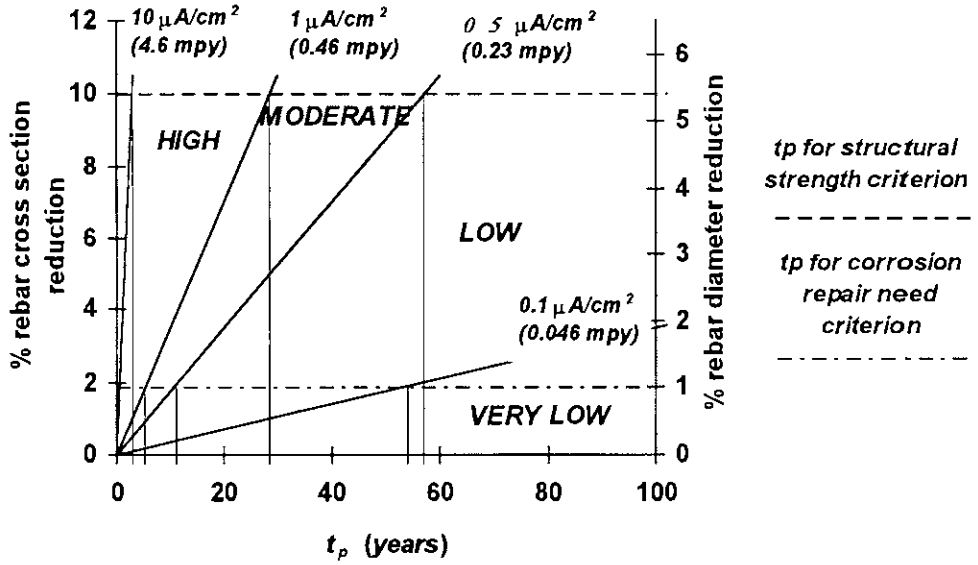

Figure I.33. Percentage of rebar cross section reduction and % of rebar diameter reduction as a function of the time of corrosion propagation for a rebar No. 4 with $\varnothing_o$ = 1/2 *in.* (1.27 *cm*). (curves for 10, 1, 0.5, and 0.1 $\mu A/cm^2$ corrosion rate are represented) [I.24].

3.3.3.3.3 Estimation of t_p Based on the Corrosion Repair Need Criterion. The rate and extent of cracking and spalling caused by corrosion of reinforcement depends on the properties of hardened concrete (quality, tensile strength, modules of elasticity), on the corrosion products (type of rust, quantity),

on the size (diameter) of the reinforcement and on the thickness of the concrete cover [I.16]. It has been found that in typical service conditions just 10 to 50 μm (0.4 to 2 *mils*) of corrosion penetration is enough to produce a visible (0.05 *mm* width) crack in the concrete cover [I.19]. This in terms of rebar diameter reduction (assuming a rebar type # 4) represents a 0.16 to 0.8 %. For the purpose of this investigation a 1 % reduction in rebar diameter will be considered as the unacceptable degree of cracking and spalling that limits the structure service life.

The estimated values of t_p obtained when considering the *corrosion repair need* criterion outlined by a 1 % rebar diameter reduction can be visualized in Figure I.33. The estimated time for corrosion propagation for the different values of corrosion rate indicated in the figure are: $t_p \approx 0.8$ year for $CR = 10\ \mu A/cm^2$, $t_p \approx$ 5 *years* for $CR = 1\ \mu A/cm^2$, $t_p \approx 11$ *years* for $CR = 0.5\ \mu A/cm^2$, and $t_p \approx 54$ *years* for $CR = 0.1\ \mu A/cm^2$.

3.3.3.4 Estimation of the Service Life (*SL*)

The estimated service life (***SL***) of a reinforced concrete structure is given by the sum of both the initiation and the propagation period (t_o and t_p). The following section presents the estimated values of ***SL*** that result from considering the particular cases analyzed previously where the time for

corrosion initiation was less than 75 years. In all cases a rebar type No. 4 with a diameter of 1/2" (1.27 *cm*) was assumed.

3.3.3.4.1 Estimation of *SL* for the Case of Concrete Carbonation. According to the values of t_{Ca} calculated in section **3.3.3.1**, the only significant case where the service life could be less than 75 years, is the so called *severe* case. The *severe* case considerate a carbonation coefficient value ($Kc_{(90\%)}$) that exceeds 90% of the measurements reported and a concrete cover $cc_{(10\%)}$ that exceeds at least 10% of the measurements reported. Figure I.34 presents the estimations of ***SL*** for two values of time for corrosion initiation analyzed previously (Table 1.7), t_{Ca} = 75 *years* obtained when considering the entire ***Kc*** data set, and t_{Ca} = 70 *years* obtained when considering the worst ***Kc*** subset ($Kc_{D(90\%)}$).

Table I.10 presents the estimated values of ***SL*** that correspond to the *structural strength* and the *corrosion repair need* criteria for the cases presented previously, assuming typical values of corrosion rate of steel in carbonated concrete

Therefore, when considering the *structural strength* criterion, the estimated ***SL*** exceeds the ***NSL*** target of 75 years even when the reinforcement undergoes a high corrosion rate. On the other hand, when the *corrosion repair need* criterion is considered, values of ***SL*** close to 75 years are obtained.

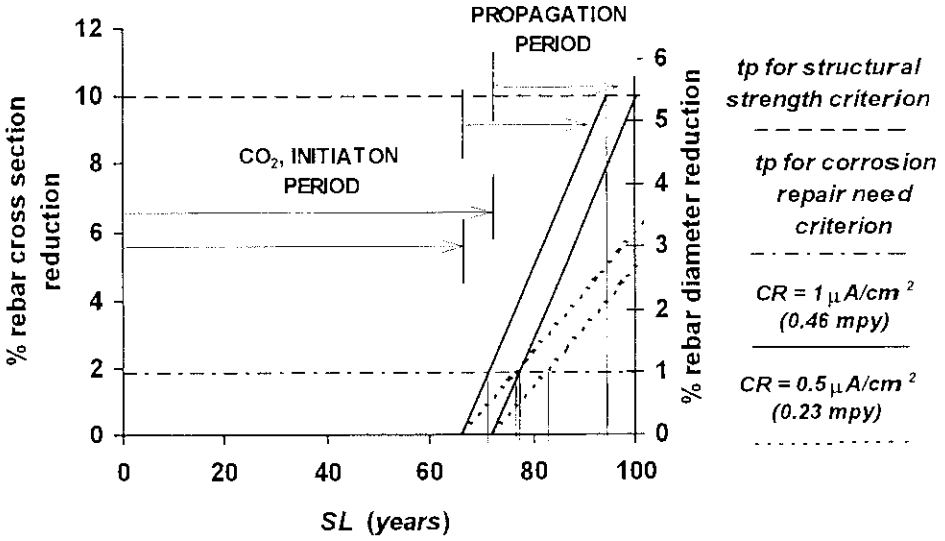

Figure I.34. Estimated service life (***SL***) prediction for concrete carbonation representing the values of t_{cl} that were obtained for $Kc_{(10\%)}$ and $cc_{(10\%)}$, and assuming typical values of ***CR*** of steel in carbonated concrete. A rebar diameter of 1/2 *in.* (1.27 *cm*) was assumed.

Table I.10. Estimated service life (***SL***) prediction for concrete carbonation based on the *structural strength* and the *corrosion repair need* criteria.

Service Life Criterion	***SL*** (*years*)			
	t_{Ca} = 70 *years*		t_{Ca} = 75 years	
	CR = 1 $\mu A/cm^2$	***CR*** = 0.5 $\mu A/cm^2$	***CR*** = 1 $\mu A/cm^2$	***CR*** = 0.5 $\mu A/cm^2$
Structural Strength	94	123	102	131
Corrosion Repair Need	75	81	80	86

Consequently, the projected service life of reinforced concrete structures presenting carbonation are governed by the duration of the initiation period, and

only on structures that present relatively high corrosion rates, cracking and spalling may occur before a period of 75 years. Bridges decks and over land structures present higher risk of showing corrosion damage due to concrete carbonation as they usually show the shortest time for corrosion initiation.

3.3.3.4.2 Statistical Implications. Appendix 3.4 presents a tentative approach to evaluate the overall distribution of carbonation-related corrosion damage in the present FDOT bridge inventory.

3.3.3.4.3 Estimation of *SL* for the Case of Chloride Induced Corrosion. As it was indicated earlier, the most severe condition from the point of view of chloride induced corrosion corresponded to the substructure and the deck of over water bridges exposed to marine environment. The conjunction of high ***Cs*** and D_{eff} values gave rise to very low values of t_{Cl}. In addition, the higher corrosion rate typically observed in reinforced concrete contaminated with chlorides result in very low values of ***SL*** compared to the case of concrete carbonation. Conversely, the over land and over water (river) structures, presented very high estimated values of t_{Cl} and therefore values of ***SL*** that far exceeded the ***NSL*** due to the low values of ***Cs*** and D_{eff} considered in this case.

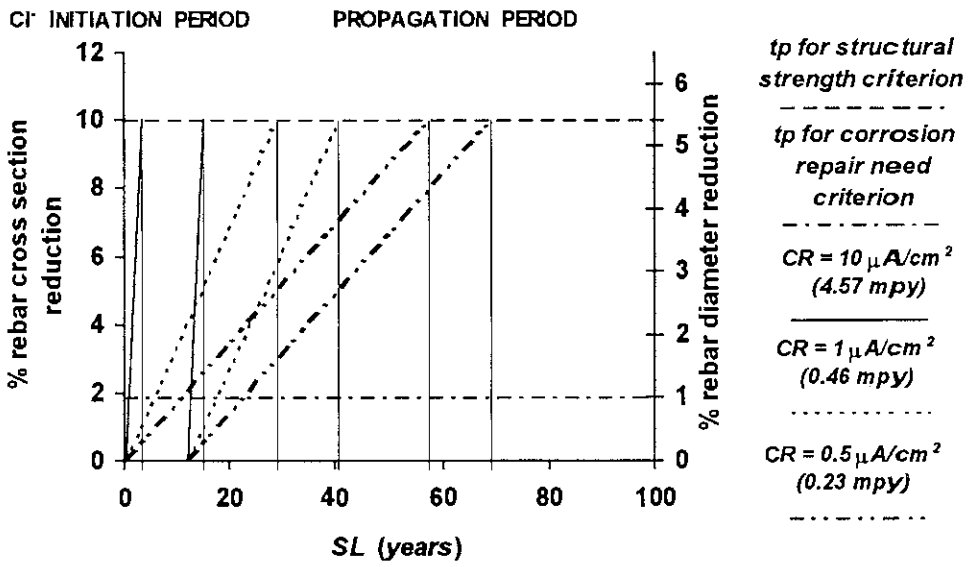

Figure I.35. Estimated service life (***SL***) prediction for chloride induced corrosion representing the values of t_{Cl} that were obtained from over water bridges exposed to marine environment and assuming typical values of ***CR*** of steel in concrete contaminated with chlorides. The initial rebar diameter is 1/2 *in.* (1.27 *cm*).

Figure I.35 shows the representation of the estimated ***SL*** curves for t_{Cl} = 0.4 *years* (case of the substructure of over water (marine) bridges, assuming ***cc*** = 1.5" (3.8 *cm*)) and for t_{Cl} = 12.2 *years* (case of the deck of over water (marine) bridges assuming ***cc*** = 2.5" (63.5 *cm*)). The results for three typical corrosion rate values of steel in concrete contaminated with chloride ions (10, 1 and 0.5 mA/cm^2) are represented in the figure. Table I.11 presents the estimated values of ***SL*** obtained for each of these conditions for both service life criteria considered. These examples are shown for illustration only; Ref [I.21] should be consulted for applicable information on chloride-induced corrosion forecasts in Florida.

Table I.11. Estimated service life ***SL*** prediction for chloride induced corrosion based on the *structural strength* and the *corrosion repair need* criteria.

Service Life Criterion	***SL*** *(years)*					
	t_{cl} = 0.4 *years*			t_{cl} = 12.2 *years*		
	CR = 10 $\mu A/cm^2$	***CR*** = 1 $\mu A/cm^2$	***CR*** = 0.5 $\mu A/cm^2$	***CR*** = 10 $\mu A/cm^2$	***CR*** = 1 $\mu A/cm^2$	***CR*** = 0.5 $\mu A/cm^2$
Structural Strength	3.2	29	57	15	41	69
Corrosion Repair Need	1.2	5.4	11.4	13	17	23

3.3.4 Comparison With Results From Other Field Investigations

Results from other field investigations revealing carbonation depth and carbonation coefficients data that were carried out by several researchers world wide are presented in Appendix 3.5. The reported values of ***Kc*** were obtained from carbonation depth measurements performed on different types of reinforced concrete structures assuming a square root of time type of relationship as shown in equation **(1)**. In order to compare these results, the concrete characteristics (compressive strength, water to cement ratio (***w/c***)) and the type of exposure condition of the inspected structures are also specified when this information was reported.

According to the results presented in section **3.2.2.2**, the value of ***Kc*** obtained in this work fall in the same range of most values reported in the

literature. The low ***Kc*** values reported by Holm et al[I.15], obtained on marine structures in the USA, are of the same order as those obtained on over water bridges in the present investigation. The results presented by Wong et al[I.29] for different civil construction types exposed to tropical humid environments are higher than those obtained in the Florida highway bridges. The reason for this may be due to the lower concrete quality (reflected in the compressive strength values reported) of the structures tested by Wong et al[I.29].

3.3.5 Additional Aspects Analyzed

3.3.5.1 Correlation Between ρ and E_{corr} Measured in the Field

The mapping of electrical resistivity (ρ) of concrete together with half-cell potential (E_{corr}) is commonly used for assessing the corrosion risk of reinforced concrete structures in service [I.8, I.31]. Figure I.14 on section **3.2.1.2** presents the ρ measurements taken in the field using a 4 point probe Wenner array. The values of ρ increased as a function of the elevation above high tide (***EAHT***) on over water structures, or the elevation above floor level (***EAFL***) on over land structures and presented considerable variation from bridge to bridge. The same type of pattern was observed on the E_{corr} measurements performed on over water bridges exposed to marine environment, where the readings also increased with the ***EAHT***. In most cases, the values of E_{corr} varied from typical

active potentials of steel in concrete (-450 to -600 *mV* vs. ***CSE***) at ***EAHT*** below 1 *ft.* (0.30 *m*) to passive potentials (> -150 *mV* vs. ***CSE***) at ***EAHT*** above 7 *ft.* (2.13 *m*). Except for underwater concrete, the incidence of rebar corrosion damage is great on areas of the structure presenting active potentials together with low values of ρ (for example 10 *kW cm*) [I.31].

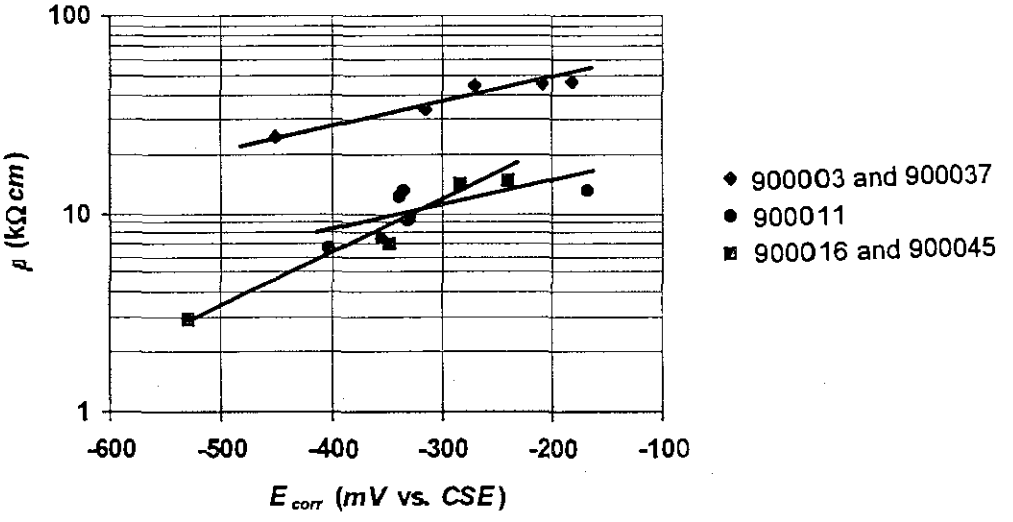

Figure I.36. Correlation between electrical resistivity of concrete (ρ) and half-cell potential (E_{corr}) measured at the same ***EAHT*** on over water bridges exposed to marine environment (see Table I.1 for bridge identification).

Figure I.36 shows the correlation between the field measurements of ρ and E_{corr} taken at equal ***EAHT*** on over water (marine) bridges. The lower readings of ρ corresponded to the more active potentials, providing symptoms that agreed with the incidence of rebar corrosion on the over water bridge substructures exposed to marine environment. This behavior was not observed

on over land bridges where the half-cell potential readings presented typical passive values that did not vary consistently with the ***EAFL***.

3.3.5.2 Correlation Between D_{eff} and Wet Resistivity (ρ_w)

The determination of the chloride diffusion coefficient (D_{eff}) by measuring chloride concentration profiles in concrete is a time consuming process that requires careful sample analysis. It is therefore of interest to establish some other way to estimate this parameter by means of a quicker method. The electrical resistivity of concrete is a function of the pore solution composition and the degree of water saturation of the concrete pores. The measurement of the electrical resistivity of saturated concrete samples provides an indication of the mobility of ions within the concrete. Therefore, it seems possible to obtain a relationship between the values of D_{eff} and the wet resistivity (ρ_w) measurements performed in concrete samples. This issue has been previously addressed by several researchers who have presented different expressions relating these parameters.

Berke and Hicks [I.32] have obtained an empirical relationship between ρ (Ω *cm*) and D_{eff} (in^2/y) by testing concrete samples exposed to a solution containing 3% ***NaCl*** for two years. This correlation is given as

$$D_{eff}\left(\frac{in^2}{y}\right) = 2.7\,\rho_{[\Omega cm]}^{-1.09} \qquad (5)$$

In a theoretical study, Andrade et al [I.33] proposed a relationship where $D_{eff} = f(Do, \rho_o)1/\rho$, where ρ_o is the concrete pore solution resistivity, and D_o is the diffusion coefficients of chlorides in the pore solution.

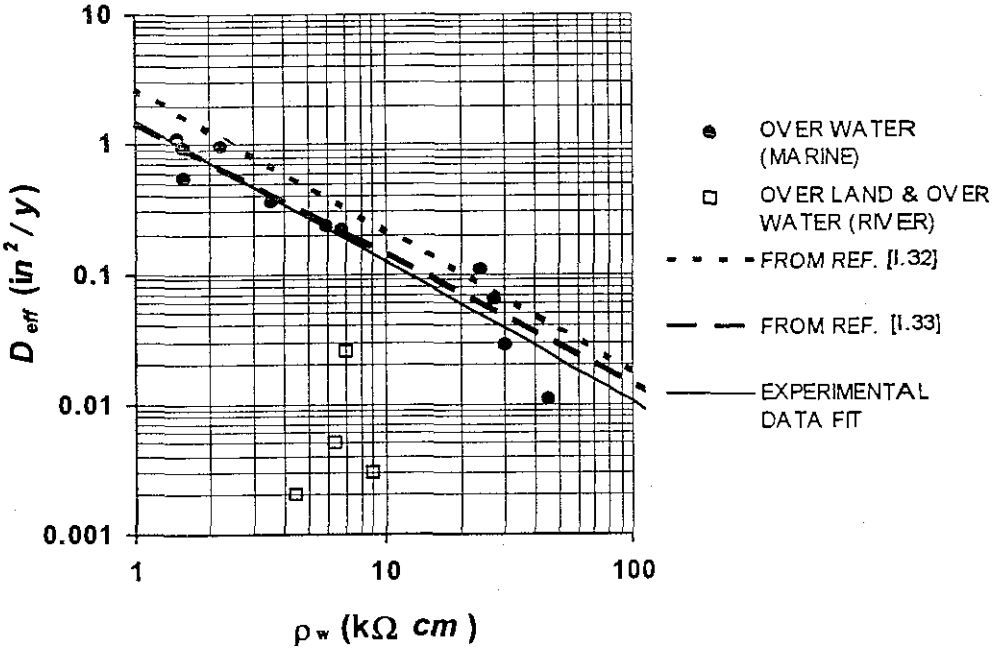

Figure I.37. Relationship between effective chloride diffusion coefficient and concrete wet resistivity.

Figure I.37 shows the relation between the values of D_{eff} calculated from chloride profiles and the ρ_w measurements obtained from cores extracted from the same bridges, at the same elevations above high tide and in some cases from the same column. The data are grouped according to the type of exposure condition. The filled symbols in the figure correspond to the data obtained from over water (marine) bridges, and the open symbols correspond to the over land and over water (river) bridges.

The best linear fit for the over water (marine) results gave the correlation

$$D_{eff}\left(\frac{in^2}{y}\right) = 1.57\,\rho_{w[\Omega cm]}^{-1.09} \qquad (6)$$

Which is represented by the solid line in Figure I.37, together with the relationships from reference [I.32] and [I.33]. The ρ_w and D_{eff} data obtained from over land and over water (river) bridges (also shown in Figure I.37) did not follow the trend observed in the over water (marine) results.

3.3.5.3 Evaluation of the concrete quality

An estimation of the original mix design water to cement ratios (***w/c***) of the structures inspected can be made based on the concrete porosity results presented in section **3.2.2.5** and assuming an aggregate to cement ratio (***a/c***) by volume of 2.33 in all the cases analyzed. According to the empirical relationship developed by Powers [I.34], the capillary porosity of the cement paste (P_c) can be calculated as

$$P_c = w/c - 0.36\,\alpha \qquad (7)$$

where α is the degree of hydration of the concrete. For the purpose of these calculations α is considered as α = 0.8 (80 % of the cement has hydrated). The total porosity of concrete (P_T) is the result of three main components, the percentage of air entrained (***Ae***), the porosity of the aggregate (A_p), and the porosity of the cement paste P_C. The value of aggregate porosity was determined in section **3.2.2.5** for limestone, being A_p = 14.2%. Assuming that ***Ae*** = 1%, and considering an ***a/c*** = 2.33, that is, 70 % by volume of the concrete is aggregate, the value of P_C can be calculated as

$$P_C = (P_T - Ae - 0.7\,A_p) / 0.3 \qquad (8)$$

From equation. **(7)** and **(8)** the ***w/c*** can be calculated as

$$w/c = P_C + 0.288 \qquad (9)$$

Figure I.38 shows the estimated water to cement ratio calculated according to this procedure, averaged for four selected structural component classes.

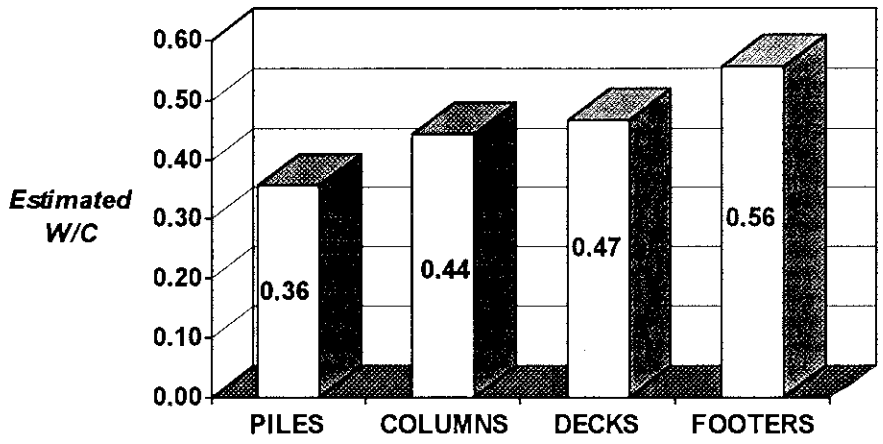

Figure I.38. Estimated values of water to cement ratio (***w/c***) based on the porosity measurements of concrete cores extracted from different structural components.

These results obtained fall in the range expected for typical mix designs used in each type of structural component. The lowest ***w/c*** value was obtained on cores extracted from prestressed piles, while the highest were obtained on cores extracted on cast in place footers.

3.4 CONCLUSIONS

1. Evidence of concrete carbonation in progress was found in 16 out of 18 Florida bridges examined.

2. Only one out of 18 bridges examined showed direct indication of carbonation induced rebar corrosion.

3. Concrete carbonation depths (x_C) measured in cores extracted from the bridges examined were as high as 50 *mm* with an average value of 9.8 *mm.*

4. Carbonation coefficients (***Kc*** = x_C / $t^{½}$) measured for extracted cores ranged from 0 to 14 $mm/y^{½}$.

5. The bridge decks presented higher values of x_C and ***Kc*** compared to the substructure. This was most evident on over water bridges, where the average values of x_C were 12.3 *mm* and 2.1 *mm* for the deck and the substructure respectively.

6. The internal relative humidity (***IRH***) measurements at a depth of 1.5" (3.8 *cm*) in the concrete, did not reveal any significant difference between over water

and over land structures. A seasonal variation of the ***IRH*** was observed on the over land bridges.

7. The most severe conditions from the point of view of concrete carbonation induced corrosion was obtained on the decks of over land bridges (highest 10 percentile ***Kc***> 4.35 $mm/y^{1/2}$). The estimated time for corrosion initiation was approximately 70 years when a concrete cover of 1.5" (3.8 *cm*) and the value of ***Kc*** = 4.35 $mm/y^{1/2}$ were considered.

8. Cores extracted from the substructure of over water (marine) bridges presented very high chloride concentrations at the rebar depths compared to the assumed threshold value for corrosion initiation (1.2 *pcy* (0.71 kg/m^3)), whereas the over land and over water (river) bridges presented very low chloride concentrations as a result of the milder exposure conditions.

9. The most severe conditions from the point of view of chloride induced corrosion were observed on the substructure of over water (marine) bridges, where the time for corrosion initiation was a fraction of a year when a concrete cover thickness of 1.5" (3.8 *cm*) and a chloride threshold value for corrosion initiation of 1.2 *pcy* (0.71 kg/m^3) were assumed.

REFERENCES

I.1. Andrade, M. C., "Report on the Background of Carbonation of Concrete Structures," Report No. 16.709-II, Institute of Construction Science "Eduardo Torroja", CSIC, Madrid, 1996.

I.2. Andrade, C., Sarría, J. and Alonso C., "Statistical study on Simultaneous Monitoring of Rebar Corrosion Rate and Internal Relative Humidity in Concrete Structures Exposed to the Atmosphere", to be published in Corrosion of reinforcement in Concrete Construction, SCI, Proc. of a Conference to be held in Cambridge, UK, June, 1995.

I.3. Papadakis, V. G., Vayenas, C. G. and Fardis, M. N., "Fundamental Modeling and Experimental Investigation of Concrete Carbonation," ACI Materials Journal, Vol. 88, No 4, p. 363, 1991.

I.4. Tuutti, K., Corrosion of Steel in Concrete, Swedish Cement and Concrete Institute, Stockholm, 1982.

I.5. Bakker, R., "Initiation Period", Corrosion of Steel in Concrete, Report of the Technical Committee 60 CSC, RILEM, Report 60 CSC, P, Schiessl, Ed., Chapman and Hall, London, p.22, 1988.

I.6. Hamada, M., "Neutralization (carbonation) of Concrete and Corrosion of Reinforcement", Proc. 5th Int. Symp. on Chemistry of Cement, Vol III, Tokyo, p. 349,1968.

I.7. RILEM Recommendation, "CPC-18 Measurement of Hardened Concrete Carbonation Depth," Materials and Structures, Vol. 21. No. 126, p. 453, 1988.

I.8. Millard, S. G., Harrison, J. A., and Eduards, A. J., "Measurement of the Electrical Resistivity of Reinforced Concrete Structures for the Assessment of Corrosion Risk", Br. J. of Nondestructive Testing. Vol. 31, p.616, 1989.

I.9. Gonzalez, J.A., Lopez, W., Rodriguez, P., "Effects of Moisture Availability on Corrosion Kinetics of Steel Embedded in Concrete," Corrosion, Vol. 49, No. 12, p. 1004, 1993.

I.10. Gregg, S. J., and Sing, K. S. W., "Adsorption, Surface Area and Porosity", 2nd Ed., Academic Press, New York, 1967.

I.11. Hagymassy, J., Stephen Brunauer, J. R. and Mikhail, R. Sh., "Pore Structure Analysis and Water Vapor Adsorption", J. of Colloid and Interface Science, Vol. 20, No. 3, p. 485, 1969.

I.12. Parrot, L., "Measurement and Modeling of Porosity in Drying Cement Paste", Microstructural Development During Hydration of Cement, L. J. Struble and P. W. Brown, Eds., Materials Research Society Symp. Proc., Vol. 85, p. 91, 1987.

I.13. Kessler, R. J., Arrebola, V.E., Lingerfelt, R.S., and Brown, R.P., "Determination of Low Levels of Chloride in Concrete and Raw Materials, FDOT Research Report 203, Florida Department of Transportation, Tallahassee, 1978.

I.14. Baweja, D., Roper, H., Guirguis, S., and Sirivatnanon, V., "Measurement of Corrosion of Steel Reinforcement under High Chloride Conditions." Fly Ash, Silica Fume, Slag and Natural Pozzolans in Concrete, Fourth International Conference, ACI SP132, Vol. II, V.M. Malhotra, Ed., American Concrete Institute, Detroit, p. 1543, 1992.

I.15. Holm, T. A., Bremner, T. W., and Vaysburd, A. "Carbonation of Marine Structural Lightweight Concrete",Concrete in Marine Environments, ACI SP 109, American Concrete Institute, Detroit, p.667, 1988.

I.16. Morris, W., Moreno, E. I. and Sagues, A. A., "Practical Evaluation of Resistivity of Concrete Test Cylinders using a Wenner Array Probe", Cement and Concrete Research, Vol. 26, No. 12, pp. 1779-1787, 1996.

I.17. FDOT Guidelines, "Florida-Concrete Design, Environmental Classification and Construction Criteria," Procedures - Structures Design Guidelines, Tallahassee, 1992.

I.18. Maldonado, L., Echeverria, M., Castro, P., and Diaz, L., "Determination of Corrosion Rates in a Tropical Marine Environment of the Yucatan Peninsula," Corrosion, Proc. of the First Mexican Symposium on Metallic Corrosion, L. Maldonado and M. Pech, Eds., UNAM - Facultad de Quimica Press, México, p. 219, 1995.

I.19. Andrade, C., and Alonso C., "Refined Methods for the Calculation of the Design Life of Reinforced Concrete", Proc. First NACE Latin American Region Corrosion Congress, Paper No. 94115, Maracaibo, 1994.

I.20. RILEM Report 60 CSC, Corrosion of Steel in Concrete, P. Schiessl, Ed.,Chapman and Hall, London, 1988.

I.21. Sagüés, A. A., "Corrosion of Epoxy Coated Rebar in Florida Bridges," Florida Department of Transportation, WPI No. 0510603, State Job No. 99700-7556-010, Nov. 1993.

I.22. Sagüés, A. A., Powers, R. G., and Kessler, R., "Corrosion Processes and Field Performance of Epoxy-Coated Reinforcing Steel in Marine Substructures," Corrosion/94, Paper No. 299, NACE, Houston, 1994.

I.23. Parrot, L. and Cheng Zhang Hong, "Some factors Influencing Air Permeation in Cover Concrete", Materials and Structures, Vol. 24, p. 403,1991.

I.24. Andrade, C., Alonso, C. Gonzalez, J. A., "An Initial Effort to use the Corrosion Rate Measurements for Estimating Rebar Durability", Corrosion Rates of Steel in Concrete", ASTM STP 1065, N. S. Berke, V. Chaker and W. D. Whiting, Eds., American Society for Testing and Materials, Philadelphia, p. 29, 1990.

I.25. Gonzalez, J.A., Algaba, S., Andrade, C., "Corrosion of Reinforcing Bars in Carbonated Concrete" British Corrosion Journal Vol. 15, No 3, p. 135, 1980.

I.26. Vaysburd, A.M., "Determination and Rehabilitation of the Elevated Roadway Bridge at Baltimore/Washington International Airport," Paul Klieger Symposium on Performance of Concrete, ACI SP 122, American Concrete Institute, Detroit, p. 401, 1993.

I.27. Parrott, L. J. "Carbonation, Corrosion and Standardization", Protection of Concrete, Proc. Conf., R.K. Dhir and J.W. Green, Eds.,Chapman and Hall, Dundee, p. 1009, 1990.

I.28. Ho, D. W. S., and Lewis, R. K., "Carbonation of Concrete and its Prediction" Cement and Concrete Research, Vol. 17, No. 3, p. 489, 1987.

I.29. Wong, W.F., Chiew, S.P., and Ho, N.Y., "Evaluation of Insitu Test Data from Existing Concrete Structures," Concrete 2000, Vol. II, R.K. Dhir and M.R. Jones, Eds., E. & F.N. Spon, London, p. 1147, 1993.

I.30. Prakash, D. S. and Aggarwat, P., "Carbonation and Corrosion in Concrete Structures", Indian Concrete Journal, Vol. 82, p. 130, 1985.

I.31. Borgard, B., Warren, C., Somayaji, S., and Heidersbach, R., "Mechanisms of Corrosion of Steel in Concrete", Corrosion Rates of Steel in Concrete, ASTM STP 1065, N.S. Berke, V. Chaker, and D. Whiting, Eds., American Society for Testing and Materials, Philadelphia, p. 174, 1990.

I.32. Berke, N. S. and Hicks, M. C. , "Estimating the Life Cycle of Reinforced concrete Decks and Marine Piles Using Laboratory Diffusion and Corrosion Data", Corrosion Forms and Control for Infrastructure, ASTM STP 1137, V. Chaker, Ed., American Society of Testing and Materials, Philadelphia, p. 207, 1992.

I.33. Andrade, C., Alonso, C., and Goñi, S., "Possibilities for Electrical Resistivity to Universally Characterize Processes in Concrete," Concrete 2000, Vol. II, R.K. Dhir and M.R. Jones, Eds., E. & F.N. Spon, London, p. 1639, 1993.

I.34. Mindes, S. and Young, J.F., Concrete , Prentice-Hall Inc, Englewood Cliffs, 1981.

Section 4. Objective (c): LABORATORY INVESTIGATION

Objective (c) is to conduct a laboratory investigation to determine the influence of mix design parameters on the carbonation rate of concrete to be used for future long term durability FDOT applications.

The approach to attain this objective was to select a number of old and actual FDOT concrete mix designs. Concrete cylinders along with reinforced concrete prisms were exposed to a carbon dioxide environment. The results were used to determine carbonation coefficients and obtain a distribution of carbonation severity as a function of water-to-cement ratio, 28-day compressive strength, and pozzolanic replacement. The results were then used to obtain projections of the length of service time before carbonation-induced corrosion would be observed in severe exposure conditions.

The test plan was developed by first choosing a set of suitable FDOT mix designs. After casting the concrete specimens were allowed to stabilize in lab air conditions previous to carbon dioxide exposure. A suitable carbon dioxide concentration was chosen to accelerate the carbonation rate and a carbonation test chamber was designed. During the carbonation exposure, concrete carbonation depth was measured at two different times. Carbonation coefficients then were converted to atmospheric exposure conditions.

At the same time concrete electrical resistance and half cell potentials were monitored using the reinforced concrete prisms. Corrosion rates of the

embedded rebars were determined using electrochemical measurements in selected specimens. A detailed indication of the test techniques and the findings is given in the following subsections.

4.1 PROCEDURE

4.1.1 Concrete Specimens

4.1.1.1 Mix Design

The control concrete mix design was representative of Florida Department of Transportation design used in moderately aggressive environments. The cementitious content, or cementitious factor, was 444 kg/m^3 (752 pcy), the coarse aggregate was limestone, and a w/c ratio of 0.37 [II.1] was used to get a minimum 28-day compressive strength of 41.4 MPa (422 kg/cm^2, 6000 psi).

A cementitious content of 80% portland cement type I (OPC) and 20% FA class "F" (by weight) was used (see Table II.1). This mix is routinely used in marine structures to reduce the heat of hydration. In addition the cement paste permeability of FA concrete is lower than standard concrete, thus reducing the chloride diffusion coefficient.

A water reducer agent (***WRAD***), 2.16 lt/m^3, was used to obtain enough workability at this low w/c ratio.

Table II.1. Mix design variations.

#	Mix	Fly Ash†		Silica Fume†		w/c ratio		Chloride	
		20%	50%	0%	8%	0.37	0.50	Yes	No
1	Control	X		X		X			X
3	w/c var.	X		X			X		X
5	Cl- var.	X		X			X	X	
8	SF var.	X			X	X			X
10	FA var.		X	X		X			X

† Percent as cement replacement.

In addition to the control mix design, the following mix variations were evaluated:

A w/c variation (w/c=0.50) was chosen to study the depth of carbonation of high porosity paste, thus simulating older construction practice.

A Cl^- variation (w/c=0.50, and 1.77 kg/m^3 (3 pcy) of chloride ions) was used to represent the effect of occasional chloride presence into the concrete mix in old structures. Chloride ions were added as sodium chloride; since it aids workability no ***WRAD*** was used in this variation.

An SF variation (8% SF as replacement) was chosen to observe the behavior of a ternary system (OPC, FA, and SF) when exposed to carbonation.

An FA variation (50% FA as replacement) was used to study the behavior of high pozzolanic replacement—as in the case of massive concrete structures where a low heat of hydration is desirable. This addresses questions from reported increases in the carbonation depth as the amount of FA increases [II.2].

Due to the small size of the specimens, a maximum coarse aggregate size of 9.5 mm (⅜") was selected. See Appendix 4.1 for detailed concrete mix designs used.

4.1.1.2 Instrumented Specimens

Instrumented concrete specimens (see Figure II.1) were designed to monitor the electrochemical behavior of steel in concrete. Concrete specimens were 20.3 cm (8") high, 10.2 cm (4") wide, and 5.1 cm (2") thick, with two embedded rebars, ends protruding through the top.

The rebars were No. 3, with a nominal 9.5 mm (⅜") diameter, 20.3 cm (8") long, placed longitudinally starting 5.1 cm (2") from the bottom, and centered 2.5 cm (1") from the sides from the planar view. The first 10.2 cm (4") of each rebar were degreased with acetone and directly exposed to the surrounding concrete. The following 6.3 cm (2½") long region was masked with epoxy-resin (1 cm protruding from the concrete specimen) to avoid direct corrosion from the external ambient. The remaining protruding region was protected from

atmospheric corrosion by coating it with a commercial oil paint. The paint was removed in an small area to attach a copper cable to each rebar by using a hose-clamp. The copper cables were later soldered to standard binding posts to make electrical connections from the test chamber. A reference electrode (activated titanium rod (***ATR***), 3.2 mm (⅛") diameter by 3.8 cm (1½") long), was placed in each concrete specimen.

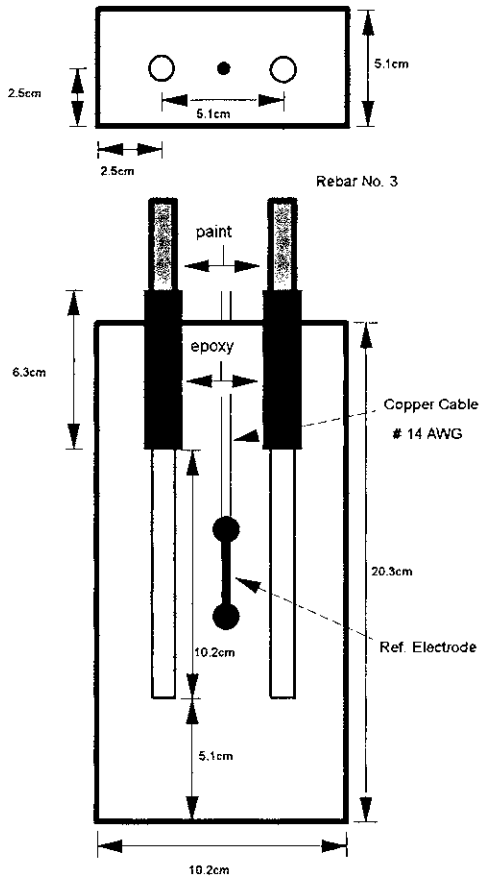

Figure II.1. Instrumented concrete specimen dimensions.

The ***ATR*** was centered in the concrete specimen between the two rebars, and it was used for electrochemical experiments of the rebars [II.3].

Six concrete specimens for each mix design were cast. Three of them underwent accelerated testing at CO_2 concentration of 5000 ppm in air and the results are presented in this report. The remaining specimens were set aside for future testing.

4.1.1.3 Plain Specimens

Plain specimens were designed for physical tests and to monitor the carbonation depth. "3 by 6" cylinders (7.6 cm diameter, 15.2 cm long) were chosen for the latter purpose.

Fourteen "3 by 6" concrete cylinders for each mix design were cast, 12 for carbonation testing, and the remaining two for natural indoor exposure as control specimens. Of the 12 specimens for carbonation testing three specimens underwent accelerated testing at a CO_2 molar concentration of 5000 ppm in air and the results are presented in this report. Of the remaining specimens, three were used for full outdoor weathering exposure; three were used for rain-sheltered outdoor exposure; and three were set aside for accelerated testing at a CO_2 molar concentration of 40000 ppm in air. The results of these additional tests will be reported in the future.

At least two "4 by 8" concrete cylinders (10.2 cm diameter, 20.3 cm long) of each mix were cast for AASHTO Rapid Chloride Permeability testing and other related tests, and three "6 by 12" concrete cylinders (15.2 cm diameter, 30.5 cm long) were cast for 28-day compressive strength tests.

All the concrete specimens except the "6 by 12" cylinders were cured for 14 days by keeping them in their respective molds and spraying water in the open surface. The open surface of the molds was covered with plastic bags to retain moisture. The "6 by 12" concrete cylinders were cured for 28 days in a 100% R.H. chamber.

4.1.2 Carbonation Test Chamber

A test chamber to hold 15 instrumented and 15 plain specimens was designed based on the scheme outlined by previous investigators [II.4, II.5].

A glass fish tank (121.9 cm (48") long, 31.7 cm (12½") wide, and 53.3 cm (21") high) was used as the test chamber. The top of the tank was closed with an acrylic sheet lid (6.4 mm (¼") thick), and sealed using weatherstrip. Electrical binding posts were placed through the lid for easy electrical connection of the internal wiring to electrochemical equipment. Small holes (3.2 mm (⅛") diameter) for hanging strings were drilled in the lid to weigh the concrete samples without removing them from the chamber. A 19 mm (¾") hole with a PVC fitting was also fitted into the lid for insertion of a R.H. measurement

gage. The lid also had holes for gas inlet and outlet. An internal hose was connected to the inlet to send the gas directly to the middle-bottom region of the tank. A fan was used to distribute the gas throughout the tank. A cardboard deflector was installed above the fan to improve the gas distribution and to prevent stagnant gas zones.

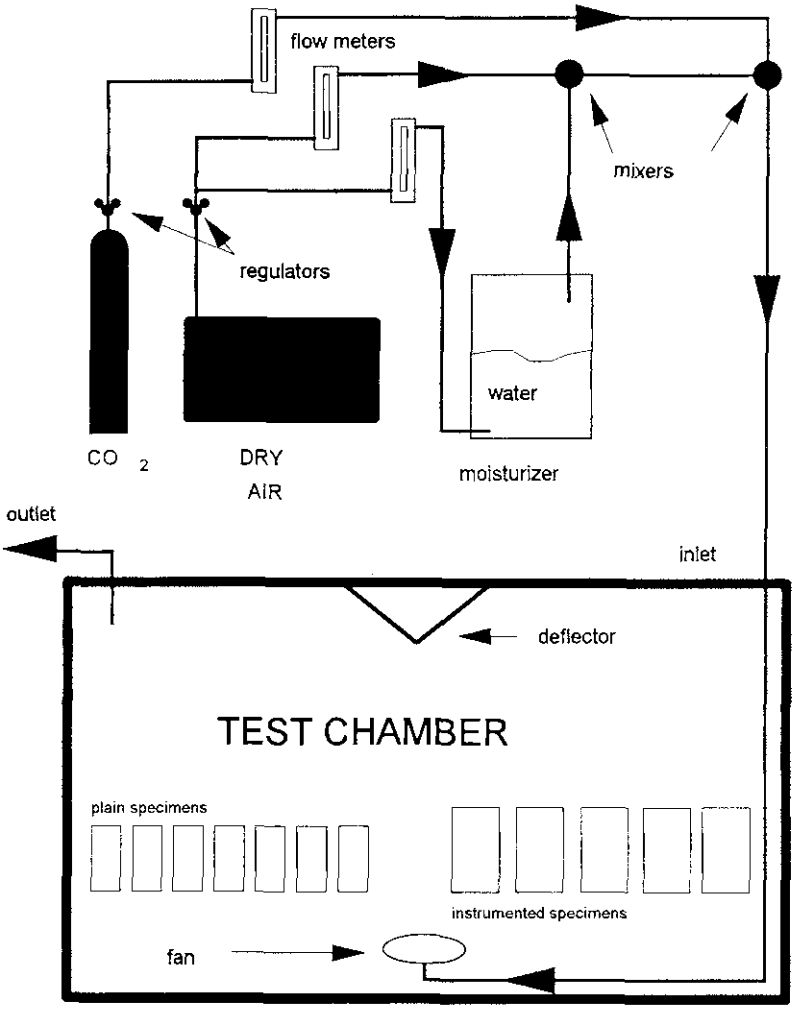

Figure II.2. Scheme of carbonation test chamber setup.

An ordinary dial hygrometer was placed inside the tank. The hygrometer was calibrated against a digital R.H./temperature Vaisala® meter model HM34 placed temporarily in the PVC fitting.

To obtain the CO_2 concentration of 5000 ppm (mol/mol) and the desired R.H. inside the chamber, a mix of carbon dioxide and air at two different moisture levels was used. Three flow meters were used to control the volume of each gas. One flow meter (maximum capacity of 1222 ml/min) was set up to control the dry air. A second flow meter (maximum capacity of 4700 ml/min) was used to control the wet air (see Figure II.2). The air source was the compressed air building supply, which provided dry air (typically 20% R.H.). From the compressor, the air went to the two air flow meters through a regulating valve. The air exiting from one of the flow meters was sent through a bubbling moisturizer. The air stream exiting from the moisturizer and the other air flow meter were mixed in the chamber inlet hose with the CO_2 gas flowing through the CO_2 flow meter (maximum capacity 40 ml/min) from a tank of commercially pure CO_2. The flow rate in the dry and wet flow meters were adjusted periodically to obtain a 60%±5% R.H. inside the chamber. This R.H. value was chosen since it was established that carbonation of concrete is fastest at this humidity range [II.5, II.6, II.7].

4.1.3 Testing During Conditioning Period

Accelerated concrete carbonation tests are not practical under normal atmospheric environment immediately after concrete demolding because the concrete pore network is filled with water. Therefore, a conditioning period under ambient room humidity conditions was scheduled for both the instrumented and plain specimens.

4.1.3.1 Mass Loss

The loss of water from drying during the conditioning period was monitored by periodically weighing the plain specimens. A Sartorious® digital balance model 1203MP with a 0.1 g resolution was used to weigh the specimens.

4.1.3.2 Concrete Resistivity

The concrete resistivity of the plain cylindrical specimens was measured indirectly using a CNS RM MKII® resistivity meter with a Wenner four-electrode array with adjustable inter-probe distance [II.8]. All the measurements were performed with an inter-probe distance of 2.5 cm (1"). The four-electrode array was longitudinally centered on the side of the cylinders and the measurements

were repeated for three different angular positions. The instrument resistivity readings were corrected for deviation from semi-infinite uniform body condition by multiplying by a geometric cell constant (C_G). The corrected values were averaged to obtain a nominal concrete resistivity for each specimen.

The geometric cell constant (C_G) was determined experimentally by empirical correlations from resistivity measurements with plastic concrete cylinder molds filled with solutions of known resistivity and verified with finite element model calculations [II.9]. C_G was 1/1.62 for the "3 by 6" cylinders, and 1/1.26 for the "4 by 8" cylinders.

4.1.4 Other Baseline Concrete Evaluations

4.1.4.1 Rapid Chloride Permeability Test

Selected "4 by 8" concrete cylinders were cured for 90 days in a 100% R.H. chamber in order to perform the Rapid Chloride Permeability Test (***RCPT***), originally developed by Whiting [II.10], now formulated as an standard test [II.11, II.12].

The tests were performed at the FDOT Materials Office Laboratory. After curing the "4 by 8" cylinder was cut into slices 5.1 cm (2") thick. Apparent concrete resistivity measurements were taken with the CNS RM MKII® resistivity meter with the Wenner probe placed on the top surface of the slices before the

RCPT. The instrumented readings were converted to resistivity values by using the appropriate geometric cell constant [II.9].

In the ***RCPT***, a measured amount of electric charge was delivered through the specimen over a six-hour period. A potential difference of 60-volt DC between the two flat surfaces was maintained during the test. Based on the amount of charge (in coulombs) measured, the concrete was classified following AASHTO ranking criteria as: very low permeability (less than 1000 C), low permeability (from 1000 to 2000 C), moderate permeability (from 2000 to 4000 C), or high permeability (more than 4000 C).

4.1.4.2 Concrete Porosity Test

The porosity of concrete was evaluated by a modification of the ASTM C 642-90 Standard Test Method for Specific Gravity, Absorption, and Voids in Concrete [II.13]. Two concrete samples (80 to 100 g) per mix design were weighed to obtain the "as received condition" weight (***ARW***). After that the samples were dried in an oven at 105 C for 48 hrs, and then weighed again to obtain the "dry condition" weight (***DCW***). Finally the samples were immersed in water for 72 hrs. The surface moisture was then removed with a towel before weighing to obtain the "wet condition" weight (***WCW***).

The weight of the water inside the voids (***WV***) was obtained as ***WV*** = ***WCW*** - ***DCW***. This water was assumed to be the total water inside the concrete. The "percentage of total voids by weight" ($TV_{\%wt}$) was defined as

$$TV_{\%wt} = 100 \quad WV / WCW \qquad (I)$$

4.1.5 Testing During Carbonation Exposure

During the carbonation exposure, electrochemical behavior of the rebars was monitored with time. Also, carbonation depths were measured in the plain specimens to determine an effective carbonation coefficient **Kc** for each concrete formulation. Electrochemical measurements of the instrumented specimens were conducted also during the conditioning period before the carbonation exposure. The start of the carbonation procedure was designated as time = 0; measurements during the conditioning period are therefore reported as negative time values.

4.1.5.1 Mass Gain

The mass of selected plain specimens was monitored during exposure in the carbonation chamber. Those specimens were weighed with an external mechanical triple-beam balance of 0.1 g resolution. To weigh the specimens, a nylon net was used to hang them from the balance. The nylon string was

threaded (taking care to minimize friction) through the small holes in the lid, so it was no necessary to remove the specimens from the chamber.

Although the mass-gain trends were very sensitive to small variations of the R.H. inside the chamber, the results provided nevertheless a rough estimation of the carbonation progression.

4.1.5.2 Half-Cell Potential Measurements

In the instrumented specimens, measurements of the half-cell potential between the rebars and the internal reference electrode were done using an MCM® voltmeter model LC-4, with an input resistance of 200 M . Since the ***ATR*** is not a true reference electrode [II.3], calibration against an external copper-copper sulfate electrode (***CSE***) was required. This measurement vs. ***CSE*** was performed periodically placing the tip of the ***CSE*** on the upper surface of the concrete prism.

4.1.5.3 Electrical Resistance Measurements

Measurements of the electrical resistance between the two embedded rebars were performed in the instrumented specimens with a soil resistivity Nilsson® meter model 400 (operating with square-wave alternating current at 97 Hz) using a two-point array configuration.

4.1.5.4 Electrochemical Impedance Spectroscopy (EIS) Tests

In the instrumented specimens, ***EIS*** tests were performed using a custom made unit [II.14]. The tests were performed in the frequency interval 0.001 to 10000 Hz, with a typical amplitude of 10 mV peak-to-peak. A three-point array method was implemented by using one bar as the working electrode (***WE***), the ***ATR*** as the reference electrode (***RE***), and the second bar as the counter electrode (***CE***)—also called the auxiliary electrode.

One concrete specimen was chosen from each concrete formulation, and both rebars (identified as X and Y) were tested with one day in between to allow the tested rebar to recover, thus avoiding unrepresentative polarization of the specimen. The same concrete specimen was tested every time.

The rebar polarization resistance ($\mathbf{Rp_{EIS}}$) was evaluated by assuming that the system behaves as an ideal Randles circuit with a simple solution resistance **Rs** and with $\mathbf{Rp_{EIS}}$ in parallel with a constant phase angle element (***CPE***) with parameters **Yo** and ***n*** [II.15]. A commercially available computer package (EQUIVCRT®) was used to obtain the values of the Randles circuit components that provided the best fit to the ***EIS*** data.

4.1.5.5 Polarization Resistance Tests

Conventional polarization resistance (***PR***) tests were performed in the instrumented specimens using a computer-controlled Gamry® potentiostat with IR compensation disabled. The electrode configuration was the same as in the impedance tests [II.15].

The same concrete specimens used in the ***EIS*** test were chosen for ***PR*** tests. Both rebars were tested with one day in between to allow the rebars to recover the initial open circuit potential after any disturbance created by the first test.

Tests were conducted by varying the potential (starting from the open circuit potential) in the cathodic direction, at an scan rate of 0.1 mV/s. The test was interrupted when the potential reached 10 mV below the starting potential. The polarization resistance ($\mathbf{Rp_{PR}}$) was evaluated by taking the slope of the potential-current curve at 10 mV excursion and subtracting the IR ohmic drop. The ohmic drop was measured independently with the Nilsson soil resistivity meter wire in a three-electrode configuration same as that used for the ***PR*** test.

4.1.5.6 Galvanostatic Step Technique

In the instrumented specimens, a custom made galvanostat was used to obtain an indication of the polarization resistance values from the rebars. In this

test all the rebars were tested in groups of 15 specimens at a time. A computer-controlled voltage source produced a 5 V voltage step with respect to the ***WE*** of each specimen. Individual large value resistors connected the ***CE*** of each specimen to the voltage source, resulting in the application to each specimen of a closely controlled current step in the range 0.0625 μA - 0.25 μA in the cathodic direction. The ***WE*** vs. ***RE*** potential of each specimen was monitored for a period of 700 s before application of the step, and for 1300 s afterwards. The potential was recorded every 40 s, thus producing a potential shift vs. time data sequence for each specimen during the experiment. From this potential shift, and by knowing the current step applied, an approximate value of the polarization resistance (which will be called $\mathbf{Rp_{ap}}$) was obtained. In addition a more sophisticated numerical analysis procedure was applied to the one of the galvanostatic step data sets (test 10). The procedure used the galvanostatic step response to estimate independently the values of the parameters of the same ideal Randles circuit employed for the ***EIS*** analysis; the polarization resistance value thus obtained is designated as $\mathbf{Rp_{GST}}$. Detailed of this procedure are given in the literature [II.16, II.17].

4.1.6 Carbonation Depth Measurement

The most common procedure for carbonation depth measurements is based on spraying pH indicators over a freshly broken concrete surface. By

reaction with the highly alkaline non-carbonated concrete, the indicator shows a change in color [II.18] revealing the carbonation front. This carbonation front is assumed to be the boundary between the colorless concrete and the reddish concrete.

Although there are tests to determine the extent of concrete carbonation like Thermogravimetric Analysis (***TGA***) [II.19, II.20], Quantitative X-ray Diffraction (***QXRD***) [II.21, II.22], Scanning Electron Microscopy (***SEM-EDAX***) [II.23] these were not used since the coarse aggregate used in this investigation is limestone rich in calcium carbonate and adequate differentiation of limestone from carbonated cement paste would be difficult [II.24].

4.1.6.1 Phenolphthalein Solution

The most popular pH indicator used for measuring the depth of carbonation in concrete is phenolphthalein. Its pH range is stated to be [II.25] from 8.2 (colorless) to 10.0 (red).

Although Kishitani [II.26] concluded that phenolphthalein solution is of high precision to measure whether or not calcium hydroxide remains in the concrete, this does not mean that the pH of the red concrete is above 12. However, the phenolphthalein solution can not delimit the exact boundary between non-carbonated and partially carbonated concrete; or the exact boundary between partially carbonated and totally carbonated concrete.

Because of this indetermination partially carbonated concrete may be present at points in the concrete deeper than the position indicated by the phenolphthalein boundary [II.19, II.27]. Therefore, likelihood of corrosion initiation in partially carbonated concrete exists even if the reddish boundary is still a few mm away from the steel surface since corrosion of the rebar can start at pH below 10.

4.1.6.2 Other pH Indicators

In addition to phenolphthalein, other suitable pH indicators such as Alizarin Yellow (pH change from 9 to 10), Thymolphthalein (pH change from 9.3 to 10.5), and Napthol Green B (pH change from 8 to 10), work with virtually identical results to phenolphthalein [II.24]. However, color changes produced by phenolphthalein are the most distinct of those produced by indicators [II.2, II.28].

4.1.6.3 Procedure

An approximately 4 cm-thick slice was split from the "3 by 6" cylinders using a chisel and a hammer. Immediately after that a 1% phenolphthalein ethyl alcohol solution or a 0.05% thymolphthalein ethanol solution was mist sprayed over the two freshly broken surfaces. After the change in color, eight carbonation depths (unless otherwise specified) at different angular positions (selected at random) were determined in both surfaces using a caliper. The

carbonation depth was measured from the edge of the specimen to the beginning of the red zone. Besides those measurements, the maximum and the minimum carbonation depths were measured. The carbonation depth measurements were averaged for each cylinder tested. The reported values are the average of two cylinders.

4.2 RESULTS

4.2.1 Conditioning Period

4.2.1.1 Mass Loss

During the conditioning period all the specimens exposed to the lab air environment were drying, thus losing mass in the form of water.

The mass loss (***ML***) for each mix design is plotted in Figure II.3 as a function of time. Each value shown is an average of 13 cylinders (see Appendix 4.2). The sets of specimens that lost most water were those of mixes 03 and 05, with w/c 0.5. Mixes 01 and 08 with a w/c of 0.37 lost the least water. The mass loss for mix 10 (also w/c=0.37) was actually closer to those of the mixes with w/c of 0.50 than to those of the other mixes with w/c of 0.37.

However, not all the mass loss came from the free water inside the pore network. To determine this amount of mass a standard concrete porosity test was performed in concrete specimens 120 days old [II.13]. The $TV_{\%wt}$ involves the weight percent of voids from entrained air ($Va_{\%wt}$), aggregate ($Vag_{\%wt}$), and pore network ($Vfw_{\%wt}$). However, during conditioning, the monitored mass loss

came exclusively from water inside the aggregate and the pore network since the voids from entrained air were empty during casting. Therefore, a correction factor (cf_{fw}) was developed to compute the mass loss from the free water. The results are shown in Table II.2.

$$cf_{fw} = Vfw_{\%wt} / [\ TV_{\%wt} - Va_{\%wt}\ ] \qquad (II)$$

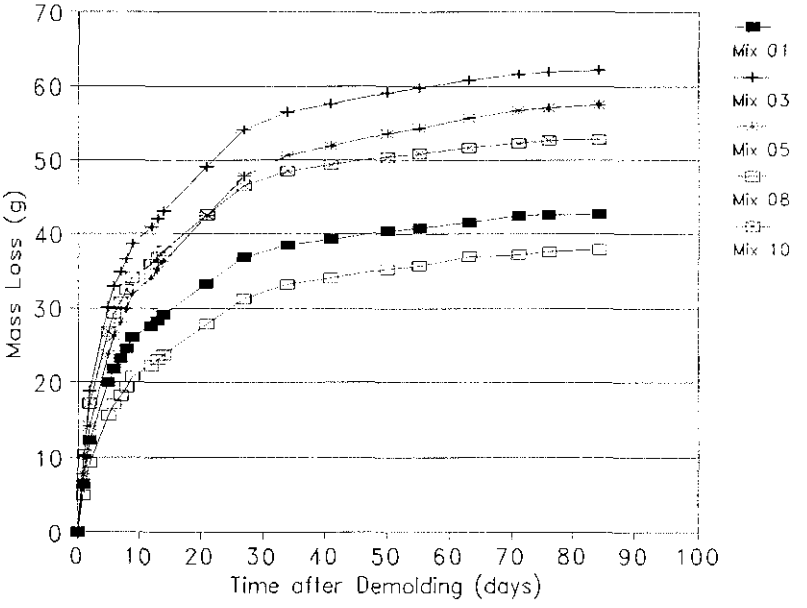

Figure II.3. Mass loss as a function of time during the conditioning period.

The drying behavior also can be described by a Water-Loss Ratio (***WLR***) figured as the mass of the free water loss (***Mfw***) divided by the mass of the mix-design water (MW_{mix}). The latter is the mass of water that needs to be added to the mix when the aggregate is assumed to be in the saturated-surface dry (***SSD***) condition.

$$Mfw = cf_{fw} \quad ML \qquad \text{(III)}$$

$$WLR = Mfw \,/\, MW_{mix} \qquad \text{(IV)}$$

The ***WLR*** is shown in Figure II.4 for all mixes as a function of time (in logarithm scale) during the conditioning period. In this representation, mixes 05 and 10 had the extreme behavior, having lost by day 85 almost 27% of the mix-design water. At the same time, mix 03 lost around 26%, mix 01 lost 22%, and mix 08 only lost 20% of the mix-design water. Figure II.4 was used to decide on the termination of the conditioning period. The period was terminated when the slope of the ***WLR*** with respect to time in a logarithm scale was consistently one half or less of that of the initial trend. This condition was reached for all mixes by day 90.

Table II.2. Concrete porosity (weight-based).

Mix	Weight % Solids[§]	Weight % Voids				Correction factor (cf_{fw})
		($TV_{\%wt}$)[§]	($Va_{\%wt}$)[†]	($Vag_{\%wt}$)[†]	($Vfw_{\%wt}$)	
01	93.83	6.17	0.53	2.35	3.29	0.58
03	92.59	7.41	0.55	2.41	4.45	0.65
05	90.27	9.73	0.55	2.41	6.77	0.74
08	93.16	6.84	0.58	2.36	3.90	0.62
10	93.39	6.61	0.81	2.38	3.42	0.59

[§]From modified ASTM C 642 test

[†]From Appendix 1

Figure II.5 shows the change in the residual w/c (***RWC***) as a function of drying time. This ***RWC*** is figured as the mass of the mix-design water used minus the mass of the free water loss, divided by the mass of the cementitious material (***Mcm***).

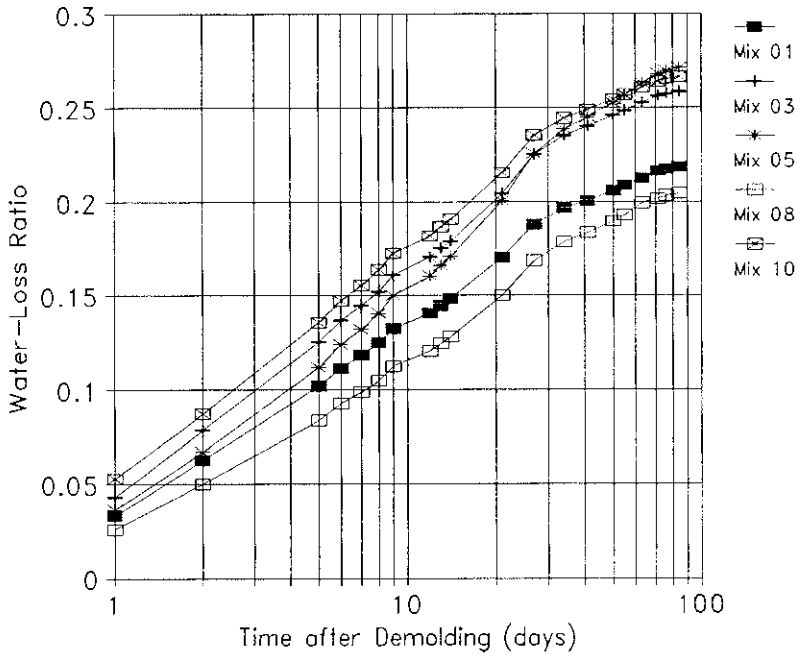

Figure II.4. Water-loss ratio as a function of time.

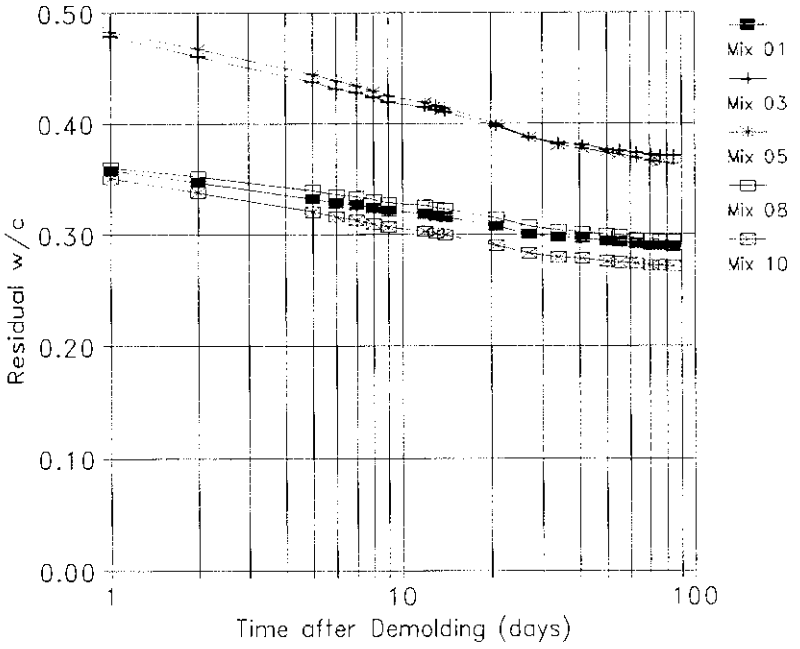

Figure II.5. Change in the residual w/c as a function of drying time.

$$RWC = [\, MW_{mix} - Mfw \,] / Mcm \qquad (V)$$

At the end of the conditioning period, the ***RWC*** for mixes 03 and 05 was about 0.37. For the mixes with low w/c (mixes 01, 08, and 10), the final ***RWC*** was between 0.27 and 0.29. Notice that during the first 10 days after demolding the slope for mix 10, which had an initial w/c of 0.37, was different from that of mixes 01 and 08, both having an initial w/c of 0.37.

4.2.1.2 Concrete Resistivity

While drying, the specimens experienced a concurrent increase in their resistivities as shown in Figure II.6. Each value is an average of 13 cylinders (see Appendix 4.3). Notice that, although the resistivity of mix 10 was in the same order as the resistivities of mixes 01, 03, and 05 at the beginning of the conditioning period, the resistivity of mix 10 increased to reach and exceed that of mix 08 after 30 days. At the end of the conditioning period the resistivities of mixes 01, 03, and 05 were very similar regardless of the design w/c value. The resistivity of mix 10 was almost twice the resistivity of mix 08, and more than four times the resistivity of the mix 01, 03, and 05 group.

The resistivity trends with time of the selected specimens kept in the 100% R.H. chamber (Figure II.7) were quite different from those exposed to laboratory air. All specimens at 100% R.H. increased their resistivities in the logarithm scale linearly with time for about 30 days after demolding (45 days after casting). This behavior may reflect the progress of pozzolanic reaction of FA with calcium hydroxide. After this period all the resistivities remained nearly stable. Notice that the behavior of the resistivity of mix 10 (50% FA) was different from the others.

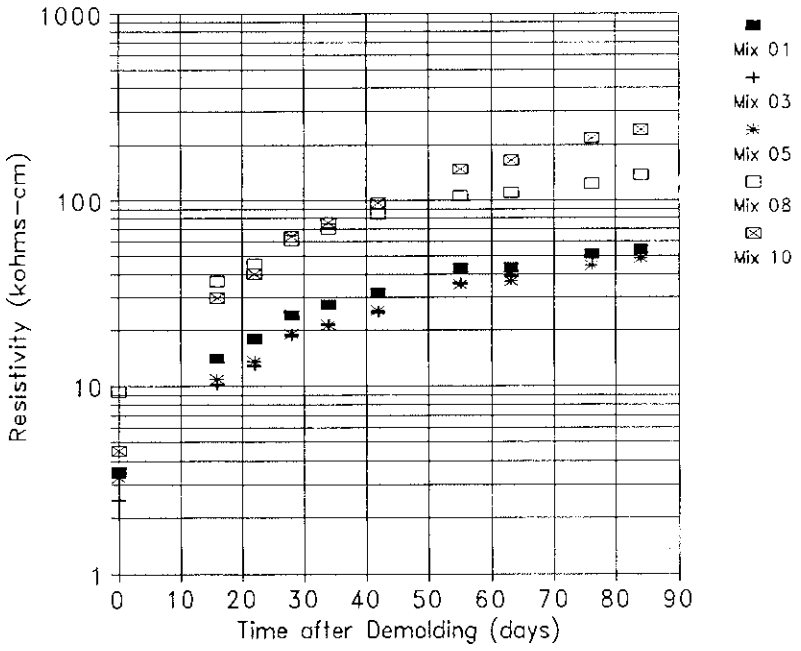

Figure II.6. Concrete resistivity of specimens during the lab air environment conditioning period.

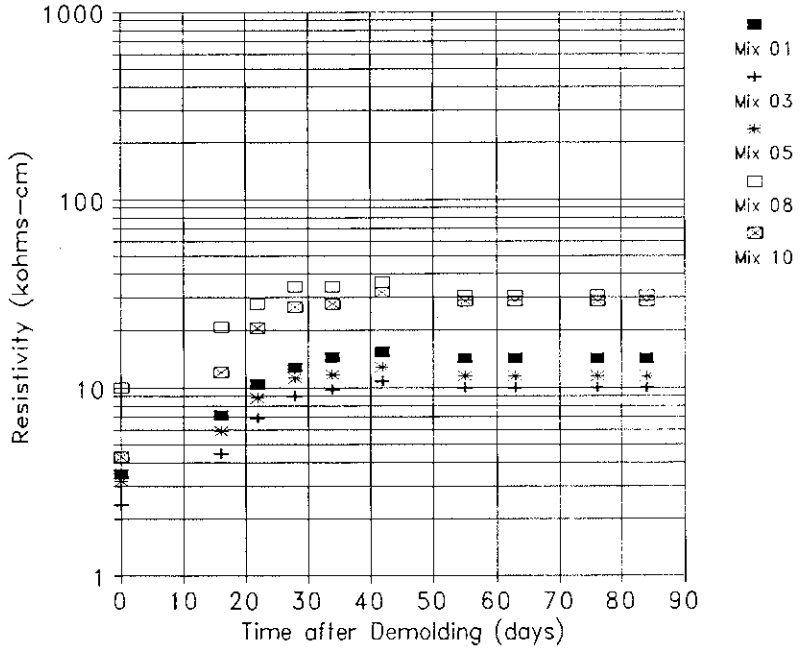

Figure II.7. Concrete resistivity of specimens in the 100% R.H. chamber.

At the beginning of the wet conditioning period, the resistivity value of mix 10 was in the same order as that of the other mixes without SF (~4 kΩ-cm) although the resistivity of mix 08 was about 10 kΩ-cm. However, after the wet conditioning period the resistivity of mix 10 was in the same order as that of mix 08 (~30 kΩ-cm)—two times more than those of the other mixes with 20% FA (~10 kΩ-cm).

4.2.1.3 Rapid Chloride Permeability Test

90 days after demolding the ***RCPT*** was performed at the FDOT Materials Office Laboratory with a set of selected "4 by 8" specimens that had been continuously kept in a 100% R.H. environment.

The results showed that mixes 03 and 05 had chloride permeability values in the "Low" classification (from 1000 to 2000 C), while mixes 01, 08, and 10 had permeability values in the "Very Low" classification (less than 1000 C). The results are plotted in Figure II.8 as a function of the resistivity (ρ) at 100% R.H. of each concrete mix at the time of ***RCPT*** determination.

There was a close correlation of the ***RCPT*** coulomb values with the resistivity values of each mix measured in the fully wet condition before the ***RCPT***. The correlation matched well the resistivity-***RCPT*** test relationship (ρ=4887 $C^{-0.832}$) obtained by Berke and Hicks [II.29], denoted by the solid line in the figure.

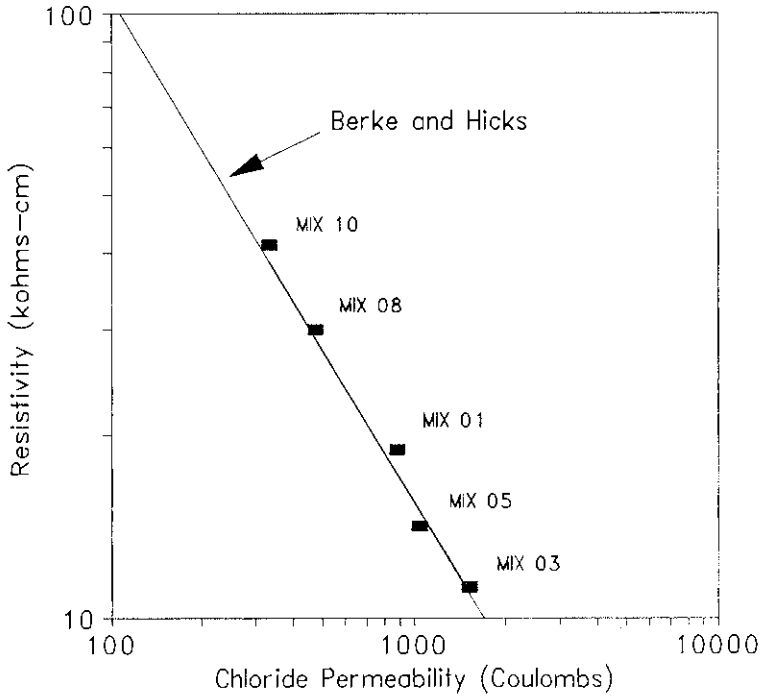

Figure II.8. Correlation between concrete resistivity and Rapid Chloride Permeability Test results.

4.2.2 CO_2 Exposure Environment

4.2.2.1 Mass Gain

The masses of the selected "3 by 6" specimens monitored during the CO_2 exposure period are plotted as a function of time in Figure II.9. This exposure started immediately after the conditioning period. The mass gain reflected the reaction with the carbonating environment. Notice that the mixes with high w/c

(mixes 03 and 05) gained more mass than the mixes with low w/c (01, 08, and 10). The mass of the specimens showed also sensitivity to the small variations of the chamber R.H. within the control range (60%±5%).

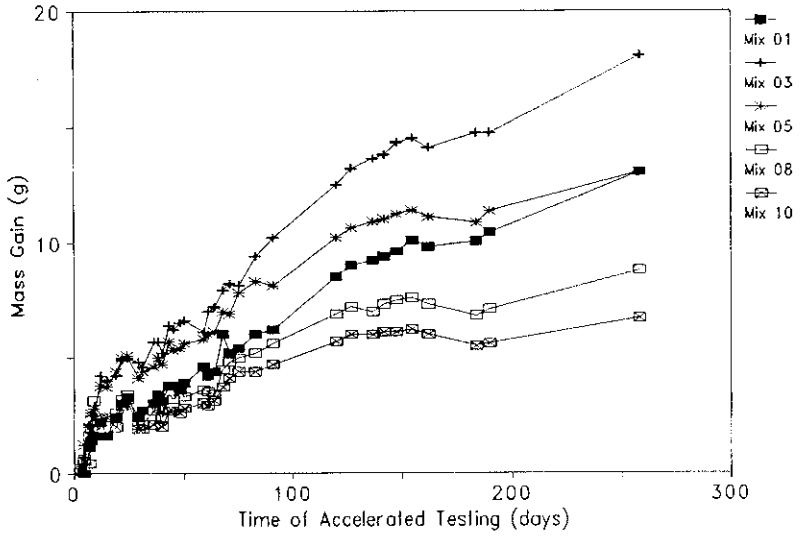

Figure II.9. Mass gained of "3 by 6" concrete specimens during carbonation in a 0.5% CO_2 environment.

4.2.2.2 Half-Cell Potential Measurements

During the conditioning period the rebar potentials from all mixes became more positive with increasing time (see Figure II.10). The more positive potential at the end of this period was found in mix 08, although at the beginning of the testing period this mix had the less positive rebar potential. The average potentials at the end of conditioning of mixes 01, 03, and 10 were near -50 mV

vs. ***CSE***. The less positive potential was found in the chloride-contaminated mix 05 (near -80 mV vs. ***CSE***).

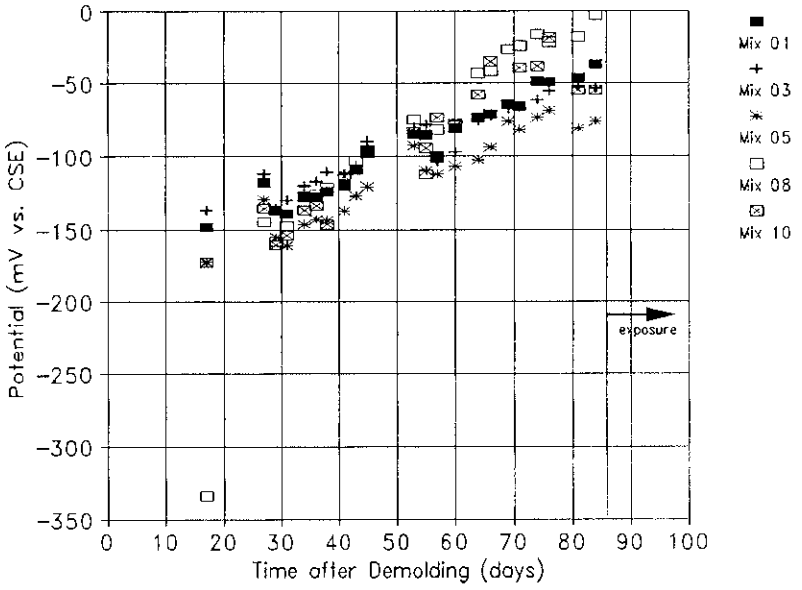

Figure II.10. Evolution of rebar potentials during the conditioning period. Each value is an average of 12 specimens.

During the actual testing (exposure to 5000 ppm of CO_2) period the average potentials for each mix remained stable for about 170 days (Figure II.11). The chloride-contaminated mix 05 was the first concrete mix where the rebars showed the onset of a trend toward less positive values (day 175 of accelerated testing). Concrete mix 03 was the second to show a transition (day 190 of accelerated testing), but after a small potential shift (25 mV) in the less noble direction, the rebar potentials became stable again. Concrete mix 10 experienced a transition in day 200 of accelerated testing. The rebar potentials in this mix showed a continuing shift in the less noble direction, but at a slower

rate than that of the rebars in mix 05. The potentials of the rebars in mixes 01 and 08 did not show significant variation. See Appendix 4.4 for the detailed listing of results.

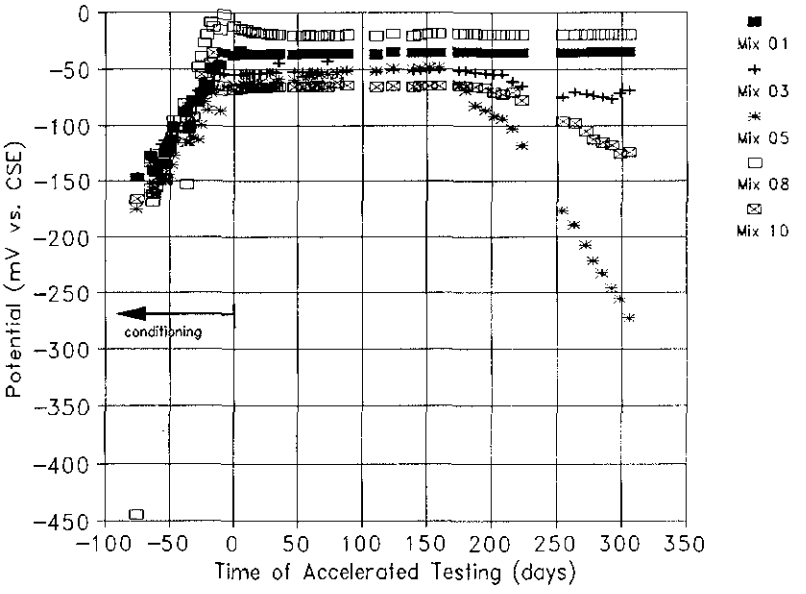

Figure II.11. Evolution of rebar potentials. Negative time values correspond to the conditioning period; positive time values denote exposure in the accelerated test chamber (0.5% CO_2). Average of 6 specimens.

4.2.2.3 Electrical Resistance Measurements

The interbar concrete resistance of the instrumented specimens is plotted as function of time in Figure II.12. Each value is an average of 3 concrete prisms. Notice that the slope of the curves for the mixes 01, 03, 05, and 10 changed at the time that the specimens were put in the accelerated test chamber (around 90 days after demolding). Also, the slope of the curve for mix 03 began

to change again after 150 days in the chamber, and the curve surpassed that of mix 08 after 280 days in the chamber. The resistance of mix 03 increased nearly 10 times during the period in the chamber. During the same period the resistance of mixes 01, 05, and 10 increased more than 4 times, and the resistance of mix 08 increased more than 3 times.

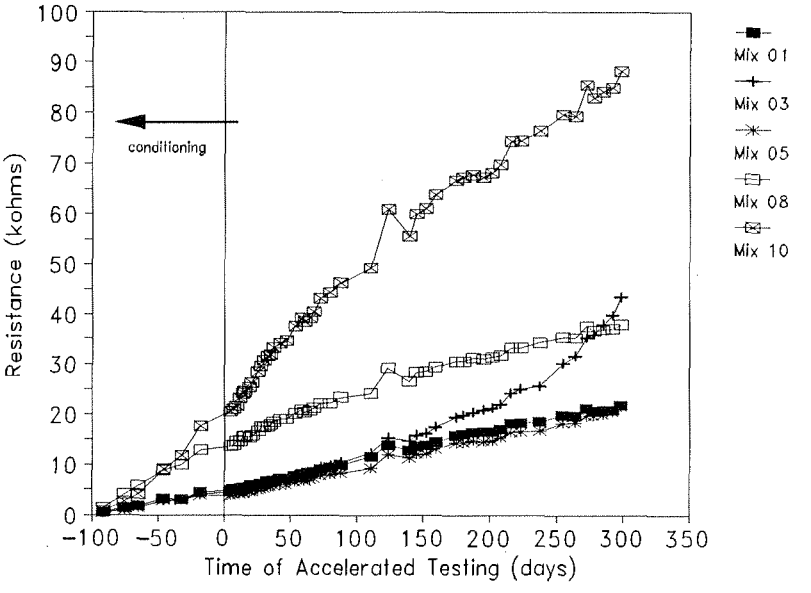

Figure II.12. Average interbar concrete resistance per mix design of instrumented specimens.

4.2.2.4 Polarization Resistance Measurements

The $\mathbf{Rp_{ap}}$ results from the galvanostatic step technique (***GST***) tests are shown in Figure II.13. Those results are the average of 6 rebar specimens per mix design (see Appendix 4.5).

The average $\mathbf{Rp_{ap}}$ values in all concrete mixes had generally increasing trends, except for mixes 05 and 10 that experienced a trend reversal starting around day 200. The relative change in trend was greater in mix 05 than in mix 10. Notice that these changes correlate well with the potential behavior transitions (Figure II.11) observed for the same specimen groups at the same time.

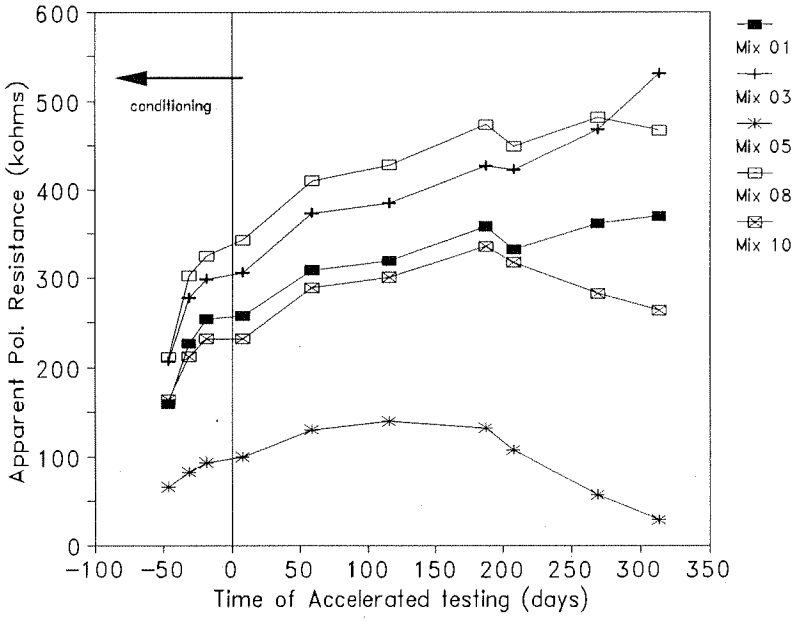

Figure II.13. Average $\mathbf{Rp_{ap}}$ as a function of time. Steel area = 31 cm^2.

Figure II.14 shows the impedance response of a rebar specimen in concrete mix 01 (20% FA, w/c=0.37, no chloride) at different dates. This response was typical of specimens having high polarization resistance values (by either of the various methods used). In contrast, Figure II.15 shows the response of a rebar specimen in concrete mix 05 (20% FA, w/c=0.50, chloride

contaminated), typical of specimens showing low polarization resistance values. Both specimens had concrete resistance values of the same order. Notice that because of the position of the ***ATR***, the concrete resistance values from the ***EIS*** diagrams are half of those reported in Figure II.12 for the same mixes and times.

The $\mathbf{Rp_{EIS}}$ was evaluated using the low frequency portion of the spectrum (f<10 Hz). The results for data obtained near day 300 are given in Table II.3. The upper limit of detection of $\mathbf{Rp_{EIS}}$ was ~4 MΩ. All reported values are in Ω. To convert to area-normalized impedance, the reported values can be multiplied by the nominal steel area in contact with concrete (31 cm^2).

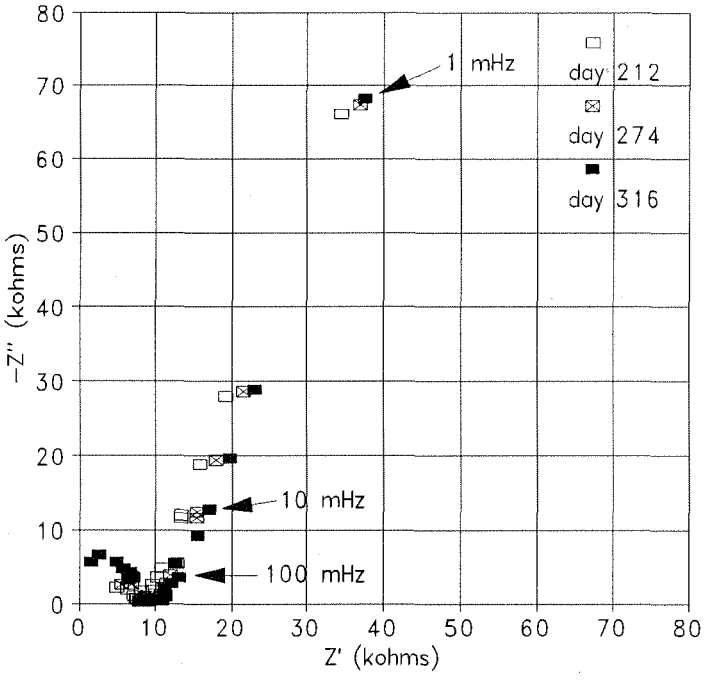

Figure II.14. Typical Nyquist plot of a rebar specimen in concrete mix 01.

A summary of the Rp_{EIS}, Rp_{PR}, and Rp_{GST} results near day 310 of accelerated testing is presented in Table II.3. The three methods gave consistent results in most cases, considering that the admittance of the corrosion reactions was often very small. The best correlation was between Rp_{PR} and Rp_{EIS} results in the range 10 - 100 kΩ.

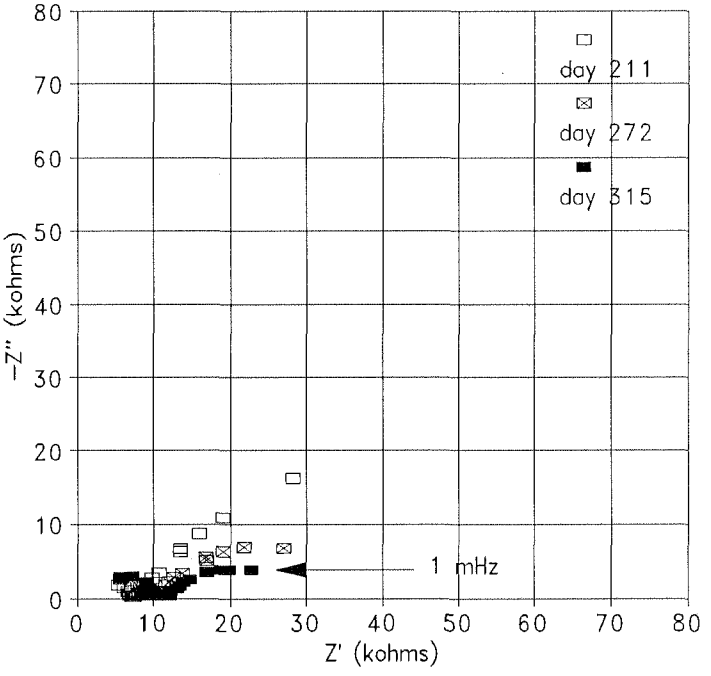

Figure II.15. Typical Nyquist plot of a rebar specimen in concrete mix 05.

Table II.4 shows the average values of Rp_{GST} and the ***CPE*** constants (**Yo** and ***n***) evaluated near day 310. Each value is an average of six rebars per mix design. The behavior of **Yo** and ***n*** with time is presented in Figure II.16. Those

Table II.3. **Rp** values from different tests near day 310 of accelerated testing.

		Rp values (kΩ)		
Concrete Mix	Specimen	***EIS***	***PR***	***GST***
01	011X			600
	012X	910	430	560
	013X			840
	011Y			940
	012Y	>4000	650	1200
	013Y			2000
03	031X	2500	680	1600
	032X			1800
	033X			1300
	031Y	>4000	940	1300
	032Y			1400
	033Y			900
05	051X	27	25	48
	052X	21	17	33
	053X	17	16	31
	051Y	25	24	22
	052Y	18	15	16
	053Y	82	52	61
08	081X	>4000	580	700
	082X			1600
	083X			1200
	081Y	>4000	1100	2400
	082Y			1400
	083Y			1200
10	101X	1900	450	600
	102X			1100
	103X			300
	101Y	3700	230	380
	102Y			500
	103Y			400

values were evaluated from ***EIS*** results and are the average of two selected rebars per mix design. Notice that the **Yo** values were decreasing with time for each mix design but mix 01. On the other hand, ***n*** values for mixes 03, 05, and 10 were decreasing with time. The values of **Yo** and ***n*** from ***EIS*** results (Figure II.16) were generally consistent with those obtained from ***GST*** (Table II.4) at day 313. The only severe discrepancy is in the results obtained from mix 05.

Table II.4. Average values of **Yo** and ***n*** from ***GST*** tests at day 313.

Mix	**Rp** (kΩ)	$10^4 \cdot$ **Yo**	σ_{Yo}	***n***	σ_n
01	1000	8	1.26	0.82	0.02
03	1400	3	0.68	0.76	0.04
05	35	12	5.80	0.70	0.13
08	1400	7.5	1.54	0.85	0.02
10	550	4	0.80	0.71	0.04

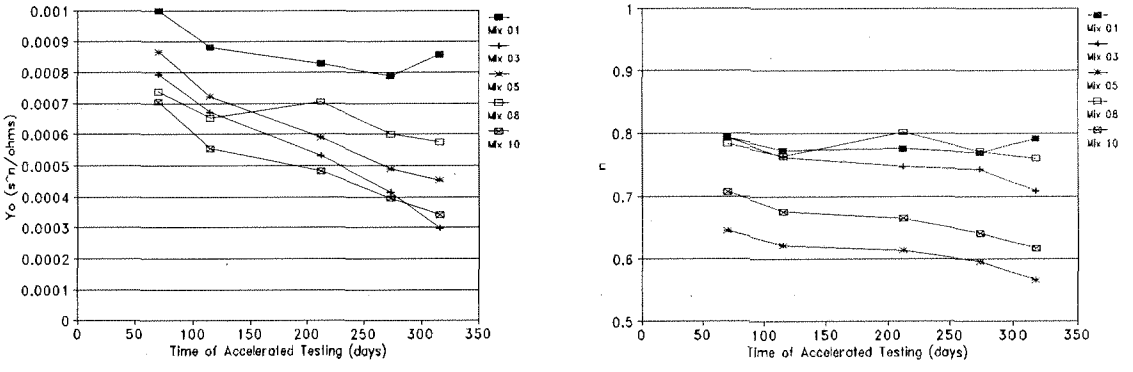

Figure II.16. Values of **Yo** and ***n*** as a function of time from ***EIS*** tests.

The values of $\mathbf{Rp_{ap}}$ (not shown in Table II.3) were in good agreement with the results from the other procedures for mix 05. As expected, the polarization resistance was somewhat underestimated by $\mathbf{Rp_{ap}}$ in the other mixes for which the admittance of the corrosion reactions was small [II.15]. $\mathbf{Rp_{ap}}$ was nevertheless useful for comparison purposes (as in Figure II.13) and was used for ease of computation in this preliminary processing of the results to date.

4.2.3 Carbonation Depth Measurements

At the end of the conditioning period, two cylinders per mix design were split open and tested with both phenolphthalein and Thymolphthalein indicators, to determine the depth of carbonation. Those specimens were previously designated as controls, and the results are shown in Table II.5, as an average of two specimens—each one in turn an average of seven measurements around the cracked section perimeter.

Table II.5. Carbonation depth at day 0 of accelerated testing.

	Mix 01	Mix 03	Mix 05	Mix 08	Mix 10
Average (mm)	1.1	2.2	2.5	1.4	2.6

These results showed an increasing carbonation depth as the cement content decreased when going from mix 01 to mix 08 to mix 10. The carbonation

depth increased as the w/c increased from 0.37 in mix 01 to 0.50 in both mixes 03 and 05 (see Table II.1 for mix designs). There was no difference in the measured carbonation depth when either phenolphthalein or thymolphthalein was used. However the color changes when using phenolphthalein were better defined, specially when examining concretes containing SF. Based on the above, thymolphthalein was not used for carbonation testing in the rest of this study.

After 120 days of accelerated testing, two specimens per mix design were split open and tested with phenolphthalein indicator. The results are shown in Table II.6. Each value is an average of the total carbonation depth of the two specimens—each one in turn an average of eight measurements.

Table II.6. Carbonation depth at day 120 of accelerated testing.

	Mix 01	Mix 03	Mix 05	Mix 08	Mix 10
Average (mm)	8.4	12.2	12.6	11.1	13.7

The correlation between carbonation depth (after subtracting the initial carbonation depths in Table II.5) and cement content is plotted in Figure 17A. Notice that for concretes with the same w/c (mixes 01, 08, and 10), the carbonation depth varies as a function of the cement content. On the other hand, for concretes with the same cementitious content (mixes 01, 03, and 05), the carbonation depth varies as a function of w/c, as plotted in Figure II.18A.

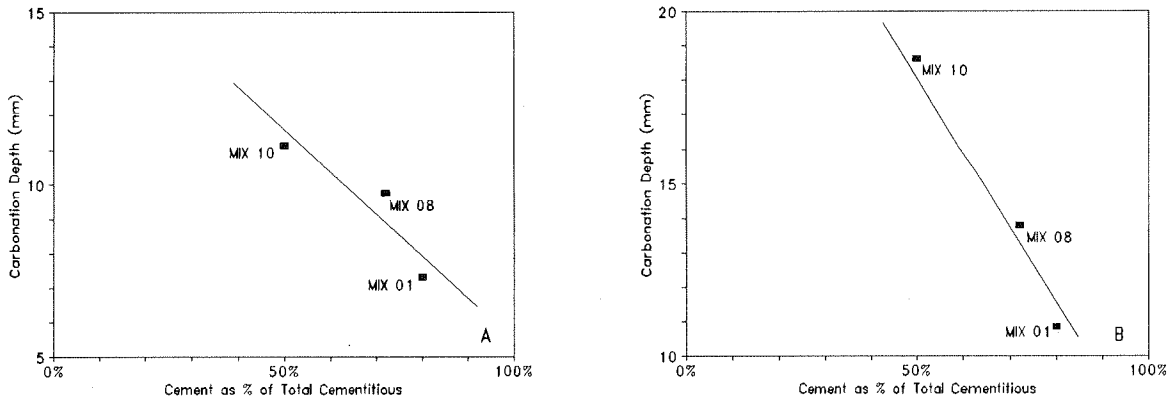

Figure II.17. Carbonation depth (initial carbonation depth subtracted) as a function of the cement content at A) 120 days of accelerated testing, B) 260 days of accelerated testing.

After 260 days of accelerated testing two specimens per mix design were tested with phenolphthalein indicator to determine the carbonation depth. The results are shown in Table II.7.

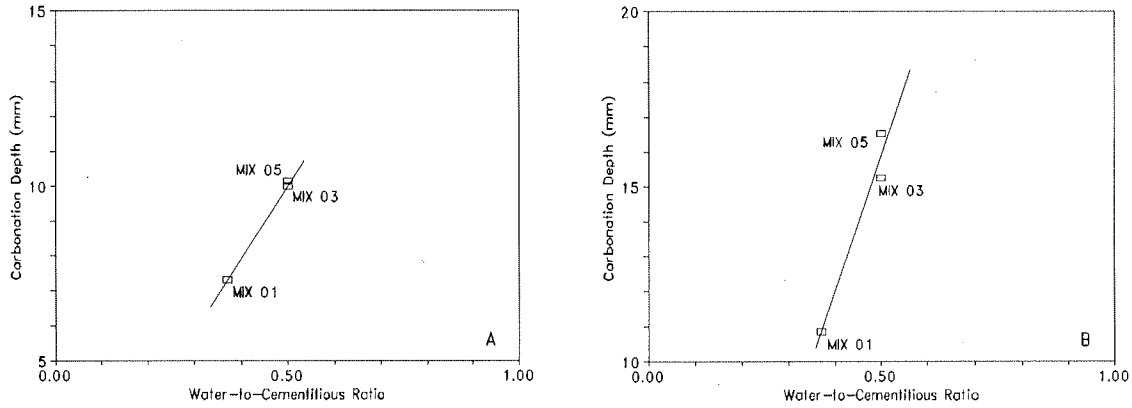

Figure II.18. Carbonation depth (initial carbonation depth subtracted) as a function of the water-to-cementitious ratio at A) 120 days of accelerated testing, B) 260 days of accelerated testing.

Table II.7. Carbonation depth at day 260 of accelerated testing.

	Mix 01	Mix 03	Mix 05	Mix 08	Mix 10
Average (mm)	12.0	17.4	19.0	15.2	21.2

Figure II.19 shows a picture of the phenolphthalein test for a sample of each concrete mix after 260 days of accelerated testing. The picture was taken just after spraying the pH indicator on the freshly broken surface of the samples. The specimens are arranged by increasing carbonation depth (from left to right). In that order, the concrete mixes are 01, 08, 03, 05, and 10. Notice the higher carbonation depth for the samples with high w/c (mixes 03 and 05) or high pozzolanic replacement (mix 10), compared with the carbonation depth of the control mix 01.

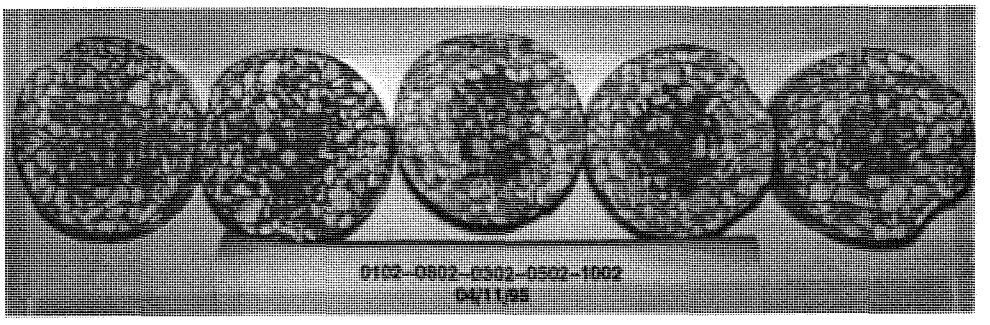

Figure II.19. Carbonation depth determination using phenolphthalein. Determination at 260 days of accelerated testing. From left to right, mixes 01, 08, 03, 05, and 10.

The trends of carbonation depth (after subtraction of initial carbonation depth) as a function of the cement content, and as a function of the w/c are plotted in Figure II.17B and Figure II.18B, respectively. These and previous

results (at days 0 and 120 of accelerated testing), indicate that the carbonation depth increases as the cement content decreases, and as the w/c increases.

The carbonation depth (after subtraction of initial carbonation depth) as a function of the 28-day compressive strength test is shown in Figure II.20. The carbonation depth decreased as the compressive strength increased when the cementitious material was the same (mixes 01, 03, and 05).

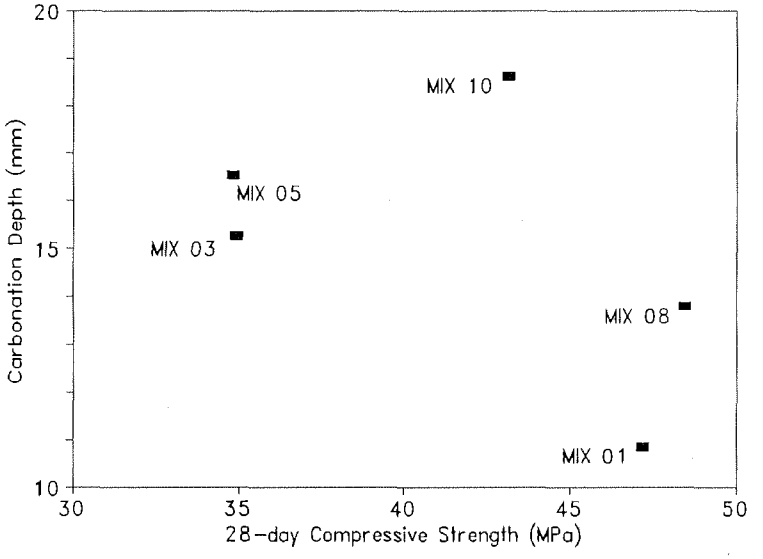

Figure II.20. Carbonation depth (initial carbonation depth subtracted) as a function of the 28-day Compressive Strength, at 260 days of accelerated testing.

The maximum, mean, and minimum carbonation depths per mix design at day 260 of accelerated testing are plotted in Figure II.21. The large variation between minimum and maximum carbonation depths underscores the variability of the carbonation depth, reflecting the existence of preferential gas transport paths as for example through porous aggregates. The carbonation penetration

depth in the instrumented specimens is expected to have been comparable (although a detailed analysis would be needed to account for the differences between the prismatic and cylindrical geometries). Notice that although in only one concrete formulation (mix 10) the average carbonation depth exceeded the steel concrete cover depth in the prismatic specimens (20.6 mm), the maximum carbonation depth values in mixes 03 and 05 also surpassed that value. This observation may account for the electrochemical activity observed in those three mixes as shown in Figures II.11 and II.13.

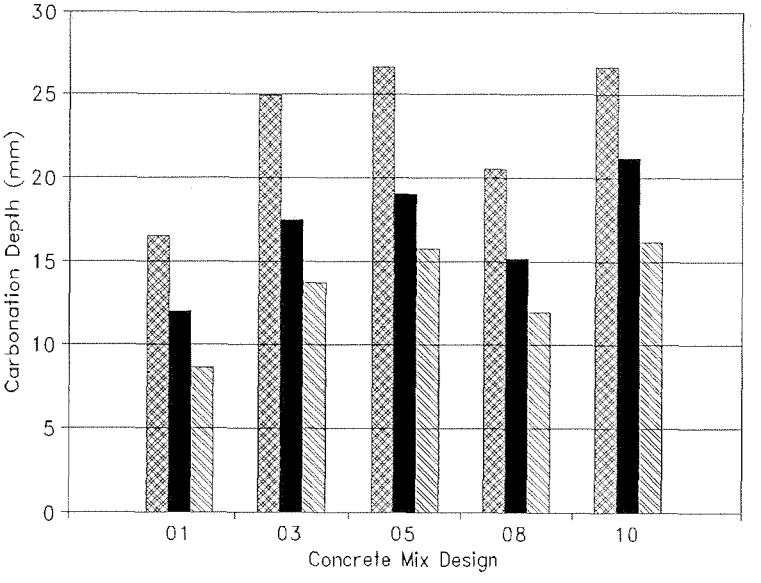

Figure II.21. Maximum, average, and minimum carbonation depth for each concrete mix at day 260 of accelerated testing.

On first approximation the carbonation progress under uniform exposure conditions may be expressed by the empirical relation:

$$x = K \cdot t^{1/2} \qquad \text{(VI)}$$

which can also be derived from simplified theoretical treatment (Appendix 4.6).

In eq. VI, x is the carbonation depth in mm; t is the carbonation time in years; and K is the carbonation coefficient in mm/y^{½}. Typical values of K in actual structures exposed to atmospheric CO_2 [II.30, II.31] are on the order of 3 mm/y^{½} (dense concretes) to up to 10 mm/y^{½} (less dense concretes).

To determine the carbonation coefficient of each concrete mix, the carbonation depths were first nominally converted from carbonation depths in a cylinder to carbonation depths in a flat surface. The procedure to make the conversion is shown in Appendix 4.7. This conversion was needed to overcome the corner effect penetration in the cylinder specimens. The converted carbonation depths at 120 and 260 days are presented in Table II.8 (see Appendix 4.8).

Table II.8. Converted carbonation depths assuming a flat surface.

	Mix 01	Mix 03	Mix 05	Mix 08	Mix 10
at 120 days	8.0	11.5	11.8	10.4	12.8
at 260 days	11.3	15.9	17.1	14.1	18.7

The values of Kc (carbonation coefficient under accelerated testing conditions) from the converted carbonation depths are presented in Table II.9. These values were also corrected from initial carbonation prior to accelerated exposure following the procedure shown in Appendix 4.6. Notice that these carbonation coefficients are for test chamber exposure to a CO_2 molar

concentration of 0.5% (5000 ppm) in air. Conversion to atmospheric exposure conditions is given in the Discussion section.

Table II.9. Values of ***Kc*** at CO_2 = 0.5% (in mm/$y^{½}$). Corrected for geometry and pre-existent carbonation.

	Mix 01	Mix 03	Mix 05	Mix 08	Mix 10
at 120 days	13.9	19.6	20.1	18.1	21.8
at 260 days	13.3	18.7	20.1	16.6	22.0

4.3 DISCUSSION

4.3.1 Conditioning Period

Fraay et al. [II.32] showed that the pozzolanic reaction of the FA class "F" begins in wet concrete typically after about 2 weeks of casting, when the OH^- concentration becomes high enough to dissolve the fly ash particles. The presence of this effect in the specimens kept in a 100% R.H. chamber was supported (Figure II.7) by the observed increase in the resistivity of all mixes for a period ending at 45 days after casting (30 days after demolding). This increment in resistivity due to the pozzolanic reaction has been reported by Bijen and Pietersen [II.33]. All this implies that during the first days the FA behaves mostly as an inert material.

Therefore, when the specimens were exposed to the lab air environment immediately after the 14-day curing period, they had an excess of water (from the w/c mix design), since the FA has not starting to react. This was true

especially for mix 10 (50% FA). The mass loss after demolding for mix 10 differs from the others (Figure II.3), in that during the first 10 days the mix 10 specimens lost water at the same rate than specimens from mixes 03 and 05, both also with w/c=0.50; but after a transition from day 10 to day 30, the rate of water-loss of mix 10 resembled that of mixes 01 and 08, both with w/c=0.37.

Because of drying, the specimens conditioned in the lab air environment experienced a concurrent increase in their resistivities. However, two well defined stages can be observed in Figure II.6. The first one involves the first 30 days after demolding, in which the increase in resistivity is most likely due to both drying of the outer concrete layer and further hydration of the inner concrete core. This early behavior resembles that of the selected specimens kept in the 100% R.H. condition (Figure II.7). Once the hydration of the concrete reached a very low rate (almost negligible) after 30 days of curing, the increase in resistivity for the specimens in the lab air environment can be expected to have been primarily due to drying.

Notice that the resistivity in mix 10 surpassed that of mix 08 at the end of the test period (Figure II.6). Also, the resistivity behavior of the mix 10 specimens in the lab air environment differed from that of the mix 10 specimens kept at 100% R.H. (in the 100% R.H. chamber the resistivity of the mix 10 specimens did not surpass that of mix 08 specimens); and that could be explained by the excess of water lost during the first 10 days after demolding due to the unreacted FA. This implies that less electrolyte (for this concrete mix with a w/c=0.37) was held in the pore network, therefore a lower conductivity concrete was obtained.

Additionally to the scope of this investigation the correlation between the ***RCPT*** and the resistivity measurements verified the findings of Berke and Hicks [II.29]. Therefore, it is suggested that instead of performing a time-consuming

semi-destructive ***RCPT***, the same results can be obtained for this type of concretes from a quick non-destructive measurement of the concrete resistivity. However, care should be exercised while trying to correlate corrosion-risk prediction with resistivity or ***RCPT*** results without considering concrete porosity, degree of water saturation, pozzolanic replacement, and pore solution composition [II.34]. Further research involving different types and amounts of pozzolanic replacement is needed to thoroughly confirm these findings.

4.3.2 CO_2 Exposure Environment

Although the weight gain in the chamber gave a rough indication of the progression of the carbonation process, the results need to be complemented by further analysis of the decomposition of CH and C-S-H by CO_2. The weight gain method is helpful when looking for complete carbonation which is reached when the specimens achieve constant weight [II.35].

The electrochemical behavior of the rebars in the control mix 01 indicated that the steel was still passive at the end of the testing period (Figure II.11). The potentials remained stable at noble values in agreement with the high polarization resistance values obtained. Both the potential and $\mathbf{Rp_{ap}}$ trends matched the expected behavior based on the average carbonation depth shown in Figure II.21. According to the carbonation depth measured at the end of the testing period, there was no carbonation in the plain specimens at the depth where the steel surface is located in the instrumented specimens, and therefore no corrosion was expected.

The potential data for steel in mix 03 showed erratic behavior after 190 days in the CO_2 chamber. The likelihood that this behavior was due to the carbonation front having reached the steel surface is supported by the total

carbonation depth shown in Figure II.21. However, this potential behavior was not matched by a transition in the $\mathbf{Rp_{ap}}$ trend (Figure II.13). This may be explained by the high concrete resistance which at the end of the testing period surpassed that of SF mix 08. According to Alonzo et al. [II.35], large $\mathbf{Rp_{ap}}$ values are commonly observed when the concrete resistance is high. In the case of the steel in the high concrete resistance (mix 03), the high baseline $\mathbf{Rp_{ap}}$ values could overshadow a small variation due to the carbonation front arrival.

Alonzo et al. [II.35] showed that there was a linear correlation (in a log-log scale) between corrosion current density and the electric concrete resistance for rebars embedded in carbonated mortars regardless of the amount and composition of the pozzolanic replacement. Feliu et al. [II.36] noted that although the resistivity and **Rp** are not necessary a function of each other, both depend on the degree of humidity of the concrete. Therefore, it was assumed by Feliu et al. [II.36] that the corrosion attack in carbonated concrete will be limited to the metal zones in contact with the pore solution and be negligible at the relatively dry zones. The authors proposed that the measured value of **Rp** is inversely proportional to the fraction of wetted surface and that if the corrosion rate of rebars embedded in carbonated concrete were under resistive control, then the application of the Stearn-Geary equation would not be valid. However, they concluded that it is not the case because, due to the low R.H. (less than 85%) normally observed in carbonation-induced corrosion processes, diffusion transport of oxygen (needed for the cathodic reaction) is not likely to be limiting the rate of the corrosion reaction. Any variation in the R.H. affects the moisture inside the concrete, thus changing the anodic reaction rate. Glass et al. [II.37] stated that in carbonation-induced corrosion processes the anodic reaction rate is under resistive control and the overall corrosion rate is under anodic control. All the above arguments appear to be applicable to the findings of this

investigation, and in summary it may be proposed that the corrosion rate is limited by electrolyte availability.

In the chloride contaminated mix 05 the steel potential data showed a continuous shift toward less noble potentials after 175 days of testing. At the end of the testing period the potential data showed values typically associated with steel depassivation. This change was observed also in the $\mathbf{Rp_{ap}}$ trend that showed a continuous decrement after the same time. The assumption that both these changes were due to the carbonation front arrival was supported by the carbonation depth measurements (Figure II.21). Due to the chloride contamination, low concrete resistance was observed in spite of the high carbonation depth measured. The chloride contamination provided additional ionic charge carriers and the hygroscopic properties of the salt may have caused more water to be retained by the concrete [II.37]. Therefore a larger amount of electrolyte which was also more conductive was available (compared with mix 03 for the same w/c ratio). Although already during the first ***PR*** tests the steel rebars in mix 05 showed low $\mathbf{Rp_{ap}}$ values, these decreased by more than a half after the concrete was carbonated. This two-fold increase in the apparent corrosion current may be explained by assuming that the carbonation process released the bound chlorides [II.38], thus increasing further the amount of free chlorides in the pore solution. Since the carbonation process decreased the pH of the pore solution (which means a reduction in the concentration of OH^-), the Cl^-/OH^- ratio is expected to have increased as a result therefore elevating the corrosion risk even more [II.39, II.40].

The electrochemical behavior of steel in mix 08 showed no change during the testing period. The rebars in this concrete mix had the more noble potentials and the highest $\mathbf{Rp_{ap}}$ values among all mixes. However, it was confirmed in this

investigation that SF concrete experienced higher carbonation depth than the control FA concrete mix 01 [II.45].

The potential data from steel specimens in mix 10 showed a continuous shift toward less noble values after 200 days. At the same time the $\mathbf{Rp_{ap}}$ values decreased although only moderately. This could be explained by the high concrete resistance of mix 10, that increased the $\mathbf{Rp_{ap}}$ values as discussed earlier [II.35]. An assumption that the potential and polarization resistance behaviors were due to the carbonation front arrival was supported by the average carbonation depth measured in this mix, which was highest than in any other (Figure II.21). Notice that due to pronounced drying during the conditioning period (as discussed in previous section **4.3.1**), this mix had also the highest concrete resistance among all mixes, which generally means low electrolyte amount in the pore network (although low pH pore solution may have also contributed to high resistivity). Therefore, in spite of the onset of corrosion, the corrosion rate was likely to be limited by the high concrete resistivity.

The influence of w/c ratio on the carbonation process was evident only when the cementitious content and cement percent replacement was constant, as for mixes 01, 03, and 05. For those mixes, the higher the w/c ratio, the higher the carbonation rate. This was expected due to the high porosity of mixes 03 and 05 compared with mix 01, that allowed for a faster influx of CO_2. On the other hand, for the same cementitious content and w/c ratio, the rate of the carbonation process decreased with the cement content, as for mixes 01, 08, and 10. Let's assume that the final product of the carbonation process is primarily calcium carbonate, and recall that there was more calcium per unit volume (due to the cement content) in mix 01 than in mix 08, and more in mix 08 than in mix 10. Therefore, more CO_2 would be needed per unit volume (a higher

value of ***M*** in the terminology of Appendix 4.6) to react with all the carbonatable products, thus lowering the carbonation rate for a given CO_2 concentration.

Due to the geometry of the plain specimens a conversion from the carbonation depth in a cylinder to carbonation depth in a flat surface was needed. The conversion was calculated as shown in Appendix 4.7.

The calculated flat-front carbonation depth at day 260 is plotted in Figure II.22 as a function of the water-to-cement ratio (w/c^*) instead of the water-to-cementitious ratio. The penetration depth appears to be determined primarily by the cement content (notice nearly linear dependence with w/c^*) and not by the extent of pozzolanic addition, which varied significantly between mixes (correction of the carbonation depths to account for the small amount of pre-existing carbonation at the beginning of the test yielded essentially the same results). This suggests that the pozzolanic material behaves as an inert material for the carbonation process in spite of the increase in resistivity and compressive strength, and the decrease in porosity that usually results from pozzolanic replacement.

No correlation was found for the carbonation depth as a function of the 28-day compressive strength except for mix groups with the same cementitious content and percent replacement. This behavior paralleled the behavior from carbonation depth as a function of w/c described in Figure II.18.

This lack of correlation was expected since both the w/c and the 28-day compressive strength are related to the concrete porosity under the same conditions (i.e. curing time). It is worthy to mention that no correlation between

the 28-day compressive strength and the carbonation rate was found when different amounts and/or types of pozzolanic replacements were used in other investigations [II.42, II.43].

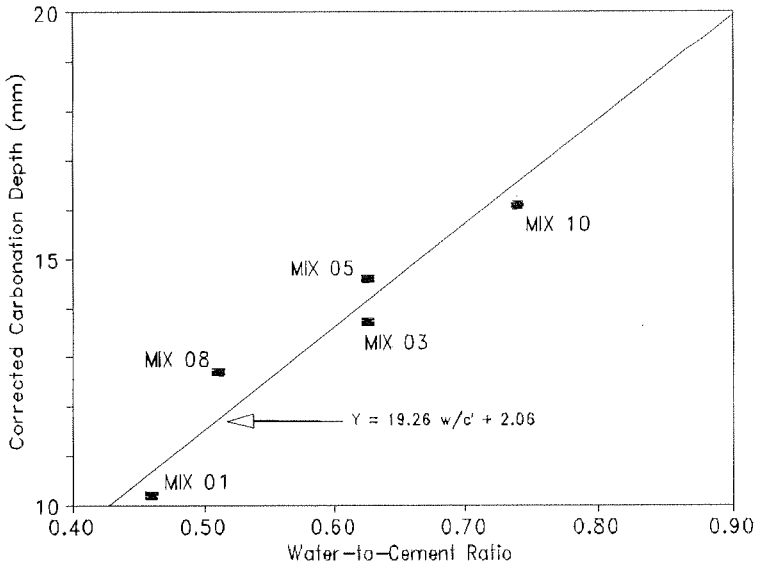

Figure II.22. Flat-front corrected carbonation depth for 260-day exposure at Pco_2 = 0.005 Atm., as a function of the water-to-cement ratio.

Visual inspection of the freshly broken concrete surface after spraying phenolphthalein (during carbonation depth measurements) showed a very irregular carbonation front, specially where coarse aggregate was located. Presumably, this aggregate was very porous and quickly lost the water inside,

allowing the air to flow deeper into the concrete. Experiments using a different type of stone (river-rock) are now in progress to clarify this issue.

4.3.3 Implications for Service Life Prediction

The end of the initiation period of carbonation-induced corrosion can be assumed to occur when the carbonation depth exceeds the rebar cover thickness X_c. The nominal time t_c for corrosion initiation is then given by eq. (6.6) in the Appendix 4.6.

$$t_c = X_c^2 / K_a^2 \qquad \text{(VII)}$$

where K_a is the carbonation coefficient under atmospheric exposure conditions (CO_2 about 0.03%). The value of K_a can be estimated from the accelerated exposure tests by using the simplifying assumptions of Appendix 4.6 that yields K_c $(C_{CO_2})^{1/2}$. Since in the experiment C_{CO_2} = 0.5%, then $K_a = (4.08)^{-1} K_c$. This correlation was used also by Papadakis et al. [II.5] while comparing carbonation depths from different investigators. The values of the carbonation coefficients thus estimated for natural exposure under adverse R.H. conditions are presented in Table II.10. Carbonation coefficients estimated from the shallow carbonation depth experienced during the atmospheric conditioning period at 65% R.H. are also presented in Table II.10, showing good agreement despite the relative short conditioning time and changing concrete conditions.

In a reinforced structure with a concrete cover of 5.1 cm (2"), and a desired service life of 75 years without steel depassivation, the carbonation coefficient should be less than 5.8 mm/y^{½} [II.44]. Under those assumptions all the concrete mixes tested had a low-enough carbonation coefficient even at the severe 60% R.H. regime used (see Table II.10). However, if the concrete cover for the same structure were only 2.5 cm (1"), the required carbonation coefficient should be less than 2.9 mm/y^{½}. For a 2.5 cm cover, mix 01 (20% FA) would start to show steel depassivation after 54 years. For mix 08 (20% FA + 8% SF cement replacement) the steel would start to show depassivation after 34 years. By increasing the FA replacement from 20% to 50% the steel depassivation would begin after only 21 years. In other words, the corrosion initiation period would be reduced by 60% when increasing the FA content (as cement replacement) from 20% to 50%; by 50% by increasing the w/c from 0.37 to 0.50; and by 35% by adding 8% SF (as cement replacement). The calculated effect of reducing cover lends support to establishing specifications for thick concrete cover, such as those used by FDOT [II.45] that required 5.1 cm (2") of cover for Cast-in-Place superstructures and 7.6 cm to 10.1 cm (3" to 4") for Cast-in-Place substructures. The calculations suggest that with proper construction control, new structures reflecting present design may be expected to be free of carbonation-induced corrosion over long service lives.

The estimated K_a values are likely to be representative only of inland concrete structures covered from rainfall. Actual K_a values ranging from 1 to 5

mm/y$^{1/2}$ were obtained from measurements in inland concrete bridges in Florida [II.31]. An average K_a = 3 mm/y$^{1/2}$ was found in the substructures, and an average K_a = 2.5 mm/y$^{1/2}$ was found in the superstructures of those bridges. The somewhat lower K_a values found in the field (compared with those in Table II.10) may be attributed to the wet periods due to rainfall and to variations in R.H. A worst-scenario case was used in this investigation (no wet periods and R.H. of 60%).

Table II.10. Average converted values of K_a (in mm/y$^{1/2}$).

	Mix 01	Mix 03	Mix 05	Mix 08	Mix 10
From accelerated exposure	3.4	4.7	4.9	4.3	5.4
From initial conditioning	2.3	4.4	5.0	2.7	5.2

4.3.4 Comparison with other Investigations

The correlation between carbonation depth and the w/c* described in the previous section can be discussed in terms of the carbonation coefficient K_a. The advantage in doing so is that the results can be compared with results from other investigators. The K_a values are shown in Figure II.23 along with trends extracted from the results by Loo et al. [II.46] and Ho and Lewis [II.47]. The results from those investigators were converted to K_a values using the same procedure described in the previous section. The research from Loo et al. was

done using a CO_2 concentration of 7%, R.H. of 65%, and w/c* ranging from 0.40 to 0.70. No FA was used in that investigation. The research from Ho and Lewis involve a CO_2 concentration of 4%, R.H. of 50%, w/c ranging from 0.40 to 0.80, and FA replacement from 0% to 40%. Similar trends of dependence of K_a with w/c* (although at somewhat different offsets) were found for the results of those investigations and the present work.

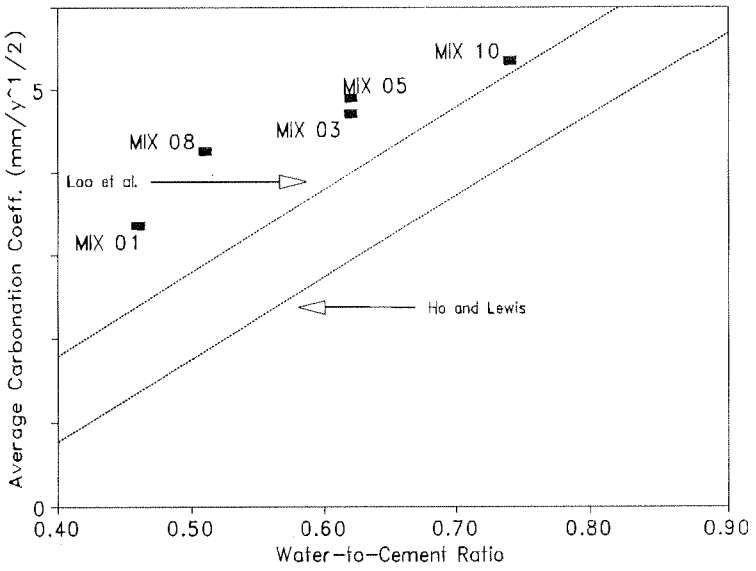

Figure II.23. Flat-front corrected carbonation coefficient K_a as a function of the water-to-cement ratio.

4.4 CONCLUSIONS

1. For concrete mixes with 20% FA replacement and 444 kg/m^3 of cementitious material, the carbonation depth increased directly proportional as the water-to-cementitious ratio increased from 0.37 to 0.50.

2. For concrete mixes with a 0.37 water-to-cementitious ratio and 444 kg/m^3 of cementitious material, the carbonation depth increased as the percent of cement content decreased from 80% to 50%.

3. For concrete mixes with 20% FA replacement and 444 kg/m^3 of cementitious material, the carbonation depth decreased as the compressive strength increased.

4. For concretes with pozzolanic replacement carbonation depth increased nearly linearly as the water-to-cement (as opposed to water-to-cementitious) ratio increased.

5. The combined effect of chloride and carbonation-induced corrosion was synergetic even in the low relative humidity test environment used.

6. The estimated corrosion initiation period can be shortened by about 60% if the amount of FA is increased from 20% to 50% (as cement replacement); by about 50% if the water-to-cementitious increased from 0.37 to 0.50; and by about 35% if 8% of SF is added as cement replacement.

7. Comparison between carbonation coefficients obtained in the accelerated test exposure and initial atmospheric conditions agreed approximately with a square root dependence of Kc with P_{CO_2}.

8. Extrapolation to atmospheric conditions of the Kc values obtained in the accelerated test resulted in atmospheric carbonation coefficients in the range $3 < Ka < 5$ (in $mm/y^{1/2}$). Those values compared favorably with the range of values obtained in the field investigation presented in Section 3.

REFERENCES

II.1 FDOT Specifications (1993). "Portland Cement Concrete." *Section 346*, Tallahassee, Fl.

II.2 Al-Amoudi, O.S.B., Rasheeduzzafar, and Maslehuddin, M. (1991). "Carbonation and Corrosion of Rebars in Salt Contaminated Concrete." *Cem. Concr. Res.*, 21(1),38-50.

II.3 Castro, P., Sagüés, A.A., Moreno, E.I., Maldonado, L., and Genescá, J. (1996). "Characterization of Activated Titanium Solid Reference Electrodes for Corrosion Testing of Steel in Concrete." *Corros.*, 52(8), 609-617.

II.4 Dhir, R.K., Jones, M.R., and Munday, J.G.L. (1985). "A Practical Approach to Studying Carbonation of Concrete." *Concrete*, 19(10), 32-34.

II.5 Papadakis, V.G., Vayenas, C.G., and Fardis, M.N. (1991a). "Fundamental Modeling and Experimental Investigation of Concrete Carbonation." *ACI Mats. J.*, 88(4), 363-373.

II.6 Verbeck, G. (1956). "Carbonation of Hydrated Portland Cement." *Cement and Concrete ASTM-205*, American Society for Testing and Materials, Philadelphia, Pa., 17-36.

II.7 Parrott, L.J. (1990). "Carbonation, Corrosion and Standardization." *Protection of Concrete*, R.K. Dhir and J.W. Green, eds., E. & F.N. Spon, London, 1009-1023.

II.8 Millard, S.G., Harrison, J.A., and Gowers, K.R. (1991). "Practical Measurement of Concrete Resistivity." *Br. J. Non-Destr. Test.*, 33(2), 59-63.

II.9 Morris, W., Moreno, E.I., and Sagüés, A.A. (1996). "Practical Evaluation of Resistivity of Concrete in Test Cylinders using a Wenner Array Probe." *Cem. Conc. Res.*, 26(12), 1779-1787.

II.10 Whiting, D. (1981). "Rapid Measurement of the Chloride Permeability of Concrete." *Public Roads*, 45(3), 101-112.

II.11 AASHTO (1989). "Standard Method of Test for Rapid Determination of the Chloride Permeability of Concrete." *T 277-89*, Washington, D.C.

II.12 ASTM (1991). "Standard Test Method for Electrical Indication of Concrete's Ability to Resist Chloride Ion Penetration." *C1202-91*, Philadelphia, Pa.

II.13 ASTM (1990). "Standard Test Method for Specific Gravity, Absorption, and Voids in Hardened Concrete." *C642-90*, Philadelphia, Pa.

II.14 Sagüés, A.A. (1988). "A System for Electrochemical Impedance Corrosion Testing using a PC with Isaac-Cyborg Interface." *Proc., CORROSION/88*, National Association of Corrosion Engineers, Houston, Tx., paper No. 104.

II.15 Sagüés, A.A., Kranc, S.C., and Moreno, E.I. (1995). "The Time Domain Response of a Corroding System with Constant Phase Angle Interfacial

Component: Application to Steel in Concrete." *Corros. Sci.*, 37(7), 1097-1113.

II.16 Sagüés, A.A., Kranc, S.C., and Moreno, E.I. (1996). "Evaluation of Electrochemical Impedance with Constant Phase Angle Component from the Galvanostatic Step Response of Steel in Concrete." *Electroquim. Acta*, 41, 1239-1243, 2661.

II.17 Moreno, E.I., Sagüés, A.A., and Powers, R.G. (1996). "Performance of Plain and Galvanized Reinforcing Steel during the Initiation Stage of Corrosion in Concrete with Pozzolanic Additions." *Proc., CORROSION/96*, NACE International, Houston, Tx., paper No. 326.

II.18 RILEM Recommendation (1988). "CPC-18 Measurement of Hardened Concrete Carbonation Depth." *Mater. Struct.*, 21(126), 453-455.

II.19 Rahman, A.A., and Glasser, F.P. (1989). "Comparative Studies on the Carbonation of Hydrated Cements." *Adv. Cem. Res.*, 2(6), 49-54.

II.20 Pihlajavaara, S.E., and Pihlman, E. (1974). "Effect of Carbonation on Microstructural Properties of Cement Stone." *Cem. Concr. Res.*, 4(2), 149-154.

II.21 Kobayashi, K., Suzuki, K., and Uno, Y. (1994). "Carbonation of Concrete Structures and Decomposition of C-S-H." *Cem. Concr. Res.*, 24(1), 55-61.

II.22 Moorehead, D.R. (1986). "Cementation by the Carbonation of Hydrated Lime." *Cem. Concr. Res.*, 16(5), 700-708.

II.23 Nishikawa, T., Suzuki, K., and Ito, S. (1992). "Decomposition of Synthesized Ettringite by Carbonation." *Cem. Concr. Res.*, 22(1), 6-14.

II.24 Forrester, J.A. (1976). "Measurement of Carbonation." *Colloquium on Carbonation of Concrete*, International Union of Testing and Research Laboratories for Materials and Structures, Cement and Concrete Association, Wexham Springs, U.K., Theme 2 Paper 1.

II.25 CRC (1973). *Handbook of Chemistry and Physics* 54th. ed., R.C. West, ed., CRC Press, Boca Raton, Fl., D-112.

II.26 Kishitani, K. (1969). "Studies of Carbonation and Coloration of Phenolphthalein at Time of Determination of Carbonation." *Durability of Concrete-Preliminary Report*, vol. II, International Union of Testing and Research Laboratories for Materials and Structures, Academia, Prague, D43-D58.

II.27 Parrott, L.J., and Killoh, D.C. (1989). "Carbonation in a 36 Year Old, In-Situ Concrete." *Cem. Concr. Res.*, 19(4), 649-656.

II.28 Meyer, A. (1968). "Investigations on the Carbonation of Concrete." *Proc. Fifth Int'l Symposium on the Chemistry of Cement*, vol. III, Tokyo, Japan, 394-401.

II.29 Berke, N.S., and Hicks, M.C. (1992). "Estimating the Life Cycle of Reinforced Concrete Decks and Marine Piles Using Laboratory Diffusion and Corrosion Data." *Corrosion Forms and Control for Infrastructure ASTM STP 1137*, V. Chaker, ed., American Society for Testing and Materials, Philadelphia, Pa., 207-231.

II.30 Andrade, C., and Alonso, C. (1993). "Life Time of Rebars in Carbonated Concrete." *10th European Corrosion Congress*, Barcelona, Spain, Paper No. 165.

II.31 Morris, W. (1996) *Influence of Concrete Carbonation on the Durability of Highway Bridges in Florida*, M.S. Thesis, University of South Florida, Tampa, Fl.

II.32 Fraay, A.L.A., Bijen, J.M., de Haan, Y.M. (1989). "The Reaction of Fly Ash in Concrete—A Critical Examination." *Cem. Conc. Res.*, 19 (2), 235-246.

II.33 Bijen, J., Pietersen, H. (1994). "Mineral Admixtures: Reactions, Micro-Structure and Macro-Properties." *Advances in Cement and Concrete*, M.W. Grutzeck and S.L. Sarkar, eds., American Society of Civil Engineers, New York, NY, 292-328.

II.34 Andrade, C., and Whiting, D. (1996). "A comparison of Chloride Ion Diffusion Coefficients derived from Concentration Gradients and Non-Steady State Accelerated Ionic Migration." *Mater. Struct.*, 29, 476-484.

II.35 Alonso, C., Andrade, C., González, J.A. (1988). "Relation between Resistivity and Corrosion Rate of Reinforcments in Carbonated Mortar made with Several Cement Types." *Cem. Conc. Res.*, 18 (5), 687-698.

II.36 Feliu, S., González, J.A., Feliu, S. Jr, Andrade, C. (1989). "Relationship between Conductivity of Concrete and Corrosion of Reinforcing Bars." *Br. Corros. J.*, 24 (3), 195-198.

II.37 Glass, G.K., Page, C.L., Short, N.R. (1991). "Factors Affecting the Corrosion Rate of Steel in Carbonated Mortars." *Corros. Sci.*, 32 (12), 1283-1294.

II.38 Tuutti, K. (1982). *Corrosion of Steel in Concrete*, Swedish Cement and Concrete Research Institute, Stockholm, Sweden.

II.39 Dhir, R.K., Jones, M.R. (1990). "Influence of PFA on Proportion of Free Chlorides in Salt Contaminated Concrete." *Corrosion of Reinforcement in Concrete*, C.L. Page, K.W.J. Treadaway, and P.B. Bamforth, eds., Elsevier Appl. Sci., London, UK, 227-236.

II.40 Kayyali, O.A., Haque, M.N. (1988). "Effect of Carbonation on the Chloride Concentration in Pore Solution of Mortars with and without Fly Ash." *Cem. Concr. Res.*, 18 (4), 636-648.

II.41 Byfors, K (1985). "Carbonation of Concrete with Silica Fume and Fly Ash." *Nordic Conc. Res.*, (4), 26-35.

II.42 Skjolsvold, O. (1986). "Carbonation Depths of Concrete with and without Condensed Silica Fume." *Fly Ash, Silica Fume, Slag, and Natural Pozzolans in Concrete ACI SP-91*, vol. II, V.M. Malhotra, ed., American Concrete Institute, Detroit, Mi., 1031-1048.

II.43 Häkkinen, T. (1991). "The Influence of the Content and Quality of the Cementing Materials on the Permeability of Concrete." *Proc., Second CANMET/ACI Int'l Conference on Durability of Concrete—Supplementary Papers*, Canada Centre for Mineral and Energy Technology, Montreal, Canada, 339-367.

II.44 Weber, H. (1983). "Methods for Calculating the Progress of Carbonation and the Associated Life Expectancy of Reinforced Concrete Components." *Betonwerk+Fertig.*, 49 (8), 508-514.

II.45 FDOT Guidelines (1992). "Florida-Concrete Design, Environmental Classification and Construction Criteria." *Procedures—Structures Design Guidelines*, Tallahassee, Fl.

II.46 Loo, Y.H., Chin, M.S., Tam, T.C., Ong, K.C.G. (1994). "A Carbonation Prediction Model for Accelerated Carbonation Testing of Concrete." *Mag. Concr. Res.*, 46 (168), 191-200.

II.47 Ho, D.W.S., Lewis, R.K. (1987). "Carbonation and its Prediction." *Cem. Concr. Res.*, 17 (3), 489-504.

STATEMENT OF BENEFITS

The investigation described in this report assessed the extent of concrete carbonation in FDOT bridges and the potential for carbonation in candidate concrete mix designs for future FDOT construction. The results indicate that concrete carbonation is in progress at a moderate rate in most bridges, but that carbonation-induced corrosion affects only a small fraction of the present bridge inventory. Durability projections for existing structures indicate that, except for a few extreme cases, carbonation induced corrosion should not become an important maintenance issue during the normal service life of the bridge. The findings benefit planning for future maintenance needs by indicating direction of the FDOT resources to the more pressing problem of chloride-induced reinforcement corrosion.

Because the FDOT bridge inventory is large, the results of this investigation suggest nevertheless that routine tests for concrete carbonation be performed when periodically assessing the integrity of existing bridges, especially for older structures at inland locations. Direct benefits from this practice derive from identification of structures in need for maintenance which otherwise would have pass unnoticed.

The results from the laboratory investigation provided important confirmation that concrete mixes with moderate amounts of pozzolanic additions (a key component in the present FDOT strategy to combat chloride-induced corrosion) do not show undue susceptibility for carbonation. This finding benefits the FDOT materials selection effort by removing

uncertainty in the expected performance of these candidate concretes. The findings also provided a warning against excessive pozzolanic replacement in high performance concretes, a result that is beneficial by avoiding design choices that could have caused durability reduction.

APPENDICES

APPENDIX FOR SECTION 2

APPENDIX FOR SECTION 2

Report on the background of carbonation of concrete structures

by C. Andrade

BACKGROUND

Present report corresponds to the Contract between the University of South Florida and the Consejo Superior de Investigaciones Científicas, no.subagreement #21-04-201-LO-A.

AIM

The aims of present report are the following:

1) To summarize a state-of-the art on the processes developing during carbonation of the concrete, on the concrete itself and on the rebars.

2) To collect a list of bibliographical references on the subject.

3) To describe calculation methods of the carbonation rate.

1. SUMMARY OF THE STATE-OF-THE ART

1.1. CARBONATION REACTIONS

1.1.1. Carbonation of the solid phase of the cement paste

The action of CO_2 of the hydrated cement paste leads to some relevant changes on cement microstructure which causes the slow modification of the properties of the concrete.

When taking account the reaction mechanism of cement components it is necessary to distinghish between anhydrous and hydrated cement. Anhydrous cement is carbonated when it is stood in contact with the atmosphere. This contact makes the cement particles to be hydrated superficially and in consequence, they may become carbonated developing some kind of aggregation. The phenomenon is known as the meteorization of the anhydrous cement.

More specially important are the reactions experienced by the solid components of the hydrated cement when those components suffer carbonation. Thus, as S.L. Meyers (1) suggests that the hydrated SC_3 reacts with the CO_2 to form calcium CO_3 and hydrated SiO_2, while the SC_2 reacts directly with the CO_2 to create the same type product.

Other authors state (2)(3)(4) that in the carbonation of the hydrated SC_3 (tobermorite) it reacts directly with the CO_2 to produce $CaCO_3 + SiO_2 + H_2O$. Other authors suggest that this carbonation takes place in two stages (5) (6). In the first stage the tobermorite reacts with the CO_2 forming calcium carbonate, water and monocalcic hydrated silicate, according to the reaction.

$$C_3SH + CO_2 \rightarrow CaCO_3 + CSH + H_2O \quad [1]$$

In a second phase of the process the CSH (hydrated monocalcium silicate) reacts with the CO_2 in presence of water producing $CaCO_3$ and hydrated silica (amorphous silica). This takes place following the reaction:

$$CSH + CO_2 + H_2O \rightarrow CaCO_3 + SiO_2(OH)_2 \quad [2]$$

In this process the $CaCO_3$ appears mainly in the allotropic form of calcite, since this is more stable than the aragonite variety.

The hydrated aluminate (C_3AH) also experiences a carbonation of the type (3)(7):

$$4C_3AH + 4CO_2 \rightarrow 4\ CaCO_3 + 2\ Al(OH)_3 + 10\ H_2O \quad [3]$$

This aluminum hydroxide evolves forming aluminum oxide (Al_2O_3) which is much more stable. Carboaluminate also appear as an intermediate reaction product. This compounds decompose when more CO_2 appears to form ($CaCO_3 \cdot Al_2O_3$).

It is important to state here that carbonates act as regulators of the setting process when are added to the clinker instead of gypsum. The carbonates have the ability to react with hydrating aluminates and form carboaluminate and alumina.

The carbonation of ettringite is also of interest. Ettringite results from the hydration of cement when it reacts with gypsum and the aluminates. The process suggested for this case is: (7)(8)(9)(10).

$$C_3A(CS)_3\ H_{32} + CO_2 \rightarrow CaCO_3 + Al_2O_3 + H_2O + CaSO_4 \cdot 2H_2O \quad [4]$$

The hydrated calcium ferro-aluminates ($FeAC_4H$) in the reaction with the CO_2 decompose to form iron oxides, aluminum oxides (alumina) and $CaCO_3$ (8).

When concrete carbonates it suffers a variation of some of its properties (11) in addition to experiencing a microestructural modification as a result of the chemical transformations mentioned before. Properties affected include the mechanical resistance, the resistance to aggressive environmental agents, surface hardness, porosity, shrinkage, etc. Numerous authors (11) have found that the mechanical resistance increases with carbonation, both in tension and in compression. The tensile resistance increases and the elastic modules increases also.

The resistance to the combined tension-flexion first decreases but then increases. It has been found (12) that with carbonation there is an increase in the hardness of the concrete surface. Because of carbonation the resistance to sulfates increases but no

improvement to the resistance to the action of acid waters has been observed. Porosity decreases since part of the pores become filled by the $CaCO_3$ formed during carbonation. Verbeck (13) studied the shrinkage due to carbonation. He concluded that the shrinkage is produced by the water released by the reaction and is function of the humidity, CO_2 concentration and porosity.

It is also important to emphasize that carbonation of most of the greater part of the cement is concurrent with a weight increase, because CO_2 is used to form $CaCO_3$ and H_2O.

1.1.2.Carbonation of the aqueous phase of the concrete pores

Most carbonation studies have addressed the carbonation of the solid phases of hydrating cement disregarding the carbonation of the aqueous phase contained in the concrete pores. This aqueous phase is highly alkaline, so it will also experience a carbonation process.

When mention is made of the carbonation of water phase (3)(8) it is often only in terms of the carbonation of $Ca(OH)_2$:

$$Ca(OH)_2 + CO_2 \rightarrow CaCO_3 + H_2O \qquad [5]$$

Since the $CaCO_3$ formed by this reaction has very low solubility, the carbonate will precipitate and the amount of carbonates in solution will be very small. The result is a water phase which is practically pure water.

Relatively few authors have taken into account the previous existence of alkalines (Na^+, K^+) in the aqueous phase of concrete, when mention to the alkalines is made (14), little notice is given to the possible appearance of bicarbonates, see Figure 1. Only in few papers reference is made to the possible formation of bicarbonates in the carbonation process of the aqueous phase. Thus, Niels Aschan (15) (figure 2) proposes a carbonation mechanism of the water phase where the formation of bicarbonates is considered, although nevertheless the presence of KOH and NaOH is ignored. The reactions proposed by this author are:

$$Ca(OH)_2 + CO_2 \rightarrow CaCO_3 + H_2O \qquad [6]$$

$$CaCO_3 + CO_2 + H_2O \rightarrow Ca(HCO_3)_2 \qquad [7]$$

The $Ca(HCO_3)_2$ formed is in solution, so that in addition it may happen that:

$$Ca(HCO_3)_2 + Ca(OH)_2 \rightarrow 2CaCO_3 + 2H_2O \qquad [8]$$

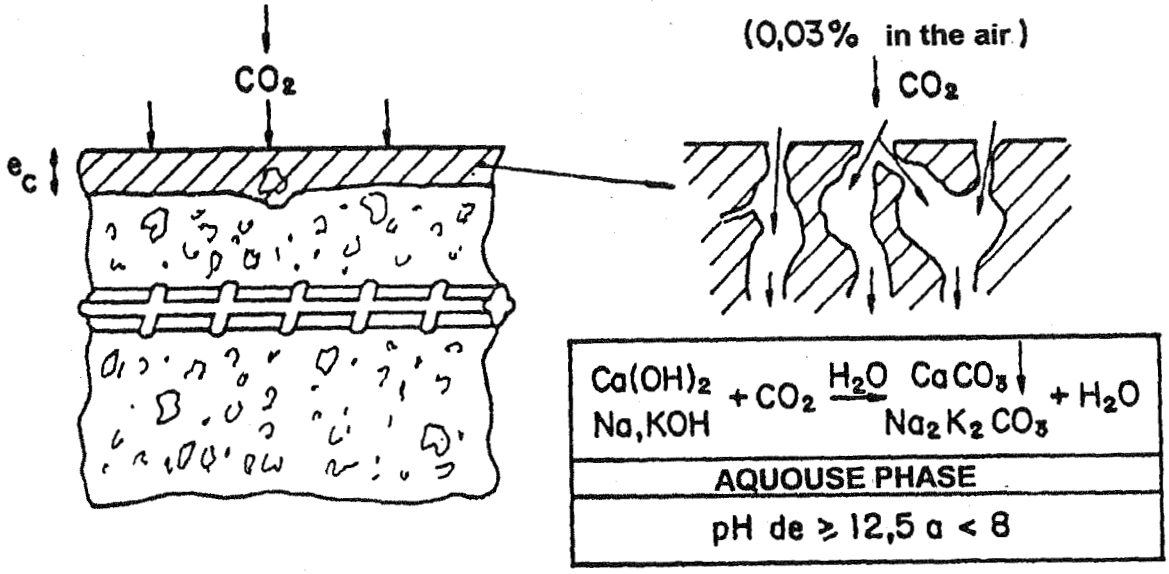

Figure 1

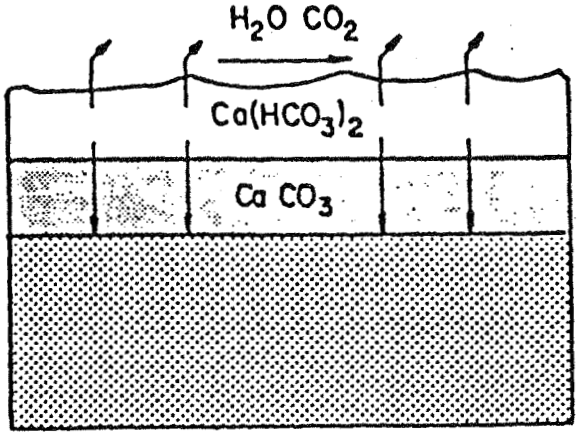

Figure 2. Model proposed by Nils Aschan for the advance of the carbonation front.

Other authors (2)(16) do consider the presence of alkalies in the medium, taking into account that they react with the CO_2 forming the corresponding $CO_3^=/HCO_3^=$ of Na and K. They observe that it is $Ca(OH)_2$ which is carbonated the fastest forming calcite, aragonite or vaterite. The appearance of one or of the other compound is attributed to: the quantity of $Ca(OH)_2$, the state of hydration of the cement, and the quantity of water in the concrete pores and the carbonation rate.

In another proposed mechanism (17) the CO_2 reacts with the alkalies forming the corresponding carbonates, which in turn react with the $Ca(OH)_2$ forming $CaCO_3$ and also with the silicates and aluminates to give the compounds already described above.

Extensive work has been done by Alonso (see bibliography in 2) in this subject. The results obtained indicate the importance of the of alkalines, Na^+, K^+, as their carbonates/ bicarbonates are soluble. The evolution of pH, potential, corrosion rate and amount of carbonates, has been monitored. This allowed to explain the phenomena happening in concrete and to state that Na^+ and K^+ ions ought to be removed from the pore solution for noticing a pH value decrease, otherwise the final pH should be around 10.5.

1.2. VARIABLES INFLUENCING THE CARBONATION RATE

Among the factors determining the rate of carbonation advance, the following are emphasized:

- Those factors of which the total amount of acid necessary for neutralizing the concrete until a certain depth, depend: 1) the cement composition and the mix design of the concrete.

- Factors from which depends the CO_2 permeability of the concrete: 2) porosity, 3) concrete compaction, 4) curing conditions and 5) relative humidity.

1.2.1. Cement composition and concrete mix design: since hydrated cement is the carbonatable component of the concrete, the carbonation depth is inversally proportional to the cement content. In addition, the amount of CO_2 needed to react with the alkaline components of the hydrated cement depends on the type of cement.

According to Bakker (17) for the same rate of diffusion of CO_2, the carbonation depth is related to the amount of alkaline components of the concrete, mainly the CaO.

Several authors (6)(21) consider that the rate of carbonation of a mortar, everything else kept being the same, is faster for blended cement than for unblended portland cements. Some authors state (22)(23) that a fly ash mortar carbonates about fifty percent faster than a portland cement mortar.

M. Venuat (7) also indicates that cements with large quantities of additions carbonate more faster, specially if the concrete has not been kept wet since the beginning of the curing process.

The carbonation rate of a mortar increases as the quantity of cement decreases. This can be seen in figure 3 in which the depth of the carbonation layer is shown in function of the square root of times for concretes where the cement factor varies from 200-400 kg/m^3.

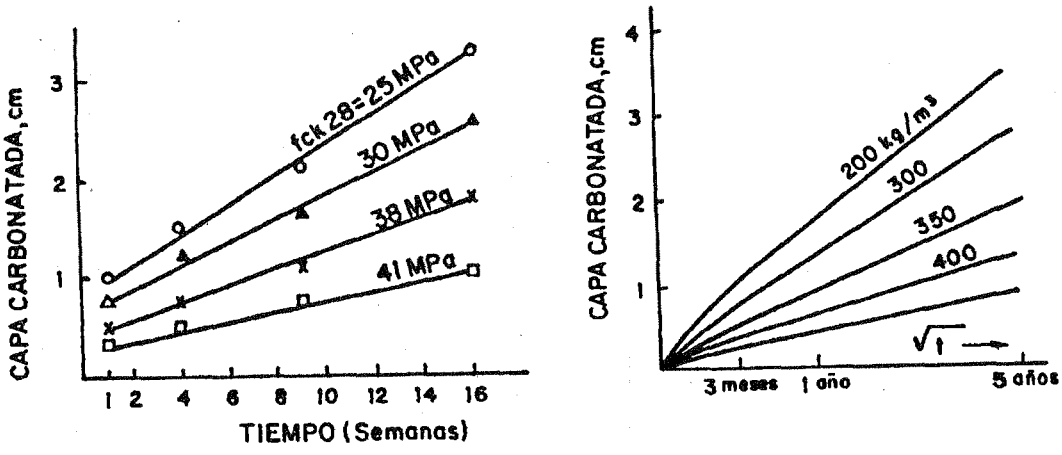

Figure 3

1.2.2. Porosity

The concrete porosity is controlled by the w/c ratio (6). Not all the mixing water is used in the hydration reactions, but some of it remains free. As this water evaporates after the curing process, it induces the formation of a network of channels and pores, which make the concrete permeable to certain gases.

The porosity of the concrete therefore increases as the w/c ratio does, which indicates that the rate of carbonation will also increase as the CO_2 diffuses more easily through the pores. Also, as the porosity increases, the diffusion of other elements that play a role in the carbonation process, such as $Ca(OH)_2$ also increases. In figure 4, it can be seen now the thickness of the carbonation layer increases as the w/c ratio increases for a concrete conserved or exposed to the atmosphere over a 3 year period (7).

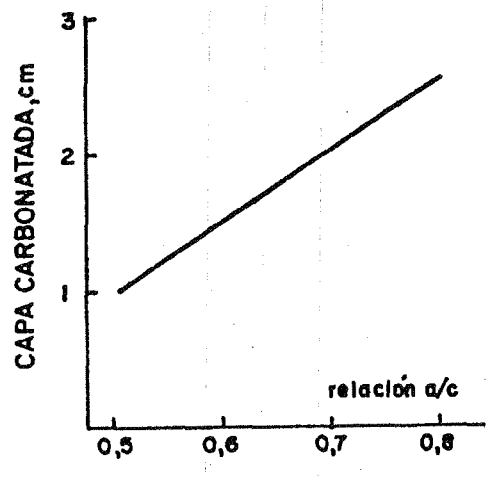

Figure 4

The porosity depends also on the grain size distribution of the aggregates. This explains how a cement paste carbonates slowly and a mortar much more rapidly, more than concrete. The reason for this is that normally a mortar is not as densily compacted as concrete. A defficient joint between the aggregate and the cement paste may lead in a very irregular carbonation front, with deep inroads in the contact zones of the two phases mentioned above (6)(17).

The porosity of a concrete depends also partly on the type of cement. Thus, slag cement give lower porosity than portland ones (24).

1.2.3. Concrete compaction

Concrete must be well compacted, otherwise the zones more permeables than other would develop voids which will conduct to a rapid carbonation of that zone.

1.2.4. Curing conditions

Curing conditions affect considerably the carbonation rate in a concrete (25)(26). For the same composition and at a given temperature, the pore permeability depends on the degree of hydration. As this increases, the permeability decreases. This is however true only if there is not water loss, which supposes curing under high humidity conditions (27). If there is loss of water, the degree of hydration is inferior, which would in turn increase the carbonation depth. This curing effect on carbonation can be seen in figure 5 for concrete cured at different degrees (29).

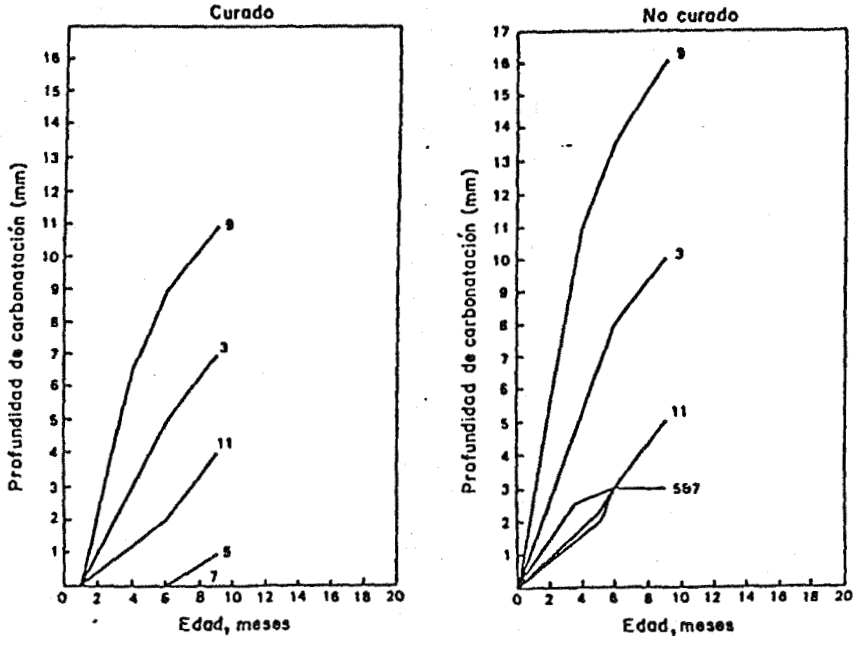

Figure 5

1.2.5. Relative humidity

In addition to the factor mentioned above carbonation depends also of variables of the environment, specially on relative humidity, since it is the humidity within the pores of the concrete which eventually determines the permeability to CO_2.
This internal humidity depends in turn on the ambient relative humidity.

As indicated earlier, carbonation in practice,. nearly takes place in either dry concrete or water saturated concrete, which means that only a concrete not saturated with water could carbonate.

Maximum penetrations appear when RH is between 50 and 65% as shown in figure 6, where the extend of carbonation is plotted in function of the RH (7).

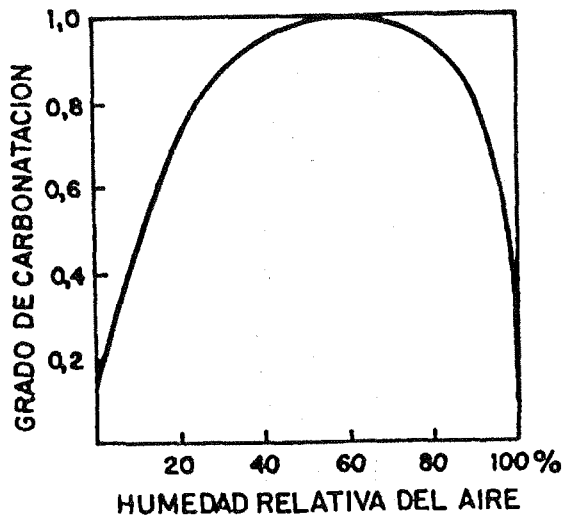

Figure 6

For humidities below 30% the carbonation phenomenon does not take place or is very slow (24)(30). This fact confirms the expectation that the hydrated components of the concrete carbonate by formation of intermediate alkaline hydroxides in solution (31)(32). At elevated humidities, carbonation cannot take place due to the slow rate of the CO_2 diffusion in water compared with that in air.

For each relative humidity in the atmosphere there is an equilibrium humidity in the concrete that tends to be approached, although the time for equilibritation may be very long when the concrete is dense and the cover thickness is considerable (33).

In any event a minimum amount of water is necessary for carbonation becomes possible starting at 0.5-1% of water by concrete weight in the concrete pores (7).

Should also be considered that the process of carbonation may increase the humidity of the pores as water is liberated during the reaction of hydrated components and the CO_2. This could in turn, facilitate the carbonation process.

1.3. METHODS TO OBTAIN THE DEPTH OF THE CARBONATED LAYER

The most precise determination of the carbonated layer depth has been obtained by microscopic observation. Cured cement paste appears dark when observed through crossed polarizers, as it is common with isotropic materials. The double refraction properties of calcium carbonate cause it to appear bright under crossed polarization. This permits positive evaluation of the penetration of carbonation through the concrete.

Due to the pronounced change in pH that accompanies the carbonation process (figure 7), it is also possible to make sufficiently exact determinations by means of a 1% solution of phenolphthalein in alcohol. Applied over a freshly fractured concrete surface, an opal red zone is observed where the carbonation has not reached, and a colorless zone is seen in the carbonated region. This procedure is often used because of its simplicity. Simultaneous use of several indicators with different color tone pH intervals allows more precise determination of the pH of the carbonated material (35).

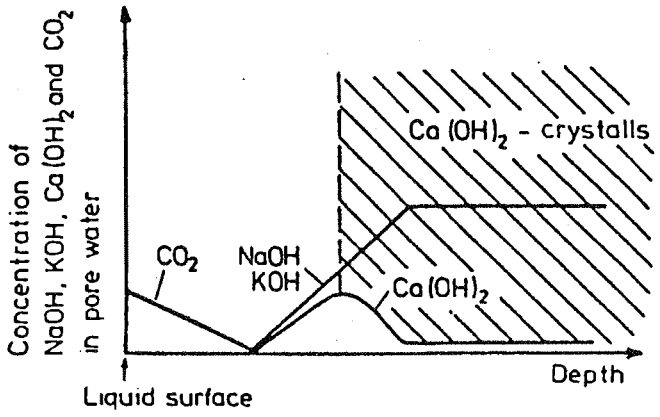

Figure 7. Schematic sketch of concentration profile for concrete carbonation.

Due to the changes in microstructure and chemical composition that result from the carbonation reaction, its advance can also be followed with a scanning electron microscope, by x-ray diffraction, or by neutron radiography (the latter, because of the moderator effect of the water freed during the carbonation reactions) (2)(7). It is also possible to determine the degree of carbonation of concrete by means of thermo gravimetric tests at different distance from the surface of the specimens (7)(15). TGA involves starting with a dry concrete sample and subjecting it to an increasing temperature ramp with time, in a thermal differential balance. The corresponding loss of weight is recorded. This loss of weight is ascribed to the "loss of free water" and the decomposition of calcium hydroxide, which takes place between 100°C and 550°C, as well as the loss of CO_2 from the $CACO_3$ between 700°C and 900°C.

1.4. CARBONATION OF CRACKED CONCRETE: TRANSVERSE AND LONGITUDINAL CRACKS.

The appearance of cracks in reinforced concrete structures is a result of the low tensile strength of concrete. This is inherent to the nature of the material and cannot be avoided, only controlled. Carbonation penetrates much faster toward the concrete interior along cracks. Carbonation affects the edges or lips of the cracks. The carbonation process in cracked concrete can be described by the scheme in Figure 8. The diffusion of carbon dioxide along a crack depends on the following:

- Size of the crack
- Permeability of the space within the crack

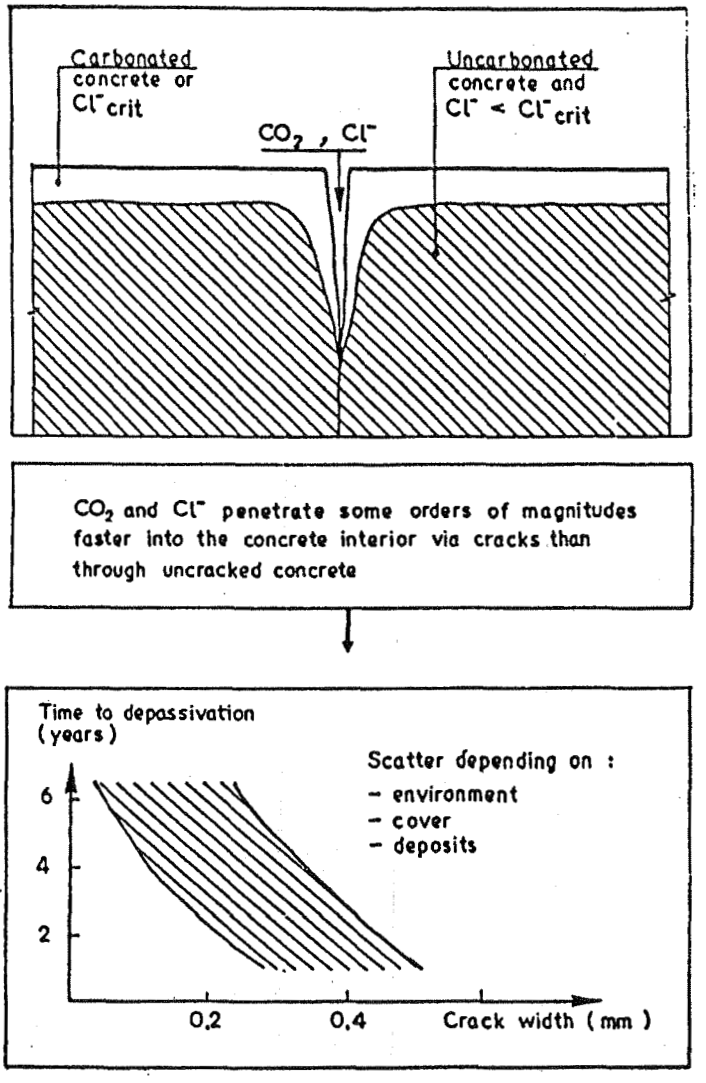

Figure 8

Size of the Crack

Structural design can be used to control the size of cracks which are perpendicular to the reinforcing bars, but no procedures are available to control the width of cracks parallel to the reinforcing steel bars. Structural cracks transverse to the rebar direction are permitted by design criteria, depending on the aggressiveness of the surface environment. For environments with low relative humidity, crack sizes between .3 and .4 millimeters (36)(37) are allowed for non-aggressive atmospheres. For high humidity conditions, the maximum crack opening must not exceed 0.2 millimeters. For highly aggressive industrial or marine environments, the recommended crack size is less that 0.2 millimeters. The most restrictive values for crack openings are between 0.3 and 0.4 millimeters, and are usually the result of aesthetic structural concerns rather than the need for extended durability (38). This was illustrated by Schiessl showing that after 10 years the crack width does not control the corrosion produced (figure 9).

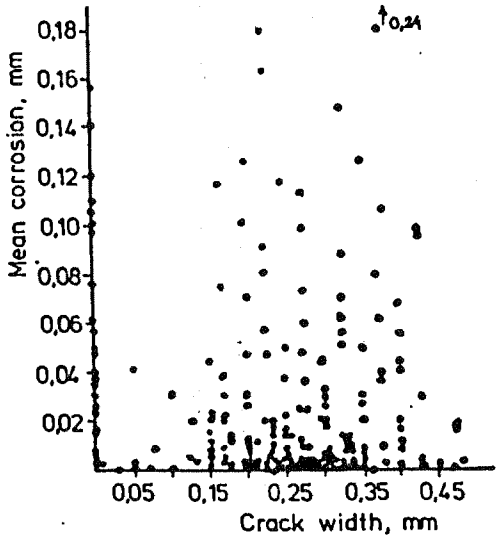

Figure 9. Mean corrosion on reinforcement as a function of the crack width after ten years exposure.

Permeability Within the Crack

Permeability within the crack depends mainly on the amount and type of deposits that form inside. These deposits depend in turn on the diffusion of alkali from the interior of the concrete toward the crack (17). Variations in humidity increase the extent of water transport toward the crack, and it is especially during the drying processes that the dissolved alkali are transported together with the water. When these alkali reach the surface of the crack, they carbonate while the water evaporates. To determine the thickness of the carbonated layer in cracked concrete, in addition to the parameters that effect the carbonation rate in the bulk, one must consider the influence of the parameters just mentioned (opening of the crack and permeability of the deposits within the crack). This situation is more complicated, and it is more difficult to propose an equation that takes into account all the parameters with the desired accuracy.

1.5. CARBONATION OF CONCRETE BY WATERS WITH HIGH CO_2 CONTENT

Waters with high contents of H_2CO_3 make up the most important group of natural waters that react with acids. Only one percent of the CO_2 dissolved in water is in the form of bicarbonate ions. The rest is gaseous CO_2 dissolved in the water. When the pH of a water is ≥ 8.5, the quantity of dissolved CO_2 is negligible, since practically all of the CO_2 is in the form of HCO_3- (39). If the free CO_2 amount is greater than the equilibrium amount of carbonic acid, the water will attack concrete. If the free CO_2 content is equal to the H_2CO_3 equilibrium amount, a state of equilibrium with exist. If the free content of CO_2 is smaller than the equilibrium amount of carbonic acid, calcium hydroxide will precipitate.

H_2CO_3 resulting from the dissolution of CO_2 in water dissolves the $CAOH_2$ of the hardened cement paste. Therefore, waters that have an H_2CO_3 content such that the pH is ≤ 7 will tend to attack concrete. The proposed attack mechanism (39) for these waters can be described in the following fashion:

For the aqueous phase:

$$H_2CO_3 + Ca(OH)_2 \leftrightharpoons CaCO_3 + H_2O \qquad [9]$$

For the paste:

(the silicates): $$C_3SH + H_2CO_3 \leftrightharpoons CaCO_3 + H_2SiO_3 \qquad [10]$$

(aluminates): $$C_3AH + H_2CO_3 \leftrightharpoons CaCO_3 + Al(OH)_3 \qquad [11]$$

According to A. Steope (40), the carbonic acid after the dissolution of carbon hydroxide, attacks the dehydrated calcium silicate from the hardened cement until only the insoluble silicic acid remains.

1.6. DIFFERENCE BETWEEN NATURAL AND ACCELERATED CARBONATION

The material addressed above refers only to natural carbonation of concrete, either due to atmospheric carbon dioxide or to natural waters that contain a high content of CO_2.

Because natural carbonation is slow, laboratory studies use accelerated conditions, consisting often of increasing the concentration of CO_2 above the natural levels, sometimes reaching 100% CO_2. The use of atmospheres saturated with CO_2 can result in carbonation rates 3,000 times greater than those that would be observed in a regular atmosphere. The formulas to calculate advance of the carbonation rate indicated earlier are not expected to be accurate. Although laboratory conditions allow for an easier control of the exposure, the diffusion rate and mechanism of CO_2 may have changed considerably from natural conditions, in part because the diffusion rate of CO_2 can change dramatically with pressure and concentration of the gas in the carbonation chamber. As a result, in an accelerated carbonation test, the crystal

size of final products such as calcium carbonate (which appears in the form of calcite) is much smaller than in the case of natural carbonation. The carbonation of the solid phases of cement in an accelerated test gives products which are different form those that appear in natural carbonation processes. The pH of the aqueous phase in the accelerated carbonation case is lower than that observed in natural carbonation, possibly even smaller than neutral, because the bicarbonates are present in greater concentration as a result of additional dissolution of calcium carbonate provoked by the excess of CO_2. Calcium bicarbonate is very soluble (15).

It is necessary to take into account these differences in behavior when attempting to interpret the results of laboratory carbonation tests for the purpose of extrapolation to actual surface conditions.

1.3. MODELS OF ADVANCE OF THE CARBONATION FRONT

1.3.1. Semi-empirical models

Many authors (13)(14)(27)(28) in their concrete carbonation studies have proposed models of how the carbonation front progresses, **Niels Askhan** (27) proposes that carbonation takes place in the manner described in figure 2 involving three stages. In the first stage the $Ca(OH)_2$ dissolves in water, reacts with the CO_2 also dissolved to form $CaCO_3$. The $CaCO_3$ later reacts with the excess of CO_2 forming $Ca(HCO_3)_2$ which is soluble and penetrates through the pores of the concrete and when it encounters uncarbonated concrete it reacts with $Ca(OH)_2$ forming $CaCO_3$. Thus, resulting in the advance of the carbonation front.

Alexeyeev in (20) proposes also diffusion of $Ca(OH)_2$ towards the exterior and proposes several methods of calculating the progression of the carbonation.

According **Venuat and Alexandre** (7) the carbonation rate is initially constant $dx/dt=k$. By integrating $x= Axt$, where $x=$ carbonation depth and $t=$time.

The authors also suggest, that after a relatively short time and over a subsequent period of years, the carbonation front advances proportional to the $\sqrt{}$time. This is expected since if the diffusion of CO_2 is the controlling step of the global process, the CO_2 must travel through the already carbonated layer before finding new material suceptible to carbonation.

The obstacle to this transport is excepted to be proportional to the thickness of the carbonated layer. Therefore, $dx/dt=k/x$, which by integration gives $x=a\sqrt{t} + b$, where **a** and **b** are coefficients which incorporated the effect of parameters described earlier. This equation approximates a parabolic behaviour.

Parabollic growth has also been proposed for formulations not based on the diffusion of CO_2, but on the mechanical strength on the concrete (27). In equation of the type:

$$x = a\left(\frac{w/c}{t} - b\right)\sqrt{t} \qquad [12]$$

is proposed in which: x= depth of carbonation, t= time of carbonation, w/c= water/cement ration, Rt= compression strength in concrete in days, **a** and **b** are constants which depend on the carbonation conditions. For example, for a carbonatin process without taken into consideration rain time, a=250 and b= 625, whereas in a carbonation process in a sheltered environment, a= 180 and b= 780.

Later other authors (30)(34) tried to modify this equation calculating the value of the diffusion coefficient by application of Fick's laws obtaining expressions of the type:

$$x = \sqrt{\left(2D\frac{C_1}{C_2}\right).(t)} \qquad [13]$$

where X is the carbonation depth in millimeters, D is the diffusion coefficient of CO_2 in millimeters per year, C the concentration of CO_2 in the atmosphere, which is 0.69 g/m^3, C_2 is the amount of CO_2 per m^3 concrete, and t is the carbonation time in years. The carbonation coefficient is defined as

$$C = \sqrt{2D\frac{C_1}{C_2}} \qquad [14]$$

and the equation reduces to $C = x/\sqrt{t}$, where C's units are millimeters per square root of year. For small values of C, the concrete is more resistant to carbonation, which will imply a longer service life. D is usually not time or depth independent. In fact, equations whereby x is proportional to the square root of t are not justified in fundamental terms. The resulting formulas of that type are only empirical.

According to **Smolczyk** (41) this equation provides good agreement with experimental data and theoretical predictions for the range 5 to 30 years. However, this simple relationship does not give good results in situations in which other factors are in play. These factors include variables dependent on time, such as the variation of porosity with the degree of hydration, and the moisture content. To address these shortcomings, variations to the basic equation:

$$x = A\sqrt[n]{t} \qquad [15]$$

have been proposed, such as, for example, N is a variable greater than one, which is found tabulated in the literature (41). Other authors have proposed different values for A in

Table 3

AUTHOR	EQUATION	COMMENTS
LE SAGE DE FONTENAY, 1985	$X_{CO_2} = 0,43\left(\frac{a}{c} - 0,4\right)\sqrt{12(t-1)} + 0,1$ $X_{CO_2} = 0,53\left(\frac{a}{c} - 0,2\right)\sqrt{12t} + 0,2$	CURED 28 DAYS NOT CURED
DAIMON ET AL., 1971	$X_{CO_2} = A\sqrt{(t-t_i)T^{0,75}\frac{C_1}{C_2}}$	t_i = INDUCTION TIMET = TEMPERATURE (K) C_1 = $[CO_2]$ IN THE AIR C_2 = COMBINED $[CO_2]$
VENUAT, 1969	$X_{CO_2} = 15\sqrt{t} + 2$ $X_{CO_2} = 12\sqrt{t} + 2$ $X_{CO_2} = 5\sqrt{t} + 2$ $X_{CO_2} = 5\sqrt{t}$ $X_{CO_2} = 5\sqrt{t} - 2$	
BOB, 1990	$X_{CO_2} = \frac{150CKd}{f_C}\sqrt{t}$ $K = 1,0(INDOOR)$ $K = 0,7(OUTDOORSHELTERED)$ $K = 0,5(OUTDOOR)$ $K = 0,3(DAMP)$ $d = 1,0(0,03\%CO_2)$ $d = 2,0(0,1\%CO_2)$	
BETONTECHNISCHE BERICHTE, 1972	$X = 7\left(\frac{10\,a/c}{\sqrt{N_T}} - 0,175\right)\sqrt{t - 0,50}$	
	$T = 5 + 0,003\frac{N_5 - 100}{10\,a/c}t$	
	$X = \left(84,62\frac{a/c}{\sqrt{N_T}} - 0,64\frac{a}{c} - 1,63\right)\sqrt{t} + 0,95$	
PARROTT, 1991	$d = 1875\frac{K^{0,4}}{c}t_i^n$ *where:* $n = 0,0491r - 0,000374r^2 - 1,01$	d = carbonation depth (mm) K = air permeab. (10^{-16} m^2) r = relative humidity (%) C = cement content (Kg/m^3)

Table 2

AUTHOR	EQUATION	COMMENTS
NISCHER, 1984	$X_{CO_2} = 10,3\, e^{-0,123 * R_{28}}$ $X_{CO_2} = 3,4\, e^{-0,034 * R_{28}}$	SHELTERED FROM RAIN NON SHELTERED FROM RAIN
LE SAGE DE FONTENAY, 1985	$X_{CO_2} = 680\left(R_{28} + 25\right)^{-1,5} - 0,6$	AT TWO YEARS
SCHOLZ Y WIERING, 1984	$X_{CO_2} = 1 - \frac{B}{\sqrt{R_{28}}} + \frac{C}{\sqrt{CaO - 46}}$	AT 1 YEAR
SCHUBERT Y BERG, 1979	$X_{CO_2} = \left(\frac{0,508}{\sqrt{R_{35}}} - 0,047\right)\sqrt{365\,t}$	
SMOLCZYK, 1976	$X_{CO_2} = 0,846\left(10\frac{\frac{a}{c}}{R_7^{10}} - 0,193 - 0,076\, a/c\right)\sqrt{12t} + 0,095$	
MATTHEWS, 1984	$X_{CO_2} = 73,74 - 1,69R_{28}$ $X_{CO_2} = 63,00 - 1,30R_{28}$ $X_{CO_2} = 13,94 - 0,30R_{28}$ $X_{CO_2} = 11,00 - 0,2523R_{28}$ $X_{CO_2} = 65,14 - 1,2384R_{28}$ $X_{CO_2} = 61,0972 - 1,1140R_{28}$ $X_{CO_2}(5-8\,years) = 50,00 - 0,8865R_{28}$ $X_{CO_2}(5-8\,years) = 46,2995 - 0,8686R_{28}$ $X_{CO_2}(5-8\,years) = 15,30 - 0,1972R_{28}$ $X_{CO_2}(5-8\,years) = 7,7993 - ,12092R_{28}$	
MOPU, 1985	$X_{CO_2}(mm) = 16,98 - 0,0399R_{28}$ $X_{CO_2}(mm) = 24,73 - 0,0546R_{28}$	AT 1 YEAR AT TWO YEARS

Equation [15] for the estimation of the penetration depth (see Table 1). Other authors have also correlated the value of 28 days compression strength and the carbonation depth (Table 2).

Finally, Table 3 presents other relations in which parameters such as the water/cement relation, temperature, carbon dioxide concentration, and others are contemplated.

Table 1

	$X_{CO_2} = A\sqrt{t}$	
AUTHOR	COEFICIENT A	COMMENTS
KISHSTANI	γ	
KASAMI ET AL, 1986	$\alpha.\beta.\gamma$	SEE TABLES 4,5 y 6
HAMADA, 1968	$\frac{R}{\sqrt{K}}$. $R = r_c * r_a * r_s$. $K = \frac{0,3\left(1,15 + 3\frac{a}{c}\right)}{\left(\frac{a}{c} - 0,25\right)^2}$	SEE TABLES 7 y 8
NAGATAKI ET AL, 1986	$A * B * \left(\frac{a}{c} * \alpha - \beta\right)$	SEE TABLE 9 A = f(CURED) B y C = f(% FLY-ASH)
VESIKARI, 1985	$2,6\left(\frac{a}{c} - 0,3\right)^2 + 0,16$ $\left(\frac{a}{c} - 0,3\right)^2 + 0,07$	SHELTERED FROM RAIN NON SHELTERED FROM RAIN
SMOLCZYCK, 1968	$a\left(\frac{1}{\sqrt{B}} - \frac{1}{\sqrt{B_G}}\right)$	B = CHEMICAL STRENGTH AT 28 d B_G = LIMITING RESISTANCE TO CARBONATE (CTE.)
SMOLCZYK, 1976	$a\left(\frac{a/c}{\sqrt{N_t}} - b\right)$	N_t = Chemical strength at t days OUTDOOR INDOOR a: 250 180 b: 625 780

Table 4

Ambient	Indoor	Outdoor
α	1,7	1
Standard deviation	0,61	-

Table 5

	INDOOR							OUTDOOR			
	TYPE OF FINISHING										
	1	2	3	4	5	6	7	1	4	7	6
β	1,0	0,79	0,41	0,29	0,15	0,12	0,57	1,0	0,28	0,80	0,07
σ	-	0,15	0,23	0,23	0,11	0,14	0,24	-	0,23	-	0,01

TYPE OF FINISHING

1. NONE
2. GYPSUM
3. MORTAR AND GYPSUM
4. MORTAR
5. MORTAR AND PAINT
6. TILES
7. PAINT

Table 6

WATER/CEMENT > 0,60	WATER/CEMENT < 0,60
$\gamma = \frac{R\,(A/C - 0{,}25)}{(0{,}31(1{,}15+3\,A/C))^{1/2}}$	$\gamma = 0{,}37\,R\,(4{,}6\,A/C - 1)$
R= Coefficient which depends on the aggregate and cement type.	

Table 7

CEMENT TYPE	OPC	BFSC	POZZ. CEMENT	FLY ASH CEMENT
	Initial Resistance	Slags		Fly ash
(r_c)	Normal High 1 0,0	30-40% 60% 1,4 2,2	1,7	20% 1,9
AGGREGATES	aggregates river	sound river Gravel:Pumici-ta	. Pumicita	Cinder
(r_a)	1	1,2	2,9	3,3
ADMIXTURES	WITHOUT ADMIXTURES	AIR-ENTRAINING	PLASTIFIER	
(r_s)	1	0,6	0,4	

Table 8

Coefficient R

CEMENT	AGGREGATES	SAND AND GRAVEL			SAND AND LIGHT WEIGHT GRAVEL			SAND AND LIGHT WEIGHT GRAVEL		
	ADMIXTURE	N	AEA	DA	N	AEA	DA	N	AEA	DA
OPC		1	0,6	0,4	1,2	0,8	0,5	2,0	1,8	1,1
RAPID HARDENING BFSC:30-40%		0,6	0,4	0,3	0,7	0,4	0,3	1,8	1,0	0,7
BFSC: _ 60%		1,4	0,8	0,6	1,7	1,0	0,7	4,1	2,4	1,6
SILICA FUME		2,2	1,3	0,9	2,6	1,6	1,1	6,4	3,8	2,6
CEMENTO CON CENIZAS (FLY ASH:20%)		1,7	1,0	0,7	2,0	1,3	0,8	4,9	3,0	2,0
		1,9	1,1	0,8	3,3	1,4	0,9	5,5	3,3	2,2

N : WITHOUT ADMIXTURES
AEA : AIR - ENTRAINING AGENT
DA : PLASTIFIER

Table 9

EXPOSURE CONDITIONS	F/(C+F) (%)	A	B (* Water curing)	α	β	γ
OUTDOOR	0	0,55	1	4,211	1,831	0,25
	30	0,77		3,311	1,777	
INDOOR	0	1,50	1,00 (7 days*)	1,656	0,622	0,5
	30	1,61	0,78 (91 days*)	1,445	0,619	

1.3.2. Rigourous models

They are based in Fick's laws of diffusion. Considering that the neutralization reaction of concrete, for which the reactant is immobilized, is very fast when compared with the process of diffusion, it may be assumed that there is an equilibrium between the free and the fixed reactants. In the simplest case, the concentration of the immobilized substance, is

$$S = R \cdot C \qquad [16]$$

where R is a constant and C is the concentration.

When diffusion is accompanied by the chemical reaction of the diffusing substance, the

$$\frac{\partial C}{\partial t} = D\frac{\partial^2 C}{\partial x^2} - \frac{\partial S}{\partial t} \qquad [17]$$

equation in one dimension has the form:

$$\frac{\partial C}{\partial t} = \frac{D}{R+1}\frac{\partial^2 C}{\partial x^2} \qquad [18]$$

Assuming that the diffusion coefficient D is constant, and substituting, one obtains:
If the relation between S and C is not linear, for example,

$$S = R \cdot C^n \qquad [19]$$

with R and n as constants, then the solution to this problem can only be obtained by numerical integration methods (42). In practice, approximations are used that greatly simplify the computation of the prediction of the carbonation front advance. Next, several of these models are presented.

Based in diffusion models **Schiessl**, (24) (figure 10), was the first to propose an expression that took into account a variation of D with carbonation depth, indicating that diffusion is increasingly more difficult as the carbonation front progresses. Thus, Schiessl defines a carbonation retardation factor, which is the one that controls the rate of the process. In this model the carbonation depth tends toward a finite limit. The model, however, does not take into consideration the diffusion of alkaline substances (although this factor may be of only limited importance) (figure 7), or the effect of humidity gradients within the concrete.

In his model, the amount of CO_2 which penetrates the concrete cover is given by the equation:

$$dq = c_c F \frac{C_1 - C_2}{x} dt$$

where dq= amount of CO_2 which has penetrated (kg)
Dc= diffusion coefficient of CO_2 at 90 days (m^2/s)
F= cross section (m^2)
C_1-C_2= concentration difference of CO_2 between the air and the carbonation front (kg/m^3)
x= carbonation depth (m)
t= time (s)

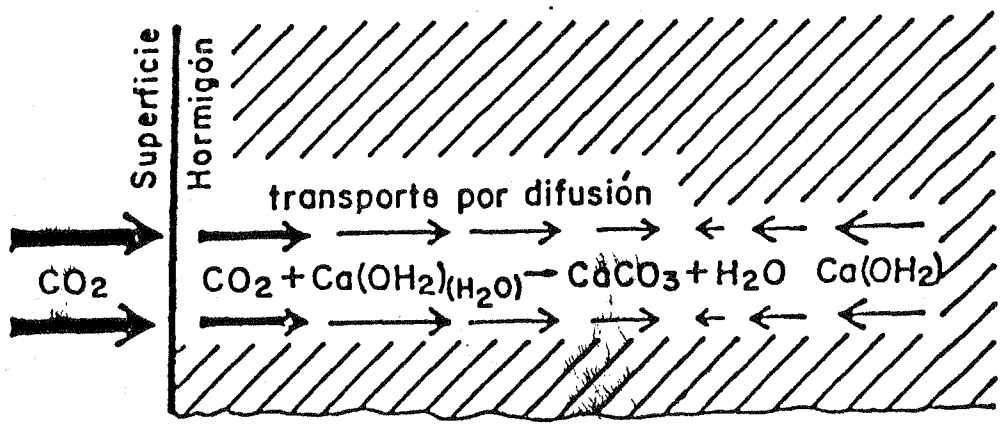

Figure 10

In turn, the amount of CO_2 needed to carbonate the concrete constituents is:

$$dq = adv \qquad [20]$$

being a= amount of alkaline components (kg/m^3) and dv= concrete volume (m^3).

By substitution it is obtained:

$$D_{cF}\frac{C_1 - C_2}{x}dt = adv = aFdx$$

Assuming that D_c and C_1-C_2 are constant, it can be arrived to a lineal dependence of x with the square root of time x= f($\sqrt{t}$). However, D_c is dependent on the time and depth.

Schiessl introduced as mentioned earlier, the factor **f**, which figures this dependence with the depth and a "retarding factor" **b**, which depends on the amount of alkalines diffusion from the interior to the exterior.

By this way, from D_c at 90 days (D_{90}), it can be obtained:

$$dq = D_{90}(1 - fx)F_D\frac{C_1 - C_2}{x}dt \qquad [21]$$

which by integration gives:

$$x = \frac{D_{90}(C_1 - C_2)}{b + f\,D_{90}(C_1 - C_2)} \qquad [22]$$

Schiessl considered that the retarding factor is not dominant, while Bakker (28) opposes to this, as although the diffusion of alkaline substances may be negligeable, is not the same with the effect of the humidity gradient also encountered in the retarding factor **b**.

Bakker (28) suggested that the observed discrepancy between the actual carbonation rates and those predicted by simplified application of a fixed law may be due to the latter not taking into consideration a variable diffusion coefficient. He indicates that the moisture profile and the concrete permeability depend on both time and distance from the surface, and also that the reaction between the CO_2 and the concrete components complicates the response compared to the case of a pure diffusional process.

In atmospheric exposure of concrete, the diffusion coefficient of the various levels within the concrete, is strongly dependent on the presence of periods of rain and/or high relative humidity. During the latter, the concrete absorbs water again, which means that the

carbonation depth is not parabolic with time (figure 11), but instead is a function of the finite limit . This limit value can be estimated as follows: a: assuming that concrete absorbs water more easily than it loses it, and b: assuming that the time between consecutive periods of waiting is constant (Figure 12). For example, at time t_i, the carbonation depth is x_i, and if after that there is a wetting period, when the drying process starts again, the carbonation front will move into position x_{i+1}. The effective length of the carbonation period is each time smaller, and the longer the concrete is wet during the curing period, the more slowly the concrete will dry out, and the less it will become carbonated.

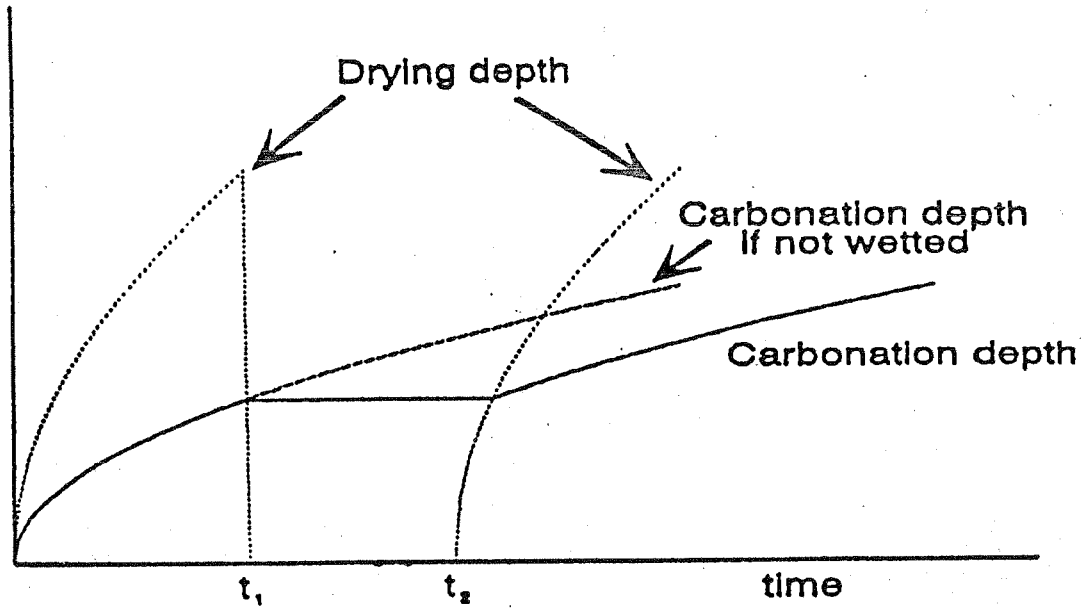

Figure 11. Shifting of the carbonation curve due to wetting

A more refined model to determine the carbonation limit (45), was proposed in which the diffusion coefficient of water vapor was taken into consideration, in addition to the variations of the diffusion coefficient of CO_2 addressed above. The resulting equation for the carbonation depth was as follows:

$$x_n = \sqrt{\frac{2D_c}{a}(c_1c_2)(t_{d1} + t_{d2}(x_1 overb)^2 + t_{d3}(\frac{x_2}{b})^2 \ldots\ldots + t_{dn}(\frac{x_{n1}}{b})^2)} \qquad [23]$$

$$b = \sqrt{\frac{2D_v}{b}(c_3c_4)}$$

x = carbonation depth
a = CaO content in the concrete
b = amount of water which evaporates from concrete
D_c = diffusion coef. of CO_2 at a particular RH
D_v = diffusion coef. of water vapour
C_1-C_2 = difference of CO_2 concentration between air and concrete
C_3-C_4 = difference in RH between air and concrete

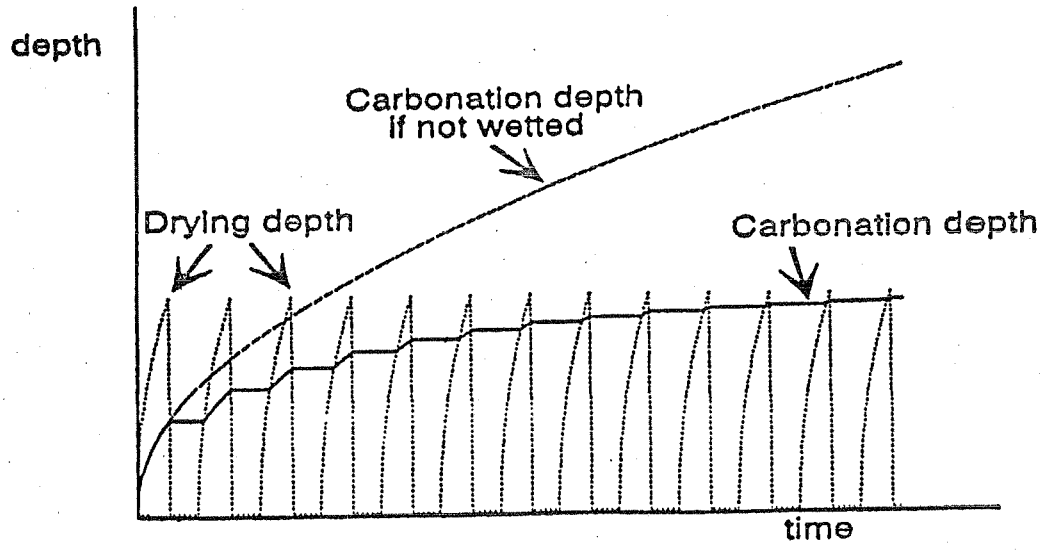

Figure 12. Carbonation front reaching the limit

In this formula:

$$(\frac{x_{n-1}}{B})^2 \qquad [24]$$

represents the time necessary to evaporate the water after N-1 wetting periods with their corresponding N-1 drying period. The wetting time is neglected by assuming that wetting takes place instantaneously. The variables in the two formulas are:

X= carbonation depth and time, t
$T_{N=}$ length of N drying periods
X_n=carbonation depth after N drying periods

Two square roots

D_C=future coefficient of CO_2 for a given moisture content in the pores
$D_{V=}$ diffusion coefficient of water vapor at the given moisture content in the pores
A= alkaline content in the concrete

C_1-C_2= the difference of CO_2 concentration between the air and the carbonation front
C_3-C_4= the difference in moisture between the air and the evaporation front.

As it can be seen in this model, Fick's diffusion equation is used twice, once to describe the drying period of carbonated concrete, and another to address the carbonation of dry concrete.

If drying terms were not considered, one would arrive at the expression, $X=A\sqrt{t}$; however, because of the wetting periods, there is a limit that will depend on the length of the drying period. This limit is expressed by $X_N = D\sqrt{t_N}$, and is reached as long as

$$m-(\frac{x_{n-1}}{B})^2 = 0 \qquad [25]$$

and therefore, if T = 0, this presupposes that there is no drying, and if X = 0, there is no carbonation (26) (figure 13).

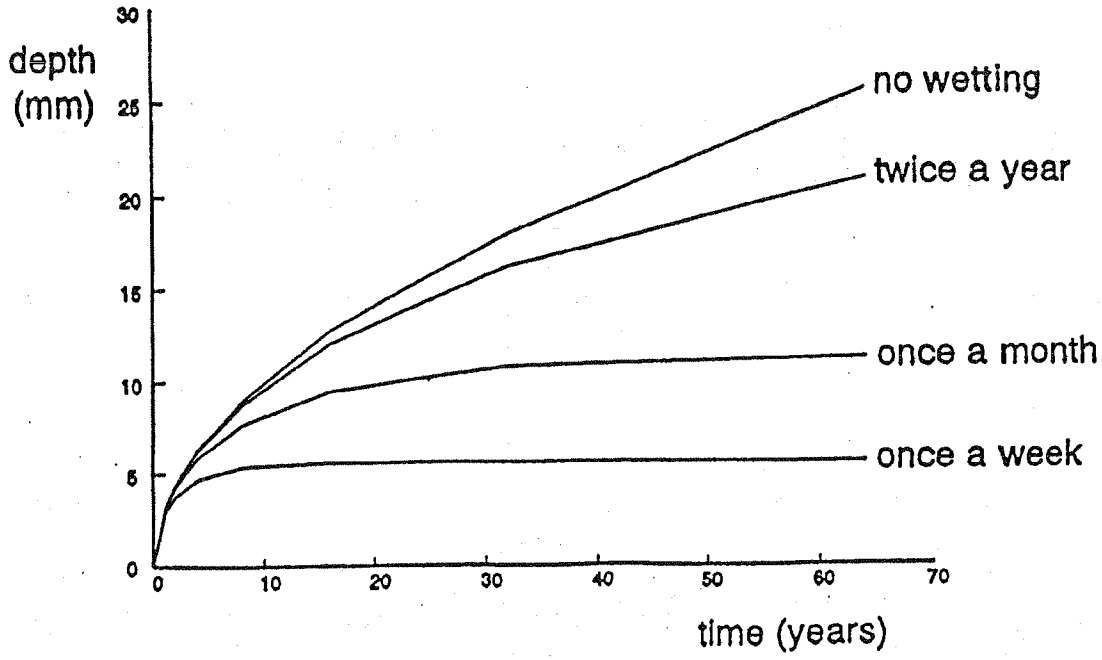

Figure 13. Influence of wetting and drying on rate of carbonation.

The relationships described above to determine the rate of carbonation take into account in one way or another the influence of one or more selected variables that may effect the carbonation process. However, no single expression has yet been defined that includes all relevant parameters. An exact theoretical relationship, predicting the carbonation depth, is therefore not available, in part because some of the relevant parameters are not practically measurable.

Tuutti (16) also proposed a diffusional model for carbonation rate. It is based in the concept of moving boundaries, which considers the diffusion plus a complete reaction (inmovilization) of the CO_2 (figure 14).

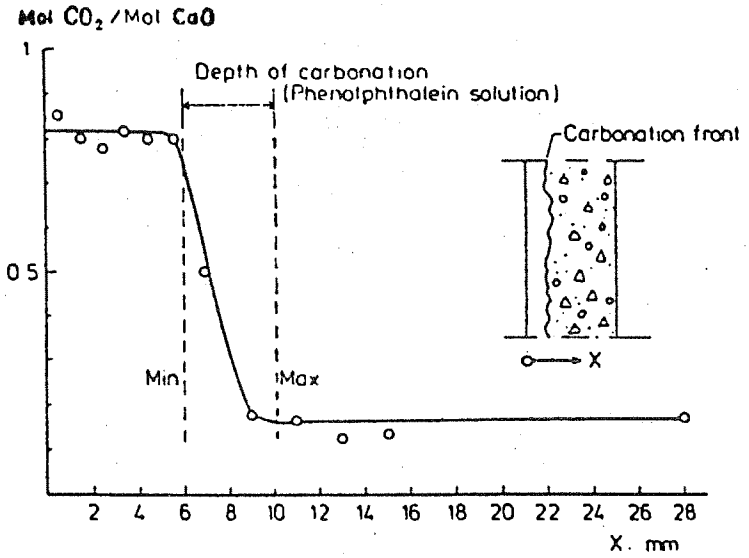

Figure 14. Measured CO_2/CaO in carbonated concrete designated 25 D concrete

He arrives to the following expression:

$$\frac{C_s}{C_x} = \sqrt{\pi}\left[\frac{x/\sqrt{t}}{2\sqrt{D}}\right]\exp\left[\frac{x^2}{4Dt}\right]erf\left(\frac{x/\sqrt{t}}{2\sqrt{D}}\right) \qquad [26]$$

where:

C_s = CO_2 concentration in the atmosphere
C_x = amount of bound CO_2 (cement phases pore solution), mol/m^3
D = CO_2 diffusion coefficient
x = Carbonation depth
t = time

An example of plots log x-logt is shown in figure 15.

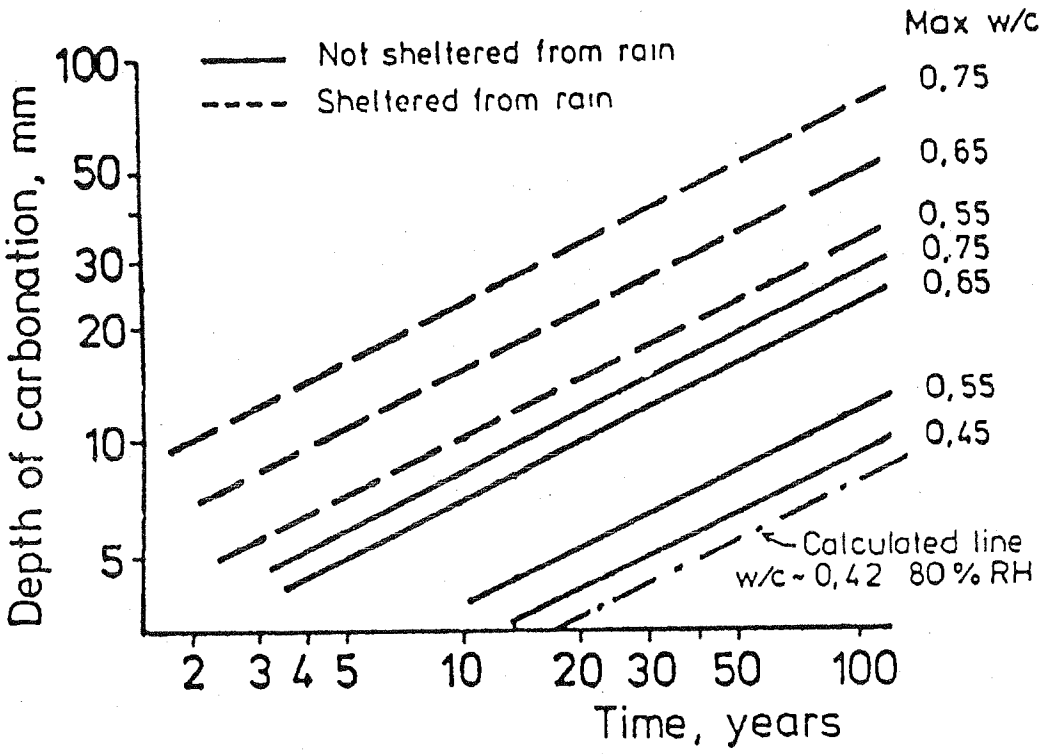

Figure 15

Papadakis (43)(44) model is based in chemical considerations. He tries to model the kinetics of the expected reactions of the CO_2 with the cement phases in combination with the hydration reactions of the cement. However, he does not take into account the alkaline hydroxides of Na and K, which supposes an important defficit in his model.

He proposes an expression, in which the carbonation constant K_c is function of the reaction ability of the cement constituents.

$$x = \sqrt{\frac{2[CO_2]\,D_{CO_2}}{[Ca(OH)_2] + 3[C_3S] + 2[C_2S]}}\sqrt{t} \qquad [27]$$

Finally, **Parrott** (45) proposes a completely empirical model, based in the fitting of a parabollic curve to carbonation data obtained in a large set of real structures. This fitting was made with a 90% of confidence. That is, by leaving out only 10% of the results (see figure 16).

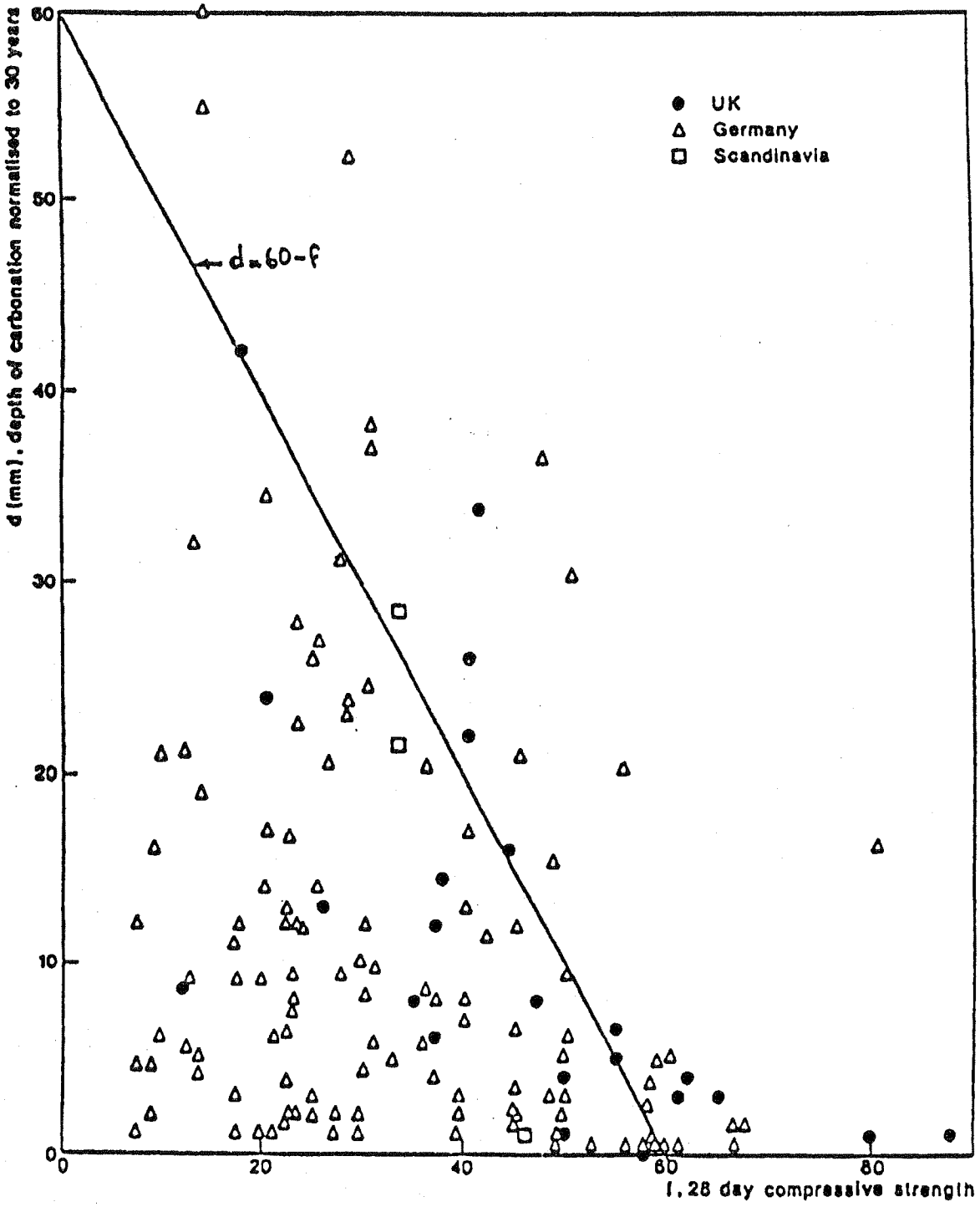

Figure 16. Carbonation depths normalized to 30 years plotted against 28 day compressive strength. Outdoor exposure sheltered from rain.

He arrives so to an expression:

$$x = ak^{0.4} t^{n} / c^{0.5} \qquad [28]$$

where:

k= (in units of $10^{-16}m^2$) is the air permeability of cover concrete and depends upon the relative humidity, r% in the cover concrete (10,11). If k is unknown it can be estimated from the permeability of a test specimen dried at 60% relative humidity, k_{60} (11) using the equations:
$k = mk_{60}$
$m = 1.6 - 0.00115\, r - 0.0001475 r^2$
or $m = 1.0$ if $r < 60$

n= is a power exponent that is close to 0.5 for indoor exposure but decreases as the relative humidity rises above 70% to account for the slower rates of carbonation observed under wetter conditions (1,6).
$n = 0.02536 + 0.01785\, r - 0.0001623\, r^2$

c= is the calcium oxide content in the hydrated cement matrix of the cover concrete (in kg/m^3 of cement matrix) that can react with and effectively retard the rate of carbon dioxide penetration; it depends upon the cement composition, exposure condition and the proportions of cement reacted. Some estimates of c are given in Ref. (45) for a range of relative humidities and different European (EN 197) cement types, together with corresponding values of m and n.

a= is a coefficient that can be assigned a value of 64.

REFERENCES

1. MEYERS, S.L. - Rock-Products. U.S.A., N° 52, pg. 96-98 (1949).
2. VENUAT, M. and ALEXANDRE, J. - CERILH, publicación n° 195.
3. GASPAR TEBAR, D. and MUÑOZ PLAZA, M. - Materiales de Construcción n° 165, pg.1, (1977).
4. NORMAN MAYCOCK, J. and SKALNY, J. - Cement and Concrete Research, vol.4, pg. 69-76 (1974).
5. FERNANDEZ PARIS, J.M. - Monografía n° 310. I.E.T.c.c. Madrid (1973).
6. SHRÖDER, F. and SMOLZYK, H.G. - 5th International Symposium on the Chemistry of Cement, pg. 188, Tokio (1968).
7. VENUAT, M. - Rencontres Cefracor, 77, IEBTP - CATED (1977).
8. CALLEJA, J. - 7° Congreso Internacional de París, Tema VII, pg.6 (1980).
9. MANNS, W. and WESCHE, K. - 5th Int. Symposium on the Chemistry of Cement. Tokio (1968).

10. GASPAR TEBAR, D., DEL OLMO RODRIGUEZ, C. and VAZQUEZ MORENO, T. - RILEM. Int. Symposium, Abril (1976).
11. MEYERS, S.L. - Revue des Materiaux, Nov. (1949).
12. LEBER Y BLAKEY - Journal of Amr. Concr. Inst. Sept. (1956)
13. VERBECK, G. - Carbonation of Hydrated Portland Cement, Wahington, (P.C.A. Boletín nº 87) febrero, (1958).
14. WIERING - RILEM Seminar, Hannover, Marzo (1984).
15. ASCHAN, N. - Nordisk-Beton, nº 3, pg.275 (1963).
16. TUUTTI, K. - Corrosion of steel in concrete, CBI Forskning research, Stockholm (1982).
17. BAKKER - Corrosion of steel in Concrete, state of the art. Report. RILEM. Technical commite 60-CSC. Abril (1986).
18. SCHIESSL, M. and MARTIN, H. - Betonwerk + Fertigteil, Hefh 2, pg.588-590, (1975)
19. SCHIESSL, P. - Corrosion of reinforcement - durability of concrete structures, CEB-RILEM, Mayo (1983) Copenague.
20. ALEKSEEV, S.N. and ROZENTAL, N.K. - Rilem Int. Symposium carbonation of concrete, Abril, U.K. (1976).
21. HAMADA, H. - 5th International Symposium onthe Chemistry of Cement. pg. 343, Tokio (1968).
22. HO, D.W.S. and LEWIS, R.K. - International Conference Fly Ash, Silica Fume, Slag and Natural Puzzolans in Concrete. SP79-17, pg.333-346 Detroit.
23. PAILLERE, A.M., RAVERDY, M. and GRIMALDI, G. - 2th Int. Conference of fly ash, silica fume, slag and natural puzzolans in concrete, SP91-25, pg.541 (1986).
24. LITVAN, G.G. and MEYER, A. - 2nd Int. Conference of fly ash silica fume, slag and natural puzzolans in concrete. SP91-71, pg.1445 (1986).
25. SKJOLSVOLD,O. - 2nd Int. Conference of fly ash, silica fume slag and natural puzzolans in concrete, SP91-51 pg.1031 (1986).
26. FATTUHI, N.I. - Materiaux et constructions vol. 19, nº 110, pg 131, (1986).
27. SMOLCKYK, H.G. - RILEM Int. Symposium carbonation of concrete, U.K. Abril (1976).
28. SHIGEYOSHI NAGATAKI, HYROYUKIOHYO and EUNKYUMKIM - 2nd Int. Conference of fly ash, silica fume, slag and natural puzzolans in concrete - SP91-24, pg.521 (1986).
29. TREADAWAY, K.W.J. - Corrosion of reinforcement in concrete construction Edt. Alan P. Crane, Cap. 11, pg159 (1983).
30. WEBER, H. - Betonwork + Fertigteil - Technik pg. 5-8, (1983).
31. SUZUKI, K., NISHKAWA, T. and ITO, S. - Cement and concrete research, vol.15, pg.213, (1985).
32. BLENKIN, R.D., CURRED, B.R. MIDGLEY, H.G. and PERSONAGE, J.R. - Cement and concrete research, vol.15, nº 2, pg.276, (1985).
33. WOODS, H. - Mat. perf. 13 (10), g 31, (1974).
34. ALEKSEEV, S.N. and ROZENTAL, N.K. - Beton, Korrosion Von Stahlbeton in aggressiver Industrieluft; cap.4, pg65, (1976).

35. SHIESSL, P. - DAFSTB, n°255, pg. 39, (1976).
36. EH-82 - Instruccion para el proyecto y la ejecución de obras de hormigón en masa o armado. Comisión permanente del hormigón (1982).
37. Código Modelo CEB - FIP para las estructuras de hormigón, comité Europeo del hormigón (1978).
38. RODRIGUEZ, J. and ANDRADE, C. - I Congreso de patología en la edificación, Feb.(1985) Barcelona.
39. BIZOCK, I. - La corrosión del hormigón en masa o armado. Edt. URMO, Cap.4, pg.220, (1963).
40. STEOPOE, A. - Zement, n° 50, (1935).
41. SMOLCZYK, H. - 5th Int. Conf. on Chem. of Cement, Vol. 3, Tokyo. (1968). pp. 369-384.
42. CRANK, J.- Oxford University Press. Oxford. (1975).
43. PAPADAKIS, V. G., Vayenas, C. G. and Fardis, M. N. - AIChE Journal, Vol. 35, N° 10. (1989). pp. 1639-1648.
44. PAPADAKIS, V. G., VAYENAS, C. G. and FARDIS, M. N. - "Durability on building materials." Brighton. (1990). pp. 27-38
45. PARROTT, L.J. - SP-145-15 International Congress on Durability of Concrete, Nice (France) Canmet - Malhotia Ed., pp.283-298 (1994).

2. GENERAL BIBLIOGRAPHY ON CARBONATION

2.1 Carbonation and corrosion

AL-AMOUDI, O.S.B., RASHEEDUZZAFAR, MASLEHUDDIN, M. - Carbonation and corrosion of rebars in salt contaminated OPC/PFA concretes -Cement and Concrete Research. Vol. 21, pp.38-50, 1991.

AL-RABIAH, A.R., BAGGOT, R. and RASHEEDUZZAFAR - Construction and Durability Considerations for King Fahd Causeway - A Case Study. ACI. SP 109-32 pp. 705-735. 1988.

BYFORS, K. - Carbonation of concrete with silica fume and fly ash - Till Nordic Concrete Research 1985.

BOB, C. - Some aspects concerning corrosion of reinforcement - Protection of Concrete - Dundee 1990. pp.53-61, Ed.R.K.Dhir and J.W. Green. - Chapman and Hall Editorial.

BONNET, D. and RUBAUD, M. - Influence des variations du pH du milieu - Cahiers du Centre Scientifique et Technique du Batiment. n° 168. Cahier n° 1371. Abril 1976

BONNET, D. and RUBAUD, M. - Contribution à l'étude du comportement des métaux dans les bétons carbonatés. Cahiers du Centre Scientifique et Technique du Batiment. n° 169. Cahier n° 1378. Mayo 1976.

GLASS, G.K., PAGE, C.L. and SHORT, N.R. - Factors affecting the corrosion rate steel in carbonated mortars - Corrosion Science, Vol. 32, n° 12, pp. 1283-1294, 1991.

GOUDA, V.K. and MOURAD, H.M. - Galvanic cells encountered in the corrosion of steel reinforcement. I.Differential pH cells. Corrosion Science, vol.14, pp. 681-690, 1974.

HAQUE, M.N. and KAWAMURA, M. - Carbonation and Chloride-Induced Corrosion of Reinforcement in Fly Ash Concretes - ACI Materials Journal. Vol. 89, n° 1, Jan-Feb 1992.

KAMASI, H., IZUMI, I., TOMOSAWA, F. and FUKUSHI, I. - Carbonation of concrete and corrosion of reinforcement in reinforced concrete - 2nd CEB-RILEM International Workshop. October 1986.

KAYYALI, O.A. and HAQUE, M.N. - Effect of carbonation on the chloride concentration in pore solution of mortars wiht and wihtout flyash. Cement and Concrete Research. Vol. 18, pp.636-648, 1988.

MEDGYESI, I, KEMPER, M., KELEMEN, M. - L'effet de la carbonisation sur la durabilité des structures en béton armé. RILEM-ACI. Colloque international sur L'observation a long terme des structures en beton. Sep.1984. Budapest, pp. 147-159.

NAGATAKI, S., MANSUR, M.A and OHGA, H. - Carbonation of Mortar in Relation to Ferrocement Construction - ACI Materials Journal -Title n° 85-M3. pp. 17-25, January-February 1988.

PARROT, L.J. - Damage caused by carbonation of reinforced concrete - Rilem technical committees commissions techniques de la Rilem. 104-DCC: Damage classification of concrete structures evaluation des domages des ouvrages en beton. Matériaux et Constructions, 1990, 23, 230-234.

PARROTT, L.J. - Carbonation in reinforced concrete: A bibliography - Cement and Concrete Association.U.K. Report 20, July 1987.

PARROTT, L.J. and KILLOH, D.C. - Carbonation in a 36 year old, in-situ concrete - Cement and Concrete Research, Vol. 19, Report 25, pp 649-656, 1989.

PARROTT, L.J. - A review of carbonation in reinforced concrete BCA-Report 19, July 1987.

PAZINI, E.J., and RECENA, F.A.P. - Aspectos da tecnologia da argamassa armada que podem définir sua durabilidade - Reunião anual de 1991.Durabilidade do concreto estructural, São Paulo, 26 a 30 Agosto. 1991.

SCHIESSL, P. - Relation between the crack width and the amount of corrosion at the reinforcement - Betonwerk+Fertigteil-Technik, pp. 594-598, Heft 12/1975.

SCHRÖDER, F. and SMOLCZYK, H.G. - Carbonation and Protection against Steel Corrosion - Discusión del informe principal de la sesión I.V. 3. Slags and Slag Cements (Fritz Schröder/Part. IV. Proceedings of the Fifth International Symposium on the Chemistry of Cement, pag. 149, Tokyo 1968).

SHORT, N.R., PAGE, C.L. and GLASS, G.K. - A galvanic sensor for monitoring corrosion of steel in carbonated concrete - Magazine of Concrete Research, 1991, 43, nº 156, pp. 149-154, Sept.1991.

SORETZ, S. - La corrosion des constructions en beton arme - Un nouveau slogan? - Betonstahl in entwicklung. Tor-Isteg Steel Corporation. Luxembourg. Cahier 67.Vienne, Octobre 1979.

STOLTE, E. and BOHNENKAMP, K. - Korrosionsverhalten der bewehrung von stahlbeton. pp. 113-127.

VENUAT, M. - Relation entre la carbonatation du beton et les phenomenes de corrosion des armatures du beton. Rencontres CEFRACOR 77 ITBTP-CATED "La protection contre la corrosion dans le bâtiment". Journées des 25-26 Octobre, 1977.

WEBER, H. - Methods for calculating the progress of carbonation and the associated life expentancy of reinforced concrete components. Heft 8. pp.508-514. 1983.

2.2 Carbonation/Skrinkage

HISAKA, M., MANO, T., YASUDA, M. and KANDA, A. - Study on Method of Cracking Test of Concrete Due to Drying Shrinkage. Nº 101, pp. 326-329 CAj Review 1988.

KONISHI, M., ASAGA, K., DAIMON, M. and GOTO, S. - Drying Shrinkage of Hardened Cement Pastes. Nº 99, pp. 318-321. Caj Review, 1988.

LEA, F.M. and DESH - Química del cemento y el hormigón - Publicaciones de la Escuela Técnica Superior de Ingenieros de Caminos, Canales y Puertos. Traducción de Manuel Benitez y Manuel Galán. Edición original publicada por Edward Arnol, Editores. Londres. Traducción de la obra inglesa The chemistry of cement and concrete.

MARTINEZ YNZENGA, J.I. - Retracción de morteros y hormigones - Monografías del Instituto Eduardo Torroja de la Construcción y del Cemento. nº 260, Madrid, febrero de 1967.

MOSKVIN, V., IVANOV, F., ALEKSEYEV, S. and GUZEYEV, E. - Concrete and Reinforced Concrete Deterioration and Protection - Edited by Prof. V. Moskvin, Moscow.

SOROKA, I. - Portland Cement Paste and Concrete - Unwin Brothers Limited, Old Woking, Surrey. British Library Cataloguing in Publication Data. I.Soroka 1979.

VENUAT, M. - Influence du milieu de conservation sur le retrait hydraulique apres prise - RILEM-CEMBUREAU. The shrinkage of hydraulic concretes. Vol.II, Madrid, 1968.

2.3 Measurement of carbonation rate

CURRIE, R.J. - Carbonation depths in structural-quality concrete: an assessment of evidence from investigations of structures and from other sources - BRE. Report 1986.

CURTIL, L., GIELLY, J. and MURAT, M. - The polarizing microscope: A tool of interest for investigation on concrete; application to carbonation - Cement and Concrete Research. Vol.23, pp.329-334, 1993.

LEVY, C. - La carbonatation acceleree des betons. Comparaison entre des betons courants et des betons a hautes performances.- Seminaire durabilite des betons a hautes performances. 29-30 Mayo 1990.

PARROTT, L.J. - Assessing carbonation in concrete structures - Durability of Building Materials and Components. Proceedings of the Fifth International Conference held in Brighton, U.K., 7-9, pp. 575-586, November 1990.

REIJONEN, H. and PIHLAJAVAARA, S.E. - On the determination by neutron radiography of the thickness of the carbonated layer of concrete based upon changes in water content - Cement and Concrete Research. Vol. 2, pp 607-615, 1972.

RENCHER, J, and POLSTER, H. - Schnellmethode zur Bestimmung der Alkalität von Betondeckungen mit Indikatoren (Método rápido para determinar la alcalinidad de los recubrimientos de hormigón, mediante indicadores) - Bauplanung-Bautechnik, 25.Jg. Helt 8, August 1971.

RILEM DRAFT RECOMMENDATION. Concrete permanent committee. Measurement of hardened concrete carbonation depth CPC-18. Matériaux et Constructions, vol. 17. nº 102.

RILEM RECOMMENDATIONS. TC56- MHM Hydrocarbon Materials. CPC-18 Measurement of hardened concrete carbonation depth.

2.4 Models of carbonation rate

ALEKSEEYEV, S.N. - Method of permeability control of concrete protective layer in products - Fourth International Conference on Durability of Building Materials & Components, Singapore 1987.

ALEXANDRE, J. - Construction au CERILH d'une armoire de conservation en atmosphère carbonique. Publication du CERILH nº 198.

BAKKER, R. - Corrosion of steel in concrete (state of the art report). Rilem technical committee 60-CSC, Abril 1986.

BAKKER, R. - Permeability of Blended Cement Concretes - SP79-30, pp. 589-605.

BETONTECHNISCHE BERICHTE. Karbonatisierung des betons: einflüsse und auswirkungen auf den korrosionsschutz der bewehrung. (1972). 128 pp.

BOB, C. Some aspects concerning corrosion of reinforcement. En "Protection of Concrete". Recopilado por R. K. Dhir y J. W. Green, University of Dundee. (1990). pp. 53-61.

BROWN, G.E. - "Discussion" Hydration and Carbonation of Pozzolanic Cements (Papadakis, V.G. ...) - ACI Materials Journal. p.102. Jan-Feb.1993.

DAIMON, M.; AKIBA, T. y KONDO, R. Through pore size distribution and kinetics of carbonation reaction of OPC mortars. J. Amer. Ceramic Soc., Vol. 54, Nº 9. (1971). pp. 423-428.

DHIR, R.K., HEWLETT, P.C., and CHAN, Y.N. - Near-surface characteristics of concrete: prediction of carbonation resistance. Magazine of Concrete Research, 41, nº 148, pp.137-143, Sept. 1989.

FUKUSHIMA, T. - Predictive Methods on the Progress of Neutralization (Carbonation) of Concrete by Unsteady State Dynamic Analysis - Caj Review, pp 210-213.1988.

HAMADA, M. - Neutralization (Carbonation) of Concrete and Corrosion of Reinforcing Steel. 5th Int. Symposium on the Chemistry of Cement - Tokyo 1968.

KASAMI, H. e IZUMI, I. et al. Carbonation of concrete & corrosion of reinforcement in reinforced concrete. Durability of RC Japan, Tukuba. (Septiembre-Octubre, 1986). 12 pp.

KISHITANI, K., SHIIRE, T., TOMOSAWA, F., FUKUSHI, I. and KASAMI, H. - Carbonation of concrete in existing structures up to 55 years old and a porposal of reliability design technique for cover thickness of reinforcement - Annex 2. 2nd CEB-Rilem Workshop 1986.

LE SAGE DE FONTENAY, C. Effect of concrete admixtures, composition & Exposure on carbonation in Bahrain. En "Deterioration & Repair." Bahrain. (1985). pp. 467-483.

NAGATAKI, S.; OHGA, H. y KIM, E. Effect of curing conditions on carbonation and corrosion in fly ash concrete. Proc. ACI SP-91, Vol. 1, Madrid. (1986a). pp. 521-540.
NAGATAKI, S.; UJIKE, I. y KONISHI, N. Influence of moisture content on air permeability of concrete. Review of 40 Meeting of Cement Association of Japan, Tokio. (1986b). pp. 158-161.

NISCHER, P. Effect of environment and concrete quality on carbonation. Betonwerk + Fertigteil + Tech., Nº 11. (1984). pp. 752-757.

MATTHEWS, J. D. Carbonation of ten-year-old concretes with and with out added pulverised-fuel ash. Proceedings of 2nd International Conference on Ash Technology and Marketing, Barbican Centre, Londres. (1984). Abstract Paper 398a.

MOPU. Relación entre la profundidad de carbonatación y distintas características fisicomecánicas del hormigón. MOPU, COAAT, Murcia. (1985). 8 pp.

PAPADAKIS, V.G., FARDIS, M.N. and VAYENAS, C.G. - Fundamental concrete carbonation model and application to durability of reinforced concrete - Symposium Durability of Building Materials and Componments - Brighton (U.K.) pp. 27-38. 1990.

PAPADAKIS, V.G., VAYENAS, C.G. and FARDIS, M.N. - Fundamental Modeling and Experimental Investigation of Concrete Carbonation - ACI Materials Journal, v.88, nº 4, July-Aug. 1991.

PAPADAKIS, V.G., VAYENAS, C.G. and FARDIS, M.N. - A Reaction Engineering Approach to the Problem of Concrete Carbonation - ACI Materials Journal. Vol.35, nº 10, p.1639. Oct.1989.

PAPADAKIS, V.G., FARDIS, M.N. and VAYENAS, C.G. - Effect of composition, environmental factors and cement-lime mortar coating on concrete carbonation - Materials and Structures, 25, 293-304, 1992.

PARROTT, L. J. Factors influencing relative humidity in concrete. Magazine of Concrete Research, Vol. 43, Nº 154. (1991a). pp. 45-52.

PARROTT, L. J. CEN TC 104/WG1/TG1/ Panel 1. Paper Nº 20. (1991b).

SAETTA, A.V., SCHREFLER, B.A. and VITALIANI, R.V. - The carbonation of concrete and the mechanism of moisture, heat and carbon dioxide flow through porous materials - Cement and Concrete Research, Vol. 23, pp 761-772, 1993.

SCHOLZ, E. y WIERIG, H. Carbonation of fly ash concrete. Proc. RILEM Seminar, Hannover. (1984). pp. 258-265.

SCHUBERT, P. y BERG, W. Coal fly-ash to DIN. Betonwerk + Fertigteil + Tec. (1979). pp. 692-696.

SMOLCZYK, H. Discussion of principal paper on carbonation of concrete by Hamada. 5th Int. Conf. on Chem. of Cement, Vol. 3, Tokyo. (1968). pp. 369-384.

SMOLCZYK, H. Physical an chemical phenomena of carbonation. RILEM Symp. on Carbonation of Concrete. (1976). p. 10.

TOMOSAWA, F. and FUKUSHI,I. - A preliminary study on the prediction of service life of reinforcing concrete based on carbonation and corrosion of reinforcement. Annex 1. 2nd CEB-RILEM Workshop 1986.

TOMOSAWA, F., FUKUSHI, I., MORINAGA, S. - A Preliminary study on the prediction of service life of reinforced concrete based on carbonation and corrosion of reinforcement - First Joint Workshop on Durability of Reinforced Concrete. Australia. 1986.

VENUAT, M. - De la carbonatation du béton - Publication du CERILH, nº 195.

VENUAT, M. y ALEXANDRE, J. Publicación del C.E.R.I.L.H., Nº 195. (1969). 30 pp.

VESIKARI, E. Prediction of service life of concrete structures and reinforcement corrosion. Tech. Res. Centre Finland Prelim Report. (1985). 25 pp.

WIERIG, H.J. - Longtime studies on the carbonation of concrete under normal outdoor exposure - Rilem - Hannover (1984).

2.5 General on concrete carbonation

ASCHAN, N. - Investigación termogravimétrica del fenómeno de carbonatación en el hormigón. Nordisk Betong, nº 3, pág. 275, 1963.

BENTUR, A. and JAEGERMANN, C. - Effect of curing and composition on the development of properties of the outer skin of concrete - ASCE J. Mater.Civil Eng.
BICKLEY, J.A. - Potential for carbonation of concrete in Canada. SP 122-16.

COAAT de Murcia y MOPU - Relación entre la profundidad de carbonatación y distintas características fisicomecánicas del hormigón. Gabinete Técnico del Laboratorio de Ensayos del Colegio Oficial de Aparejadores y Arquitectos Técnicos de Murcia, 1985.

EWERTSON, C. and PETERSON, P.E. - The influence of curing conditions on the permeability and durbility of concrete. Results from a field exposure test - Cement and Concrete Research. Vol.23, pp.683-692, 1993.

FATTUHI, N.I. - Carbonation of concrete as affected by mix constituents and initial water curing period. Matériaux et Constructions. Vol. 19, nº 110, pp 131-136, 1986.

FATTUHI, N.I. - Carbonation of concrete as affected by mix constituents and initial water curing period. Matériaux et Constructions, Vol. 19, nº 110, pp.131-136.

FATTUHI, N.I. - Concrete carbonation as influenced by curing regime. Cement and Concrete Research. Vol. 18, pp. 426-430, 1988.

FUKUSHIMA, T. - Theoretical investigation on the influence of various factors on carbonation of concrete - Fourth International Conference on Durability of Building Materials & Components, Singapore 1987.

HAYES, A.J. - Corrosion damage to a precast concrete grandstand facility. Corrosion 87. Paper 141. March 9-13. San Francisco. 1987.

IZUMI, I. - Effects of Concretes Constituents on Carbonation of Concrete - First Joint Workshop on Durability of Reinforced Concrete. Australia - Japan Science and Technology Agreement. Japan, September 30 - October 2, 1986.

JAEGERMANN, C. - Chloride penetration and carbonation in concrete exposed to mediterranean marine environment. - FIP Symposium. Israel 1988, pp.1-10.

JEGOROW, M. - Contribution of brick skins to the corrosion protection of steel reinforcement in concrete - Z International, 2, pp 89-94, February 1980.

MORI, T., SHIRAYAMA, K. and YODA, A. - The Neutralization of Concrete, the Corrosion of Reinforcing Steel and the Effects of Surface Finish. pp. 249-255.

NISCHER, P. - Einfluß der Betongüte auf die Karbonatisierung. Zement und Beton, 29 Jahrgang, Heft 1, pp.11-15, 1984.

NISCHER, P. - Effect of Environment and Concrete Quality on Carbonation. Betonwerk+Fertigteil-Technik, Heft 11, pp.752-757. 1984.

PARROTT, L.J. - Carbonation, moisture and empty pores - Advances in Cement Research, 4, nº 15, pp.111-118, July 1991/92.

POMEROY, C.D., SC, D., PHYS, C., INST P, F.,FACI, FSS. - ENV 197 CEMENTS: Perspective in relation to EC2 and ENV 206 - Seminar: Performance of limestone-filled cements: report of joint BRE/BCA/Cement working party. Paper nº 10. Nov. 1989.

ROBERTS, M.H. - Carbonation of concrete made with dense natural aggregates - BRE Information IP 6/81. April 1981.

SAUMAN, Z. - Effect of CO_2 on porous concrete. Cement and Concrete Research. Vol. 2, pp.541-549, 1972.

SKAARUP, J. and FONTENAY - The influence of exposure conditions on the rate of carbonation of different concretes in Bahrain. pp-203-223.

VENUAT, M. - Carbonatation. La Commission Technique 16-C. Matériaux et Constructions - vol. 11, nº 62 pp.142-146

2.6 Blending materials influence

BAWAJA, D., HOPER, H., COOK, D.J. - Carbonation characteristics of in-situ portland cement and fly ash concretes in Australia, England and the United States - Fourth International Conference on Durability of Building Materials & Components, Singapore 1987.

BUTTLER, F.G., DECTER, M.H., and SMITH, G.R. - Studies on the Desiccation and Carbonation of Systems Containing Portland Cement and Fly Ash. SP 79-19. pp. 367-381. V.M. Malhotra Ed. Vol. I.

CALLEJA, J. - En torno a las cenizas volantes en los cementos y en los hormigones, a la luz de un trabajo presentado en el 7º Congreso Internacional de la Química de los Cementos. Materiales de Construcción, nº 165, pp. 3-13, 1982.

DE CEUKELAIRE, L. and VAN NIEUWENBURG, D. - "Accelerated carbonation of a blast-furnace cement concrete - Cement and Concrete Research, Vol. 23, pp.442-452, 1993.

DHIR, R.K., JONES, M.R. and McCARTHY, M.J. - Pulverized-fuel ash concrete: carbonation-induced reinforcement corrosion rates - Proc. Instn. Civ. Engrs Structs & Bldgs, 94, pp-335-342, Aug. 1992.

HO, D.W.S. and LEWIS, R.K. - Carbonation of Concrete Incorporating Fly Ash or a Chemical Admisture - SP 79-17, pp.334-346.

HOBBS, D.W. - Carbonation of concrete containing pfa - Magazine of Concrete Research, Vol.40, nº 143. June 1988.

KASAI, Y., MATSUI, I., FUKUSHIMA, Y. and KAMOHARA, H. - Air Permeability and Carbonation of Blended Cement Mortars - SP 79-23 pp-435-451, M.M. Malhotra Ed. vol.I.

KIKUCHI, M. and MUKAI, T. - Carbonation of Concrete Containing Sintered Fly-ash Coarse Aggregate. Caj Review, pp-228-231, 1988.

LIN, X.X., FU, Y. - Influence of microstructure on carbonation of concrete containing fly ash - Fourth International Conference on Durability of Buildings Materials & Components, Singapore, 1987.

MELAND, I. - Carbonation in Hardened fly ash cements. Blended Cements in Construction, Elsevier Ed., R.N. Swamy Ed. Sheffield, Sept. 1991, pp.329-335.

NAGATAKI, S., MANSUR, M.A., OHGA, H. - Carbonation of mortar and con concrete with mineral admixtures - Fourth International Conference on Durability of Building Materials & Components, pp.671-678, Singapore 1987.

PAPADAKIS, V.G., FARDIS, M.N. and VAYENAS, C.G. - Hydration and Carbonation of Pozzolanic Cements - ACI Materials Journal. Vol.89, nº 2, p.119. Mar-Apr.1992.

SCHIESSL, P. - Carbonation of Concretes Using Various Cements - Betonwerk+Fertigteil-Technik, pp. 588-590, Heft 12/1975.

THOMAS, M.D.A. and MATTHEWS, J.D. - Carbonation of fly ash concrete. Magazine of Concrete Research, nº 140, 44, September, 217-228, 1992.

2.7 Influence of cement Chemistry

BENSTED, J. - Some hidration investigations involving Portlnad cement - effect of calcium carbonate substitution of gypsum. World Cement Technology, pp. 395-406, Oct. 1980.

BERGER, R.L. and KLEMM, W.A. - Accelerated curing of cementitious systems by carbon dioxide. Part II. Hydraulic calcium silicates and aluminates. Cement and Concrete Research. Vol. 2, pp. 647-652, 1972.

BERGER, R.L. - Stabilization of silicate structures by carbonation. Cement and Concrete Research. Vol. 9, pp. 649-651, 1979.

BUIL, M. and BARON, J. - Le retrait autogène de la pâte de ciment durcissante. 7th Int. Congress on Cement Chemistry - Paris 1980, VI-pp.37-42.

FERNANDEZ PARIS, J.M. - La carbonatación de la pasta hidratada de cemento portland. Interpretación físico-química. Monografías del Instituto Eduardo Torroja de la construcción y del cemento. nº 310, Madrid, Mayo 1973.

GASPAR TEBAR, D., DEL OLMO RODRIGUEZ, C. y VAZQUEZ MORENO, T. - Influencia del CO_2 sobre un cemento portland anhidro. Materiales de Construcción, nº 161, Ene-Feb-Marzo 1976.

GASPAR-TEBAR, D. y MUÑOZ-PLAZA, M. - Acción del CO_2 sobre un cemento portland. I. Influencia sobre las características químicas y fisicomecánicas. Materiales de Construcción. nº 165, Ene-Feb-Marzo 1977.

GASPAR-TEBAR, D., MUÑOZ-PLAZA, M. y VAZQUEZ-MORENO, T. - Acción del CO_2 sobre un cemento portland. II. Estudio por espectroscopía infrarroja. Materiales de Construcción. nº 168, Oct.Nov.Dic. 1977.

KLEMM, W.A. and BERGER, R.L. - Accelerated curing of cementitious systems by carbon dioxide. Part I. Portland Cement. Cement and Concrete Research, vol. 2, pp.567-576, 1972.

KOBAYASHI, K. and UNO, Y. - Influence of alkali on carbonation of concrete, Part I. Preliminary tests with mortar specimens. Cement and Concrete Research. Vol. 19, pp. 821-826, 1989.

KOBAYASHI, K. and UNO, Y. - Influence of alkali on carbonation of concrete, Part II. Influence of alkali in cement on rate of carbonation of concrete. Cement and Concrete Research, Vol. 20, pp. 619-622, 1990.

KOELLIKER, E. - Skins of Calciumcarbonate and their Significance for the Corrosion of Concrete. 8th International Conference on the Chemistry of Cement. Río de Janeiro 1986 - Vol. 4, Session 2.

MAYCOCK, N. and SKALNY, J. - Carbonation of hydrated calcium silicates. Cement and Concrete Research, Vol. 4, pp. 69-76, 1974.

MOOREHEAD, D.R. - Cementation by the carbonation of hydrated lime. Cement and Concrete Research. Vol. 16, pp. 700-708, 1986.

RAMACHANDRAN, V.S., CHUN-MEI, Z. - Influence of $CaCO_3$ on hydration and microstructural characteristics of tricalcium silicate. Il cemento, 3, pp. 129-152. 1986.

NISHIKAWA, T., SUZUKI, K., ITO, S., SATO, K. and TAKEBE, T. - Decomposition of synthesized ettringite by carbonation. Cement and Concrete Research, Vol. 22, pp. 6-14, 1992.

RAFAI, N., LETOLLE, R., BLANC, P., PERSON, A. and GEGOUT, P. - Isotope Geochemistry (^{13}C, ^{18}O) of carbonation processes in Concretes. Cement and Concrete Research, Vol. 21, pp. 368-377, 1991.

RAHMAN, A.A. and GLASSER, F.P. - Comparative studies of the carbonation of hydrated cements. Advances in Cement Research, 2, nº 6, Apr., pp. 49-54, 1989.

ROSSI, P. and ACKER, P. - A new approach to the basic creep and relaxation of concrete. Cement and Concrete Research, Vol. 18 pp.799-803, 1988.

RUIZ DE GAUNA, A.- Relaciones entre la carbonatación del cemento portland, el grado de cocción del clínker y algunos fenómenos expansivos en el ensayo de autoclave. Materiales de Construcción, nº 162. Abr.Mayo.Junio 1976.

RUIZ DE GAUNA, A., TRIVIÑO, F. y VAZQUEZ, T. - On the carbonation mechanism of calcium aluminate hexahydrate in hydrated high-alumina cement. The VI International Congress on the Chemistry of Cement, Supplementary paper, Section III, III-4, Moscow, Sep. 1974.

RUIZ DE GAUNA, A. - Relaciones entre la carbonatación del cemento portland, el grado de coccción del clínker y algunos fenómenos expansivos en el ensayo de autoclave. Materiales de Construcción nº 160. Oct.Nov.Dic. 1975.

SLEGERS, P.A., and ROUXHET, P. - Carbonation of the Hydration Products of Tricalcium silicate. Cement and Concrete Research, Vol. 6, pp.381-388, 1976.

SUZUKI, K., NISHIKAWA, T., ITO, S. - Formation and carbonation of C-S-H in water. Cement and Concrete Research, vol. 15, pp.213-224, 1985.

2.8 Chemical equilibrium $CO_3^{=}/HCO_3^{-}$

ARIAS, J.M. - Equilibrios en las aguas naturales. CP - pp.37-40, Junio-Julio 1977. Corrosion y Protección, pp.37-40.

BURSTEIN, G.T. and DAVIES, D.H. - The Electrochemical Behavior of Scratched Iron Surfaces in Aqueous Solutions. Electrochemical Science and Technology, Vol. 128, nº 1, pp.33-39, January 1981.

CROLET, J.L. and BONIS, M.R. - pH Measurements in Aqueous CO_2 Solutions Under High Pressure and Temperature. Corrosion, Vol. 39, nº 2, February 1983.

DUGSTAD, A. - The importance of $FeCO_3$ Supersaturation on the CO_2 Corrosion of carbon steels. Corrosion 92, Paper nº 14, 1992.

GRAY, L.G.S., ANDERSON, B.G., DANYSH, M.J. and TREMAINE, P.T. - Effect of pH and temperature on the mechanism of carbon steel corrosion by aqueous carbon dioxide. Corrosion 90. Paper nº 40, April 23-27, Las Vegas, 1990.

HIXSON, D. and UHLIG, H.H. - Stress Corrosion Cracking of Mild Steel in Ammonium Carbonate Solution. Corrosion Nace, Vol. 32, nº 2, February, 1976.

JALLERAT, N., PARI, F.L., BOURELIER, F., VU QUANG, K. - Specific inhibition effect of carbonate and bicarbonate ions on pitting corrosion of stainless steels and nickel base alloys. 9th Int. Cong. of Metallic Corrosion - Toronto - Junio 1984.

MARTI DEULOFEU, J.M. - Efectos de un agua incrustante. Procedimientos que permiten disminuir su dureza y evitar la incrustación. Corrosion y Protección - pp.11-14, Junio-Julio 1977.

MCINTIRE, G., LIPPERT, J. and YUDELSON, J. - The Effect of Dissolved CO_2 and O_2 on the Corrosion of Iron. Corrosion, vol. 46, nº 2, pp 91-94, Feb. 1990.

PARKINS, R.N., ALEXANDRIDOU, A. and MAJUMDAR, P. - Stress corrosion cracking of C-Mn steels in environments containing carbon dioxide. Materials Performance, pp.20-27, 1986.

PEREZ SANCHEZ, M., BARRENA, M. y GONZALEZ, S. - Comportamiento electroquímico del cobre en medios alcalinos acuosos de carbonato y bicarbonato de sodio. XI Reunión Grupo Electroquímica. Valladolid - Sep. 1989.

RANGEL, C.M., FONSECA, I.T. and LEITAO, R.A. - Some aspects of the electrochemical behaviour of mild steel in carbonate/bicarbonate solutions. Electrochimica Acta, Vol. 31, nº 12, pp. 1659-1662, 1986.

STOLL, F. and KAESCHE, H. - Passivity and Stress Corrosion Cracking of Prestressing Steel in Concrete at pH-Values between 7 to 12.6. Mainz 1981 - 8th Int. Congress on Metallic Corrosion, pp. 530-535.

THOMAS, J.G.N. and DAVIS, J.D. Influence of Hydrogen Carbonate and Chloride Ions on the Stability of Oxide Films on Mild Steel in Near-Neutral Solutions. Br. Corros. J., Vol. 12, nº 2, 1977.

VALENTINI, C.R., MOINA, C.A., VILCHE, J.R. and A.J. ARVIA - The electrohcemical behaviour or iron in stagnant and stirred potassium carbonate-bicarbonate solutions in the 0-75^{0}C temperature range. Corrosion Science, 1985.

VIDEM, K. and KOREN, A.M. - Corrosion, Passivity and Pitting of carbon steel in aqueous solutions of HCO_3^-, CO_2 and Cl^-. Corrosion 92, Paper nº 12, 1992.

2.9 Publications of IETcc on carbonation

ALONSO, C., ANDRADE, C. - "The effect of nitrite as corrosion inhibitor in carbonated mortar containing or not chlorides" - Journal ACI, Materials, Mar, pp 130-137 (1990).

ALONSO, C., BABLE, B., ANDRADE, A., RODRIGUEZ, J. - "Accelerated testing methods for evaluating Carbonation resistance of Concrete coatings" - FIP Symposium, Jerusalem. Sep. 1988.

ALONSO, C., ANDRADE, C. - "Life time of rebars in carbonated concrete" - 10th European Corrosion Congress - (EFC) - Barcelona (Spain) July 1993.

ALONSO,C., ANDRADE,C. - "Electrochemical behaviour of steel reinforcements in Na_2CO_3 and $NaHCO_3$ solutions in relation to stress corrosion cracking" - Corrosion Science vol. 29, nº 9, pp 1129-1139 (1989).
ALONSO,C., ANDRADE, C., "Corrosion of steel reinforcement in carbonated mortar containing chlorides" Advances in Cement Research, vol.1, nº 3, pp 155-164, 1988.

ALONSO,C., ANDRADE,C., GONZALEZ, J.A. - "Relation between resistivity and corrosion rate of reinforcements in carbonated mortar made with several cement types" Cement and Concrete Research - vol.8, pp 687-698 (1988).

ANDRADE, C., ALONSO, C., SANTOS, P., MACÍAS, A. - "Corrosion behaviour of steel during accelerated carbonation of solutions which simulate the pore concrete solution" - 8th. Int. Congress on Cement Chemistry, vol. V, Theme 4 pp 256-262, Río de Janeiro (Brasil), Sep 1986.

GARCÍA, A.M., ALONSO, C., ANDRADE, C. - "Evaluation of the resistance of concrete coatings against carbonation and water penetration" - Symposium on Protection of Concrete - Dundee (U.K), Sep 1990.

GARCÍA, A.M., ANDRADE, C., ALONSO, C. - "Metodología de ensayo evaluadora de la capacidad protectora de pinturas para hormigón frente a la carbonatación" - Hormigón y Acero pp 135-140 (1990).

GONZÁLEZ, J.A. y ANDRADE, C. - "Relaciones cuantitativas entre la carbonatación del hormigón y la corrosión de las armaduras" Revista Iberoamericana de Corrosión y Protección, nº 1, pp 15-24 (1980).

GONZÁLEZ, J.A. y ANDRADE, C. - "Avance sobre el comportamiento de armaduras galvanizadas en morteros carbonatados y sin carbonatar" - Revista de Metalurgia (CENIM) vol.15, nº 2, pp 83-90 (1979)

GONZÁLEZ, J.A., VÁZQUEZ, A.J., ANDRADE, C. - "Les effets des cyces d'humidité sur la corrosion des armatures galvanisées dans les mortiers carbonatés et non carbonatés" - Matériaux et Constructions (Rilem) - vol.15, nº 88, pp271-278 (1982).

GONZÁLEZ,J.A., ALONSO,C., ANDRADE, C. - "Corrosion rate of reinforcements during accelerated carbonation of mortar made with different types of cement" - Corrosion of steel in Concrete Construction. Ed.

GONZÁLEZ, J.A.,ALGABA, S., ANDRADE, C. - "Corrosion of Reinforcing bars in carbonated concrete" - British Corrosion Journal vol. 15, nº 3, pp 135-139, (1980).

MACÍAS, A., ANDRADE, C. - "Corrosion of galvanized steel in $Ca(OH)_2$ diluted solutions (pH range from 11, 10 to 12.6)" - British Corrosion Journal, vol 22, nº 3, pp 162-171 (1987).

NEPOMUCENO, A.A., ANDRADE,C. - "Chloride and carbonation resistance of several repair mortars" - Conference on Rehabilitation of Concrete Structures. Ed. D.W.S. Ho, Rilem, Melbourne (Australia) Sep. 1992.

3. EXAMPLES OF COMPARATIVE CALCULATION OF CARBONATION RATE

3.1. MODELS CONSIDERED

Only three of the different above mentioned models have been selected to make a comparison. Thus the main features of the proposals of Bakker (B), Tuutti (T) and Parrott (P) are described and after calculations for several conditions, are made. Finally some comments on the differences found are presented.

Bakker proposal (B)

The formula to be used is:

$$X = A\sqrt{t_{eff}}_n$$

$$A = \sqrt{\frac{2Dc}{a}(C_1C_2)}$$

where:

$$t_{eff} = [t_{d1} + t_{d2}(\frac{x_1}{B})^2 + t_{d3} \ldots\ldots\ldots t_n(\frac{x_{n1}}{B})^2]$$

x = carbonation depth
a = CaO content in the concrete
b = amount of water which evaporates from concrete
D_c =diffusion coef. of CO_2 at a particular RH
D_v =diffusion coef. of water vapour
C_1-C_2 = difference of CO_2 concentration between air and concrete
C_3-C_4 = difference in RH between air and concrete

The main aspects to be commented in this formula are:

1. It considers steady state condition (applies first Fick 1aw).

2. It considers cycles of wet and drying in the humidity. This introduces an attenuation factor much higher when these cycles vary continuosly, (short period), than if the wet-dry periods have a longer period although are equal in total length/year.

3. It needs for the calculation the following parameters: D_c (CO_2), D_u(H_2O), (C_1 - C_2), (C_3- C_4), wet period length, dry period length (for the meanings please consult Bakker's paper) and alkaline and water content.

Tuutti proposal (T)

It is the mathematical solution for a non-steady-state diffusion process where the penetration rate is combined with a reaction of such importance that the profile of concentration is very sharp (carbonation front) (42).

The expression is:

$$\frac{C_s}{C_x} = \sqrt{\pi}[\frac{K_c}{2\sqrt{D}}].e^{(\frac{K_c^2}{4D})}.erf[\frac{K_c}{2\sqrt{D}}]$$

C_s = CO_2 concentration in the atmosphere
C_x = amount of bound CO_2 (cement phases pore solution), mol/m^3
D = CO_2 diffusion coefficient
x = Carbonation depth
t = time

$$X = K_c \sqrt{t}$$

Once calculated K_c from this expression, the penetration rate is:
The main comments to be made are:

1. It considers non-steady-state conditions.

2. It does consider an average mean humidity (not moisture cycling although this could be introduced after k_c is obtained, even using the same assumptions than Bakker).

3. It needs for the calculation the following parameters: D_{O2}, cement and CaO content, degree of hydration (w/c ratio), and CO_2 concentration in the atmosphere.

Parrott proposal (P)

As was mentioned, this expression is:

$$X = \frac{64.K^{0.4}.t^{n}}{c^{0.5}}$$

x = carbonation depth in mm
k = oxygen permeability coefficient in 10^{-16} m^2
t = time in years
c = CaO content in the concrete in kg/m^3

Following previous comments, the main in this case are:

1. It is empirical, however based in real data. It should give conservative design values. It does not predict rate of carbonation, but gives a safe value of concrete cover to avoid risk of carbonation at the rebar level in the 90% of the cases.

2. It considers variation in humidity by introducing the root power n (attenuation factor) to an averaged humidity.

3. It needs the following parameters: oxigen permeability, relative humidity (average), alkaline content of the cement.

NUMERICAL EXAMPLES

1) It has been used as reference a concrete with the following composition.

cement content - 320Kg/m^3
degree of hydration - 50%
CaO - 65%
water content - 192 Kg/m^3
service life - 75 years

The reference relative humidity used is of 60%. The service life taken is of 75years.

Example 1

[B] **$D_{CO2} = 4x10^{-8}$ m^2/sec**
$D_{H2O} = 4{,}8x10^{-7}$ m^2/sec $(C_1 - C_2) = 0.00066$ kg/m^3
HR= 60% → no wetting period $(C_3 - C_4) = 0.0062$ kg/m^3

[T] $C_s = 1{,}23x10^{-5}$ Kmol CO_2/m^3
$C_x = (320/56)(0.65)(0.5) = 1{,}85$ Kmol/m^3
$D_{O2} = 4x10^{-8}$ cm^2/sec

[P] $D_{O2} = 2{,}833 \times 10^{-8} K_{60}^{0.922} \rightarrow K_{60} = 1.453 \times 10^{-16}$
RH= 65%
CE= 743 Kg CaO/m^3 matrix

Example 2: The same than 1 but using $D_{CO2} = 8x10^{-8}$ m^2/sec

Example 3: The same than 1 but using $D_{CO2} = 2x10^{-8}$ m^2/sec

Example 4: The alkaline content is reduced to the half in the reference concrete.

Example 5: Half a year cycle (6 months dry - 6 months wet)

Example 6: month cycle (one month wet-one dry)

With these assumptions the results obtained are presented in Table 10 and plotted in figure 17.

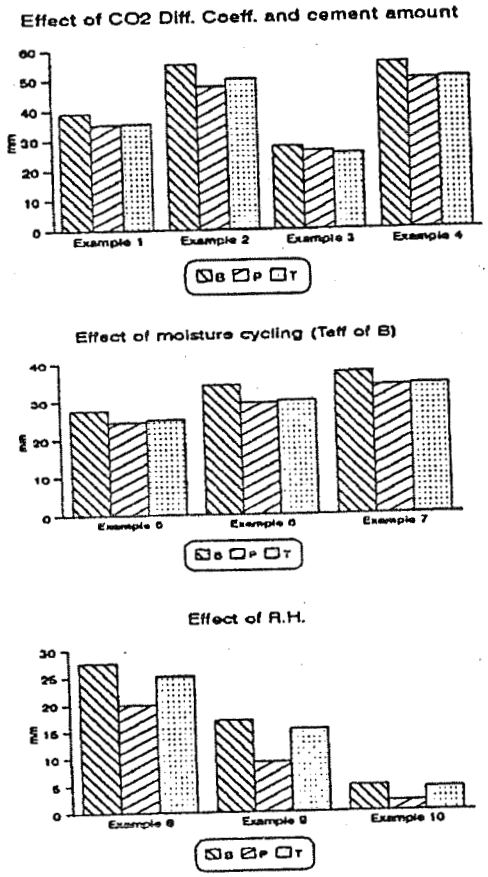

Figure 17

Table 10

Cement - 320 kg
Degree Hyd - 50%
Reference RH - 60%

Water - 192 l
CaO% - 65%
t= 75 years

BAKKER

Exam.	D_{CO2}	D_{H2O}	a	b	C_{CO2}	C_{H2O}	X(mm)	t_{dry} (days)	t_{wet} (hours)
1	$4x10^{-8}$	$4.8x10^{-7}$	82	119.2	0.00066	0.0074	39	27375	.0
2	$8x10^{-8}$	$4.8x10^{-7}$	82	119.2	0.00066	0.0074	55.2	27375	0
3	$2x10^{-8}$	$4.8x10^{-7}$	82	119.2	0.00066	0.0074	27.6	27375	0
4	$4x10^{-8}$	$4.8x10^{-7}$	41	119.2	0.00066	0.0074	55.2	27375	0
5	$4x10^{-8}$	$4.8x10^{-7}$	82	119.2	0.00066	0.0074	27.5	13650	327600
6	$4x10^{-8}$	$4.8x10^{-7}$	82	119.2	0.00066	0.0074	34.2	21075	151200

PARROTT

Examp.	D_{CO2}	K_{60}	HR	CE	X	t_{eff} (Bak)
1	$4x10^{-8}$	$1.453x10^{-16}$	60	371.5	35.18	
2	$8x10^{-8}$	$3.083x10^{-16}$	60	371.5	47.53	
3	$2x10^{-8}$	$0.685x10^{-16}$	60	371.5	26.04	
4	$4x10^{-8}$	$1.453x10^{-16}$	60	185,75	49.75	
5	$4x10^{-8}$	$1.453x10^{-16}$	60	371.5	24.61	37.35
6	$4x10^{-8}$	$1.453x10^{-16}$	60	371.5	29.39	52.81

TUUTTI

Examp.	D_{CO2}	C_S	C_X	X	t_{eff}(Bak)
1	$4x10^{-8}$	$1.23x10^{-5}$	1.85	35.46	
2	$8x10^{-8}$	$1.23x10^{-5}$	1.85	50.1	
3	$2x10^{-8}$	$1.23x10^{-5}$	1.85	25.0	
4	$4x10^{-8}$	$1.23x10^{-5}$	0.928	50.1	
5	$4x10^{-8}$	$1.23x10^{-5}$	1.85	25.0	37.35
6	$4x10^{-8}$	$1.23x10^{-5}$	1.85	29.7	52.81

2) Another example is presented next. Here, the situation is the reverse: what is known is the carbonation depth in real structure and what is calculated by the three formulae is the diffusion coefficient D. Thus, the structures selected was made with two types of cement (**At** having 64% CaO and **As** having fly ashes and CaO= 46%). They were held indoors (60% RH) and outdoors (averaged RH= 80%).

amount of cement - 400 kg
% CaO - At - 0.64
As - 0.46
water content - 150 l
Degree of hydration - 50%
R.H. - 60% and 80%

The carbonation depth after 3 years of storage were (Table 11):

Table 11

	x(mm) (Experimental)	
	60% RH	80% RH
At	7,21	2,36
As	7,71	2,74

From these real penetration depths, the D value are calculated by means of Parrot and Tuutti formulae. In the case of Bakker, a D value is assumed and x is calculated.

It is interesting to notice that the diffusion coefficients obtained by means of the three models (Table 12) are quite similar, giving a value of $D= 5x10^{-8} m^2/s$ for indoor conditions and of $D= 0.5x10^{-8}$ m^2/s for Madrid outdoor environment not sheltered from rain.

Table 12. Results of calculation of D_{CO2} with the three models.

	PARROT			**TUUTTI**		**BAKKER**				
	CE	K_{60}	D	C_x	D	D	a	b	C_{H2O}	X
At-60%RH x=7,21	460,1	$2,22x10^{-16}$	$5,9x10^{-8}$	2,28	$5,1x10^{-8}$	$5x10^{-8}$	100,6	59	0,0074	7,9
At-80%RH x= 2,36	483,1	$0,34x10^{-16}$	$1x10^{-8}$	2,28	$0,54x10^{-8}$	$0,5x10^{-8}$	100,6	59	0,00352	2,5
As-60%RH x=7,71	330,7	$1,74x10^{-16}$	$4,72x10^{-8}$	1,64	$4,2x10^{-8}$	$4,2x10^{-8}$	72,3	59	0,0074	8,5
As-80%RH x=2,74	347,2	$0,32x10^{-16}$	$1x10^{-8}$	1,64	$0,53x10^{-8}$	$0,5x10^{-8}$	72,3	59	0,00352	2,9

3.2. CONCLUSIONS

If properly applied the three formulae give very similar results, which shows that the three may be reliably used.

Also, it has to be stressed that the concept of effective time of carbonation t_{eff}, can be incorporated to Parrott and Tuutti's models which enables to avoid the estimation of a CO_2 diffusion coefficient for each humidity, although on the other hand, may complicate the calculation as the lengths of the wetting-dry periods are needed.

It can be then summarized that the preference of one of the models will depend on the possibility of knowing the different parameters introduced in the formulae.

APPENDICES FOR SECTION 3

APPENDIX 3.1 SUMMARY OF RESULTS FROM TEST PERFORMED IN THE FIELD

BRIDGE NUMBER	BENT - COLUMN	EAHT or EAFL (ft.)	RESIST. kohm cm	HALF-CELL (mV)	CARB. D. (inch)	IRH (%)	OBSERVATIONS
700352	6 - A	3			< 1/16		
	6 - A	6			< 1/16		
	6 - D	5			< 1/16		
	6 - K	5			< 1/16		
720011	15 - A	4.5	40		< 1/8		
	15 - A	15			< 1/8		
	15 - A	2	30	-130	1/2		
	15 - A	9			1/16 - 3/8		
	15 - B	15			1/16 - 3/8		
	19 - A	6			1/8 - 3/8		Spall & Crack on column
720057	9 - E	5	62		< 1/16		
	9 - CAP	6	85		< 1/16		Cracks on pile
	12 - A	4	38				
	12 - CAP	5	35 - 45		< 1/16		
	14 - A	5			< 1/16		
900003	3-2	2	38	-304			
	3-2	4	45	-280 to -307	1/4	[80.7]	[IRH] taken after 7.5 hrs.
	15 - 2	6	45.5	-138 to -222	1/4	[74.5]	[IRH] taken after 5.5 hrs.
900037	15-2	5		-189 to -205	1/4 to 3/8		
	28-2	5		-280 to -319	1/4 to 3/8		Cracks on pile
	28-2	2	23.5	-451			
	28-2	4	33.5	-315			Cracks on pile
	28-2	6	42.4	-271	1/4 to 3/8		
900011	6 - A	3	6.7	-403			Spall & Crack on column
		4	9.2	-332		[77.9]	[IRH] taken after 10 hrs.
		5	12.3	-339	3/8 to1/2		
		6	12.9	-335	3/8 to1/2		
		7		-265			
	6 - A	4	7.5	-336			Cracks on piles
		5	9.4	-330	3/8 to1/2	[71.2]	[IRH] taken after 5.5 hrs.
		6	13	-217	3/8 to1/2		
		7		-11			
900016	4 - 3	1		-424			Cracks on pile
		2		-416			Cracks on pile
		3		-413			
		4		-405			
		5		-338	1/8 to 1/4	[89.0]	[IRH] taken after 6 hrs.
		6		-222	1/8 to 1/4		
900045	4 - 3	1	1.5	-424			
		2	2.9	-369			
		3	3.4	-334			
		4	7	-286			
		5	14	-205	1/8		Cracks on pile
		6	14.8	-141			
	29 - A	2	1.9	-515	1/8 to 1/4		Spall & Crack on column

RESIST. = Resistivity
CARB. D. = Carbonation Depth
IRH = Internal Relative Humidity of Concrete
[IRH] = Measured value of IRH in the field
IRH* = Calculated value of IRH according to Appendix 3.3
Note: See Table I.1 for bridge identification

EAHT = Elevation Above High Tide
EAFL = Elevation Above Floor

APPENDIX 3.1 (Continued)

BRIDGE NUMBER	BENT - COLUMN	EAHT or EAFL (ft.)	RESIST. kohm cm	HALF-CELL (mV)	CARB. D. (inch)	IRH (%)	OBSERVATIONS
900045		4	2	-431	1/8 to 1/4		
		5	2.1	-324	1/8 to 1/4		
900035				Only concrete cores were extracted from this bridge			
150107	158 - A	3	30		1/16 to 1/4		Spall & Crack on column
		4	36.4		1/16 to 1/4	[81.2] | 89.0*	[IRH] taken after 24 hrs.
		5	43		1/16 to 1/4		IRH winter
		6	54.9				
	164 - A	3	5.6		1/16 to 1/4	[80.1] | 80.7*	[IRH] taken after 24 hrs.
		4	20.2		1/16 to 1/4		Cracks on column
		5	60		1/16 to 1/4		IRH winter
		6	66.2				
		14.9				[74.3] | 82.7*	[IRH] taken after 24 hrs.
	167 - A	3	49	-440 (cp)		[77.3] | 78.4*	[IRH] taken after 24 hrs.
		4	60	-220(cp)			IRH winter
		5	80	-140(cp)	1/16 to 1/4		
		6	87.7	-50 (cp)	1/16 to 1/4		
100172	1 - C	1	53			72.0* | 88.5*	IRH winter | IRH summer
		2	112				Concrete spalls and
		3	493				rebar corrosion
		4	1338				
		5	1632		1 1/2		
	CAP				1	77.1* | 84.9*	IRH winter | IRH summer
100153	1 - A	1	282				
		2	1690				
	1 - B	1	357				
		2	586				
		3	750				
		4	896		1/2		
		5	929	42 to 50	1/2	72.3* | 83.9*	IRH winter | IRH summer
	CAP			42 to 50	3/4	74.3* | 80.5*	IRH winter | IRH summer
100198	1 - B	1	64				
		2	321				
		3	753				
		4	868		1/4 to 1/2		
		5	1950		1/4 to 1/2	71.4* | 80.5*	IRH winter | IRH summer
						76.8* | 80.2*	IRH winter | IRH summer
100920	1 - C	1	54				
		2	56				
		3	96				
		4	136		1/4		
		5	333		1/4	76.3* | 82.9*	IRH winter | IRH summer
870034	1 - C	1	29.5				
		2	287.5				
		3	1463				
		5		-87 to -102	5/8		IRH probe placed

RESIST. = Resistivity
CARB. D. = Carbonation Depth
IRH = Internal Relative Humidity of Concrete
[IRH] = Measured value of IRH in the field
IRH* = Calculated value of IRH according to Appendix 3.3
cp = structure under cathodic protection
EAHT = Elevation Above High Tide
EAFL = Elevation Above Floor
Note: See Table I.1 for bridge identification

APPENDIX 3.1 (Continued)

BRIDGE NUMBER	BENT - COLUMN	EAHT or EAFL (ft.)	RESIST. kohm cm	HALF-CELL (mV)	CARB. D. (inch)	IRH (%)	OBSERVATIONS
870049	1 - B	1	41				
		2	417				
		3	1597				
		5			3/4 to 1		IRH probe placed
	CAP				3/4		
870081	1 - C	1	99.5				
		2	377				
		5		-10 to -72	3/4		IRH probe placed
	CAP				1/2		
870053	1 - C	1	60.5				
		2	115.5				
		3	570				
		4	1501				
		5			3/4		IRH probe placed
	CAP				3/43/4 to 1		

RESIST. = Resistivity
CARB. D. = Carbonation Depth
IRH = Internal Relative Humidity of Concrete
[IRH] = Measured value of IRH in the field
IRH* = Calculated value of IRH according to Appendix 3.3
Note: See Table I.1 for bridge identification

EAHT = Elevation Above High Tide
EAFL = Elevation Above Floor

APPENDIX 3.2 MASTER TABLE OF CORE CHARACTERISTICS

CORE IDENT. NUM.	BRIDGE NUMBER	BRIDGE AGE (years)	PIER NUM.	COL.	FACE ORIEN.	EAHT or EAFL (feet)	STEEL EXP.	CONC. COVER (inches)	CORE INITIAL WEIGHT (gr)	CORE LENGTH (inches)	WET RESIST. (kΩ cm)	CARB. DEPTH (mm)	CARB. COEFF. ($mm/y^{1/2}$)	Cs (pcy)	Deff (in^2/y)
1	720011		15	A	S	5.8	NO			7.9	33				
2	720011	13	15	A	S	6.7	NO			6.66		1	0.28	0.92	0.011
3	720011	13	15	A	S	7.5	NO			7	57.8	7	1.94		
4	720011	13	15	A	S	8.3	NO			8.75	46.7				
5	720057	29	9	F	E	3.0	YES			5.4	25.5	1.5	0.28		
6	720057	29	9	F	E	2.0	NO			6	21.7				
7	900003	21	3	2	E	0.0	YES	3.75	333	3.75	2.2				
8	900003	21	3	2	E	6.0	YES	3.75	325.1	3.75		1	0.22		
9	900003	21	15	2	N	0.0	NO		312.5	3.5					
10	900003	21	15	2	N	6.0	YES	3.5	344.2	3.66		0	0		
11	900003	21	28	2	S	0.0	YES	3.75	434.9	4.75	6.75				
12	900003	21	28	2	S	5.0	YES	3.5	534.7	6.25	11.25				
13	900003	21	28	2	S	10.0	NO		554.5	5.25	21.25				
14	900037	13	3	2	E	0.0	NO		305.4	3.5					
15	900037	13	3	2	E	0.0	NO		508.6	5.5				16.8	0.911
16	900037	13	3	2	E	7.0	YES	3.6	449.5	5					
17	900037	13	15	2	N	0.0	NO		434.9	5					
18	900037	13	15	2	N	7.0	YES	3.5	351.8	4					
19	900037	13	28	2	S	0.0	NO		428.9	5				32	0.22
20	900037	13	28	2	S	5.0	YES	3.5	341.1	3.75					
21	900037	13	28	2	S	10.0	YES	3.6	343.3	3.75		3.5	0.97		
22	900003	21	SP28	DK			NO		529.9	6.75	21.48				
23T	900003	21	SP1	DK-T			YES	2.4		2.5/2.25		12	2.62		
23B	900003	21	SP2	DK-B			YES	1.75		1.75		22	4.80		
24	900003	21	SP1	DK			NO		685.1	8					
25	900037	13	SP1	DK			YES	3	398.8	5					
26	900037	13	SP1	DK			YES	1.6	660.1/340.2	2.25/4.25		50	13.87		
27T	900037	13	SP1	DK-T			YES	2.6	211.3	2.75		40	11.09		
27B	900037	13	SP1	DK-B			NO		407.9	5		2.5	0.69		
28	900037	13	SP1	DK			NO		436.2	2.5					
29	900037	13	SP1	DK			NO		804.4	7.65					
30	900037	13	SP22	DK			NO		210.5	2.75		4.5	1.25		
31	900011	13	SP22	DK			NO		659.7	7.75				4.2	0.108
32	900011	13	6	EF	E	0.5	NO		393.2	4.5	1.55				
33	900011	13	6	E	N	6.5	NO		304.7	3.5		4.5	1.25		
34	900011	13	6	E	W	12.0	NO		409.4	4.75					
35	900011	13	12	EF	E	0.5	NO		440.9	5				22.8	0.59
36	900011	13	12	E	W	6.5	NO		413.6	4.5	3.09				
37	900011	13	12	E	W	12.5	NO		423.8	4.75					
38	900011	13	SP 1	DK			NO		685.1	8					
39	900011	13	SP 1	DK			NO		696.2	8.25					
40	900011	13	SP 18	DK			NO		339.9	4.25	6.63				

APPENDIX 3.2 (Continued)

CORE IDENT. NUM.	BRIDGE NUMBER	BRIDGE AGE (years)	PIER NUM.	COL.	FACE ORIEN.	EAHT or EAFL (feet)	STEEL EXP.	CONC. COVER (inches)	CORE INITIAL WEIGHT (gr)	CORE LENGTH (inches)	WET RESIST. (kΩ cm)	CARB. DEPTH (mm)	CARB. COEFF. ($mm/y^{1/2}$)	Cs (pcy)	Deff (in^2/y)
41	900011	13	SP 18	DK			NO		734.8	8.9				7	0.032
42	900011	13	SP 1	DK			NO		705.4	8.75	17.26				
43	900016	25	4*	3	N	0.0	YES	2	209.8/237.9	2.25/2.5		1	0.20		
44	900016	25	4*	3	N	5.0	YES	2	446.5	2.4		9	1.80		
45	900016	25	4*	3	N	10.0	YES	2		4.9					
46	900016	25	14*	EF	E	0.5	NO		422.6	4.75					
47	900016	25	14*	EC	N	5.0	NO		357	4.1		1.5	0.30		
48	900016	25	14*	EC	E	10.0	NO		390.1	4.4					
49	900016	25	29*	WC	E	0.0	NO		420.4	4.5				20	1.104
50	900016	25	29*	WC	W	5.0	NO		416.8	4.5				12	0.357
51	900016	25	29*	WC	W	10.0	NO		436.7	4.6					
52	900016	25	L SP	DK			YES	2.5	632.5	7.25					
53	900016	25	L SP	DK			YES	3	362.5	4.4		1	0.20		
54	900016	25	L SP	DK			NO		605.7	7.25				16.2	0.02
55	900016	25	M SP	DK			NO								
56	900016	25	M SP	DK			NO		394.7	4.75	3.5	1	0.20		
57	900016	25	M SP	DK			NO		213.7	3.25					
58	900016	25	M SP	DK			NO		582.6	7		10	2.00		
59	900045	22	4*	3	N	0.0	YES	2.25	235.3	2.5		0	0		
60	900045	22	4*	3	N	5.0	YES	2.5	239.5	2.5		2	0.43		
61	900045	22	4*	3	N	10.0	NO		397.6	4.25		1	0.21		
62	900045	22	14*	EF	E	0.5	NO		402.3	4.5	1.5				
63	900045	22	14*	EC	E	5.0	NO		282.7	3.25		1.5	0.32		
64	900045	22	14*	EC	E	10.0	NO		367.3	4					
65	900045	22	29*	EF	E	0.5	NO		427.6	4.65				21.6	0.949
66	900045	22	29*	EC	E	5.0	NO		536.9	5.75	3.52				
67	900045	22	29*	EC	E	10.0	YES	4.5	403.1	4.5					
68	900045	22	L SP	DK			NO		303.7/261.5	3.75/3.25		6	1.28		
69T	900045	22	L SP	DK-T			NO		563.4	6.75		1	0.21		
69B	900045	22	L SP	DK-B			NO					13	2.77		
70	900045	22	L SP	DK			YES	3.8	318.2	4					
71	900045	22	M SP	DK			NO		436.2	5.45					
72	900045	22	M SP	DK			NO		328.5	3.9					
73	900045	22	M SP	DK			YES	1.5	124.1	1.5		1	0.21		
74	900045	22	M SP	DK			NO		360.7	4.5	29.72				
75	900045	22	M SP	DK			NO		599.3	7					
76	900035	34	SP 1	DK			YES	4.5	803.3	9.75					
77	900035	34	SP 1	DK			NO		467.4	5	5.84				
78	900035	34	SP 1	DK			NO		804.4	9.75				20.4	0.238
79	900035	34	SP 1	DK			YES	3.6	313.1	3.75		8	1.37		
80	150107	36	158	A	E	2.7	YES	2.75	246.5	2.75		1.5	0.25		

CORE IDENT. NUM.	BRIDGE NUMBER	BRIDGE AGE (years)	PIER NUM.	COL.	FACE ORIEN.	EAHT or EAFL (feet)	STEEL EXP.	CONC. COVER (inches)	CORE INITIAL WEIGHT (gr)	CORE LENGTH (inches)	WET RESIST. (kΩ cm)	CARB. DEPTH (mm)	CARB. COEFF. ($mm/y^{1/2}$)	Cs (pcy)	Deff (in^2/y)
81	150107	36	158	A	E	2.8	YES	3.75	357.2	3.87	24.4				
82	150107	36	158	A	S	17.8	NO		643.3	7		3	0.50		
83	150107	36	164	B	W	3.1	YES	3.4	343	3.62		0	0		
84	150107	36	164	B	W	14.8	NO		294.7	3.25		0	0		
85	150107	36	167	A	W	3.1	YES	2.75	250	2.75		1	0.16		
86	150107	36	167	A	W	14.7	NO		451	5		1	0.16		
87	100172	34	1	C	N	5.0	NO		423.2	5		28	4.80		
88	100172	34	1	C	N	6.0	NO		443.7	5					
89	100172	34	1	C	N	15.0	NO		463.9	5					
90	100172	34	1	C	N	15.0	YES	1.5	148.9	1.5		14	2.40		
91T	100172	34	SP 1	DK-T			NO		642.4	7.6		7.5	1.29		
91B	100172	34	SP 1	DK-B			NO					27	4.63		
92T	100172	34	SP 1	DK-T			YES	3	598.6	7.8		26	4.46		
92B	100172	34	SP 1	DK-B			NO					24.5	4.20		
93	100172	34	SP 1	DK			NO		468.8	5.7	6.59				
94	100172	34	SP 1	DK			NO		207.9	2.9					
95	100172	34	SP 1	DK			NO		151.8	1.9		9	1.54		
96	100153	33	1	B	E	5.0	NO		496	5.6		20.5	3.57	2.7	0.003
97	100153	33	1	B	E	5.8	YES	2	187.8	2.25		23	4.00		
98	100153	33	1	B	E	6.0	NO		467.9	5.4					
99	100153	33	1	B	E	15.0	YES	2.5	216.5	2.5		12	2.09		
100	100153	33	1	B	E	15.0	NO		456.8	5.5		27	4.70		
101	100153	33	SP 1	DK			NO		482.2	5.6	4.57				
102	100153	33	SP 1	DK			NO		408.3	5		16	2.79		
103	100153	33	SP 1	DK			NO		614.1	7.2	6.32	7.5	1.31		
104	100153	33	SP 1	DK			NO		602.8	7.2				1.3	0.005
105	100198	31	1	B	N	5.0	YES	2	157.8	2		21	3.77		
106	100198	31	1	B	N	6.0	NO		443.7	5					
107	100198	31	1	B	N	15.0	NO		476.1	5.3	5.5				
108	100198	31	1	B	N	15.0	YES	2.75	269	3		5.5	0.99		
109	100198	31	SP 1	DK			YES	1	636.7	7.3		18.5	3.32		
110	100198	31	SP 1	DK			NO		629.2	7.3		18	3.23	1.1	0.025
111	100198	31	SP 1	DK			NO		447.5	5.2	7.29				
112	100920	56	1	C	N	5.0	NO		490	4.6	9.2	4	0.53		
113	100920	56	1	C	N	6.0	NO		437.9	5.1				0.9	0.003
114	100920	56	SP 1	DK			YES	2.25	634	6.8		17	2.27		
115T	100920	56	SP 1	DK-T			NO		645.9	6.9		10	1.33		
115B	100920	56	SP 1	DK-B			YES	1.5				0	0		
116	100920	56	SP 1	DK			NO		592.2	6.8	10.93				
117T-a	870034	32	SP 1	DK-T			NO			4.25		15	2.65		
118B-a	870034	32	SP 1	DK-B			NO			4		15.5	2.74		
119T	870034	32	SP 1	DK-T			NO			3.5		9	1.59		
119B	870034	32	SP 1	DK-B			NO			4.25		4	0.71		
120	870034	32	SP 1	C	E		NO			5.875		16.5	2.92		

CORE IDENT. NUM.	BRIDGE NUMBER	BRIDGE AGE (years)	PIER NUM.	COL.	FACE ORIEN.	EAHT or EAFL (feet)	STEEL EXP.	CONC. COVER (inches)	CORE INITIAL WEIGHT (gr)	CORE LENGTH (inches)	WET RESIST. (kΩ cm)	CARB. DEPTH (mm)	CARB. COEFF. ($mm/y^{1/2}$)	Cs (pcy)	Deff (in^2/y)
121	870034	32	SP-1	DK			NO		681.5	7.75					
122	870034	32	SP-1	DK			NO		553	6.75	8.4				
123	870049	31	SP-1	B	E	0.0	NO			5.5		20.25	3.64		
124	870049	31	SP-1	DK			NO		573.2	7					
125	870049	31	SP-1	B	E		YES	4		4		16.25	2.92		
126B	870049	31	SP-1	DK			YES	1.25		2.25		8.5	1.53		
127	870049	31	SP-1	B	E	5.0	NO			2.5		27	4.85		
128	870049	31	SP-1	DK			NO		573.3	7	12.1				
129	870053	33	SP-1	C	E	5.0	NO			6.5		1.75	0.30		
130	870053	33	SP-1	C	E		YES	1.9		1.875		0	0		
131T	870081	31	SP-1	DK-T			NO			2.5		1	0.18		
131B	870081	31	SP-1	DK-B			NO			4.75		0	0		
132T	870081	31	SP-1	DK-T			NO			2.75		3.5	0.63		
132B	870081	31	SP-1	DK-B			NO			4.25		0	0		
133	870081	31	SP-1	DK			NO		600.8	7.25	10.9				
134T	870081	31	SP-1	DK-T			NO			2.5		1.5	0.27		
134B	870081	31	SP-1	DK-B			YES	1.25		3.5		12	2.16		
135	870081	31	SP-1	DK			YES	1.9		2.5		11	1.98		
136T	870081	31	SP-1	DK-T			NO			2		10	1.80		
136B	870081	31	SP-1	DK-B			YES	1.25		5.5		14	2.51		
137	870081	31	SP-1	DK			NO		393.7	4.75	6.9				
138	870053	33	SP-1	DK			YES	2.13		5		3.5	0.61		
139	870053	33	SP-1	DK			NO		387.2	4.75	8				
140	870053	33	SP-1	DK			YES	1.88		5.5		4.75	0.83		
141	870053	33	SP-1	DK			YES	1.88		5.25		8.25	1.44		
142	870053	33	SP-1	DK			NO		590.3	7.125	8.5				
143	870034	32	SP-1	C	E		NO			2.75		17.5	3.09		
144	870034	32	SP-1	C	E		NO			2.5		17	3.01		
All deck cores correspond to top portion of the deck unless otherwise indicated															
a- Cores 177 and 188 are the top and the bottom of the same core															

APPENDIX 3.3 INTERNAL RELATIVE HUMIDITY DETERMINATION.

EXAMPLE OF INTERNAL CONCRETE RELATIVE HUMIDITY CALCULATION

Bridge: Howard Frankland P158 Elevation from Footer at 2 ft.

DATA INPUT:

$$RH := \begin{pmatrix} 84.0 \\ 86.0 \\ 88.6 \\ 89.1 \end{pmatrix} \quad t := \begin{pmatrix} 30 \\ 60 \\ 180 \\ 300 \end{pmatrix}$$

Value of RH % measured at t intervals of time (t in seconds)

$RH0 := 80.5$

Initial value of RH.

$$F(t, A, \tau) := RH0 + A \cdot \left[1 - e^{\left(\frac{-t}{\tau}\right)}\right]$$

Function assumed for modeling the variation of RH with time.

$i := 0..3$

$$s(A, \tau) := \sum_i \left(RH_i - F\left(t_i, A, \tau\right)\right)^2$$

Square error function.

$A := 5$

Guess value of ΔRH.

Given

Solve Block.

$s(A, \tau) = 0$

Setting square error = 0

$f(\tau) := Minerr(A)$

Creating f(τ) such that gives value of A that satisfies S(A,τ) = 0

$j := 0..10$

$\tau_j := 50 + j$

Iterating through different values of time constants (τ).

$f_j := f\left(\tau_j\right)$

$g_j := s\left(f_j, \tau_j\right)$

Calculating square error for each value of Δ and τ.

APPENDIX 3.3 (Continued)

$m := \min(g)$		Calculating the minimum error.
$k_j := if(g_j = m, j, 0)$		Calculation of the index of minimum error
$in := \lvert k \rvert$	$in = 8$	Index must be: $0 < in < 10$.
$\Delta RH := \lvert f_{in} \rvert$	$\Delta RH = 8.569$	Calculated value of ΔRH.
$T := \tau_{in}$	$T = 58$	Calculated value of time constants τ.
$ERR := g_{in}$	$ERR = 0.016$	Minimum error
$RHF := RH0 + \Delta RH$		Value of RH when t tends to infinity.

DATA OUTPUT:

$RHF = 89.069$

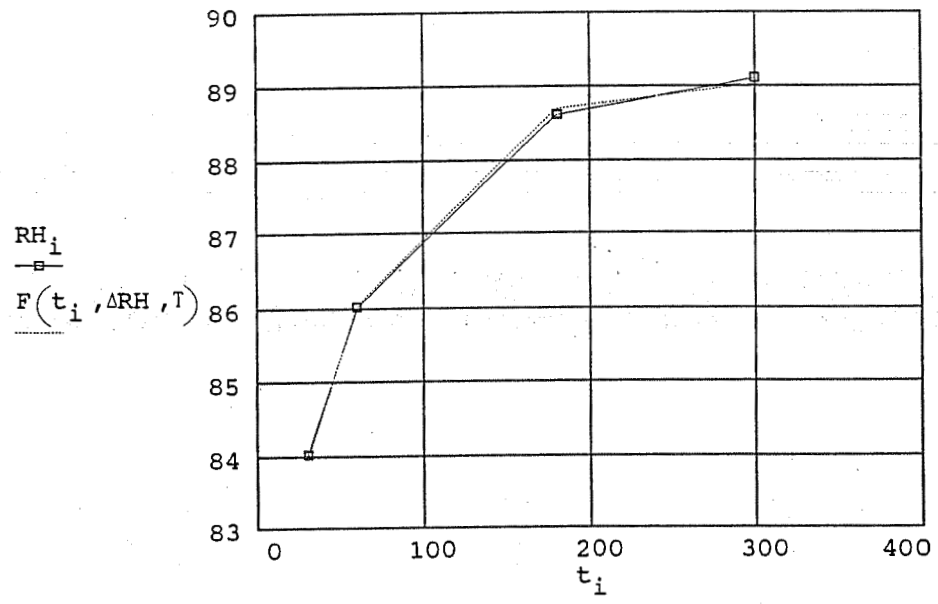

Figure 46. Representation of the variation of IRH with time (boxes are measured data points and dashed line is the minimum square root error fit).

APPENDIX 3.4 STATISTICAL APPROACH FOR ESTIMATING THE EXTENT OF CARBONATION-INDUCED CORROSION DAMAGE IN THE PRESENT FDOT INVENTORY

The calculations in this appendix are aimed to a simplified statistical indication of the extent to which carbonation-induced corrosion may be present in the current FDOT bridge inventory. This is a tentative approach based on the limited statistical information available.

For simplicity, an initial assumption will be made that the cores examined in this study are representative of the conditions of the 18 bridges examined. The overall distribution of concrete cover thickness (*cc*; Figure I.17) and carbonation depths (x_c: Figure I.18) are also assumed to be similarly representative.

For these calculations, the cumulative percentage distributions (0 to 100 %) in Figures I.17 and I.18 are expressed in terms of a fraction (0 to 1) functions *N'r(cc)* and *N'c(x_c)* respectively. Thus, given a specific concrete cover value *x*, *N'r(x)* is the fraction of the total number of cores examined that have *cc*<*x*. Furthermore, the actual distributions *N'r* and *N'c* will be replaced by idealized continuous mathematical functions *Nr* and *Nc* that approximately fit the discrete results from the limited number of cores examined. In addition, the probability distribution function *Pc(x)* will be defined as *Pc(x)* = *dNc(x)/dx*. It will also be assumed that the following discussion applies to a large core population where every core has been drilled to intersect a rebar segment.

The functional form chosen for *Nr* is that of a cumulative normal distribution function. The form chosen for *Nc* is a combination of exponentials of x_c that provides reasonable fit to the empirical distribution. These function, as well as the resulting *Pc* function are detailed later in this Appendix.

From the definitions of *Nc* and *Pc*, the fraction *f(x,dx)* of total cores having $x<x_c<x+dx$ is

$$f(x,dx) = Pc(x)\,dx \qquad (1)$$

From that fraction, the sub-fraction of cores that has rebar covers $x_c>x+dx$ (or simply $x_c>x$ in the limit) will be considered to be experiencing carbonation-induced corrosion. Calling that sub-fraction *fc(x+dx)* and from the definition of *Nr*:

$$fc(x,dx) = Pc(x)\,Nr(x)\,dx \qquad (2)$$

Repeating this procedure for every value of *x* from 0 to ∞ (or a value well in excess of the highest rebar cover and carbonation depth expected) and integrating the results, provides the value of the fraction *Fc* of the total core population expected to include rebar with carbonation-induced corrosion:

$$Fc = \int_{0}^{\infty} Pc(x)\,Nr(x)\,dx$$

This calculation has been performed in the following printout, yielding *Fc* = 0.015

The idealized calculation results indicate that an extensive survey of the bridges examined could turn approximately one core with rebar undergoing carbonation-induced corrosion for every hundred cores (with rebar) extracted. Since less than 50 cores that were extracted contained a rebar piece, it is not surprising that no instances of carbonation depth exceeding rebar cover occurred in this investigation.

The 18 bridges examined in this study are not a large unbiased sample of the overall FDOT bridge inventory. Nevertheless, these bridges are representative of a group of structures with an average age about 28.5 years. Extrapolating to the entire bridge inventory (assuming an average age of 3 decades), the results of this survey suggest that carbonation-induced corrosion may be at present affecting roughly 1% or less of the nominal surface of exposed reinforced concrete. Actual carbonation-induced spalling of concrete cover would require furthermore that the propagation stage should be exceeded. Since the estimated propagation stage is on the order of one decade (Section 3.3.3.3, assuming moderate corrosion rates), then some fraction of the areas undergoing corrosion would not be expected to have reached at present the spalling stage.

These statistical inferences can only be used as a crude estimate of the FDOT inventory given the small sample size and selection bias of the bridge population in this study. However, the results suggest that only a small fraction of the exposed reinforced concrete surface is affected by carbonation-induced damage. It is likely that the dispersion in the variables of importance in determining carbonation damage (concrete cover, concrete quality) is more on a bridge-to-bridge basis than as a distribution among the components in each individual bridge. In that case, these results can be interpreted as indicting that only a small fraction of the bridges in the present FDOT inventory is likely to be showing extensive signs of carbonation-induced corrosion damage. The observation of damage in only one of the bridges examined in this survey lends credence to this interpretation.

APPENDIX 3.4 (Continued)

$i := 1..1000$ Graphing Array for Continuous functions

$j := 0..46$ Graphing Array for Discrete Functions

$\eta cc := mean(cc)$ Mean of the concrete cover data set

$\eta cc = 67.296$

$\sigma cc := stdev(cc)$ Standard Deviation of the concrete cover data set

$\sigma cc = 23.612$

$$x_i := \frac{150 i}{1000}$$

$$Nc_i := cnorm\left(\frac{x_i - \eta cc}{\sigma cc}\right)$$ Curve fit to the normal distribution

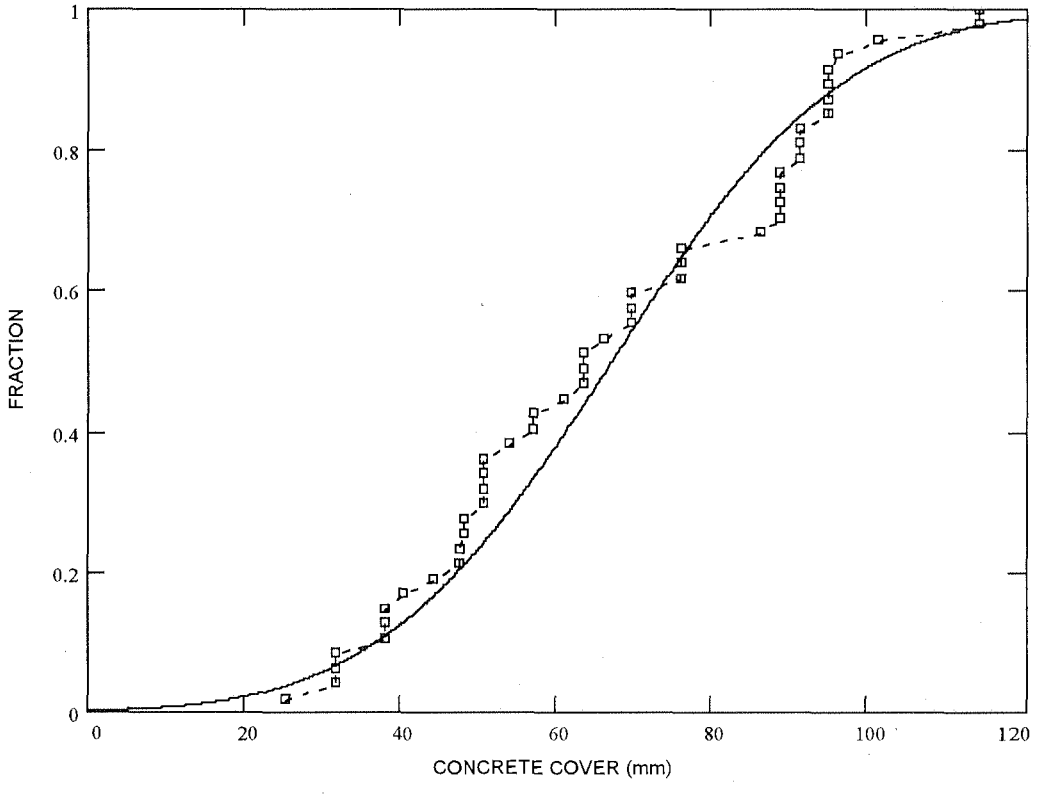

Figure 3.4.1: Cumulative normal distribution function (smooth) and experimental data (boxes) describing concrete cover.

APPENDIX 3.4 (Continued)

Carbonation Depth

$k := 0 .. 79$ Graphing Array for Carbonation Values

$z_i := \frac{100 \cdot i}{1000}$ Graphing Array for integral

$u_0 := 10$ Exponential parameter describing Xc data

$u_2 := 2$ Parameter describing Xc data

$u_1 := 2$ Parameter describing Xc data

$$Nc_i := \left(1 - \exp\left(\frac{-z_i}{u_0}\right)\right) \cdot \left[\left(u_1 \cdot \exp\left(\frac{-z_i}{u_2}\right)\right) + 1\right]$$ Experimental Curve fit of data

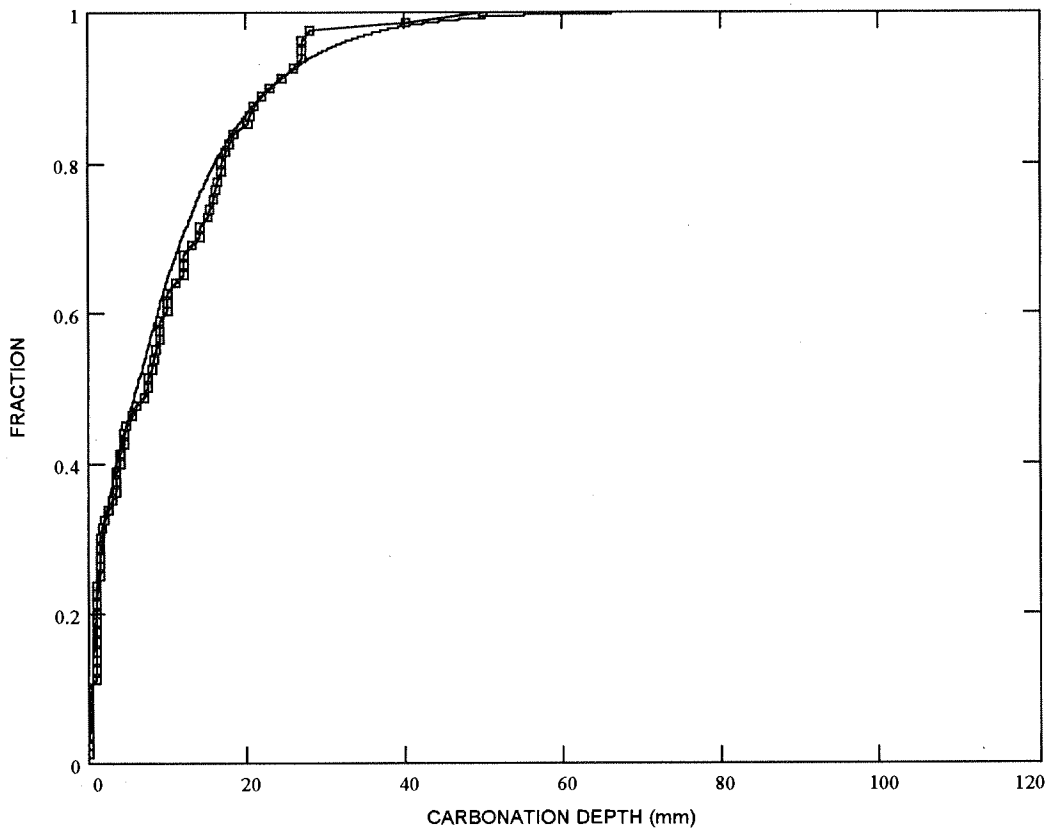

Figure 3.4.2: Experimental data (boxes) and empirical distribution function (line) for xc.

APPENDIX 3.4 (Continued)

$$Xc(i) := \left(1 - e^{\frac{-z_i}{10.909}}\right) \cdot \left[\left(1.925\, e^{\frac{-z_i}{2.172}}\right) + 1\right]$$

$$Xg(z) := \left(1 - e^{\frac{-z}{10.909}}\right) \cdot \left[\left(1.925\, e^{\frac{-z}{2.172}}\right) + 1\right]$$

$$Pxc(z) := \frac{d}{dz}\left(1 - e^{\frac{-z}{u_0}}\right) \cdot \left[\left(u_1 \cdot e^{\frac{-z}{u_2}}\right) + 1\right]$$

$$Pxc(z) := \frac{1}{u_0} \cdot \exp\left(\frac{-z}{u_0}\right) \cdot \left(u_1 \cdot \exp\left(\frac{-z}{u_2}\right) + 1\right) - \left(1 - \exp\left(\frac{-z}{u_0}\right)\right) \cdot \frac{u_1}{u_2} \cdot \exp\left(\frac{-z}{u_2}\right)$$

Probability Distribution of Xc

$$Fc := \int_0^{500} cnorm\left(\frac{z - \eta cc}{\sigma cc}\right) \cdot Pxc(z)\, dz$$

$Fc = 0.015$ 1.5 % chance of finding core with Xc>cc (see above).

APPENDIX 3.5 CARBONATION COEFFICIENTS REPORTED IN THE LITERATURE

[REF. #] RESEARCHERS	SURVEY LOCATION	EXPOSURE CONDITION	COMPRESSIVE STRENGTH (MPa)	CARBONATION COEFFICIENT (*mm/y1/2*)	STRUCTURE CHARACTERISTICS
[I.15] HOLM et al.	USA (VA.)	MARINE ENVIRONMENT	LWC 35	0.2 to 0.3	Concrete Ship
[I.15] HOLM et al.	USA (MD.)	MARINE ENVIRONMENT	LWC 24	0.2 to 1.4 0.8 to 2.2	Top of Bridge Deck Bottom Bridge Deck
[I.15] HOLM et al.	USA (NY.)	MARINE ENVIRONMENT	LWC 27	1.3 2.6	Top of Bridge Deck Bottom Bridge Deck
[I.26] VAYSBURD et al	USA (WA.)	IN LAND	35	2.6	Bottom Bridge Deck
[I.27] PARROT	U.K.	SEVERAL ENVIRONMENTS	15 to 20 35 to 40 45 to 50	4.4 to 7.7 6.2 to 0.9 1.1 to 0.3	
[I.27] PARROT	GERMANY	SEVERAL ENVIRONMENTS	15 to 20 25 to 35 45 to 50	11 to 0.3 9.7 to 0.3 6.5 to 0.2	
[I.27] PARROT	SCANDINAVIA	SEVERAL ENVIRONMENTS	32 44	5.1 to 4.0 0.3	
[I.15] HOLM et al.	JAPAN	MARINE ENVIRONMENT	LWC 23 LWC 26	3.7 4.1	Bridge Deck Bridge Deck
[I.27] PARROT	JAPAN		30	2.8 to 16.6	Harbor Structures
[I.27] PARROT	MIDDLE EAST	IN LAND		4 to 11.9	In Buildings
[I.27] PARROT	MIDDLE EAST	IN LAND	28 (w.c = 0.5)	0.3 to 3	In Buildings
[I.27] PARROT	MIDDLE EAST	IN LAND	(w/c = 0.7)	2.5 to 6.3	In Buildings
[I.28] HO and LEWIS	AUSTRALIA	IN LAND	20 to 25	4 to 6.5 6.5 to 11.5	In Buildings Bridge
[I.29] WONG, CHIEW and HO	SINGAPORE MALAYSIA	TROPICAL HUMID ENVIRONMENT	19.9 to 14.3 27.5 to 11.3 36.6 to 11.4 14.0 to 12.9	4.2 to 13.2 4.1 to 17.2 2.4 to 14.4 3.3 to 12.9	Administ. Building Industrial Building Commercial Buildings Residential Buildings
[I.30] PARAKASH et al	INDIA		35 25	1.3 to 1.6 3.1 to 3.8	Prestressed Beam Reinforced Concrete

REF. # = Reference Number
LWC = Light Weight Concrete
Administ. = Administrative

APPENDICES FOR SECTION 4

APPENDIX 4.1. CONCRETE MIX DESIGNS

Mix 01

BATCH ID # Sag #1 BATCH SIZE 1.5 CF DATE 4/12/94

W/C SELECTED .37
GAMMA = 62.215
DESIGN AIR = 2.0 %

	DESIGN WEIGHTS (LBS)	BATCH WEIGHTS (LBS)
CEMENT	601.6	33.4
ASH/SLAG	150.4	8.4
SILICA FUME	0.0	0.0
WCOR	0.0	0.0
OUNCES OF DCI	0.0	0.0
WIDCI	0.0	0.0
WATER	278.2	14.3
FINES	1119.8	61.9
COARSE	1669.9	94.2
UNIT WGT.	141.5 lb/cf	
WRDA 79	56.4oz	3.1oz 91.7 ml

MATERIALS

PROPERTY	COARSE	FINES
SPECIFIC GRAVITY	2.44	2.63
ABSORBTION	5.04	0.50
TOTAL MOISTURE	6.58	0.00
FREE MOISTURE	1.54	-0.50

%AIR NA

TEMP

APPENDIX 4.1. (Continued)
Mix 03

BATCH ID # Sag #3 BATCH SIZE 1.5 CF DATE 4/12/94

W/C SELECTED .50
GAMMA = 62.215
DESIGN AIR = 2.0 %

	DESIGN WEIGHTS (LBS)	BATCH WEIGHTS (LBS)
CEMENT	601.6	33.4
ASH/SLAG	150.4	8.4
SILICA FUME	0.0	0.0
WCOR	0.0	0.0
OUNCES OF DCI	0.0	0.0
WIDCI	0.0	0.0
WATER	376.0	19.7
FINES	862.7	47.7
COARSE	1669.9	94.2
UNIT WGT.	135.6 lb/cf	
WRDA 79	56.4oz	3.1oz

	MATERIALS	
PROPERTY	COARSE	FINES
SPECIFIC GRAVITY	2.44	2.63
ABSORBTION	5.04	0.50
TOTAL MOISTURE	6.58	0.00
FREE MOISTURE	1.54	-0.50

SLUMP 12"
TEMP
%AIR 1.2

APPENDIX 4.1. (Continued)
Mix 05

BATCH ID # Sag #5 BATCH SIZE 1.5 CF DATE 4/12/94

W/C SELECTED .50
GAMMA = 62.215
DESIGN AIR = 2.0 %

	DESIGN WEIGHTS (LBS)	BATCH WEIGHTS (LBS)
CEMENT	601.6	33.4
ASH/SLAG	150.4	8.4
SILICA FUME	0.0	0.0
WCOR	0.0	0.0
OUNCES OF DCI	0.0	0.0
WIDCI	0.0	0.0
WATER	376.0	19.7
FINES	862.7	47.7
COARSE	1669.9	94.2
UNIT WGT.	135.6 lb/cf	
WRDA 79	56.4oz	3.1oz (No WRDA 79 ADDED) 124.6 g NaCl

PROPERTY	COARSE	FINES
SPECIFIC GRAVITY	2.44	2.63
ABSORBTION	5.04	0.50
TOTAL MOISTURE	6.58	0.00
FREE MOISTURE	1.54	-0.50

SLUMP 8.5"
TEMP
%AIR 1.2

APPENDIX 4.1. (Continued)
Mix 08

BATCH ID # Sag #8 BATCH SIZE 1.5 CF DATE 4/12/94

W/C SELECTED .37
GAMMA = 62.215
DESIGN AIR = 2.0 %

	DESIGN WEIGHTS (LBS)	BATCH WEIGHTS (LBS)
CEMENT	541.4	30.1
ASH/SLAG	150.4	8.4
SILICA FUME	125.8	7.0 SLURRY
WCOR	65.6	3.6 (NOT ADDED; FROM SLURRY)
OUNCES OF DCI	0.0	0.0
WIDCI	0.0	0.0
WATER	278.2	10.7
FINES	1098.1	60.7
COARSE	1669.9	94.2
UNIT WGT.	140.7 lb/cf	
WRDA 79	56.4oz	3.1oz

MATERIALS

PROPERTY	COARSE	FINES
SPECIFIC GRAVITY	2.44	2.63
ABSORBTION	5.04	0.50
TOTAL MOISTURE	6.58	0.00
FREE MOISTURE	1.54	-0.50

SLUMP 8.75
TEMP
%AIR 1.3

APPENDIX 4.1. (Continued)
Mix 10

BATCH ID # Sag #10 BATCH SIZE 1.5 CF DATE 4/12/94

W/C SELECTED .37
GAMMA = 62.215
DESIGN AIR = 2.0 %

	DESIGN WEIGHTS (LBS)	BATCH WEIGHTS (LBS)
CEMENT	376.0	20.9
ASH/SLAG	376.0	20.9
SILICA FUME	0.0	0.0
WCOR	0.0	0.0
OUNCES OF DCI	0.0	0.0
WIDCI	0.0	0.0
WATER	278.2	14.3
FINES	1044.4	57.7
COARSE	1669.9	94.2
UNIT WGT.	138.7 lb/cf	
WRDA 79	56.4oz	3.1oz

MATERIALS

PROPERTY	COARSE	FINES
SPECIFIC GRAVITY	2.44	2.63
ABSORBTION	5.04	0.50
TOTAL MOISTURE	6.58	0.00
FREE MOISTURE	1.54	-0.50

SLUMP 3.75"
TEMP
%AIR 1.8

APPENDIX 4.2. CONCRETE WEIGHT DATA (g)
(Conditioning Period)

SPECIMEN	Date	4/27/94	4/28/94	4/29/94	5/2/94	5/4/94	5/6/94	5/11/94	5/18/94	5/24/94	5/31/94	6/7/94	6/16/94	6/21/94	6/29/94	7/7/94	7/12/94	7/20/94
NUMBER	Time	0	1	2	5	7	9	14	21	27	34	41	50	55	63	71	76	84
MIX 01																		
101	MAS	1574.7	1569.9	1563.7	1556.3	1553.4	1550.8	1548.0	1543.2	1539.8	1538.2	1537.6	1535.4	1534.9	1534.2	1533.2	1533.1	1532.9
102	MAS	1556.3	1551.1	1545.0	1537.4	1534.3	1531.5	1528.4	1524.2	1520.7	1519.0	1518.3	1517.3	1516.7	1516.0	1515.1	1514.9	1515.2
103	MAS	1560.1	1556.0	1550.9	1544.1	1541.1	1538.5	1535.6	1531.6	1528.2	1526.5	1525.8	1524.8	1524.3	1523.6	1522.8	1522.6	1522.6
104	MAS	1574.6	1566.5	1560.4	1552.7	1549.4	1546.6	1543.5	1539.3	1535.8	1534.2	1533.5	1532.4	1531.9	1531.3	1530.5	1530.3	1530.0
105	MAS	1546.6	1539.8	1534.0	1525.9	1522.5	1519.6	1516.3	1512.0	1508.5	1506.7	1506.0	1504.9	1504.4	1503.8	1502.9	1502.7	1502.4
106	MAS	1565.0	1559.0	1553.3	1545.3	1542.2	1539.5	1536.4	1532.3	1528.8	1527.1	1526.5	1525.4	1525.0	1524.3	1523.5	1523.3	1523.0
107	MAS	1553.7	1547.1	1542.3	1534.8	1532.0	1529.6	1526.8	1522.8	1519.3	1517.6	1517.0	1515.9	1515.4	1514.8	1513.9	1513.7	1513.4
108	MAS	1560.4	1554.4	1548.5	1540.7	1537.9	1535.4	1532.5	1528.6	1525.1	1523.6	1523.0	1522.0	1521.6	1521.0	1520.2	1520.1	1519.9
109	MAS	1571.5	1564.1	1557.3	1549.0	1545.5	1542.6	1539.3	1534.8	1531.2	1529.5	1528.7	1527.6	1527.1	1526.4	1525.4	1525.3	1525.0
110	MAS	1560.9	1552.6	1546.6	1538.8	1535.2	1532.3	1529.1	1524.7	1521.2	1519.5	1518.8	1517.7	1517.2	1516.6	1515.7	1515.5	1515.2
111	MAS	1541.6	1536.1	1529.7	1522.0	1518.6	1515.6	1512.5	1508.2	1504.7	1503.1	1502.4	1501.3	1500.9	1500.2	1499.4	1499.3	1499.0
112	MAS	1576.0	1570.3	1564.6	1557.0	1553.7	1550.7	1547.5	1543.2	1539.6	1537.8	1537.0	1535.8	1535.3	1534.1	1533.7	1533.5	1533.2
113	MAS	1557.3	1547.5	1542.5	1534.7	1531.2	1528.3	1525.1	1520.7	1517.1	1515.3	1514.5	1513.4	1512.9	1512.1	1511.4	1511.2	1511.3
Stand. Dev.		10.78	10.86	10.75	10.81	10.87	10.90	10.94	10.88	10.89	10.90	10.90	10.76	10.76	10.70	10.72	10.73	10.71
Avg.		1561.4	1555.0	1549.1	1541.4	1538.2	1535.5	1532.4	1528.1	1524.6	1522.9	1522.2	1521.1	1520.6	1519.9	1519.1	1518.9	1518.7
MIX 03																		
301	MAS	1514.5	1505.2	1498.4	1487.7	1483.3	1479.6	1475.3	1469.4	1464.6	1462.1	1461.0	1459.6	1459.0	1458.2	1457.1	1456.9	1457.0
302	MAS	1543.0	1533.7	1525.6	1514.4	1510.2	1506.6	1502.5	1496.9	1492.1	1489.8	1488.6	1487.3	1486.7	1485.8	1484.7	1484.5	1484.8
303	MAS	1530.8	1520.5	1510.0	1497.1	1492.4	1488.6	1484.1	1478	1473.1	1470.7	1469.6	1468.2	1467.6	1466.8	1465.8	1465.5	1465.7
304	MAS	1512.4	1499.1	1489.6	1477.8	1473.0	1469.1	1464.7	1458.9	1454.1	1451.8	1450.8	1449.4	1448.9	1448.1	1447.0	1446.8	1446.6
305	MAS	1526.5	1516.5	1507.6	1496.8	1492.2	1488.3	1484.0	1478.2	1473.4	1471.0	1469.9	1468.5	1467.9	1467.1	1466.0	1465.7	1465.4
306	MAS	1510.2	1500.4	1490.9	1479.3	1474.4	1470.2	1465.5	1459.3	1454.3	1451.7	1450.4	1448.9	1448.2	1447.2	1446.2	1445.9	1445.5
307	MAS	1509.5	1498.2	1490.7	1479.9	1475.1	1471.1	1466.6	1460.5	1455.5	1452.9	1451.6	1450.1	1449.5	1448.3	1447.4	1447.2	1446.8
308	MAS	1505.4	1495.9	1488.0	1477.3	1472.8	1468.8	1464.3	1458.1	1452.9	1450.2	1448.9	1447.3	1446.6	1445.2	1444.5	1444.2	1443.9
309	MAS	1524.2	1515.0	1506.0	1494.6	1489.8	1485.9	1481.2	1474.9	1469.7	1467.1	1465.7	1464.2	1463.5	1461.7	1461.4	1461.1	1460.7
310	MAS	1511.8	1500.1	1493.1	1482.6	1478.1	1474.4	1470.1	1464.1	1459.1	1456.6	1455.4	1454.0	1453.4	1452.5	1451.4	1451.2	1450.9
311	MAS	1527.3	1517.4	1507.7	1495.8	1491.1	1487.3	1482.8	1476.8	1471.7	1469.2	1468.0	1466.6	1466.0	1465.1	1464.0	1463.7	1463.4
312	MAS	1529.5	1519.3	1510.0	1499.1	1494.6	1490.8	1486.4	1480.6	1475.7	1473.3	1472.3	1470.8	1470.2	1469.0	1468.2	1468.0	1467.7
313	MAS	1519.4	1509.9	1501.2	1490.3	1485.7	1481.9	1477.5	1471.6	1466.7	1464.2	1463.1	1461.6	1461.0	1459.9	1459.0	1458.7	1458.4
Stand. Dev.		10.89	11.37	11.01	10.66	10.97	11.07	11.15	11.26	11.31	11.38	11.41	11.46	11.47	11.51	11.49	11.49	11.63
Avg.		1520.3	1510.1	1501.4	1490.2	1485.6	1481.7	1477.3	1471.3	1466.4	1463.9	1462.7	1461.3	1460.7	1459.6	1458.7	1458.4	1458.2

Key: specimen number XYZ; 0X is mix number; YZ (01 to 13) is replication number.
Time (0-84) in days.

SPECIMEN	Date	4/27/94	4/28/94	4/29/94	5/2/94	5/4/94	5/6/94	5/11/94	5/18/94	5/24/94	5/31/94	6/7/94	6/16/94	6/21/94	6/29/94	7/7/94	7/12/94	7/20/94
NUMBER	Time	0	1	2	5	7	9	14	21	27	34	41	50	55	63	71	76	84
MIX 05																		
501	MAS	1508.3	1499.0	1491.2	1480.6	1475.6	1471.3	1466.3	1459.6	1454.2	1451.4	1449.9	1448.3	1447.5	1446.0	1445.1	1444.7	1444.6
502	MAS	1513.0	1504.5	1499.6	1491.0	1486.9	1483.2	1478.9	1472.7	1467.4	1464.7	1463.2	1461.6	1460.8	1459.4	1458.4	1458.0	1458.1
503	MAS	1537.4	1528.0	1522.7	1513.8	1509.6	1505.9	1501.6	1495.4	1490	1487.2	1485.7	1484.0	1483.2	1481.7	1480.7	1480.3	1480.2
504	MAS	1518.0	1511.8	1505.3	1495.6	1491.5	1487.7	1483.3	1477	1471.6	1468.9	1467.5	1465.9	1465.2	1463.7	1462.8	1462.4	1461.9
505	MAS	1543.9	1537.6	1531.6	1522.3	1518.1	1514.3	1509.9	1503.7	1498.3	1495.6	1494.2	1492.5	1491.8	1490.6	1489.3	1488.9	1488.4
506	MAS	1507.7	1499.8	1492.2	1481.8	1477.6	1473.8	1469.5	1463.4	1458	1455.4	1454.1	1452.6	1451.8	1450.8	1449.5	1449.1	1448.7
507	MAS	1517.6	1510.6	1502.8	1492.7	1488.4	1484.5	1479.4	1473.1	1467.8	1464.5	1463.3	1461.5	1460.8	1459.3	1458.4	1458.0	1457.6
508	MAS	1534.9	1527.0	1520.9	1511.9	1507.9	1504.2	1500.2	1494.3	1489.3	1486.6	1485.4	1483.8	1483.0	1481.6	1480.6	1480.2	1479.7
509	MAS	1536.2	1527.4	1520.7	1510.7	1506.1	1502.0	1497.3	1490.8	1485.5	1482.7	1481.4	1479.7	1478.9	1477.4	1476.5	1476.1	1475.6
510	MAS	1547.2	1539.8	1534.4	1525.2	1521.1	1517.4	1512.9	1506.7	1501.4	1498.6	1497.1	1495.3	1494.5	1492.9	1492.0	1491.6	1491.0
511	MAS	1524.5	1518.1	1511.3	1502.1	1497.9	1494.3	1490.0	1483.8	1478.4	1475.7	1474.3	1472.6	1471.8	1470.3	1469.3	1468.9	1468.3
512	MAS	1503.6	1497.4	1491.4	1482.3	1478.3	1474.7	1470.5	1464.3	1459.1	1456.5	1455.2	1453.7	1453.0	1451.9	1450.8	1450.4	1450.0
513	MAS	1543.5	1535.0	1527.9	1517.9	1513.7	1509.9	1505.4	1499.1	1493.7	1491.0	1489.7	1488.1	1487.4	1486.2	1485.0	1484.6	1484.1
Stand. Dev.		15.40	15.30	15.65	15.86	15.93	15.98	16.05	16.10	16.11	16.11	16.11	16.05	16.05	16.01	16.00	16.00	15.90
Avg.		1525.8	1518.2	1511.7	1502.1	1497.9	1494.1	1489.6	1483.4	1478.1	1475.3	1473.9	1472.3	1471.5	1470.1	1469.1	1468.7	1468.3
MIX 08																		
801	MAS	1564.1	1559.6	1553.8	1547.3	1544.4	1541.8	1539.0	1534.8	1531.3	1529.5	1528.6	1527.5	1527.0	1525.5	1525.4	1525.1	1525.1
802	MAS	1573.3	1568.7	1563.5	1556.9	1553.9	1551.1	1548.0	1543.6	1540	1538.1	1537.1	1535.9	1535.3	1533.9	1533.6	1533.3	1533.4
803	MAS	1600.2	1594.0	1589.6	1583.2	1580.2	1577.6	1574.7	1570.5	1567	1565.1	1564.1	1563.0	1562.4	1561.1	1560.8	1560.5	1560.4
804	MAS	1574.7	1569.0	1565.2	1558.7	1555.9	1553.3	1550.3	1546.1	1542.5	1540.6	1539.6	1538.4	1537.9	1536.5	1536.2	1535.7	1535.3
805	MAS	1555.5	1551.8	1548.2	1542.1	1539.6	1537.2	1534.4	1530.2	1526.6	1524.8	1523.8	1522.6	1522.1	1520.6	1520.4	1520.1	1519.7
806	MAS	1570.8	1565.7	1562.4	1556.7	1554.2	1551.9	1549.2	1545.3	1541.9	1540.1	1539.2	1538.1	1537.6	1536.3	1536.0	1535.7	1535.4
807	MAS	1560.8	1556.2	1551.9	1545.2	1542.4	1539.9	1536.8	1532.5	1528.9	1527.1	1526.1	1525.0	1524.4	1523.4	1522.8	1522.5	1522.2
808	MAS	1579.9	1574.7	1570.1	1562.9	1560.2	1557.8	1554.8	1550.7	1547	1545.3	1544.4	1543.3	1542.8	1542.0	1541.2	1540.9	1540.6
809	MAS	1555.3	1551.2	1545.8	1539.3	1536.4	1533.9	1531.2	1527.3	1524.1	1522.4	1521.7	1520.7	1520.2	1519.0	1518.7	1518.4	1518.1
810	MAS	1573.2	1568.8	1564.0	1558.0	1555.1	1552.6	1549.9	1546	1542.8	1541.0	1540.3	1539.2	1538.7	1537.5	1537.1	1536.8	1536.5
811	MAS	1569.7	1564.6	1560.6	1554.9	1552.3	1549.8	1547.1	1543.3	1540	1538.2	1537.4	1536.3	1535.8	1534.3	1534.2	1533.9	1533.5
812	MAS	1559.3	1554.8	1550.6	1544.2	1541.4	1538.8	1535.8	1531.6	1528.1	1526.2	1525.3	1524.1	1523.6	1522.4	1522.0	1521.7	1521.3
813	MAS	1568.1	1562.9	1559.3	1553.4	1550.7	1548.4	1545.6	1541.5	1538	1536.1	1535.2	1534.0	1533.5	1532.0	1531.9	1531.6	1531.3
Stand. Dev.		11.96	11.40	11.44	11.41	11.37	11.35	11.33	11.33	11.31	11.29	11.27	11.27	11.26	11.28	11.25	11.25	11.29
Avg.		1569.6	1564.8	1560.4	1554.1	1551.3	1548.8	1545.9	1541.8	1538.3	1536.5	1535.6	1534.5	1533.9	1532.7	1532.3	1532.0	1531.8

Key: specimen number XYZ; 0X is mix number; YZ (01 to 13) is replication number.
Time (0-84) in days.

APPENDIX 4.2. (Continued)

SPECIMEN	Date	4/27/94	4/28/94	4/29/94	5/2/94	5/4/94	5/6/94	5/11/94	5/18/94	5/24/94	5/31/94	6/7/94	6/16/94	6/21/94	6/29/94	7/7/94	7/12/94	7/20/94
NUMBER	Time	0	1	2	5	7	9	14	21	27	34	41	50	55	63	71	76	84
MIX 10																		
1001	MAS	1580.1	1569.4	1563.1	1554.0	1550.3	1547.1	1543.6	1538.8	1534.9	1533.0	1532.1	1531.0	1530.5	1529.3	1529.0	1528.8	1528.9
1002	MAS	1575.0	1565.6	1559.3	1550.0	1546.3	1543.2	1539.8	1535.1	1531.2	1529.4	1528.5	1527.4	1526.9	1525.9	1525.5	1525.2	1525.5
1003	MAS	1564.0	1553.9	1546.6	1536.5	1532.7	1529.4	1525.9	1521.1	1517.2	1515.3	1514.4	1513.4	1512.9	1512.2	1511.5	1511.2	1511.3
1004	MAS	1573.3	1563.6	1556.2	1545.8	1541.5	1538.1	1534.5	1529.8	1526.1	1524.2	1523.4	1522.3	1521.8	1521.1	1520.4	1520.1	1519.9
1005	MAS	1545.5	1535.6	1527.9	1517.6	1513.5	1510.0	1506.2	1501.4	1497.5	1495.6	1494.7	1493.6	1493.0	1492.4	1491.6	1491.3	1491.1
1006	MAS	1556.7	1545.1	1539.2	1529.7	1525.8	1522.4	1518.7	1513.8	1509.8	1507.8	1506.9	1505.7	1505.2	1504.5	1503.7	1503.4	1503.2
1007	MAS	1588.1	1575.2	1569.9	1561.0	1557.3	1554.0	1550.5	1545.7	1541.7	1539.7	1538.8	1537.6	1537.1	1536.4	1535.7	1535.3	1535.1
1008	MAS	1572.2	1563.3	1555.1	1545.6	1541.6	1538.2	1534.6	1529.7	1525.7	1523.7	1522.7	1521.7	1521.1	1520.5	1519.7	1519.4	1519.2
1009	MAS	1574.7	1567.4	1560.4	1551.2	1547.3	1544.0	1540.4	1535.7	1531.7	1529.9	1529.0	1528.0	1527.5	1526.9	1526.1	1525.8	1525.7
1010	MAS	1576.5	1565.5	1558.8	1549.5	1545.4	1541.8	1538.0	1533.1	1529.2	1527.3	1526.4	1525.3	1524.8	1524.1	1523.4	1523.1	1522.8
1011	MAS	1573.1	1561.5	1555.4	1546.5	1542.4	1539.1	1535.4	1530.4	1526.4	1524.5	1523.6	1522.5	1521.9	1521.3	1520.5	1520.2	1520.0
1012	MAS	1582.7	1572.1	1565.4	1555.7	1551.8	1548.5	1544.9	1540.1	1536	1534.1	1533.2	1532.1	1531.6	1530.9	1530.1	1529.8	1529.6
1013	MAS	1556.6	1545.0	1537.3	1526.7	1522.8	1519.4	1515.8	1510.9	1506.9	1505.0	1504.2	1503.2	1502.7	1502.0	1501.3	1501.0	1500.8
Stand. Dev.		11.88	11.86	12.23	12.62	12.68	12.74	12.80	12.82	12.81	12.82	12.81	12.80	12.81	12.75	12.81	12.80	12.83
Avg.		1570.7	1560.2	1553.4	1543.8	1539.9	1536.6	1532.9	1528.1	1524.2	1522.3	1521.4	1520.3	1519.8	1519.0	1518.3	1518.0	1517.9

Key: specimen number XYZ; 0X is mix number; YZ (01 to 13) is replication number.
Time (0-84) in days.

APPENDIX 4.3. CONCRETE RESISTIVITY DATA (kΩ-cm)
(Conditioning Period)

	4/27/94	5/13/94	5/19/94	5/25/94	5/31/94	6/08/94	6/21/94	6/29/94	7/12/94	7/20/94
	0	16	22	28	34	42	55	63	76	84
Mix 01										
St. Dev.	0.27	0.66	0.89	1.07	1.26	1.91	2.82	2.66	3.30	5.49
0101	3.83	14.42	18.15	24.07	26.69	30.78				
0102	3.40	14.07	17.86	22.47	27.00	29.88	39.51	46.77	54.28	51.30
0103	4.07	14.22	18.02	23.46	27.74	32.72	41.07	47.45	54.12	55.00
0104	3.33	14.09	18.91	24.07	26.98	33.31	43.93	49.40	54.42	61.54
0105	3.40	13.77	17.57	24.88	28.35	33.23	44.24	47.57	56.95	62.47
0106	3.58	14.65	18.74	24.81	28.19	34.63	45.95	47.86	57.51	62.33
0107	3.70	13.35	17.14	22.86	25.41	27.67	38.19	44.51	55.04	51.44
0108	3.89	14.05	18.50	24.94	28.83	32.72	45.56	48.11	59.94	66.05
0109	3.27	13.33	17.22	23.70	25.58	29.79	40.74	44.96	53.19	57.96
0110	3.40	15.66	18.46	26.48	27.45	32.12	45.78	52.49	61.95	65.82
0111	3.64	14.26	19.32	24.32	29.44	33.62	43.07	50.62	60.27	67.00
0112	3.46	13.15	15.93	23.40	25.76	31.17	39.84	42.70	51.11	55.49
0113	3.15	13.60	17.92	23.02	27.94	31.48	45.84	47.88	53.62	60.49
Avg.	3.55	14.05	17.98	24.05	27.33	31.78	42.81	47.53	56.03	59.74
Mix 03										
St. Dev.	0.46	0.60	0.66	1.37	1.04	1.68	2.50	4.16	3.71	5.56
0301	2.47	11.28	13.40	19.51	23.11	25.27	38.52	45.64	57.16	54.32
0302	2.53	10.27	13.05	19.32	21.48	24.22	34.86	37.45	51.17	50.43
0303	2.28	10.91	13.99	20.93	23.17	27.67	39.55	47.37	53.97	53.50
0304	2.22	10.45	13.77	20.74	22.72	27.41	39.32	49.38	62.53	72.20
0305	2.47	9.86	13.48	18.40	21.63	24.14	35.06	43.50	55.16	60.53
0306	2.28	9.65	12.53	17.65	21.63	24.53	36.46	41.11	54.55	56.17
0307	2.22	9.44	12.37	17.04	20.78	24.18	32.80	41.46	52.72	55.33
0308	2.35	9.12	11.60	16.79	19.81	22.30	33.11	37.86	52.74	58.11
0309	2.16	9.94	12.30	18.09	20.12	24.30	33.15	38.27	50.47	55.10
0310	3.95	9.96	13.25	18.83	21.40	26.01	37.26	37.76	52.65	62.86
0311	2.22	9.55	13.29	17.28	22.14	23.58	33.21	38.42	48.19	59.47
0312	2.41	10.45	12.78	19.81	21.67	27.24	34.88	39.73	52.94	61.75
0313	2.28	10.29	12.82	17.53	20.84	23.35	33.05	36.48	48.89	54.44
Avg.	2.45	10.09	12.97	18.61	21.58	24.94	35.48	41.11	53.32	58.02
Mix 05										
St. Dev.	0.18	0.67	0.88	1.39	1.58	1.47	2.56	3.18	4.25	4.66
0501	2.90	12.20	14.12	20.00	23.62	25.99	36.15	41.26	54.84	53.46
0502	3.64	11.21	13.81	19.51	21.79	27.61	36.83	43.83	50.60	50.56
0503	3.27	11.46	13.60	18.52	21.91	26.26	35.68	41.42	48.19	46.54
0504	3.27	11.21	14.24	18.40	22.39	24.71	37.35	40.45	49.44	59.14
0505	3.21	10.51	12.51	17.41	19.40	23.68	32.63	36.87	45.80	50.64
0506	3.09	10.64	13.87	18.95	20.99	24.98	33.40	38.29	46.95	54.53
0507	3.15	10.80	12.80	19.88	21.34	25.62	34.53	40.27	49.30	54.34
0508	3.33	9.96	12.06	16.67	19.47	23.17	31.58	33.85	41.28	44.12
0509	3.09	10.97	14.05	20.37	22.06	25.31	35.39	41.09	47.63	54.96
0510	3.21	9.71	13.25	17.90	19.30	23.58	31.07	34.77	41.01	48.09
0511	3.27	10.80	12.65	17.53	18.79	23.81	33.42	37.59	45.53	50.14
0512	3.46	11.75	14.71	21.73	23.35	26.65	38.42	44.38	55.19	59.96
0513	3.21	11.03	14.96	19.20	22.14	27.43	39.26	40.76	49.40	55.31
Avg.	3.24	10.94	13.59	18.93	21.27	25.29	35.05	39.60	48.09	52.44

See key in Appendix 4.2.

APPENDIX 4.3. (Continued)

	4/27/94	5/13/94	5/19/94	5/25/94	5/31/94	6/08/94	6/21/94	6/29/94	7/12/94	7/20/94
	0	16	22	28	34	42	55	63	76	84
Mix 08										
St. Dev.	0.45	1.36	1.32	2.61	3.46	3.44	4.08	4.74	12.94	10.83
0801	9.26	35.04	45.86	56.60	70.08	81.15	102.00	117.28	134.36	132.92
0802	8.70	35.04	45.66	57.41	66.30	79.49	102.49	121.81	131.28	135.19
0803	8.83	37.55	45.12	61.36	74.81	85.64	107.28	122.02	139.71	134.77
0804	9.01	36.28	42.22	61.48	69.73	83.99	107.06	126.54	132.10	155.35
0805	9.69	34.38	43.07	59.57	67.65	83.11	106.56	109.26	93.00	143.21
0806	9.88	37.14	45.12	58.64	67.67	82.80	101.56	113.58	131.69	148.77
0807	8.89	38.85	45.49	61.73	73.68	89.90	113.56	122.63	140.95	165.64
0808	9.63	38.68	46.17	65.19	76.83	90.53	113.13	123.46	147.94	151.85
0809	8.83	37.35	46.73	61.60	72.43	88.87	107.59	118.72	137.65	155.56
0810	9.81	36.77	44.51	56.91	64.44	82.39	101.75	114.40	127.57	139.30
0811	9.69	37.63	46.11	61.60	70.12	81.79	102.74	116.26	131.48	151.03
0812	9.38	36.13	45.62	63.83	70.37	83.91	108.77	116.87	134.16	158.44
0813	9.88	36.67	46.63	59.38	70.49	82.82	104.65	116.26	137.65	161.93
Avg.	9.34	36.73	45.25	60.41	70.36	84.34	106.09	118.39	132.27	148.77
Mix 10										
St. Dev.	0.20	0.88	1.61	2.46	2.63	4.15	5.40	7.29	7.25	12.92
1001	4.69	29.59	40.70	63.77	75.74	91.42	148.15	185.60	228.40	239.51
1002	4.57	31.42	40.53	65.06	80.78	101.95	151.44	171.60	241.36	251.65
1003	4.63	29.44	41.42	62.84	74.79	100.29	143.00	175.31	229.84	226.75
1004	4.32	28.89	41.40	61.54	74.18	90.51	139.30	162.55	225.10	254.32
1005	4.32	28.77	37.43	60.37	73.62	93.64	139.09	179.84	227.98	262.96
1006	4.38	30.47	38.87	61.30	70.91	95.76	143.83	176.54	227.57	256.17
1007	4.57	28.64	40.88	63.02	77.92	97.98	146.71	178.60	228.60	262.14
1008	4.32	30.99	38.37	61.54	75.06	93.15	142.80	174.90	232.51	268.93
1009	4.94	29.77	39.75	64.32	75.82	95.93	149.18	172.43	237.04	255.97
1010	4.38	30.95	43.23	67.22	76.98	103.00	153.09	191.56	243.83	264.20
1011	4.63	30.16	42.51	66.73	77.24	102.70	158.02	184.16	247.94	276.34
1012	4.63	30.12	39.92	62.04	80.00	97.30	145.88	176.13	227.16	265.84
1013	4.26	29.96	40.82	68.02	75.12	96.48	147.12	182.72	234.57	263.37
Avg.	4.51	29.94	40.45	63.68	76.01	96.93	146.74	177.84	233.22	257.55

See key in Appendix 4.2.

APPENDIX 4.4. REBAR POTENTIAL DATA (CSE Scale, mV)

(Starting at day 150 of the accelerated carbonation exposure)

Date	12/26/94	1/02/95	1/18/95	1/23/95	1/30/95	2/07/95	2/13/95	2/20/95	2/28/95	3/07/95	4/07/95	4/17/95	4/25/95	5/01/95	5/08/95	5/15/95	5/22/95	5/29/95
Time	152	159	175	180	187	195	201	208	216	223	254	264	272	278	285	292	299	306
Potentials vs. CSE (mV)																		
011X	-23	-24	-23	-23	-23	-24	-24	-24	-24	-23	-24	-24	-24	-24	-24	-24	-24	-24
012X	-30	-30	-30	-29	-29	-30	-30	-30	-30	-29	-29	-29	-29	-27	-29	-29	-29	-28
013X	-48	-47	-47	-47	-47	-48	-48	-47	-47	-47	-47	-47	-47	-46	-46	-46	-46	-46
011Y	-24	-24	-24	-24	-24	-25	-25	-25	-25	-25	-25	-25	-25	-25	-25	-25	-25	-25
012Y	-35	-35	-35	-35	-35	-36	-36	-36	-35	-36	-35	-35	-35	-37	-35	-35	-35	-34
013Y	-53	-53	-53	-53	-53	-54	-54	-54	-53	-53	-53	-53	-53	-53	-53	-53	-53	-53
031X	-53	-53	-54	-54	-56	-57	-59	-58	-57	-58	-56	-55	-55	-52	-51	-50	-48	-49
032X	-42	-42	-42	-42	-43	-44	-44	-43	-82	-93	-89	-67	-82	-79	-77	-86	-71	-60
033X	-53	-53	-53	-54	-55	-56	-56	-57	-57	-58	-74	-62	-69	-78	-94	-82	-82	-101
031Y	-57	-57	-56	-56	-57	-57	-57	-57	-57	-57	-59	-59	-60	-59	-59	-59	-58	-58
032Y	-44	-44	-44	-44	-45	-46	-46	-46	-47	-48	-82	-90	-72	-68	-78	-80	-69	-62
033Y	-57	-57	-60	-61	-62	-64	-65	-65	-65	-76	-89	-90	-94	-103	-94	-102	-99	-85
051X	-39	-39	-59	-66	-87	-87	-97	-98	-113	-141	-224	-228	-246	-258	-268	-280	-297	-315
052X	-54	-54	-52	-52	-52	-63	-62	-64	-73	-95	-164	-174	-213	-240	-255	-262	-274	-285
053X	-37	-36	-36	-35	-37	-45	-50	-58	-78	-93	-177	-189	-213	-230	-232	-246	-254	-268
051Y	-50	-50	-77	-85	-121	-123	-132	-142	-142	-151	-176	-197	-205	-221	-227	-239	-251	-274
052Y	-58	-58	-104	-125	-147	-149	-156	-152	-158	-173	-225	-238	-251	-252	-275	-291	-294	-302
053Y	-52	-51	-51	-51	-51	-52	-52	-52	-52	-53	-93	-110	-118	-126	-137	-155	-162	-190
081X	0	0	0	1	0	0	0	0	0	0	0	0	0	0	0	0	0	0
082X	-7	-7	-7	-7	-7	-8	-8	-8	-8	-8	-8	-8	-7	-8	-7	-7	-7	-7
083X	-50	-51	-51	-50	-51	-51	-51	-51	-51	-51	-50	-51	-50	-50	-50	-51	-50	-50
081Y	10	10	10	10	10	10	9	10	10	9	9	9	8	8	8	8	8	7
082Y	-18	-18	-18	-18	-18	-19	-19	-19	-19	-19	-18	-18	-18	-18	-17	-17	-17	-17
083Y	-52	-52	-52	-52	-52	-53	-53	-53	-53	-53	-53	-53	-53	-53	-53	-53	-53	-53
101X	-59	-59	-59	-59	-60	-61	-61	-61	-60	-60	-59	-59	-61	-59	-69	-71	-95	-92
102X	-55	-55	-56	-56	-57	-58	-58	-57	-57	-57	-57	-57	-59	-75	-77	-72	-66	-64
103X	-75	-75	-75	-75	-76	-77	-100	-114	-107	-131	-157	-160	-168	-174	-181	-181	-182	-178
101Y	-58	-58	-58	-58	-58	-59	-58	-57	-57	-57	-55	-55	-70	-79	-85	-99	-102	-106
102Y	-53	-53	-53	-53	-55	-55	-55	-55	-54	-55	-98	-93	-106	-116	-100	-114	-118	-122
103Y	-90	-90	-89	-89	-90	-90	-90	-89	-88	-105	-150	-165	-168	-176	-181	-170	-188	-180
Average																		
Mix 01	-36	-36	-35	-35	-35	-36	-36	-36	-36	-36	-36	-36	-36	-35	-35	-35	-35	-35
Mix 03	-51	-51	-52	-52	-53	-54	-55	-54	-61	-65	-75	-71	-72	-73	-76	-77	-71	-69
Mix 05	-48	-48	-63	-69	-83	-87	-92	-94	-103	-118	-177	-189	-208	-221	-232	-246	-255	-272
Mix 08	-20	-20	-20	-19	-20	-20	-20	-20	-20	-20	-20	-20	-20	-20	-20	-20	-20	-20
Mix 10	-65	-65	-65	-65	-66	-67	-70	-72	-71	-78	-96	-98	-105	-113	-116	-118	-125	-124
St. Dev.																		
Mix 01	12.50	12.11	12.31	12.40	12.40	12.40	12.40	12.21	11.93	12.23	12.03	12.03	12.03	12.11	11.84	11.84	11.84	11.97
Mix 03	6.48	6.48	7.04	7.33	7.40	7.56	8.02	8.24	11.84	16.47	14.55	15.60	14.32	18.02	17.69	18.93	17.93	19.65
Mix 05	8.45	8.65	24.03	32.16	43.94	41.72	44.68	43.92	41.88	44.77	48.45	45.72	47.86	48.57	50.44	48.51	49.62	43.96
Mix 08	26.06	26.30	26.30	26.21	26.30	26.44	26.21	26.44	26.44	26.21	25.99	26.23	25.87	25.77	25.89	26.12	25.89	25.67
Mix 10	14.52	14.52	14.04	14.04	13.99	13.81	19.46	24.14	21.84	32.47	47.35	51.79	51.41	51.41	51.76	47.70	49.35	46.91

Key: Specimen Number BXYZ; BX is mix number; Y (1 to 3) is concrete replicate number; Z (X/Y) is rebar identification.
Time (152-306) in days.

APPENDIX 4.5. APPARENT POLARIZATION RESISTANCE Rp_{ap} DATA (Ω)

	06/11/94	06/26/94	07/09/94	08/04/94	09/24/94	11/20/94	1/30/95	2/20/95	4/22/95	6/05/95
	-46	-31	-18	8	59	116	187	208	269	313
Polarization Resistances			(ohms)							
011X	146308	170171	189321	192363	230214	254666	267873	260780	262253	285219
012X	131976	152598	170870	170830	206767	231812	250420	243630	245084	267251
013X	173535	211280	248285	250450	295984	327868	345605	341027	338083	376604
031X	170602	206686	232688	232993	280491	305017	329898	342036	403358	490349
032X	168153	211106	237632	242943	294894	323902	335697	342961	339810	490979
033X	170609	310896	352513	363799	439408	477048	500786	508463	658358	692174
051X	80253	90843	103215	111953	139804	163261	152267	143302	29012	37155
052X	60531	74359	82772	87151	105888	122107	134412	131423	29830	31384
053X	15979	17124	21605	24027	34957	47109	53534	53670	17777	23784
081X	143509	177718	204177	214020	266439	304257	327569	319682	314803	354188
082X	164371	372112	403694	412693	475124	496044	520905	510139	551341	600015
083X	163588	256216	294599		391096	440339	471520	466556	469185	321547
101X	162714	209998	262558	233869	288431	318748	326144	328869	331185	284726
102X	161623	249921	279714	282785	337304	372514	380928	381453	379920	412355
103X		198421	224962	229689	282893	314165	329091	302767	201393	191503
011Y	166439	238829	247117	249048	302079	304731	350878	321816	368997	357694
012Y	167885	222139	230110	231970	282381	282847	334110	311122	323390	313993
013Y	168926	365107	442655	447549	534132	518025	604334	513855	630270	616257
031Y	257990	324475	333612	343102	414944	404545	450603	447985	524022	494771
032Y	205285	264141	271234	279678	347208	338464	403688	387896	415264	485146
033Y	271037	344113	361313	369657	458899	460161	537501	505774		
051Y	106641	123145	145480	144470	195503	192704	157236	102706	61872	16024
052Y	53723	87012	89605	102723	137178	149314	90008		37288	12574
053Y	80606	103217	113416	125214	169120	164806	207747		167287	51661
081Y	321115	395728	406662	417303	500126	489628	544743	491631	586611	574582
082Y	272178	346279	358582	372029	452804	455094	526697	488356	529199	518599
083Y	202003	267639	278517	296975	376152	379401	449135	419706	439465	430400
101Y	123303	154742	151088	157649	201015	186448	236023	209286	221887	173375
102Y	195698	245746	252313	256794	328103	325584	391395	361017	279171	283766
103Y	176407	216556	224345	234998	295546	285316	350236	320497	284232	235167
Average Polarization Resistance (kohms)										
MIX 01	159	227	255	257	309	320	359	332	361	370
MIX 03	207	277	298	305	373	385	426	423	468	531
MIX 05	66	83	93	99	130	140	133	108	57	29
MIX 08	211	303	324	343	410	427	473	449	482	467
MIX 10	164	213	232	233	289	300	336	317	283	263
Stand. Dev. (kohms)										
MIX 01	16.34	75.16	97.30	98.64	116.85	102.89	127.39	96.51	139.78	127.84
MIX 03	46.61	58.92	58.09	61.26	75.99	73.21	85.46	76.12	125.27	90.34
MIX 05	30.82	36.09	41.20	41.71	55.83	50.93	54.24	39.89	55.92	14.50
MIX 08	70.61	82.92	79.59	86.57	85.22	73.47	80.06	70.70	97.88	115.89
MIX 10	26.56	34.82	45.34	41.80	48.34	62.57	55.55	60.08	66.52	86.17

See key in Appendix 4.4.

APPENDIX 4.6. PARABOLIC CARBONATION PROGRESSION

Parabolic progression of the carbonation thickness

The following simplifying assumptions are made:

- one dimensional system, fixed CO_2 concentration Cs at the surface.

- CO_2 diffuses through the carbonated layer obeying Fick's first law.

$$Jco_2 = - D \cdot \partial Cco_2 / \partial x \qquad (6.1)$$

where Jco_2 is the flux of CO_2 through the concrete

D is the effective diffusion coefficient of CO_2

Cco_2 is the surface concentration of CO_2

x is the carbonated concrete distance from the surface

- carbonation of concrete progresses at a rate determined only by how fast CO_2 is diffused to the carbonation front (i.e. CO_2 reactions at the carbonation front are instantaneous).

- Pco_2 is negligible at the carbonation front (i.e. CO_2 is completely consumed at the reaction place).

- diffusion of CO_2 through the carbonated concrete proceeds as if in a succession of steady state regimes (i.e. the carbonation front moves very slowly and the CO_2 concentration at any point inside the carbonated concrete can be treated at each moment as if it were the solution of a time-invariant value with boundary conditions determined by the position of the carbonation front).

- D is constant in time and space.

APPENDIX 4.6. (Continued)

- the magnitude M = dn / dV is constant in time and space, where dn is the number of moles of CO_2 needed to carbonate a volume of concrete dV.

Based on the above assumptions, the problem statement can be summarized graphically in the following figure.

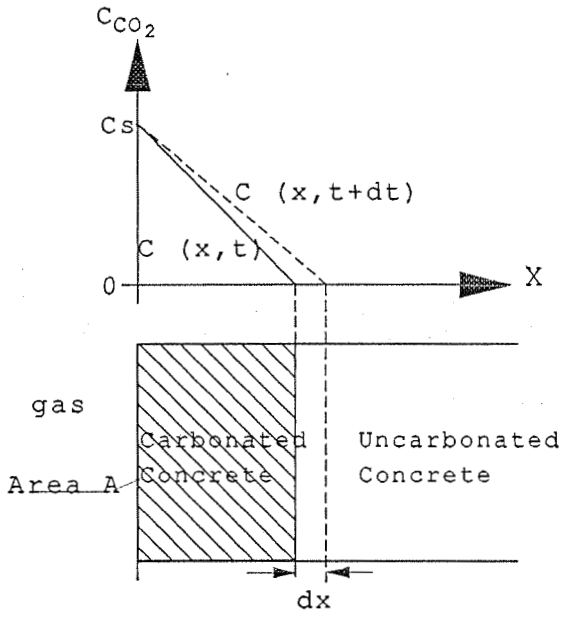

Figure 24. Problem conditions.

Between t and t + dt, a carbonated volume equal to dV = A·dx has been created. The amount of CO_2 needed to carbonate that volume is $Jco_2 \cdot A \cdot dt$. The CO_2 concentration gradient is (0-Cs) / x, thus $Jco_2 = D \cdot Cs / x$. Therefore, the amount of CO_2 needed to carbonate volume dV is $M \cdot dV = M \cdot A \cdot dx$.

APPENDIX 4.6. (Continued)

Thus,

$$Jco_2 \cdot A \cdot dt = M \cdot A \cdot dx \qquad (6.2)$$

$$(D \cdot Cs / x)\, dt = M \cdot dx \qquad (6.3)$$

$$dt = (M / D \cdot Cs)\, x \cdot dx \qquad (6.4)$$

$$\int_0^t dt = (M / D \cdot Cs) \int_0^x x \cdot dx \qquad (6.5)$$

$$t = (M / 2 \cdot D \cdot Cs)\, x^2 \qquad (6.6)$$

by calling $$K = (2 \cdot D \cdot Cs / M)^{1/2} \qquad (6.7)$$

then,

$$x = K \cdot t^{1/2} \qquad (6.8)$$

which indicates (under the above assumptions) that the carbonation distance x is proportional to the square root of time. Notice that the depth of penetration is proportional to the square root of the concentration of CO_2 at the concrete surface.

Carbonation progression after an initial carbonation layer is present

If a system is examined between time t_1 and t_2, then by adapting (6.5):

$$\int_{t_1}^{t_2} dt = (M / D \cdot Cs) \int_{x_1}^{x_2} x \cdot dx \qquad (6.9)$$

and by (6.6)

$$(x_2^2 - x_1^2) = K^2 (t_2 - t_1) \qquad (6.10)$$

If a system exhibits a carbonated layer of thickness x_1 at the beginning of the test, and that layer is assumed to have characteristics similar to those of the carbonated concrete formed subsequently during the test, then the carbonation coefficient using the condition of the test is given by

APPENDIX 4.6. (Continued)

$$K = (x2^2 - x1^2)^{½} / (t')^{½} \qquad (6.11)$$

where $t' = t_2 - t_1$ is the duration of the test. Under the above assumptions, eq (6.11) is valid even if the initial carbonation layer had developed at a faster or slower rate than in the present test.

APPENDIX 4.7. FLAT-FRONT CARBONATION DEPTH CALCULATION FROM CYLINDRICAL FRONT MEASUREMENT

Carbonation progression in a concrete cylinder

The following simplifying assumptions are made:

- Specimen is a cylinder of length L, with an external radius re (see Figure 25 below), where L⟩⟩re; Cs is the CO_2 surface concentration, and the CO_2 concentration is equal to 0 at the position of the carbonation front (radius=rf).

- CO_2 diffuses through the carbonated layer obeying Fick's first law. Therefore, from rf to re:

$$J_t CO_2 = -\frac{C(r) - C(r+dr)}{dr} D\,(2\cdot\pi\cdot r)\,L \qquad (7.1)$$

where $J_t CO_2$ is the integrated flux of CO_2 through the concrete (outward positive, inward negative)

C(r) is the CO_2 concentration at radius r

C(r+dr) is the CO_2 concentration at radius r+dr

D is the effective diffusion coefficient of CO_2

- The magnitude M = dn / dV is constant in time and space, where dn is the number of moles of CO_2 needed to carbonate a volume of concrete dV.

$$J_t CO_2\,dt = drf\,(2\cdot\pi\cdot rf)\,L\cdot M \qquad (7.2)$$

- The other assumptions made are as in Appendix 4.6.

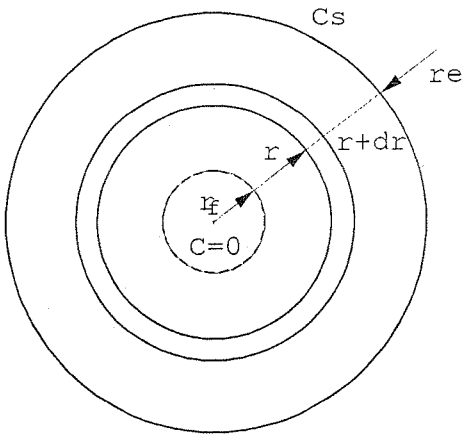

Figure 25. Cylindrical front problem.

From (7.1)

$$- \frac{dC}{dr} D\,(2\cdot\pi\cdot rf)\,L = J_t co_2 \qquad (7.3)$$

$$- \int_{rf}^{re} dC = J_t co_2\,(1/\,2\cdot\pi\cdot D\cdot L) \int_{rf}^{re} (1/r)\,dr \qquad (7.4)$$

$$-C_{re} + C_{rf} = (J_t co_2 / 2\cdot\pi\cdot D\cdot L)\,\ln(re/rf) \qquad (7.5)$$

If $C_{rf} = 0$

$$J_t co_2 = -2\cdot\pi\cdot D\cdot L\cdot C_{re} / \ln(re/rf) \qquad (7.6)$$

APPENDIX 4.7. (Continued)

From (7.2)

$$(drf/dt)\ 2\cdot\pi\cdot rf\cdot L\cdot M = -2\cdot\pi\cdot D\cdot L\cdot C_{re} / \ln(re/rf) \qquad (7.7)$$

$$dt = (M / D\cdot C_{re})\ rf\cdot\ln(rf/re)\ drf \qquad (7.8)$$

$$t = (M / D\cdot C_{re}) \int_{rf0}^{rf} rf\cdot\ln(rf/re)\ drf \qquad (7.9)$$

Analytically:

$$\int rf\cdot\ln(rf/re)\ drf = \tfrac{1}{2}rf^2\ \ln(rf/re) - \tfrac{1}{4}rf^2 \qquad (7.10)$$

Assuming that at t=0, rf=re, then:

$$t = (M / D\cdot C_{re})\ [\tfrac{1}{2}rf^2\ \ln(rf/re) - \tfrac{1}{4}(rf^2 - re^2)] \qquad (7.11)$$

Carbonation progression in a flat-front

From (6.6) in Appendix 4.6

$$t = (M / 2\cdot D\cdot C_s)\ x^2 \qquad (7.12)$$

Calling the penetration depth:

in a cylinder p_r=re-rf,

in a flat-front p_f=xf

Therefore, for a given time t and calling $K = 1/(M / 2\cdot D\cdot C_{re})^{1/2}$

$$t = K^{-2}\ [(re-p)^2\ \ln(1-p/re) - \tfrac{1}{2}(p^2 - 2\cdot p\cdot re)] \qquad (7.13)$$

$$t = K^{-2}\cdot p_f^2 \qquad (7.14)$$

If K is the same for the flat and cylindrical specimens, then the carbonation depth for the same exposure time can be corrected as using $p_f = cf_K \cdot p_r$, where cf_K is the correction factor (see Figure 26).

APPENDIX 4.7. (Continued)

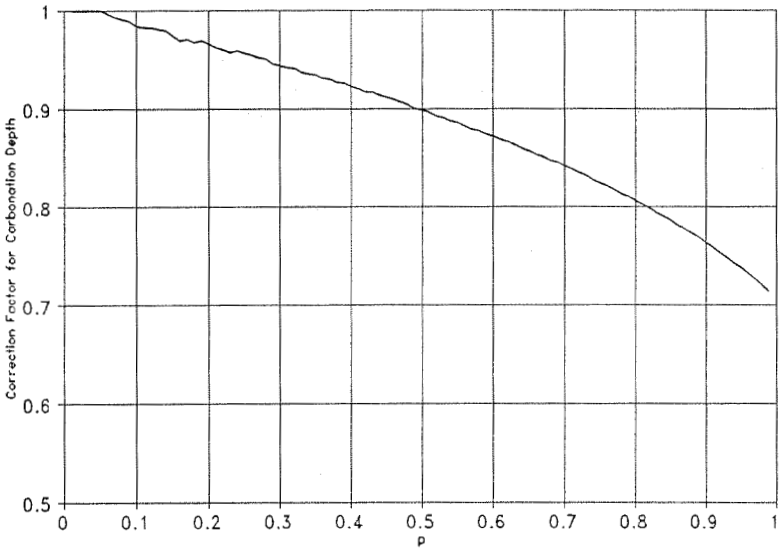

Figure 26. Correction factor (cf_K) for carbonation depth as a function of a normalized penetration depth $p = p_r / re$ in a cylinder.

APPENDIX 4.8. CONCRETE CARBONATION DEPTH DATA (mm)

Raw Carbonation Depth

Time		90		210		350	
		Depth	St. Dev.	Depth	St. Dev.	Depth	St. Dev.
Mix 01	Spc. 1	1.18	0.19	8.75	1.04	12.32	1.88
	Spc. 2	1.08	0.33	8.13	1.89	11.63	1.78
	Avrg.	1.13	0.26	8.44	1.465	11.98	1.83
Mix 03	Spc. 1	2.02	0.43	12.25	1.83	17.73	2.59
	Spc. 2	2.36	0.58	12.13	1.87	17.15	1.37
	Avrg.	2.19	0.505	12.19	1.85	17.44	1.98
Mix 05	Spc. 1	2.59	0.6	13	2.14	20.07	2.06
	Spc. 2	2.4	1.07	12.25	1.73	17.98	2.34
	Avrg.	2.5	0.835	12.63	1.935	19.03	2.2
Mix 08	Spc. 1	1.41	0.38	10.81	1	13.84	1.37
	Spc. 2	1.3	0.48	11.39	2.68	16.46	1.42
	Avrg.	1.36	0.43	11.1	1.84	15.15	1.395
Mix 10	Spc. 1	2.64	0.49	13.25	1.49	21.03	3.48
	Spc. 2	2.5	0.55	14.13	1.43	21.34	2.06
	Avrg.	2.57	0.52	13.69	1.46	21.19	2.77

Flat Carbonation Depth

Time		90	210	350
		Depth	Depth	Depth
Mix 01	Spc. 1	1.18	8.382	11.4681
	Spc. 2	1.08	7.6962	11.1252
	Avrg.	1.13	8.0391	11.3157
Mix 03	Spc. 1	2.02	11.4681	16.2306
	Spc. 2	2.36	11.4681	15.621
	Avrg.	2.19	11.4681	15.9258
Mix 05	Spc. 1	2.59	12.1158	17.9832
	Spc. 2	2.4	11.4681	16.2306
	Avrg.	2.5	11.7729	17.1069
Mix 08	Spc. 1	1.41	10.1346	12.7635
	Spc. 2	1.3	10.7823	15.0114
	Avrg.	1.36	10.4394	14.0589
Mix 10	Spc. 1	2.64	12.4587	18.5547
	Spc. 2	2.5	13.1064	18.8214
	Avrg.	2.57	12.7635	18.7071